Effects of the mid-Miocene Climatic Optimum on ecosystem structure and plant-animal interactions: a phytolith and stable isotope perspective

Elisha B. Harris

A dissertation

submitted in partial fulfillment of the

requirements for the degree of

Doctor of Philosophy

University of Washington

2016

Reading Committee:

Caroline A.E. Strömberg, Chair

Janneke Hille Ris Lambers

Gregory P. Wilson

Program Authorized to Offer Degree:

Biology

University of Washington

Abstract

Effects of the mid-Miocene Climatic Optimum on ecosystem structure and plant-animal
interactions: a phytolith and stable isotope perspective

Elisha B. Harris

Chair of the Supervisory Committee:
Professor Caroline A.E. Strömberg
Biology Department

The mid-Miocene Climatic Optimum (MMCO, 17–14.75 Ma) is one of Earth's most

recent, prolonged global warming events that is thought to have promoted ecological change

across the globe. Although there is general agreement about the timing of broad-scale ecosystem

changes associated with the MMCO, specific details of its influence on local paleo-communities

remain obscure, as no studies have been able to characterize plant and animal responses in the

context of long-term, local climate. However, new radiometric dates for the Railroad Canyon

section (RCS; 22.9–15.2 Ma) of Idaho firmly establish this region as a critical field area for

testing hypotheses about the biotic consequences of long-term global warming during the early–

middle Miocene. The RCS is an exceptionally important sequence of rocks preserving a nearly-continuous record of animals and plants that inhabited the Northern Rocky Mountain, USA, during pre- and peak-MMCO times. Results from stable carbon and oxygen isotopes from fossilized mammalian-herbivore tooth enamel establish that local climate was consistently warm and dry through the early–middle Miocene, clearly decoupled from global climate change. Phytolith (plant silica) data indicate that the RCS was a mosaic of C_3-grass dominated, open habitats and woodland patches during the early–middle Miocene, which pushes back the timing of when open-habitats spread in this region by approximately five million years. And lastly, stable carbon isotopes from tooth enamel indicate that horses and rhinos inhabiting the RCS consistently fed on C_3 vegetation leading into the MMCO. Ultimately, these data have, for the first time, allowed us to develop a comprehensive picture of climate and ecosystem change in a single basin leading into the MMCO. These results highlight how crucial it is to study many different regions to gain a full understanding of the local impacts of climate change in deep time. Specifically, data from the RCS provide insight into the response of a high-elevation site located in the continental interior to global warming during the MMCO. Given that inland, high-elevation sites are generally under-represented in the fossil record, the RCS is an important field area that has the potential to provide a unique perspective on the climate, ecology, and evolution of ecosystems during the early–middle Miocene.

TABLE OF CONTENTS

ii

iv

LIST OF FIGURES

CHAPTER 2: Vegetation response during the lead-up to the middle Miocene warming event in the Northern Rocky Mountains, USA

Appendix for Chapter 2

LIST OF FIGURES (*continued*)

CHAPTER 3: Stable isotope compositions from herbivore teeth indicate climatic stability leading into the middle Miocene in Idaho

CHAPTER 4: Stable isotopes reveal differential dietary evolution in large ungulates during the early–middle Miocene in the Northern Rocky Mountains, USA

LIST OF TABLES

ACKNOWLEDGEMENTS

My graduate school experience has been one of the most intellectually stimulating, challenging, eye-opening, and awesome adventures I have ever undertaken. I could not possibly have made it to where I am today without the enduring support of the many amazing people and organizations acknowledged here.

First and foremost I would like to express my sincere gratitude to my advisor, Caroline Strömberg, for her unending support and enthusiasm throughout the course of my dissertation. Caroline is an incredible advisor and scientist who is dedicated to her students, pushing us to be better scientists and science advocates. I am grateful to have had the opportunity to work with her and learn from her these past 5.5 years. Additionally, I would like to thank my committee members (present and past), Jody Bourgeois, Janneke Hille Ris Lambers, Matt Kohn, Liz Nesbitt, and Greg Wilson, for their questions, insights, encouragement, and advice.

Before any of my dissertation data were gathered, the rocks and fossils that produced those data needed to be collected, and so I have many field assistants to thank for their efforts. In particular I want to thank Christopher Bitting, Ashly Padgett, Cassandra Trinh-Le, and Alysen Vilhena for being awesome field assistants during the summers of 2012–2014. These undergrads toughed it out through long, summer days, wildfire scares, tumultuous lightning storms, and wind storms all so we could collect the rock and tooth fossils used in this dissertation. I am grateful for their energy, enthusiasm, endurance, and willingness to adventure with me. In addition, I am grateful to the field support I received from many other individuals including Meredith Dennis, Erik Fredrickson, Ethan Hyland, Tony Jijina, Thien-Y Le, Nathan Sheldon, Kim Smith, and Selena Smith.

Thank you also to my fellow grad students Will Brightly, Jonathan Calede, Marie Clifford, Peter Conlin, Camilla Crifó, Stephanie Crofts, Lauren DeBey, Dave DeMar, Jaquan Horton, Yasmeen Hussain, Max Maliska, Matt McElroy, Frazer Meacham, Brandon Peecook, and Stephanie Smith (to name a few) for being such a wonderful group of individuals to work and socialize with. I also especially want to thank Regan Dunn (who is the best academic sibling a grad student could ever have) for being a fantastic human being, scientist, and friend.

I also want to thank my awesome family for their endless love and support in all of my academic and personal adventures. They are a great group of talented, witty, loving, and passionate individuals and I am so thankful to have them in my life. And lastly, I would like to thank my partner in crime, Daril Vilhena, who is quite possibly one of the most gifted, intelligent, inspiring, and optimistic individuals I have ever met. I would not be where I am today if it were not for his unconditional support, encouragement, and love, and for that I am eternally grateful.

CHAPTER 1. Introduction and overview

Over the course of the past 65 million years, Earth's biota have experienced both rapid and gradual climate change events (Zachos et al., 2001, 2008) that have had profound impacts on the evolution of individual taxa and composition of biotic communities (e.g., Blois and Hadly, 2009; Figueirido et al., 2012; McInerney and Wing, 2011; Woodburne et al., 2009). Biotic turnover has been documented in plants and animals during the Paleocene-Eocene Thermal Maximum (ca. 56 million years ago, Ma), Terminal Eocene Event (ca. 33 Ma), mid-Miocene Climatic Optimum (ca. 17-14.75 Ma), and Pleistocene cooling and drying intervals (beginning ca. 2.6 Ma; see review in Blois and Hadly, 2009). Each of these events had an impact on the evolution of biotic communities around the world. Deep-time geological records give paleontologists the opportunity to study the impacts of wide ranges of environmental conditions on organisms and communities over macroevolutionary timescales (Dietl and Flessa, 2011). Understanding how taxa have adapted and evolved in response to abiotic and biotic change in the past is invaluable for understanding, managing, and mitigating future change (Dietl and Flessa, 2011; Froyd and Willis, 2008; MacDonald et al., 2008).

Notable among the climatically tumultuous intervals of the Cenozoic is the Miocene epoch (23-5.3 Ma). The Miocene was a critical transitional period in Earth's geologic history when long-term global climatic cooling was punctuated by extreme climatic optima as modern ecosystems were established around the world (Zachos et al., 2001). Grass-dominated ecosystems, which cover up to 40% of Earth's land surface today (Gibson, 2009), spread from low- to mid-latitudes in North America, Eurasia, Australia, and Africa (Jacobs et al., 1999;

1

Strömberg, 2011). Meanwhile evolutionary changes in many mammalian lineages occurred

across the world as browsers were replaced by grazers, hypsodonty in some grazers evolved

(e.g., horses), and immigration events took place (e.g., North America: Barnosky and Carrasco,

2002; Janis et al., 2004; MacFadden, 2000; Eurasia: Fortelius et al., 2006; van Dam, 2006;

Africa: Bobe, 2006; South America: Flynn et al., 2003; Pascual, 2006). These biotic

transformations continued through the late Miocene as C_4 grasses spread and became dominant

in some ecosystems, and grazers began incorporating these plants into their diets (e.g., Cerling et

al., 1997; Edwards and Smith, 2010; Quade et al., 1989). While these biotic transformations were

taking place, the Mid-Miocene Climatic Optimum (MMCO) peaked from ca. 17-14.75 Ma

marking the warmest period in the last 24 million years (Zachos et al., 2001). This global

warming event coincided with relatively warm ocean bottom and surface water temperatures, as

well as decreased ice cover at the poles (e.g., Flower and Kennett, 1994; Lear et al., 2010;

Shevenell et al., 2004; Zachos et al., 2001). Terrestrial atmospheric p_{CO2} records and Global

Circulation Models for the middle Miocene suggest p_{CO2} was also elevated at this time (>500-

700 ppmv, possibly as high as 850 ppmv; Beerling and Royer, 2011; Henrot et al., 2010; Herold

et al., 2011; Kürschner et al., 2008; Retallack, 2009; You et al., 2009). Additionally, fossil plants

suggest that warmer and wetter conditions spread to higher latitudes (e.g., Hinojosa and

Villagrán, 2005; Mosbrugger et al., 2005; Wolfe, 1994). Despite these general patterns, the

details of the influence of the MMCO on flora and fauna in North America remain obscure, as no

rigorous study has investigated paleocommunity responses to local climate during this time. A

primary reason for this gap in our knowledge is that there are very few, continuous, long-term

records in North America that preserve fossil remains leading into the MMCO. However, the

Railroad Canyon section (RCS) of Idaho is a rare example that provides a unique opportunity in

which we can compare local climate data to ecosystem-level floral and faunal change leading in the middle Miocene.

The Railroad Canyon section (RCS) exposes nearly 360 meters of sedimentary rock deposited during the early–middle Miocene of central-eastern Idaho, USA. The RCS preserves a wealth of plant silica remains (Strömberg, 2005), paleosols (Retallack, 2007, 2009) and animal fossils (Barnosky et al., 2007), making it an ideal place to study the biotic effects of the MMCO at the ecosystem level in North America. Previous work in the RCS focused on floral and faunal turnover (e.g., Barnosky, 2001; Strömberg, 2005; Barnosky et al., 2007), paleoclimatic reconstructions (Retallack, 2009), and relative age determinations of the site (Zheng, 1996; Barnosky et al., 2007). Magnetostratigraphy and biostratigraphy of local taxa were used to estimate the age of the RCS as ca. 17.3-13 Ma (Zheng, 1996; Barnosky et al., 2007). However, an alternative age model for the site was proposed by Retallack (2009) who suggested that RCS sediments were deposited between 16.4–10.7 Ma. Therefore, prior to this work the age of the RCS remained poorly constrained.

In addition to documentation of local taxa within the RCS, previous studies used regional data from the NRM to suggest an increase in grazers in faunal communities during the early–middle Miocene as well as a transition from oreodont-, camel- and rhino-dominated communities in the early Miocene to equid-dominated communities in the middle Miocene (Barnosky, 2001; Barnosky et al., 2007, 2003). Previous floral studies in the RCS have shown a transition toward more open (i.e., pooid-dominated) habitats during the late early Miocene (Strömberg, 2005). Although the timing of these biotic transitions appear to broadly coincide with global warming and a local peak in atmospheric CO_2 at the MMCO (Retallack, 2009; Zachos et al., 2001), results from these previous studies have not been synthesized or compared at high enough resolution to

discern whether or not global climate change during the middle Miocene had an impact on the local climate or biota of the Railroad Canyon. Together, the chapters presented here attempt to address this issue by presenting the first systematic analysis of local climate, vegetation, and faunal diets in a single North American basin leading into the MMCO.

In Chapter 2 phytolith and carbon isotope data from fossil soils are used to explore the habitat structure and composition of vegetation throughout the RCS. These data provide the first direct, detailed, and continuous record of long-term changes in vegetation leading up to the MMCO. This chapter also provides the first absolute age model for the Railroad Canyon sequence, using U/Pb dating of zircons extracted from three volcanic ash layers. These new geochronologic results are compared with previously published magnetostratigraphy data to resolve the conflicting age models for the RCS. The end result of this work is one of the best-dated, high-resolution Cenozoic records of long-term floral response to climatic warming in the continental interior of the United States.

In Chapter 3 stable oxygen and carbon isotope data extracted from dental enamel of equids and rhinos are used to reconstruct climate through the RCS. The oxygen isotopic compositions of enamel ($\delta^{18}O_{enamel}$) from bulk tooth samples provide information about the composition of local meteoric water through time, which can potentially offer clues about local to regional topographic changes or generally about temperature change through time. The carbon isotopic composition of enamel ($\delta^{13}C_{enamel}$) from bulk samples yields information about mean annual precipitation through time. Lastly, data from serial sampling of enamel provides clues about seasonal changes in $\delta^{18}O_{enamel}$, which can be linked to seasonal fluctuations in temperature. This chapter builds on the vegetation results provided in Chapter 1 by drawing climatic inferences from the presence of palm phytoliths in the RCS. Since palms are climatically limited

4

today, their presence in the RCS provides minimum estimates of mean annual temperature and cold month mean temperatures through the section. The results of this climate analysis are then compared to results from previous climate studies to provide a comprehensive understanding of local climate during the early–middle Miocene.

In Chapter 4 the stable carbon and oxygen isotope data from Chapter 2 is further analyzed in an attempt to understand the long-term effects of climate and biotic change on mammalian dietary patterns leading into the mid-Miocene Climatic Optimum. In particular, this chapter explores the diets and partitioning of resources among some of the herbivores that inhabited the RCS. This chapter also explores the likelihood that these herbivores exhibit seasonal shifts $\delta^{13}C$ reflecting seasonal changes in diet. This work provides a long-term perspective on the effects of climate and vegetation change on mammalian herbivore diets and niche partitioning in the RCS leading into the middle Miocene Climatic Optimum.

REFERENCES

Barnosky, A.D., 2001. Distinguishing the effects of the Red Queen and Court Jester on Miocene mammal evolution in the northern Rocky Mountains. J. Vertebr. Paleontol. 21, 172–185.

Barnosky, A.D., Bibi, F., Hopkins, S.S.B., Nichols, R., 2007. Biostratigraphy and magnetostratigraphy of the Mid-Miocene Railroad Canyon Sequence, Montana and Idaho, and age of the Mid-Tertiary Unconformity west of the Continental Divide. J. Vertebr. Paleontol. 27, 204–224.

Barnosky, A.D., Carrasco, M.A., 2002. Effects of Oligo-Miocene global climate changes on mammalian species richness in the northwestern quarter of the USA. Evol. Ecol. Res. 4, 811–841.

Barnosky, A.D., Hadly, E. a., Bell, C.J., 2003. Mammalian Response To Global Warming on Varied Temporal Scales. J. Mammal. 84, 354–368.

Beerling, D.J., Royer, D.L., 2011. Convergent Cenozoic CO2 history. Nat. Geosci. 4, 418–420.

Blois, J.L., Hadly, E.A., 2009. Mammalian Response to Cenozoic Climatic Change. Annu. Rev. Earth Planet. Sci. 37, 181–208.

Bobe, R., 2006. The evolution of arid ecosystems in eastern Africa. J. Arid Environ. 66, 564–584.

Cerling, T.E., Harris, J.M., Macfadden, B.J., Leakey, M.G., Quade, J., Eisenmann, V., Ehleringer, J.R., 1997. Global vegetation change through the Miocene/Pliocene boundary. Nature 389, 153–158.

Dietl, G.P., Flessa, K.W., 2011. Conservation paleobiology: putting the dead to work. Trends Ecol. Evol. 26, 30–7.

Edwards, E.J., Smith, S.A., 2010. Phylogenetic analyses reveal the shady history of C4 grasses. Proc. Natl. Acad. Sci. U. S. A. 107, 2532–7.

Figueirido, B., Janis, C.M., Perez-Claros, J.A., De Renzi, M., Palmqvist, P., 2012. Cenozoic climate change influences mammalian evolutionary dynamics. Proc. Natl. Acad. Sci. 109, 722–727.

Flower, B.P., Kennett, J.P., 1994. The Middle Miocene climatic transition: East Antarctic ice sheet development, deep ocean circulation and global carbon cycling. Palaeogeogr. Palaeoclimatol. Palaeoecol. 108, 537–555.

Flynn, J.J., Wyss, A.R., Croft, D.A., Charrier, R., 2003. The Tinguiririca Fauna, Chile: biochronology, paleoecology, biogeography, and a new earliest Oligocene South American Land Mammal "Age." Palaeogeogr. Palaeoclimatol. Palaeoecol. 195, 229–259.

Fortelius, M., Eronen, J., Liu, L., Pushkina, D., Tesakov, A., Vislobokova, I., Zhang, Z., 2006. Late Miocene and Pliocene large land mammals and climatic changes in Eurasia. Palaeogeogr. Palaeoclimatol. Palaeoecol. 238, 219–227.

Froyd, C. a., Willis, K.J., 2008. Emerging issues in biodiversity and conservation management: The need for a palaeoecological perspective. Quat. Sci. Rev. 27, 1723–1732.

Gibson, D.J., 2009. Grasses and Grassland Ecology. Oxford University Press, New York.

Henrot, A.-J., Franc, L., Favre, E., Butzin, M., Ouberdous, M., Munhoven, G., 2010. Effects of CO_2 , continental distribution, topography and vegetation changes on the climate at the

Middle Miocene: a model study. Clim. Past 489–535.

Herold, N., Huber, M., Müller, R.D., 2011. Modeling the Miocene Climatic Optimum. Part I: Land and Atmosphere*. J. Clim. 24, 6353–6372.

Hinojosa, L.F., Villagrán, C., 2005. Did South American Mixed Paleofloras evolve under thermal equability or in the absence of an effective Andean barrier during the Cenozoic? Palaeogeogr. Palaeoclimatol. Palaeoecol. 217, 1–23.

Jacobs, B.F., Kingston, J.D., Jacobs, L.L., 1999. The origin of grass-dominated ecosystems. Ann. Missouri Bot. Gard. 86, 590–643.

Janis, C.M., Damuth, J., Theodor, J.M., 2004. The species richness of Miocene browsers, and implications for habitat type and primary productivity in the North American grassland biome. America (NY). 207, 371 – 398.

Kürschner, W.M., Kvacek, Z., Dilcher, D.L., 2008. The impact of Miocene atmospheric carbon dioxide fluctuations on climate and the evolution of terrestrial ecosystems. Proc. Natl. Acad. Sci. U. S. A. 105, 449–53.

Lear, C.H., Mawbey, E.M., Rosenthal, Y., 2010. Cenozoic benthic foraminiferal Mg/Ca and Li/Ca records: Toward unlocking temperatures and saturation states. Paleoceanography 25, 1–11.

MacDonald, G.M., Bennett, K.D., Jackson, S.T., Parducci, L., Smith, F. a., Smol, J.P., Willis, K.J., 2008. Impacts of climate change on species, populations and communities: palaeobiogeographical insights and frontiers. Prog. Phys. Geogr. 32, 139–172.

MacFadden, B.J., 2000. Cenozoic mammalian herbivores from the Americas: reconstructing

ancient diets and terrestrial communities. Annu. Rev. Ecol. Syst. 31, 33–59.

McInerney, F. a., Wing, S.L., 2011. The Paleocene-Eocene Thermal Maximum: A Perturbation

of Carbon Cycle, Climate, and Biosphere with Implications for the Future. Annu. Rev.

Earth Planet. Sci. 39, 489–516.

Mosbrugger, V., Utescher, T., Dilcher, D.L., 2005. Cenozoic continental climatic evolution of

Central Europe. Proc. Natl. Acad. Sci. U. S. A. 102, 14964–14969.

Pascual, R., 2006. Evolution and Geography: The Biogeographic History of South American

Land Mammals. Annu. Missouri Bot. Gard. 93, 209–230.

Quade, J., Cerling, T.E., Bowman, J.R., 1989. Development of Asian monsoon revealed by

marked ecological shift during the latest Miocene in northern Pakistan. Nature 342, 189–92.

Retallack, G.J., 2009. Refining a pedogenic-carbonate CO2 paleobarometer to quantify a middle

Miocene greenhouse spike. Palaeogeogr. Palaeoclimatol. Palaeoecol. 281, 57–65.

Retallack, G.J., 2007. Cenozoic Paleoclimate on Land in North America. J. Geol. 115, 271–294.

Shevenell, A.E., Kennett, J.P., Lea, D.W., 2004. Middle Miocene Southern Ocean cooling and

Antarctic cryosphere expansion. Science 305, 1766–1770.

Strömberg, C. a. E., 2011. Evolution of Grasses and Grassland Ecosystems. Annu. Rev. Earth

Planet. Sci. 39, 517–544.

Strömberg, C.A.E., 2005. Decoupled taxonomic radiation and ecological expansion of open-

habitat grasses in the Cenozoic of North America. Proc. Natl. Acad. Sci. U. S. A. 102,

11980–4.

van Dam, J.A., 2006. Geographic and temporal patterns in the late Neogene (12-3 Ma)

aridification of Europe: The use of small mammals as paleoprecipitation proxies. Palaeogeogr. Palaeoclimatol. Palaeoecol. 238, 190–218.

Wolfe, J., 1994. Tertiary climatic changes at middle latitudes of western North America. Palaeogeogr. Palaeoclimatol. Palaeoecol. 108, 195–205.

Woodburne, M.O., Gunnell, G.F., Stucky, R.K., 2009. Climate directly influences Eocene mammal faunal dynamics in North America. Proc. Natl. Acad. Sci. 106, 13399–13403.

You, Y., Huber, M., Müller, R.D., Poulsen, C.J., Ribbe, J., 2009. Simulation of the Middle Miocene Climate Optimum. Geophys. Res. Lett. 36.

Zachos, J., Pagani, M., Sloan, L., Thomas, E., Billups, K., 2001. Trends, rhythms, and aberrations in global climate 65 Ma to present. Science 292, 686–93.

Zachos, J.C., Dickens, G.R., Zeebe, R.E., 2008. An early Cenozoic perspective on greenhouse warming and carbon-cycle dynamics. Nature 451, 279–83.

Zheng, J., 1996. Magnetostratigraphy of a Miocene sedimentary sequencen Railroad Canyon, Idaho. University of Pittsburgh.

CHAPTER 2. Vegetation response during the lead-up to the middle Miocene warming event in the Northern Rocky Mountains, USA

Elisha B. Harris, Caroline A.E. Strömberg, Nathan D. Sheldon, Selena Y. Smith, Mauricio Ibañez-Mejia, and Daril A. Vilhena

ABSTRACT

The mid-Miocene climatic optimum (MMCO; initial warming beginning ca. 18 Ma and with peak warming ca. 17–14.75 Ma) constitutes the Earth's most recent greenhouse episode, characterized by a transient shift to higher global atmospheric CO_2 levels and warmer, possibly wetter, climatic conditions. Biotic responses to these changes are thought to be significant turnover and modernization of fauna and flora as grass-dominated habitats continued to spread. However, records documenting local vegetation change during the MMCO are rare, hence this hypothesis remains largely untested. Herein, we combine phytolith assemblages and $\delta^{13}C$ records from paleosol organic matter from the Railroad Canyon section (RCS), eastern Idaho, to provide the first direct, detailed, and continuous, long-term record of vegetation composition and structure in a single basin during the lead-up to the MMCO. New U-Pb dated ashes suggest that the RCS deposits formed ca. 22.9–15.2 Ma (late Arikareean–early Barstovian), ca. 5 million years older than previously suggested. Phytolith assemblage analysis indicates that grasses, primarily C_3 pooids, dominated early–middle Miocene vegetation. Potential C_4 PACMAD grasses were present by ca. 21.6–20.7 Ma (late Arikareean) and vary (0.4–17.2% of diagnostic

phytoliths) through the section. Although overall relatively rare, PACMAD grasses decrease

significantly through time, in parallel with declining diatom abundances and an increase in pooid

grasses. In contrast, paleosol $\delta^{13}C_{org}$ indicates 0–49.3% C_4 vegetation but no consistent temporal

change. However, where both phytolith- and isotope-based estimates are made from the same

paleosol, they are within error 82% of the time. Thus, the apparent discrepancy in temporal

trends could either be due to differences in the resolution of the two records, or could be

explained if many PACMADs were actually water-loving C_3 species. Overall, these data suggest

that open-habitat mosaic vegetation with grass-dominated grasslands and open woodlands

occurred in the North Rocky Mountains, USA, by at least the early Miocene, more comparable to

the timing for the spread of grass-dominated habitats in the Great Plains than previously thought.

Additionally, phytolith data suggest that overall vegetation structure remained relatively stable

throughout the RCS, inconsistent with published paleosol morphology data. This points to

regionally unique floral patterns decoupled from global climate change leading into the MMCO.

1. INTRODUCTION

Ecological research has shown that climatic warming can drastically restructure terrestrial

communities (e.g., Parmesan, 2006; Root et al., 2003; Walther et al., 2002). Data from the fossil

record support this idea, with many severe climatic events in Earth's history linked to substantial

alterations of paleocommunities (e.g., Jaramillo et al., 2010; Retallack et al., 2004; Wing et al.,

2005). The mid-Miocene climatic optimum (MMCO, 17–15 Ma) is Earth's most recent,

prolonged global warming event since the early Eocene climatic optimum (ca. 52–50 Ma).

During the MMCO, a gradual temperature increase of 2°C per million years has been estimated

(Barnosky et al., 2003) and a potential transient shift to higher atmospheric CO_2 levels coincided with massive reorganization and modernization of floras and faunas world-wide (e.g., Beerling and Royer, 2011; Kürschner et al., 2008; Leopold and Denton, 1987; Tedford et al., 2004). Many floras from around the world suggest that during the MMCO, many mid- to high-latitude sites were characterized by lush, forest vegetation containing an abundance of broadleaved plants (e.g., Hinojosa and Villagrán, 2005; Ivanov et al., 2011; Mosbrugger et al., 2005). However, in North America, pollen, phytolith, and paleosol data from the Central Great Plains and western North America suggest that the structure and composition of vegetation changed during this period as more open vegetation (C_3 grasslands and woodlands) spread and replaced forest habitats (Leopold and Denton, 1987; Retallack, 2007; Strömberg, 2005). Although these vegetation changes have often been linked to climate change (Strömberg, 2005; Webb and Opdyke, 1995; Wing, 1998), there have been no explicit tests for a correlation between mid-Miocene climatic warming and regional- to local-scale vegetation response. In large part, this is because the detailed, local paleobotanical records through the MMCO necessary for testing such hypotheses have been lacking.

Here we use phytoliths as well as organic matter preserved in paleosols to reconstruct a temporally high-resolution vegetation record within a single depositional basin, with the aim of understanding how long-term climate change leading up to the peak MMCO warming impacted floral communities in eastern Idaho, USA. We focus on a series of early–middle Miocene-aged outcrops in the Railroad Canyon section (RCS) of Idaho that preserve a wealth of plant silica remains (Strömberg, 2005), paleosols (Retallack, 2007, 2009) and animal fossils (Barnosky et al., 2007), making it an ideal place to study the biotic effects of the MMCO at the ecosystem level in North America. Ultimately we provide one of the best-dated, high-resolution and long-

term Cenozoic vegetation records in the continental interior of the Unites States, allowing us to evaluate local floral responses to global climatic warming. Specifically, we aim to address the following questions: (1) what was the timing of the spread of open-habitat grasslands in the Northern Rocky Mountains, USA?; (2) Did higher global temperatures during the MMCO lead to an increase in biomass of warm-adapted, C_4 grasses? (3) Was the local flora and habitat structure of vegetation in the RCS impacted by climate change associated with the global MMCO?

2. GEOLOGIC SETTING

The Cenozoic was a tectonically active time in the history of western North America. Structural analysis of faults and associated magmatism indicate that early extension in the North American Cordilleran persisted since the abrupt cessation of the Laramide orogeny during the middle Eocene (Zoback et al., 1981; Fields et al., 1985; Rasmussen, 2003; Parsons, 2006). In southern Montana $\delta^{18}O_{carbonate}$ data suggest the creation of a broad regional plateau during the late Eocene–early Oligocene, the formation of which was temporally variable across Montana, Idaho, and Nevada (Chamberlain et al., 2012). By the middle Miocene (ca. 17.5 Ma) $\delta^{18}O$ and leaf physiognomic data suggest the onset of diachronous collapse of this broad plateau with the initiation of Basin and Range extension, which continued to alter the landscape in the US Northern Rocky Mountains (NRM) through the late Miocene (Atwater and Stock, 1998; Chamberlain et al., 2012). During the middle–late Hemingfordian (see North American land mammal ages in Fig. 2.4) the Yellowstone Hotspot resumed intense volcanic activity in the Snake River Plain and continued to track northward into northwestern Wyoming (Rasmussen, 2003; Parsons, 2006). To the northwest, deposits from the Columbia River Basalt flows indicate

volcanism in this region from 17.5 to 6 Ma in eastern Washington, northeastern Oregon, and western Idaho (Swanson et al., 1979). It was during this period of continued crustal extension and volcanism that the early–middle Miocene sediments within the Railroad Canyon were deposited.

The Railroad Canyon section (RCS) is located in Bannock Pass approximately 12 miles northeast of Leadore, Idaho and exposes nearly 360 m of sedimentary rock deposited during the early–middle Miocene (22.9–15.2 Ma; Fig. 2.1). The RCS contains rocks from the upper Renova Formation and lower Sixmile Creek Formation, which are thought to be separated by a regional unconformity (Barnosky et al., 2007). The Renova Formation locally consists of grey to white mudstone and siltstone deposits with occasional gypsum and halite deposits potentially indicative of an arid, closed basin with intermittent saline lakes (Fields et al., 1985; Barnosky et al., 2007). The Sixmile Creek Formation is locally distinguished by pinkish to tan siltstone and sandstone beds with occasional conglomeratic lenses indicative of a sediment-choked fluvial system (Fields et al., 1985; Barnosky et al., 2007). Overall, both units are interpreted as dominantly composed of fluvial deposits, reflecting sediment deposition in an increasingly arid floodplain environment.

3. PALEOVEGETATION RECONSTRUCTION

Phytoliths are microscopic silica bodies formed in the tissues of many vascular plants (e.g., Hodson et al., 2005; Piperno, 2006). Phytoliths have been useful for inferring local vegetation structure (i.e., closed vs. open habitats) and spatial heterogeneity of vegetation across a landscape both in modern and ancient sediments (e.g., Bremond et al., 2005; Chen et al., 2015; Fredlund and Tieszen, 1994; Piperno and Becker, 1996; Strömberg et al., 2013; WoldeGabriel et

al., 2009), although of course they do vary in their taxonomic sensitivity. Phytoliths also provide information about the relative abundances of climatically sensitive taxa, such as moisture- and temperature-limited plants (e.g., palms, spiral gingers and relatives; Chen and Smith, 2013; Miller et al., 2012), and C_4 lineages adapted to hot and/or dry climates (e.g., Chloridoideae; Piperno and Pearsall, 1998; Strömberg, 2004). Additionally, unlike pollen and most macrofossils, phytoliths can be taxonomically distinct within grasses and so can provide approximate constraints for the relative abundances of different types of closed- and open-habitat grasses (e.g., C_3 bamboos and pooids, and C_4 chloridoids and panicoids), making them particularly useful for studying the Cenozoic evolution of grasslands (e.g., Strömberg, 2005, 2011; Strömberg and McInerney, 2011; Cotton et al., 2012).

Stable isotope compositions ($\delta^{13}C$) of kerogenized rootlets from middle Miocene paleosols are used here to reconstruct local vegetation. Assuming diagenetic temperatures below 150°C, the composition of bulk soil organic material (SOM) should reflect the original carbon signature of the plants that inhabited an ancient soil, and as a result, soil organic carbon isotopes have been used regularly to reconstruct the abundance of C_3/C_4 vegetation (e.g., Quade and Cerling, 1995; Fox and Koch, 2003, 2004; Cotton et al., 2012).

By combining these different lines of evidence for plant community composition, a more detailed view of vegetation change can be attained: stable carbon isotopes and phytoliths both record the relative abundance of potential C_4 plants, and phytoliths provide information about the composition of the C_3 vegetation component (e.g., C_3 grasses, C_3 shrubs/trees, or both). The comparison also allows us to evaluate the differences between C_4 vegetation proxies, which improves our ability to reconstruct the composition of C_4 grass communities (see Materials and

Methods), and adds to recent efforts to better understand potential biases in paleo-vegetation reconstruction methods (e.g., McInerney et al., 2011; Cotton et al., 2012; Hyland et al., 2013).

4. MATERIALS AND METHODS

4.1 Sites and samples

Paleosols were sampled approximately every meter throughout the entire composite RCS (which spans 22.9–15.2 Ma) resulting in 250 total paleosol samples collected approximately every meter. Sites within the RCS originally studied by A.D. Barnosky and G.J. Retallack were re-located using photographs, topographic maps, GPS points, and field notes archived at the University of California Museum of Paleontology (Table 2.1; Barnosky et al., 2007; personal communication with A.D. Barnosky and G.J. Retallack). Site and section names follow their terminology. New stratigraphic sections were logged at eleven field sites and lithologic descriptions were taken at ~1-m intervals through the entire composite section. Correlations between exposures were based on the detailed stratigraphy published in Barnosky et al. (2007). Where possible, paleosol A-horizons were sampled. A-horizons were identified based on changes in grain size, overall color, sedimentary structures, and fossils (e.g., kerogenized rootlets, rhizoliths; Soil Survey Staff, 2014); however, identification of individual soil horizons was not always possible at all levels and, therefore, some intervals are characterized by composite or cumulative paleosols. Of the 250 rock samples taken, 25 were quantitatively analyzed for phytoliths and 40 for $\delta^{13}C_{org}$. Twelve samples were analyzed for both phytoliths and $\delta^{13}C_{org}$ allowing for a direct comparison of both proxies. In addition to the new phytolith data reported here (counts by EBH), one sample reported by Strömberg (2005; ADB89-94) was reprocessed and counted by EBH to maximize the within-study consistency of rock subsampling (linked to time-averaging, see *Discussion*).

4.2 Phytolith extraction and microscopy

An even distribution of samples (n > 100) were chosen from throughout the composite RCS and processed for phytoliths. The samples that yielded abundant phytoliths and appeared well preserved (Table A1.1) were quantitatively analyzed for their phytolith assemblage compositions. Phytoliths were extracted from paleosol samples using established procedures (Strömberg, 2005; see Appendix A1.3.1 for discussion of processing procedure).

Phytoliths were counted under an optical light microscope (Nikon i80) at 1000× magnification. Grass silica short cells (GSSC) were described and counted in oil immersion slides to allow for rotation of individual phytolith grains, which significantly aids morphotype identification (Piperno and Pearsall, 1998). On fixed slides all phytolith morphotypes were counted, which allowed for a comparison of the relative abundance of GSSC to non-GSSC morphotypes. Detailed counts from the oil immersion slides were then scaled and made comparable to those from the fixed slide (for details see Strömberg, 2005; Strömberg and McInerney, 2011). Diatoms, which can be useful as environmental indicators of local water reservoirs (Clarke, 2003), were counted in each sample to estimate their abundance relative to the abundance of phytoliths (Table A1.1). All samples and prepared slides are housed at the Burke Museum of Natural History and Culture (UWBM).

4.3 Phytolith classification and assemblage analysis

Phytoliths were classified according to the classification scheme outlined by Strömberg (2004, 2005) and Strömberg et al. (2007), and based on a modern reference collection housed at the UWBM (Strömberg, 2003, Harris and Strömberg, unpublished data). The following main categories were used for vegetation inference: (1) forest indicator (FI) forms found in palms,

woody or herbaceous dicotyledons, conifers, ferns, and gingers and relatives in the Zingiberales

(ZINGI), the sum of which is FI TOT; (2) grass silica short cells (GSSC), found exclusively in

grasses including forms typical of closed habitat grasses (e.g., bambusoid and early-diverging

grasses) and open habitat grasses, that is, grasses in the Pooideae and PACMAD clades (C_3 and

C_4 grasses in the subfamilies Panicoideae, Aristidoideae, Chloridoideae, Micrairioideae,

Arundinoideae, and Danthonioideae; Alisconi et al. 2012); (3) phytoliths from wetland plants

(AQ), including *Equisetum* and sedges; and (4) non-diagnostic and unclassified forms (OTH).

Other aquatic indicators such as chrysophyte cysts and sponge spicules were very rare in RCS

samples and were therefore not counted; however, semi-quantitative estimates are included in

Table A1.1.

Vegetation reconstructions were based on relative abundances of diagnostic

morphotypes, namely FI forms and GSSCs (Figs. 2 and 3; see Appendix A1.3.2. for additional

details about phytolith assemblage analysis), which provides information about habitat structure

and openness. In addition to tracking changes in vegetation structure, changes in grass

community composition were analyzed by tracking changes in the relative abundances of GSSC

forms produced by different grass lineages (see Appendix A1.3.2). Ninety-five percent

confidence intervals were calculated for the FI-t ratio (unconditional case, using the total

diagnostic count as the sample size) as well as other vegetation types (e.g., palms, gingers,

pooids) using a bootstrap routine (available upon request from the authors) in the statistical

software R (R core Team, 2015). Ninety-five percent confidence intervals were also calculated

for the abundance of C_3 and C_4 grasses within the GSSC portion of phytolith assemblages

(conditional case, using only the diagnostic GSSC, that is, excluding non-diagnostic or

unidentified GSSCs) using the same bootstrap routine in R (R core Team, 2015). Because it is

difficult to translate relative abundances of phytoliths in assemblages to exact abundances of plants on a landscape, mainly due to redundancy, multiplicity, and variation in phytolith production among plants (Strömberg, 2004), discussion here is focused on relative, rather than absolute, changes in vegetation structure and climatically linked morphotypes through time. However, comparison to older and younger vegetation records from southwestern Montana (e.g., Strömberg, 2005; Cotton et al., 2012; Miller et al., 2012; Chen et al., 2015) allowed us to make general inferences about vegetation type and regional change in vegetation structure through time.

4.4 Carbon isotope analysis

Where possible, organic root traces extracted from paleosols were analyzed for their carbon isotopic composition, which provides information about the photosynthetic pathways used by plants that grew in a particular paleosol. Forty samples were prepared for bulk $\delta^{13}C_{org}$ analysis by first ultrasonicating them in methanol to remove modern organic material. Samples were then treated with a 7% HCl solution at 40°C to remove carbonates. Finally, the samples were dried, loaded into tin capsules, and analyzed using a Costech ECS4010 elemental analyzer attached to a Thermo Delta V+ isotope ratio mass spectrometer at the University of Michigan. Results were normalized to the VPD scale using IAEA sucrose and caffeine standards. The analytical uncertainty determined from the standards is 0.15‰. Of the 40 samples, 17 were analyzed either in duplicate or triplicate and 95% confidence intervals were calculated for each sample from the standard deviation of the replicates. The remaining samples were analyzed singly and were assigned a conservative error estimate of ±0.3‰, which is the uncertainty typically observed for triplicate analysis (see Table A1.3).

Paleosols were identified as potentially containing C_4 biomass if their isotopic composition was, on average, greater than ~ -25‰. Isotope end members are based on the average isotopic composition of pure C_3/C_4 ecosystems in a precipitation regime of 350–800 mm yr^{-1} (Diefendorf et al., 2010; Kohn, 2010; Retallack, 2007), adjusted for changes in the $\delta^{13}C$ of atmospheric CO_2 during the early–middle Miocene using a polynomial fit to the reconstruction of Tipple et al. (2010; details in Appendix A1.2). Estimates for percent C_4 biomass within paleosol samples were determined using an average pure C_3 end member of ~ -25‰ and an average pure C_4 end member of ~ -11.1‰ (see Appendix A1.4 for discussion).

4.5 Statistical analyses

Principal component analysis (PCA) was used to visualize inter-sample, phytolith assemblage variability and to see if particular compound variables (i.e., plant functional types) clustered according to age. PCA was conducted on covariance matrices using the function 'princomp' in R (R core Team, 2015). In total, we ran three PCAs using the following phytolith relative abundance variables: Run 1) forest indicators (excluding palms and Zingiberales), pooid grasses (within entire assemblage), minimum potential C_4 grasses (within entire assemblage), aquatics, palms, Zingiberales, and diatoms; Run 2) forest indicators (excluding palms and Zingiberales), pooid grasses (within entire assemblage), maximum potential C_4 grasses (within entire assemblage), aquatics, palms, Zingiberales, and diatoms; Run 3) like Run 2 but excluding diatoms. The resulting scores on PC1 and PC2 for each run were then regressed against sample age to determine if particular plant classes changed significantly over time.

To determine if there were any changes over time in the relative abundances of individual phytolith classes and diatoms, we use a generalized linear model with a logit link function

(hereafter referred to as 'regression analysis'). The logit link function converts a morphotype proportion Y to a logarithm of the ratio $Y/(1-Y)$, which renders the data suitable to regression (see Supporting Information). The R function glm was used to run the analysis (R core Team, 2015). A Welch two sample t-test was used to determine if there was a significant difference in mean diatom relative abundances (an indicator of landscape-scale water availability) between the two most abundantly sampled grain size categories, siltstones and sandy siltstones (R core Team, 2015). Linear regression was used to determine if diatoms (an indicator of soil moisture) were correlated with particular environmentally sensitive vegetation classes (gingers, palms, chloridoids, aquatics, pooids, potential C_4 grasses, and FI) and to test for changes over time in $\delta^{13}C$ values and isotope estimates of percent C_4 vegetation (R core Team, 2015).

5. RESULTS

5.1 Geology

The majority of paleosols preserved in the RCS were identified as Entisols and Inceptisols (Soil Survey Staff, 2014). Within the Renova Formation, paleosols are predominantly developed on siltstones, whereas paleosols within the Six Mile Creek Formation can have coarser parent material consisting of sandy siltstones with occasional sandstones and conglomerate beds. The most common pedogenic features observed were root traces, burrow trace fossils, and occasional rhizoliths. In contrast to Retallack (2007), pedogenic carbonate nodules were found only at WH4 between 63–76 m above the base of the composite section. Other surficial carbonate (i.e., non-nodular and powdered) represents modern evaporative conditions.

5.2 Phytolith analysis

The preservation quality of phytolith samples was determined using criteria outlined in (Strömberg et al., 2007a; Table A1.1). In total, 25 samples were preserved well enough to warrant quantitative phytolith analysis. These new samples, along with a recount of one sample published in Strömberg (2005) resulted in a total dataset of 26 phytolith samples.

*5.2.1 Phytolith assemblage composition: FI vs. GSSC.—*Relative abundances of non-grass plants within diagnostic phytolith assemblages as an estimate of tree cover (FI-t) ranged from 1.3% (95% CI = 0.3–2.7%) to 43.2% (95% CI = 35.3–51.1%) with all but three samples having relative abundances <25% (Table A1.1). Palm-diagnostic phytoliths were occasionally observed but never constituted more than 1.4% (95% CI = 0–3.4%) of analyzed assemblages. Open-habitat GSSCs dominate all phytolith assemblages throughout the RCS (Fig. 2.4). Phytoliths from C_3 grasses (mainly Pooidae, but also closed-habitat grasses) as a proportion of the entire diagnostic count range in relative abundance from 54.6% (95% CI = 45.6–62.3%) to 98.7% (95% CI = 97.2–99.7%). Abundance of pooid GSSCs in entire phytolith assemblages ranged from 39.3% (95% CI = 31.9–45.9%) to 85.8% (95% CI = 82–89.8%; Table 2.2). Minimum estimates for the abundance of potential C_4 grasses within entire assemblages ranged from 0.4% (95% CI = 0–0.8%) to 17.2% (95% CI = 12.1–22.7%), with all but five samples having relative abundances <5%; maximum potential C_4 grass estimates within entire assemblages ranged from 2.8% (95% CI = 0.5–5.1%) to 36.2% (95% CI = 29–42.8%), respectively.

Phytoliths indicative of wetland (e.g., sedges) and moisture-limited plants (e.g., palms and spiral gingers) were relatively uncommon in the majority of samples analyzed for phytoliths.

23

Aquatic plants never constituted more than 7.7% (95% CI = 4.4–11.4%; calculated as percent of

FI + GSSC) with all but three samples having relative abundances <5%. Spiral gingers (ZINGI)

are rare in all RCS samples with all but one sample containing <0.5%.

Although there is variation in the overall composition of phytolith assemblages through

the section, regression analysis of plant functional types within entire diagnostic phytolith

assemblages reveals no statistically significant change over time in the relative abundances of

forest indicators (p = 0.97; Fig. 2.5A), C_3 grasses (including bamboo; p = 0.9; Fig. 2.5B), pooid

grasses (p = 0.1; Fig. 2.5C), potential C_4 grasses (min C_4: p = 0.07; max C_4: p = 0.054; Figs.

2.5D–5E), palms (p = 0.53; Fig. A1.4.A), aquatics (p = 0.57; Fig. A1.4.B), and spiral gingers (p

= 0.74; Fig. A1.4.C).

5.2.2 Phytolith assemblage composition: GSSC assemblages.—Morphotypes typical of

C_3 pooid grasses dominate all GSSC assemblages (Fig. A1.4.E–F) ranging in abundance from

51.2% (95% CI = 42.9–59.2%) to 96.8% (95% CI = 94.1–99.4%; Table A1.2). Minimum

estimates for percent potential C_4 forms within GSSC assemblages ranged from 0.4% (95% CI =

0–0.8%) to 22.4% (95% CI = 15.7–29.3%; Table 2.2) with all but one sample having a minimum

potential C_4 relative abundance <13%. Maximum estimates for percent potential C_4 forms within

GSSC assemblages ranged from 3.2% (95% CI = 0.6–5.9%) to 47.2% (95% CI = 38.8–55.1%;

Table 2.2) with all but six samples having a maximum potential C_4 relative abundance <25%.

Phytoliths indicative of dry-adapted chloridoid grasses are rare and never constitute more than

2.8% (95% CI = 0.6–5.1%; Table 2.2) of GSSC assemblages.

Regression analysis of vegetation types within GSSC assemblages reveals a statistically

significant change over time in the relative abundances of pooid forms (increase; p = 0.02; Fig.

2.5F) and potential C_4 grasses (decrease; min C_4: $p = 0.04$; max C_4: $p = 0.03$; Figs. 5G–H). However, there was no significant change over time in the relative abundance of chloridoid grasses ($p = 0.97$; Fig. A1.4.D) within GSSC assemblages.

5.2.3 Co-occurrence of diatoms and phytoliths.—Crysophyte cysts and sponge spicules were in very low abundance in all samples. However, diatoms appear to be very abundant (between 31%–85.1% relative to the total number of phytoliths counted) in the lower 95 m of the composite section and vary in abundance between 145–172 m (Table A1.1). From 172–352 m diatoms range in relative abundance from 0–11.4%. Regression analysis revealed a statistically significant decrease in the relative abundance of diatoms through time ($p \ll 0.05$; Fig. A1.5.A). Linear regression revealed significant positive correlations between diatoms and palms ($R^2 = 0.03$, $p \ll 0.05$; Fig. A1.5.C), spiral gingers ($R^2 = 0.15$, $p \ll 0.05$; Fig. A1.5.I), maximum percent potential C_4 estimates (within entire phytolith assemblages; $R^2 = 0.62$, $p \ll 0.05$; Fig. A1.5.D) and minimum percent potential C_4 estimates (within entire phytolith assemblages; $R^2 = 0.45$, $p \ll 0.05$; Fig. A1.5.E). Linear regression also revealed a significant negative correlation between diatoms and pooids ($R^2 = 0.33$, $p \ll 0.05$; Fig. A1.5.F). No significant correlation was found between diatoms and aquatics ($p = 0.51$; Fig. A1.5.H), chloridoids ($p = 0.43$; Fig. A1.5.G), or forest indicators ($p = 0.51$; Fig. A1.5.B). Additionally, a Welch two sample t-test showed that there is no statistically significant difference in the mean relative abundance of diatoms in siltstones and sandy siltstones ($p = 0.96$), which are the dominant grain size categories of the paleosols sampled.

5.2.4 Principal component analysis.—Principal components are interpreted based on the phytolith compound variable loadings. We chose to interpret the first two PCA axes for each run because they account for the majority of the variability in our data (>90%, see Table A1.4). Run 1) PCA axis 1 (PC1) accounts for 80.4% of the variability, with pooids loading positively and diatoms (and to a much lesser degree minimum potential C_4 grasses) loading negatively along this axis (Fig. 2.6A). PC2 accounts for 16.1% of the variability, with forest indicators loading positively and pooids (and to a lesser extent diatoms) loading negatively along this axis. Run 2) PC1 accounts for 78.1% of the variability, with pooids loading positively and diatoms (and to a lesser degree maximum potential C_4 grasses) loading negatively on this axis (Fig. 2.6B). PC2 accounts for 15% of the variability, with forest indicators loading positively and pooids (and to a lesser extent diatoms) loading negatively on this axis. Run 3) PC1 accounts for 68.8% of the variability, with forest indicators and maximum potential C_4 grasses loading positively and pooids loading negatively along this axis (Fig. 2.6C). PC2 accounts for 29.8% of the variability, with forest indicators loading positively and maximum potential C_4 grasses loading negatively along this axis. Additionally, for Runs 1 and 2, PC1 negatively correlates with time (Run 1: $p < 0.05$, $R^2 = 0.55$; Run 2: $p < 0.05$, $R^2 = 0.55$; Figs. A1.6.A, A1.6.B), and for Run 3 PC1 positively correlates with time ($p < 0.05$, $R^2 = 0.18$; Fig. A1.6.C). In contrast, there is no significant correlation between PC2 and time in any of the runs (Run 1: $p = 0.52$, $R^2 = 0.02$; Run 2: $p = 0.52$, $R^2 = 0.02$; Run 3: $p = 0.08$, $R^2 = 0.12$).

5.3 $\delta^{13}C$ analysis of paleosol organic matter

The mean $\delta^{13}C_{org}$ of kerogenized rootlets for all RCS samples was -24.37‰ (95% CI = -27.91‰ – -20.83‰) with a range of $\delta^{13}C_{org}$ values from -27.87‰ to -18.49‰ (Table A1.3). Using end-member mixing models (described in Methods), percent C_4 vegetation was calculated as ranging from 0% to 49.3%, with a mean of 7.2%. Linear regression indicates no statistically significant change through time in $\delta^{13}C_{org}$ values ($R^2 = 0.02$; $p = 0.21$; Fig. 2.7). Additionally, there is no significant correlation between percent carbon and $\delta^{13}C_{org}$ values (Fig. A1.7).

5.4 Comparison of C_4 estimates from phytolith assemblage analysis and isotope data

Phytolith and stable carbon isotope values could be directly compared for 12 paleosol samples (Fig. 2.8). For these samples, minimum estimates for percent potential C_4 forms within entire phytolith assemblages ranged from 0.97% (95% CI = 0–1.6%) to 11.9% (95% CI = 7.8–15.9%); corresponding maximum potential C_4 estimates ranged from 5.1% (95% CI = 2–7.8%) to 34.4% (95% CI = 28.6–40.7%). Estimates for percent C_4 vegetation based on isotope data indicate variable amounts of C_4 vegetation through time (Fig. 2.7), ranging in relative abundance from 0% to 49.3% (95% CI = 44.9% – 53.6%). Regression analysis indicates a statistically significant decrease over time in percent potential C_4 vegetation based on phytoliths within grass assemblages (min potential C_4 $p < 0.05$; max potential C_4 $p < 0.05$) and isotopes ($R^2 = 0.17$; $p <<$ 0.05). Of the 12 samples analyzed using both methods, nine have percent C_4 biomass estimates from carbon isotopes that fall within the range of error estimated by phytolith assemblages. Three samples have percent C_4 biomass estimates from isotopes that fall above the range of error observed for phytoliths.

6. DISCUSSION

6.1 RCS paleosols and interpretation of $\delta^{13}C_{org}$ values

Previous work by Retallack (2009) suggested that most RCS paleosols are Aridisols preserving carbonate nodules throughout. However, our survey of paleosols during the summers of 2011–2014 revealed pedogenic carbonate nodules only in a very localized part of the RCS, between 63–76 m (corresponding to ca. 21.7–21.3 Ma). This stratigraphically and temporally local distribution of carbonate nodules does not appear to coincide with phytolith assemblage compositions that are markedly different from the remainder of phytolith assemblages throughout the section (Figs. 4 & 5). One possible interpretation for the presence of pedogenic carbonate would be that it represents a brief aridification event given that in modern soils, pedogenic carbonate is generally absent when precipitation exceeds 750 mm yr^{-1} and often present under drier conditions (reviewed in Sheldon and Tabor, 2009). However, there are no other sedimentological indications of aridity within that stratigraphic interval, whereas aridity indicators such as localized evaporite deposits are found elsewhere within the RCS without any pedogenic carbonate present.

The majority of paleosols examined within the Railroad Canyon are weakly developed Entisols or Inceptisols, both of which are associated with short formation times (Sheldon and Tabor, 2009). Additionally, there is no evidence of gleying or of drab-haloed root traces in any of the paleosols, which indicates that they were well-drained during formation (e.g., Kraus, 1999). This is consistent with the relatively coarse grain size of paleosols particularly in the upper three-quarters of the composite section. The climate therefore may have been seasonal enough that the floodplain was never permanently inundated.

Where possible, paleosol A-horizons were sampled for analysis; however, because RCS paleosols are underdeveloped (i.e., lack structural features common in more developed soil profiles, such as distinct A and Bk horizons in Aridisols; Soil Survey Staff, 2014) this was not always possible. This could be a potential source of error in our C_4 estimates because we do not have the necessary data to discern if there was significant enrichment in ^{13}C as a byproduct of soil depth (Wynn, 2007; Wynn and Bird, 2007). However, ^{13}C enrichment due to microbial decomposition was tested for and showed no linear relationship between $\delta^{13}C_{org}$ values and percent carbon for all samples (Fig. A1.7). This is particularly important to test for because samples with low percent carbon are more susceptible to alteration and bias (Wynn, 2007). These results suggest that microbial decomposition did not likely result in ^{13}C enrichment of residual carbon in these samples; therefore, no additional isotope corrections were applied.

6.2 Vegetation reconstruction in the RCS: phytolith assemblages vs. carbon isotopes

Phytolith-based estimation of vegetation structure suggests that RCS habitats were relatively open and grass-dominated, with variation in the FI-t ratio suggesting patches of trees on the landscape. Grass communities appear to have been dominated by C_3 pooid, open-habitat grasses. Isotopic data largely support this reconstruction, with many of the measured paleosols (~38%) falling entirely within the range expected for C_3 plants.

Phytolith assemblages and carbon isotope estimates both suggest low to moderate relative abundances of C_4 vegetation through the RCS. For nine of the 12 samples (75%) analyzed using both methods, C_4 isotope estimates fall within the 95% CI estimated from phytoliths. In these cases, both methods agree and are giving similar estimates of percent C_4 biomass (Fig. 2.8). However, for three samples (PB30649, PB30683, PB30688) isotope C_4 estimates lie above the

29

95% CI produced by phytolith maximum C_4 estimates. The isotope estimates for these samples could be biased if these points in time represent intervals of more extreme aridity. Precipitation reconstruction from CIA-K indices of Bt horizons in six paleosols suggests that these three samples were deposited during a period (18.5–19.4 Ma) that received ~701 mm of precipitation (Retallack 2009; Fig. 2.9D). Although the data do not suggest a dramatic decrease in MAP leading into 18.5–19.4 Ma, it is still possible that the C_3 isotope end member used to establish percent C_4 relative abundance may be affected, resulting in overestimation of the relative abundance of C_4 plants. However, additional MAP estimates are necessary to test this hypothesis (note that precipitation measurements based on depth to Bk horizon from Retallack, 2009 cannot be used for most of the RCS because, as discussed above, the carbonate is not pedogenic).

Estimates of C_4 vegetation could also vary due to differences in spatial averaging between methods. Soil phytoliths often derive from *in situ* plant decay or can be transported into an area by wind or fluvial transport; eolian transport is especially important in open habitats and leads to regional mixing of phytolith assemblages (Alexandre et al., 1997; Fredlund and Tieszen, 1994; Osterrieth et al., 2009). In contrast, each isotopic measurement of SOM measures the δ^{13}C of plants that lived in the close vicinity of the sampled soil horizon before it was buried by the next paleosol or floodplain deposit (e.g., Cerling, 1984; Sheldon and Tabor, 2009). Thus, vegetation reconstructions based on isotopes might reflect a very local vegetation signal whereas phytolith assemblages, especially in open habitats—such as those reconstructed for the RCS— might preserve a more regional vegetation signal. However, the phytoliths are well preserved (i.e., not weathered as would be expected in long-distance transport; see Table A1.1. for preservation info) and contain phytoliths of a wide range of size classes (i.e., not grain size

sorted), suggesting these assemblages are not predominantly transported (Osterrieth et al., 2009; Selkin et al., 2015).

Similarly, differential temporal averaging between methods could be biasing individual reconstructions. Phytoliths typically accumulate in soil A horizons over the course of soil development on the order of hundreds to thousands of years (Fredlund and Tieszen, 1994). However, the isotopic composition of original organic carbon in a soil is preserved at each level as the soil profile builds. Thus, phytolith assemblages in a soil horizon represent an accumulation of silica over the course of generations of plant succession and thus are time averaged, whereas $\delta^{13}C_{org}$ values represent a more instantaneous snapshot of the isotopic composition of plant material (e.g., rootlets) buried at a specific period in time.

Representational bias by paleosol order should also be considered when using phytoliths for vegetation reconstructions. Hyland et al. (2013) and demonstrated that modern U.S. Mollisols and Alfisols can have a significant overrepresentation of grass phytoliths in phytolith assemblages while Entisols and Inceptisols do not. Because all of the paleosols in the RCS are either Entisols or Inceptisols we propose that the dominance of GSSCs in assemblages throughout the section is not driven by soil order taphonomic biases, but instead accurately reflect the relative abundances of grasses on the Miocene landscape.

Because of these taphonomic or methodological biases, phytoliths and isotopes must be considered complementary rather than redundant methods. Nevertheless, there is still overall agreement (82% of samples with both types of data) between the phytolith and $\delta^{13}C_{SOM}$ isotope records in the RCS, suggesting that the observed pattern is robust.

6.3 Vegetation reconstruction in the RCS: implications for the spread of grasslands in North
America

Our vegetation reconstruction for the RCS generally agree with previous phytolith work

from the Railroad Canyon (Strömberg, 2005) and phytolith and isotopic work in southwestern

Montana (Fig. 2.1; Cotton et al., 2012; Chen et al., 2015; Hyland et al., in review), all pointing to

spatially heterogeneous open, C_3 grass-dominated habitats with minor C_4 elements and some

more wooded patches during the middle Miocene. Such spatial variability in vegetation may

relate to differences in micro-climates, topography, edaphic factors, or disturbance (e.g., White,

1979; Williams et al., 1996; Hirota et al., 2011; Staver et al., 2011). However, our age revision

for RCS and the addition of more data from the base of the section leads to a much earlier

inferred timing for the spread of open, grass-dominated vegetation compared to previous work

(Strömberg, 2005). These new results have potentially major implications for how we understand

grassland evolution in North America, because it suggests that modern open-habitat grasses

expanded during a similar time-frame, by at least the early Miocene, in both the NRM (this

study) and the Great Plains (Strömberg, 2004, 2005). This pattern opens up the possibility that

driving factor, or more likely combination of factors (e.g., changes in CO_2, precipitation,

temperature seasonality, soil type, and disturbance) were not primarily dictated by latitudinal

gradients (contra Strömberg, 2005, 2011; Chen et al., 2015).

6.4 Temporal patterns of RCS diatoms, environmentally sensitive phytoliths, and environmental
drivers

6.4.1. Water availability.—The RCS shows a progressive decrease in the relative

abundance of diatoms in samples through time (Fig. A1.5.A). This pattern was not likely driven

32

by facies changes as there is no change in mean relative abundance of diatoms between the two main paleosol grain size classes (siltstone vs. sandy siltstone paleosols), but instead likely reflects a shift in landscape scale water availability in the RCS during the early–middle Miocene. Moisture-limited plants such as palms, sedges, spiral gingers and relatives were present, but appeared to have been rare in the RCS (Figs. 4, 5), consistent with local habitats that were dry, at least seasonally. Regression analysis (Fig. A1.5.I) indicates that palms and spiral gingers co-occurred with diatoms, suggesting that palms and gingers tended to grow in wetter parts of the environment, in line with the ecological preferences of these plants today (e.g., Bjorholm et al., 2005; Chen and Smith, 2013). However, the explained variance is very low, likely due to their overall low counts, preventing conclusive inferences about patterns of change through the RCS.

Diatoms also show a negative relationship with pooid forms, suggesting that open-habitat pooid grasses tended to live in drier regions, but are positively correlated with potential C_4 grass phytoliths. This latter pattern could be explained if a portion of the phytoliths typical of C_4 grasses in the Panicoideae actually derive from water-loving, C_3 panicoid (or other PACMAD) grasses (e.g., Strömberg et al., 2007b; Osborne and Freckleton, 2009; see discussion above). Further work on the exact relationships between phytolith morphology and photosynthetic pathway in modern PACMAD grasses are necessary to test this hypothesis (Erra and Strömberg, 2014).

PCA analyses shed additional light on co-occurrence of environmentally sensitive plant types within the RCS communities. Negative covariance of pooids with diatoms and potential C_4 grasses (minimum/maximum; Runs 1 & 2) drives PC1, indicating that it reflects habitat wetness, with pooids representing the dry end of the spectrum and diatoms and PACMADs signaling wetter aspects of the landscape (Figs. 6A and 6B, respectively). Given its heavier loading on

PC1, maximum potential C_4 grasses (i.e., all PACMAD forms; Run 2) appear to be more ecologically informative than minimum potential C_4 grasses (i.e., panicoid and chloridoid forms; Run 1), in keeping with the idea that these PACMADs consisted mainly of water-loving, C_3 species. PC2 is determined by the negative relationship between pooids and forest indicators, with forest indicators nearly orthogonal to PC1 (Figs. 6A and 6B), suggesting that PC2 can be interpreted as an openness gradient (from open to closed). Run 3 of the PCA (Fig. 2.3C) is consistent with this idea, indicating that tree cover was not strictly linked to water. Instead we propose that pooids, PACMADs and forest indicators reflect different vegetation associations or microhabitats (ranging from open-dry patches, to wet patches, to forest patches, respectively) on the RCS landscape.

The significant correlation of PC1 scores with time (Runs 1 and 2; Fig. A1.6.A and A1.6.B) indicates that open, pooid-dominated patches increase through the RCS, whereas the wet patches associated with diatoms and PACMADs decrease. In contrast, there is no correlation between PC2 and time (Fig. A1.6.D and A1.6.E), pointing to no temporal trend in tree cover. This pattern is in contrast to Retallack (2007) who used paleosol morphology data to propose a moderate expansion of woodlands during the early middle Miocene of Montana.

Independent support for the idea of changing water availability comes from previous studies in the region that used sedimentary structures, such as the presence of bedded gypsum and smectite-rich paleosols, to conclude that southwestern Montana, adjacent Idaho, and northwestern Wyoming were regionally arid during the middle Miocene (Thompson et al., 1982; Fields et al., 1985). Retallack (2007), on the other hand, concluded that there was an increase MAP leading into the MMCO based on Bt horizon elemental chemistry and depth to putative Bk horizons. Our new data render Retallack's (2007) climate reconstruction at best premature. First,

as discussed above, we question the validity of MAP reconstructions based on Bk depths in the RCS. Second, after re-plotting Retallack's (2007) MAP estimates based on Bt horizon chemistry considering our new age model, it appears that the only spike in estimated MAP within the RCS occurred during the earliest Miocene rather than leading into the MMCO (Fig. 2.9D).

6.4.2. Temperature.—PACMAD grasses are plesiomorphically adapted to warm habitats (Edwards and Smith, 2010), hence, another explanation for the decreased abundance of PACMAD grasses through time in the RCS could be changes in local temperature. Retallack (2007) reconstructed nine mean annual temperature (MAT) estimates based on paleosol geochemistry for the RCS, ranging between $8 \pm 4.4°C$ and $11.6 \pm 4.4°C$ (Fig. 2.9C). Thus, although global temperatures warmed during the early Miocene (Fig. 2.9A), local conditions apparently did not change to the same extent. Additionally, MAT estimates from southwestern Montana indicate that regional temperatures remained relatively stable into the late Miocene (9.2 $\pm 0.9°C$, Cotton et al., 2012; $10 \pm 4°C$, Retallack, 2007; Chen et al., 2015). These records suggest that MAT was not likely a driver of vegetation change in the NRM during the Miocene.

6.4.3. Atmospheric CO_2.—During the middle Miocene, global atmospheric CO_2 may have reached its highest levels in the past 35 million years (Beerling and Royer, 2011). However, it is less clear that there was a significant change in global atmospheric CO_2 levels during RCS deposition (linear regression: $p = 0.12$; $R^2 = 0.02$; data from Beerling and Royer, 2011) (Fig. 2.9B). Similarly, there is no significant change in atmospheric CO_2 estimates calculated from carbon isotopic values of pedogenic carbonates within the RCS (linear regression: $p = 0.34$; $R^2 = 0.01$; data from Kent-Corson et al., 2006). Therefore, it is unlikely that changes in atmospheric CO_2 had any influence on the changes in RCS vegetation.

6.5 Heterogeneity in vegetation response during the lead-up to the MMCO

Our pattern of changing grass community composition (expansion of dry-adapted pooids at the expense of PACMADs) in parallel with a local decrease in water availability, but in the context of stable temperatures and atmospheric CO_2 (Fig. 2.9), differs from what would be expected based on global climatic trends and floristic changes recorded elsewhere. For example, pollen and fossil wood remains from Europe suggest increasingly warm and humid climates associated with widespread broadleaved evergreen forests during the early–middle Miocene (e.g., Ivanov et al., 2011; Jiménez-Moreno et al., 2008). Contemporaneous phytolith data from Turkey suggests a decrease in forest vegetation leading into the middle Miocene as it was replaced by C_3 savannas or open woodlands (Strömberg et al., 2007b). Additionally, climate and vegetation data from South America suggest a transition from palm shrubland to wet sclerophyllous forest during the interval when RCS sediments were deposited (ca. 20–15 Ma; Dunn et al., 2015). Overall, data from these other regions suggest the early–middle Miocene was an interval of increasing warmth and in some instances characterized by dramatic shifts in vegetation. However, these patterns were not ubiquitous across the globe and highlight the importance of localized studies of vegetation and climate change through time.

6.6 How Did Vegetation Change in the Interior of North America During the Early Miocene and Leading into the MMCO?

The revised age model for RCS has major implications for the interpretation of patterns of grassland evolution in North America, because it suggests that the spread of open, grass-dominated habitats was initiated by at least the early Miocene in both the NRM (this study) and the Great Plains (GP; Strömberg, 2004, 2005). This pattern opens up the possibility that the

factor, or more likely combination of factors that promoted expansion of grasses at the expense of trees (e.g., changes in CO_2, precipitation, temperature seasonality, soil type, and disturbance) were important across the continent—perhaps globally—and less dictated by latitudinal gradients than previously thought (Strömberg, 2005, 2011). Work is ongoing to determine the nature and timing of vegetation changes in the NRM and GP more precisely to allow for rigorous comparison with potential abiotic and biotic drivers (Fredrickson et al., 2012).

In coeval early Miocene phytolith assemblages from the GP and NRM, the co-occurrence of abundant open-habitat, pooid grass forms with low but variable abundances of forest indicators and potential C_4 grass forms point to relatively open habitats with patches of forest vegetation (woodland, savanna, mosaic; Strömberg, 2004, 2005). These heterogeneous grass-dominated vegetation types were maintained in these regions through the middle Miocene, and only became more uniformly open during the late Miocene–Pliocene (Strömberg, 2005, 2011; Strömberg and McInerney, 2011; Hyland et al., in review). Paleosol carbonate data from the Great Plains also indicate relatively low C_4 biomass (~20% of local vegetation) during the early–middle Miocene (Fox and Koch, 2003, 2004; Fox et al., 2012), consistent with contemporaneous phytolith data (McInerney et al., 2011; Strömberg and McInerney, 2011). Taken together, these lines of evidence suggest that C_4 PACMADs were in low abundance in the interior of North America during the early–middle Miocene and only became dominant in ecosystems during the latest Miocene (Edwards et al., 2010; Strömberg and McInerney, 2011; Hyland et al., in review). Thus, it seems likely that most PACMAD grasses present in grass communities in the continental interior prior to the latest Miocene were C_3.

6.7 Vegetation Changes in the NRM as a Context for Miocene Faunal Evolution

The new results from this study indicate that the inferred changes in North American faunal richness and community composition, such as the replacement of oreodontids by equids in the NRM (Barnosky and Carrasco, 2002; Janis et al., 2002; Badgley and Finarelli, 2013, Fraser et al., 2014; Kohn and Fremd, 2007) were not associated with a drastic vegetation turnover but what appears to have been a fairly gradual and subtle environmental change, both locally in the RCS and across the NRM (Strömberg, 2005, 2011). Local changes in water availability may still have led to shifts in relative abundances of preferred foods (e.g., pooids vs. PACMADs) enough to result in local extinction of oreodonts. This untested hypothesis could be addressed by comparing patterns of vegetation change in the RCS with dietary proxy data (e.g., stable carbon isotope data from tooth enamel) from oreodontids and equids from the same strata to determine dietary preferences relative to available plant cover (Harris et al., 2016a).

7. CONCLUSION

Phytolith and isotope geochemistry data are combined here to reconstruct the first quantitative, high-resolution record of North American vegetation change leading into the mid-Miocene warming event in the Railroad Canyon section (RCS), Idaho. These records are interpreted as recording a mosaic of open, grass-dominated habitats with patches of denser woody vegetation during the early–middle Miocene. C_3 plants (in particular pooid grasses) dominated the local vegetation and although C_4 grasses (and other plants) were present on the landscape, they constituted only minor components of the local vegetation. Covariance between PACMAD grasses and diatoms suggest that most PACMADs were water-loving (C_3) plants, whereas pooids were most likely dry-adapted. Additionally, statistical and ordination analyses

reveal an increase in pooids and a decrease in diatoms and PACMAD grasses over time. These transformations occurred in parallel with a suggested decline in local mean annual precipitation or water availability, but despite unchanged local temperatures and atmospheric CO_2. Thus, regional climatic and floral patterns in the RCS cannot necessarily be predicted from global climate change leading into the middle Miocene. However, because of the low density of proxy data for temperature and precipitation seasonality locally within the RCS, it is not possible to rule out the effect these other climate variables may have had on local vegetation. Also, turnover within NRM faunas by the early Hemingfordian (ca. 18.5 Ma) cannot be easily explained by a drastic floristic change. Finally, we provide a revised age model for the RCS that constrains the age of this sequence to ca. 22.9–15.2 Ma, approximately 5 Ma older than previous age models. These new age estimates suggest a much earlier age for the spread of open, grass-dominated habitats in the Northern Rocky Mountains and indicate a concurrent spread of grasslands across the interior of North America during the early Miocene.

ACKNOWLEDGEMENTS

REFERENCES

Alexandre, A., Meunier, J.D., Lzine, A., Vincens, A., Schwartz, D., Lézine, a. M., Vincens, A., Schwartz, D., 1997. Phytoliths : indicators of grassland dynamics during the late Holocene in intertropical Africa. Palaeogeogr. Palaeoclimatol. Palaeoecol. 136, 213–229.

Atwater, T., Stock, J., 1998. Pacific-North America Plate Tectonics of the Neogene Southwestern United States–An Update. Int. Geol. Rev. 40, 375–402.

Badgley, C., Finarelli, J.A., 2013. Diversity dynamics of mammals in relation to tectonic and climatic history: comparison of three Neogene records from North America. Paleobiology 39, 373–399.

Barnosky, A.D., Bibi, F., Hopkins, S.S.B., Nichols, R., 2007. Biostratigraphy and magnetostratigraphy of the Mid-Miocene Railroad Canyon Sequence, Montana and Idaho, and age of the Mid-Tertiary Unconformity west of the Continental Divide. J. Vertebr. Paleontol. 27, 204–224.

Barnosky, A.D., Carrasco, M.A., 2002. Effects of Oligo-Miocene global climate changes on mammalian species richness in the northwestern quarter of the USA. Evol. Ecol. Res. 4, 811–841.

Barnosky, A.D., Hadly, E. a., Bell, C.J., 2003. Mammalian Response To Global Warming on Varied Temporal Scales. J. Mammal. 84, 354–368.

Beerling, D.J., Royer, D.L., 2011. Convergent Cenozoic CO2 history. Nat. Geosci. 4, 418–420.

Bjorholm, S., Svenning, J.-C., Skov, F., Balslev, H., 2005. Environmental and spatial controls of palm (Arecaceae) species richness across the Americas. Glob. Ecol. Biogeogr. 14, 423–429.

Bremond, L., Alexandre, A., Hély, C., Guiot, J., 2005. A phytolith index as a proxy of tree cover density in tropical areas: Calibration with Leaf Area Index along a forest-savanna transect in southeastern Cameroon. Glob. Planet. Change 45, 277–293.

Cerling, T.E., 1984. The stable isotopic composition of modern soil carbonate and its relationship to climate. Earth Planet. Sci. Lett. 71, 229–240.

Chamberlain, C.P., Mix, H.T., Mulch, A., Hren, M.T., Kent-Corson, M.L., Davis, S.J., Horton, T.W., Graham, S.A., 2012. The Cenozoic climatic and topographic evolution of the western North American Cordillera. Am. J. Sci. 312, 213–262.

Chen, S.T., Smith, S.Y., 2013. Phytolith variability in Zingiberales: A tool for the reconstruction of past tropical vegetation. Palaeogeogr. Palaeoclimatol. Palaeoecol. 370, 1–12.

Chen, S.T., Smith, S.Y., Sheldon, N.D., Strömberg, C.A.E., 2015. Regional-scale variability in the spread of grasslands in the late Miocene. Palaeogeogr. Palaeoclimatol. Palaeoecol. 437, 42–52.

Clarke, J., 2003. The occurrence and significance of biogenic opal in the regolith. Earth-Science Rev. 60, 175–194.

Cotton, J.M., Sheldon, N.D., Strömberg, C.A.E., 2012. High-resolution isotopic record of C4 photosynthesis in a Miocene grassland. Palaeogeogr. Palaeoclimatol. Palaeoecol. 337-338, 88–98.

Diefendorf, A.F., Mueller, K.E., Wing, S.L., Koch, P.L., Freeman, K.H., 2010. Global patterns in leaf 13C discrimination and implications for studies of past and future climate. Proc. Natl. Acad. Sci. 107, 5738–5743.

Dunn, R.E., Strömberg, C.A.E., Madden, R.H., Kohn, M.J., Carlini, A.A., 2015. Linked canopy, climate, and faunal change in the Cenozoic of Patagonia. Science. 347, 258-261.

Edwards, E.J., Osborne, C.P., Strömberg, C. a E., Smith, S. a, Bond, W.J., Christin, P.-A., Cousins, A.B., Duvall, M.R., Fox, D.L., Freckleton, R.P., Ghannoum, O., Hartwell, J., Huang, Y., Janis, C.M., Keeley, J.E., Kellogg, E. a, Knapp, A.K., Leakey, A.D.B., Nelson, D.M., Saarela, J.M., Sage, R.F., Sala, O.E., Salamin, N., Still, C.J., Tipple, B., 2010. The origins of C4 grasslands: integrating evolutionary and ecosystem science. Science (80-.). 328, 587–91.

Edwards, E.J., Smith, S.A., 2010. Phylogenetic analyses reveal the shady history of C4 grasses. Proc. Natl. Acad. Sci. U. S. A. 107, 2532–7.

Erra, G., Strömberg, C.A.E., 2014. Tracking the deep-time evolution of grasses and grasslands: duilding a key to grass short cell phytolith morphology, in: XI Congreso Latinoamericano de Botânica, Salvador, Bahia, Brazil.

Fields, R.W., Rasmussen, D.L., Tabrum, A.R., Nichols, R., 1985. Cenozoic Rocks of the Intermontane Basins of Western Montana and Eastern Idaho: a summary. Cenozoic Paleogeography of the West-Central United States 9–36.

Fox, D.L., Honey, J.G., Martin, R. a., Peláez-Campomanes, P., 2012. Pedogenic carbonate stable isotope record of environmental change during the Neogene in the southern Great Plains, southwest Kansas, USA: Oxygen isotopes and paleoclimate during the evolution of C4-

dominated grasslands. Bull. Geol. Soc. Am. 124, 431–443.

Fox, D.L., Koch, P.L., 2004. Carbon and oxygen isotopic variability in Neogene paleosol

carbonates: constraints on the evolution of the C4-grasslands of the Great Plains, USA.

Palaeogeogr. Palaeoclimatol. Palaeoecol. 207, 305–329.

Fox, D.L., Koch, P.L., 2003. Tertiary history of C4 biomass in the Great Plains, USA. Geology

31, 809.

Fraser, D., Hassall, C., Gorelick, R., Rybczynski, N., 2014. Mean annual precipitation explains

spatiotemporal patterns of Cenozoic mammal beta diversity and latitudinal diversity

gradients in North America. PLoS One 9.

Fredlund, G., Tieszen, L., 1994. Modern phytolith assemblages from the North American great

plains. J. Biogeogr. 21, 321–335.

Fredrickson, E.K., Strömberg, C.A.E., Sheldon, N.D., Smith, S.Y., 2012. Vegetation response to

the late Oligocene warming event in southwestern Montana based on a combined phytolith-

carbon isotope record. Geol. Soc. Am. Annu. Meet. abstract.

Harris, E.B., Strömberg, C.A.E., Kohn, M.J., 2016a. Stable isotopes reveal differential dietary

evolution in large ungulates during the early–middle Miocene in the Northern Rocky

Mountains. *Chapter 4*.

Hinojosa, L.F., Villagrán, C., 2005. Did South American Mixed Paleofloras evolve under

thermal equability or in the absence of an effective Andean barrier during the Cenozoic?

Palaeogeogr. Palaeoclimatol. Palaeoecol. 217, 1–23.

Hirota, M., Holmgren, M., Van Nes, E.H., Scheffer, M., 2011. Global Resilience of Tropical

Forest. Science (80-.). 334, 232–235.

Hodson, M.J., White, P.J., Mead, a., Broadley, M.R., 2005. Phylogenetic variation in the silicon composition of plants. Ann. Bot. 96, 1027–1046.

Hyland, E., Smith, S.Y., Sheldon, N.D., 2013. Representational bias in phytoliths from modern soils of central North America: Implications for paleovegetation reconstructions. Palaeogeogr. Palaeoclimatol. Palaeoecol. 374, 338–348.

Hyland, E.G., Sheldon, N.D., Smith, S.Y., Strömberg, C.A.E., n.d. Late Miocene rise and fall of C4 grasses in the western United States. Geology.

Ivanov, D., Utescher, T., Mosbrugger, V., Syabryaj, S., Djordjević-Milutinović, D., Molchanoff, S., 2011. Miocene vegetation and climate dynamics in Eastern and Central Paratethys (Southeastern Europe). Palaeogeogr. Palaeoclimatol. Palaeoecol. 304, 262–275.

Jaramillo, C., Ochoa, D., Contreras, L., Pagani, M., Carvajal-Ortiz, H., Pratt, L.M., Krishnan, S., Cardona, A., Romero, M., Quiroz, L., Rodriguez, G., Rueda, M.J., de la Parra, F., Morón, S., Green, W., Bayona, G., Montes, C., Quintero, O., Ramirez, R., Mora, G., Schouten, S., Bermudez, H., Navarrete, R., Parra, F., Alvarán, M., Osorno, J., Crowley, J.L., Valencia, V., Vervoort, J., 2010. Effects of rapid global warming at the Paleocene-Eocene boundary on neotropical vegetation. Science 330, 957–61.

Jiménez-Moreno, G., Fauquette, S., Suc, J.-P., 2008. Vegetation, climate and palaeoaltitude reconstructions of the Eastern Alps during the Miocene based on pollen records from Austria, Central Europe. J. Biogeogr. 35, 1638–1649.

Kent-Corson, M.L., Sherman, L.S., Mulch, A., Chamberlain, C.P., 2006. Cenozoic topographic and climatic response to changing tectonic boundary conditions in Western North America.

Earth Planet. Sci. Lett. 252, 453–466.

Kohn, M.J., 2010. Carbon isotope compositions of terrestrial C3 plants as indicators of (paleo)ecology and (paleo)climate. Proc. Natl. Acad. Sci. U. S. A. 107, 19691–5.

Kohn, M.J., Fremd, T.J., 2007. Tectonic controls on isotope composition and species diversification, John Day Basin, central Oregon. PaleoBios 27, 48–61.

Kraus, M.J., 1999. Paleosols in clastic sedimentary rocks: their geologic applications. Earth-Science Rev. 47, 41–70.

Kürschner, W.M., Kvacek, Z., Dilcher, D.L., 2008. The impact of Miocene atmospheric carbon dioxide fluctuations on climate and the evolution of terrestrial ecosystems. Proc. Natl. Acad. Sci. U. S. A. 105, 449–53.

Leopold, E.B., Denton, M.F., 1987. Comparative Age of Grassland and Steppe East and West of the Northern Rocky Mountain. Ann. Missouri Bot. Gard. 74, 841.

McInerney, F.A., Strömberg, C.A.E., White, J.W.C., 2011. The Neogene transition from C3 to C4 grasslands in North America: stable carbon isotope ratios of fossil phytoliths. Paleobiology 37, 23–49.

Miller, L.A., Smith, S.Y., Sheldon, N.D., Stromberg, C.A.E., 2012. Eocene vegetation and ecosystem fluctuations inferred from a high-resolution phytolith record. Geol. Soc. Am. Bull. 124, 1577–1589.

Mosbrugger, V., Utescher, T., Dilcher, D.L., 2005. Cenozoic continental climatic evolution of Central Europe. Proc. Natl. Acad. Sci. U. S. A. 102, 14964–14969.

Osborne, C.P., Freckleton, R.P., 2009. Ecological selection pressures for C4 photosynthesis in

the grasses. Proc. R. Soc. B Biol. Sci. 276, 1753–1760.

Osterrieth, M., Madella, M., Zurro, D., Fernanda Alvarez, M., 2009. Taphonomical aspects of silica phytoliths in the loess sediments of the Argentinean Pampas. Quat. Int. 193, 70–79.

Parmesan, C., 2006. Ecological and Evolutionary Responses to Recent Climate Change. Annu. Rev. Ecol. Evol. Syst. 37, 637–669.

Parsons, T., 1995. The Basin and Range Province, in: Developments in Geotectonics. pp. 277–324.

Piperno, D.R., 2006. Phytoliths: A Comprehensive Guide for Archaeologists And Paleoecologists. AltaMira Press, Lanham.

Piperno, D.R., Becker, P., 1996. Vegetational history of a site in the central Amazon basin derived from phytolith and charcoal records from natural soils. Quat. Res. 45, 202–209.

Piperno, D.R., Pearsall, D.M., 1998. The silica bodies of tropical American grasses: morphology, taxonomy, and implications for grass systematics and fossil phytolith identification. Smithson. Contrib. 85, 1–40.

Quade, J., Cerling, T.E., 1995. Expansion of C4 grasses in the Late Miocene of Northern Pakistan: evidence from stable isotopes in paleosols. Palaeogeogr. Palaeoclimatol. Palaeoecol. 115, 91–116.

Rasmussen, D.L., 2003. Tertiary history of western Montana and east-central Idaho: a synopsis, in: G., R.R., Flores, R.M. (Eds.), Cenozoic Systems of the Rocky Mountain Region. Rocky Mountain Section Society for Sedimentary Geology, Denver, pp. 459–478.

Retallack, G.J., 2009. Refining a pedogenic-carbonate CO2 paleobarometer to quantify a middle

Miocene greenhouse spike. Palaeogeogr. Palaeoclimatol. Palaeoecol. 281, 57–65.

Retallack, G.J., 2007. Cenozoic Paleoclimate on Land in North America. J. Geol. 115, 271–294.

Retallack, G.J., Orr, W.N., Prothero, D.R., Duncan, R.A., Kester, P.R., P., A.C., 2004. Eocene-Oligocene extinction and paleoclimatic change near Eugene, Oregon. Geol. Soc. Am. Bull. 116, 817–839.

Root, T., Price, J., Hall, K., Schneider, S., 2003. Fingerprints of global warming on wild animals and plants. Nature 421, 57–60.

Selkin, P.A., Strömberg, C.A.E., Dunn, R., Kohn, M.J., Carlini, A.A., Davies-Vollum, S., Madden, R.H., 2015. Climate, dust, and fire across the Eocene-Oligocene transition, Patagonia. Geology 43, 1–4.

Sheldon, N.D., Tabor, N.J., 2009. Quantitative paleoenvironmental and paleoclimatic reconstruction using paleosols. Earth-Science Rev. 95, 1–52.

Soil Survey Staff, 2014. Keys to Soil Taxonomy, 12th ed, United States Department of Agriculture. Natural Resources Conservation Service, Washington, D.C.

Staver, A.C., Archibald, S., Levin, S.A., 2011. The Global Extent and Determinants of Savanna and Forest as Alternative Biome States. Science (80-.). 334, 230–232.

Strömberg, C. a. E., 2011. Evolution of Grasses and Grassland Ecosystems. Annu. Rev. Earth Planet. Sci. 39, 517–544.

Strömberg, C.A.E., 2005. Decoupled taxonomic radiation and ecological expansion of open-habitat grasses in the Cenozoic of North America. Proc. Natl. Acad. Sci. U. S. A. 102, 11980–4.

Strömberg, C.A.E., 2004. Using phytolith assemblages to reconstruct the origin and spread of grass-dominated habitats in the great plains of North America during the late Eocene to early Miocene. Palaeogeogr. Palaeoclimatol. Palaeoecol. 207, 239–275.

Strömberg, C.A.E., 2003. The origin and spread of grass-dominated ecosystems during the Tertiary of North America and how it relates to the evolution of hypsodonty in equids.

Strömberg, C.A.E., Dunn, R.E., Madden, R.H., Kohn, M.J., Carlini, A.A., 2013. Decoupling the spread of grasslands from the evolution of grazer-type herbivores in South America. Nat. Commun. 4, 1478.

Strömberg, C.A.E., Friis, E.M., Liang, M.-M., Werdelin, L., Zhang, Y.-I., 2007. Palaeoecology of an Early-Middle Miocene late in China: preliminary interpretations based on phytoliths from the Shanwang Basin. Vertebr. Palasiat. 45, 145–160.

Strömberg, C.A.E., McInerney, F.A., 2011. The Neogene transition from C3 to C4 grasslands in North America : assemblage analysis of fossil phytoliths. Paleobiology 37, 50–71.

Strömberg, C.A.E., Werdelin, L., Friis, E.M., Saraç, G., 2007. The spread of grass-dominated habitats in Turkey and surrounding areas during the Cenozoic: Phytolith evidence. Palaeogeogr. Palaeoclimatol. Palaeoecol. 250, 18–49.

Swanson, D.A., Wright, T.L., Hooper, P.R., Bentley, R.D., 1979. Revisions in stratigraphic nomenclature of the Columbia River Basalt Group. U.S. Geol. Surv. Bull. 1457-G.

Team, R.C., 2015. R: A language and environment for statistical computing.

Tedford, R.H., Albright III, L.B., Barnosky, A.D., Ferrusquia-Villafranca, I., Hunt Jr., R.M., Storer, J.E., Swisher III, C.C., Voorhies, M.R., Webb, S.D., Whistler, D.P., 2004.

Mammalian Biochronology of the Arikareean Through Hemphillian Interval (Late Oligocene Through Early Pliocene Epochs), in: Woodburne, M.O. (Ed.), Late Cretaceous and Cenozoic Mammals of North America. Columbia University Press, pp. 169–231.

Thompson, G.R., Fields, R.W., Alt, D., 1982. Land-based evidence for Tertiary climatic variations: Northern Rockies. Geology 10, 413–417.

Tipple, B.J., Meyers, S.R., Pagani, M., 2010. Carbon isotope ratio of Cenozoic CO_2: A comparative evaluation of available geochemical proxies. Paleoceanography 25, 1–11.

Walther, G.-R., Post, E., Convey, P., Menzel, A., Parmesan, C., Beebee, T.J.C., Fromentin, J.-M., Hoegh-Guldberg, O., Bairlein, F., 2002. Ecological responses to recent climate change. Nature 416, 389–395.

Webb, S.D., Opdyke, N.D., 1995. Global climatic influence of Cenozoic land mammal faunas, in: Effects of Past Global Change on Life. National Academy Press, Washington, D.C., pp. 184–208.

White, P.S., 1979. Pattern, Process, and Natural Disturbance in Vegetation. Bot. Rev. 45, 229–299.

Williams, R.J., Duff, G.A., Bowman, D.M.J.S., Cook, G.D., 1996. Variation in the composition and structure of tropical savannas as a function of rainfall and soil texture along a large-scale climatic gradient inn the Northern Territory, Australia. J. Biogeogr. 23, 747–756.

Wing, S.L., 1998. Tertiary vegetation of North America as a context for mammalian evolution, in: Janis, C.M., Scott, K.M., Jacobs, L.L. (Eds.), Evolution of Tertiary Mammals of North America Volume 1. Cambridge University Press, Cambridge, pp. 37–60.

Wing, S.L., Harrington, G.J., Smith, F. a, Bloch, J.I., Boyer, D.M., Freeman, K.H., 2005. Transient floral change and rapid global warming at the Paleocene-Eocene boundary. Science 310, 993–6.

WoldeGabriel, G., Ambrose, S.H., Barboni, D., Bonnefille, R., Bremond, L., Currie, B., DeGusta, D., Hart, W.K., Murray, A.M., Renne, P.R., Jolly-Saad, M.C., Stewart, K.M., White, T.D., 2009. The Geological, Isotopic, Botanical, Invertebrate, and Lower Vertebrate Surroundings of Ardipithecus ramidus. Science (80-.). 326, 65e1–65e5.

Wynn, J.G., 2007. Carbon isotope fractionation during decomposition of organic matter in soils and paleosols: Implications for paleoecological interpretations of paleosols. Palaeogeogr. Palaeoclimatol. Palaeoecol. 251, 437–448.

Wynn, J.G., Bird, M.I., 2007. C4-derived soil organic carbon decomposes faster than its C3 counterpart in mixed C3/C4 soils. Glob. Chang. Biol. 13, 2206–2217.

Zoback, M.L., Anderson, R.E., Thompson, G.A., 1981. Cainozoic evolution of the state of stress and style of tectonism of the Basin and Range province of the western United States. Philos. Trans. R. Soc. London 300, 407–434.
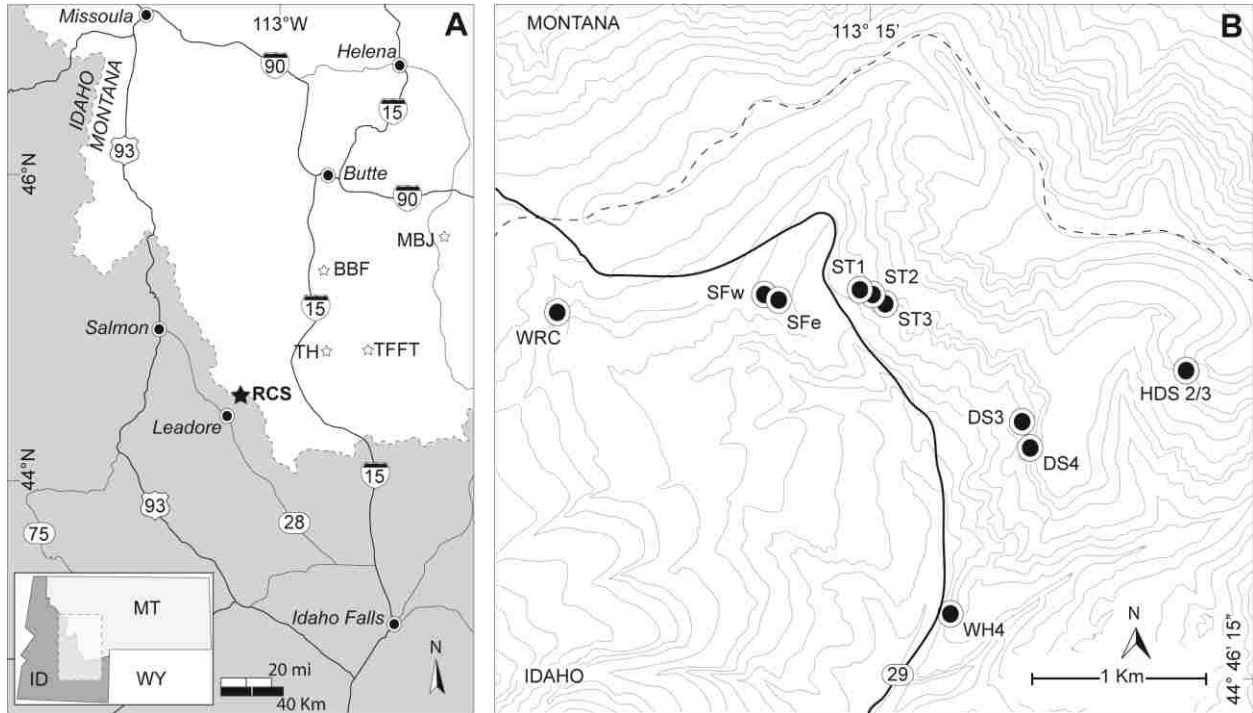
Figure 2.1. (A) Map showing the location of the Railroad Canyon Sequence (RCS) in central-eastern Idaho. The location of four additional fossil sites in southwestern Montana are also included, namely Trace Fossil Fun Time (TFFT; Cotton et al., 2012), Timber Hills A (TH; Cotton et al., 2012), Madison Buffalo Jump (MBJ; Chen et al., 2015) and Beaverhead Basin Flora (BBF; Hyland et al., in review). (B) Location of fossil sites within the RCS that were analyzed for phytoliths and stable carbon isotopes. Site name abbreviations can be found in Table 2.1.

52
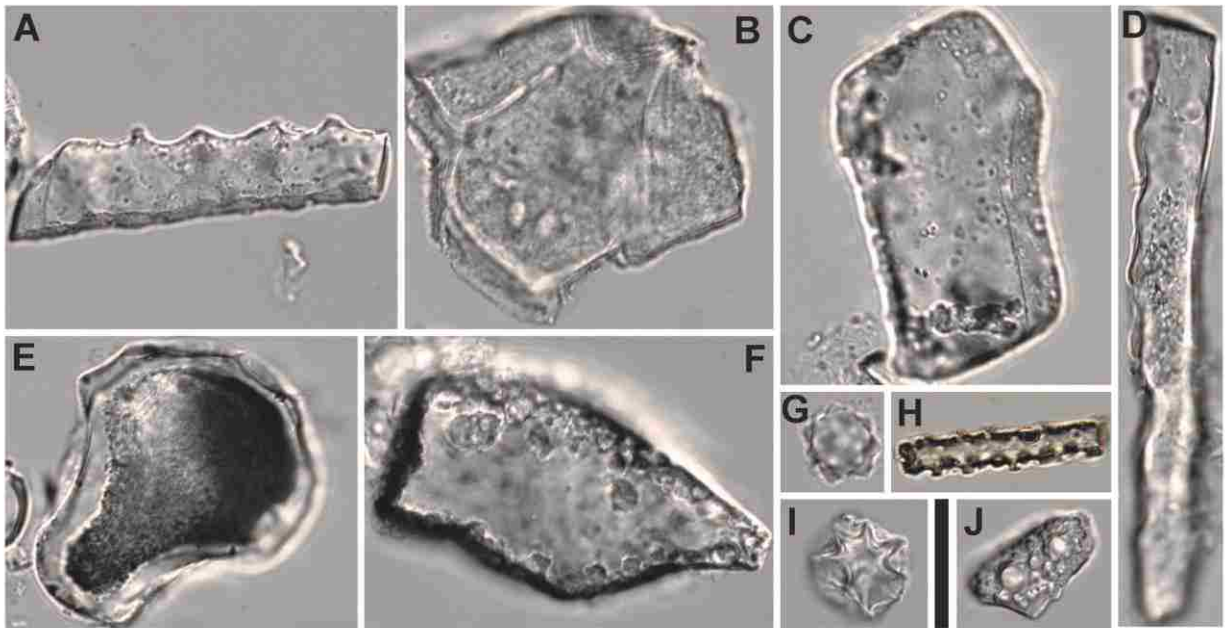
Figure 2.2. Selected non-GSSC phytoliths from the Railroad Canyon. (A) Epi-9 – spiny elongate (non-diagnostic grass/monocot), (B) Epi-1 – polyhedral epidermis (general dicot), (C) Blo-2 – thickened rectangular plate (non-diagnostic phytolith), (D) Scl-6 – slim, tapering sclereid (potential dicot), (E) Blo-10 – keystone-shaped bulliform plate (diagnostic grass), (F) Tri-8 – spindle-shaped trichome (non-diagnostic grass/monocot), (G) Clm-2 – echinate sphere (palm), (H) Elo-11 – rod with knobs (non-diagnostic phytolith), (I) Clm-4 – *Costus*-type body, (J) Epi-6 – sedge epidermal plate (sedge). Scale bar = 20 μm.
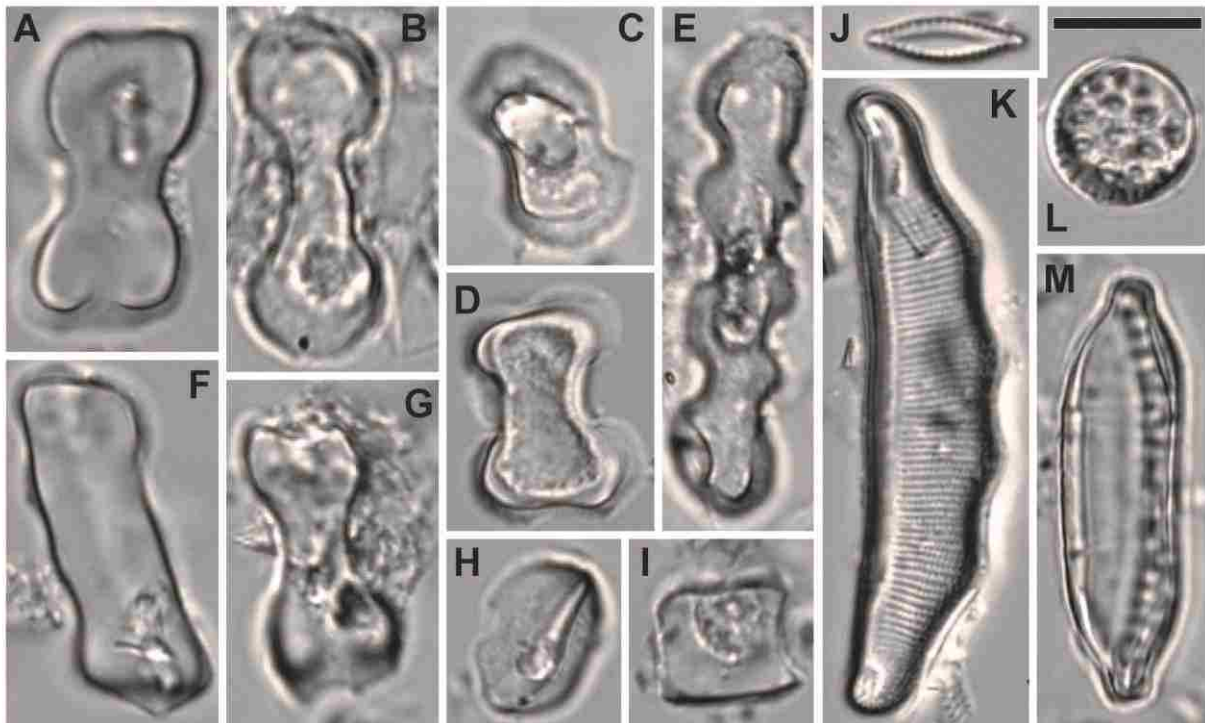
Figure 2.3. Examples of diagnostic GSSC phytoliths and diatoms from the Railroad Canyon. (A) BI-6 – inverted bilobate (PACMAD), (B) BI-5 – simple bilobate (PACMAD), (C) BI-1 – *Stipa*-type bilobate (diagnostic pooid), (D) BI-7 – Panicoid-type bilobate (PACMAD), (E) PO-1 – polylobate (diagnostic pooid), (F) CE-1 – crenate (diagnostic pooid), (G) BI-8 – Panicoid-type bilobate (Panicoid), (H) KR-1 – regular keeled rondel (non-diagnostic pooid), (I) SA-1 – true saddle (chloridoid). (J–M) examples of diatoms preserved in RCS samples. Scale bar = 10 μm.
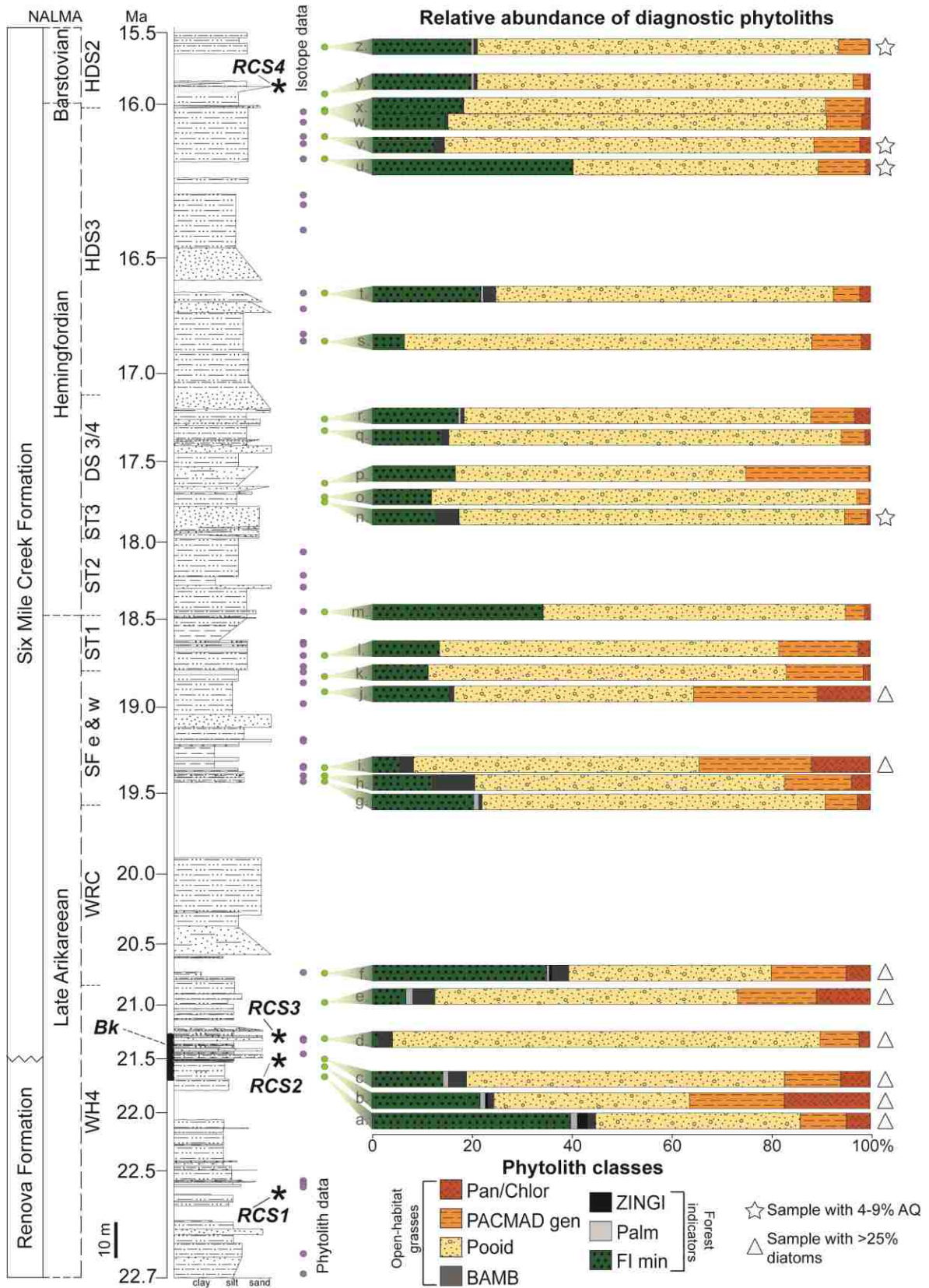
Figure 2.4. Composite stratigraphic section for the Railroad Canyon sequence. From left to right: regional rock formations observed in the RCS; estimates of relative age based on local fauna (NALMA); sites listed in stratigraphic order (abbreviations listed in Table 2.1); age estimates based on our new polynomial age model (discussed in Appendix); location of dated ash horizons (RCS1 = 22.65 ± 0.37 Ma; RCS2 = no good age estimate; RCS3 = 21.24 ± 0.27 Ma; RCS4 = 15.76 ± 0.22 Ma); location of paleosols sampled for isotope analysis; location of paleosols sampled for phytolith analysis; relative abundances of diagnostic phytoliths. a–z) sample numbers referenced in Table A1.1. Bk = location of horizons containing carbonate nodules.
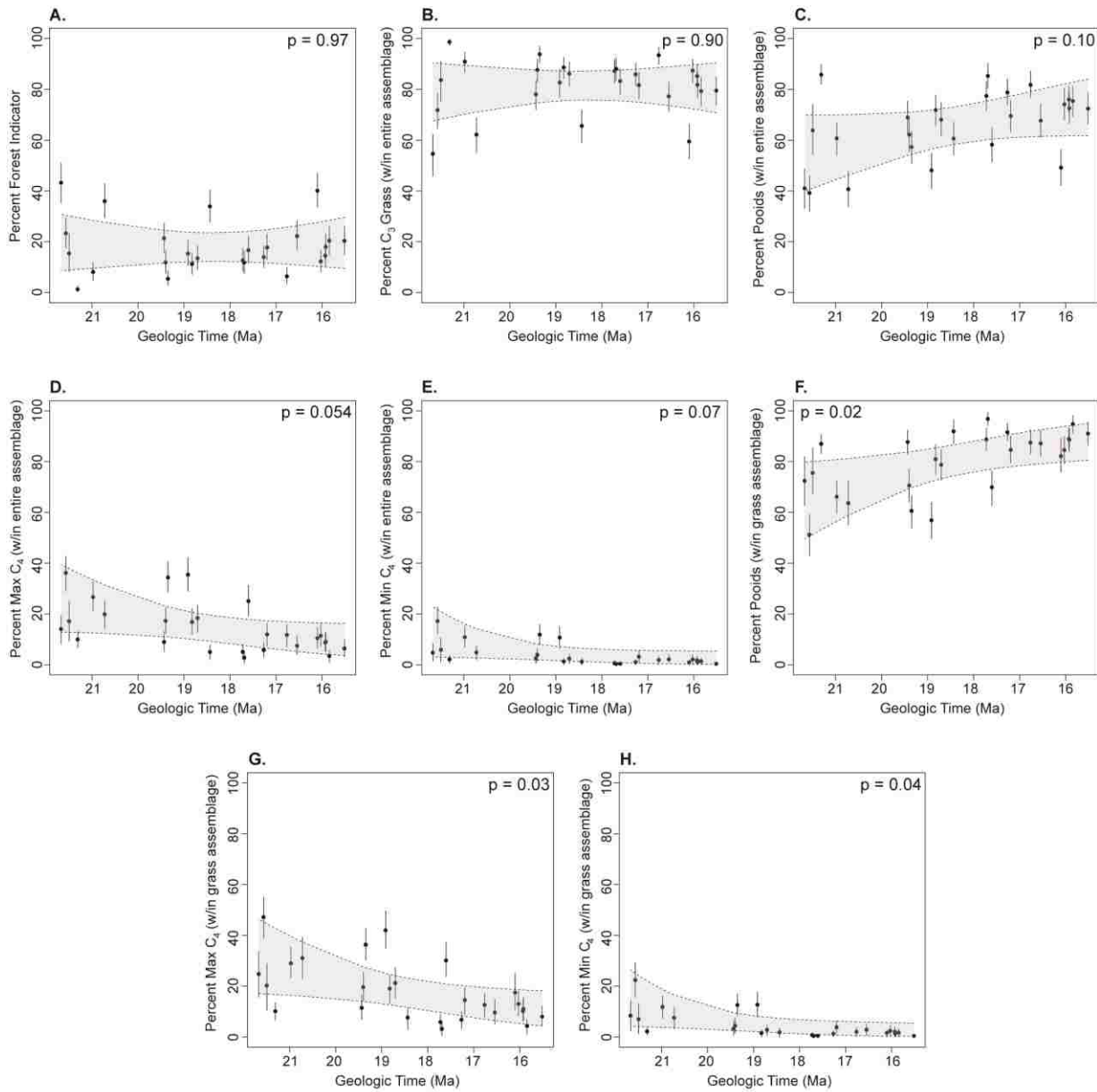
Figure 2.5. Relative abundances of various phytolith vegetation types through time. Additional plots can be found in Fig. A1.4.
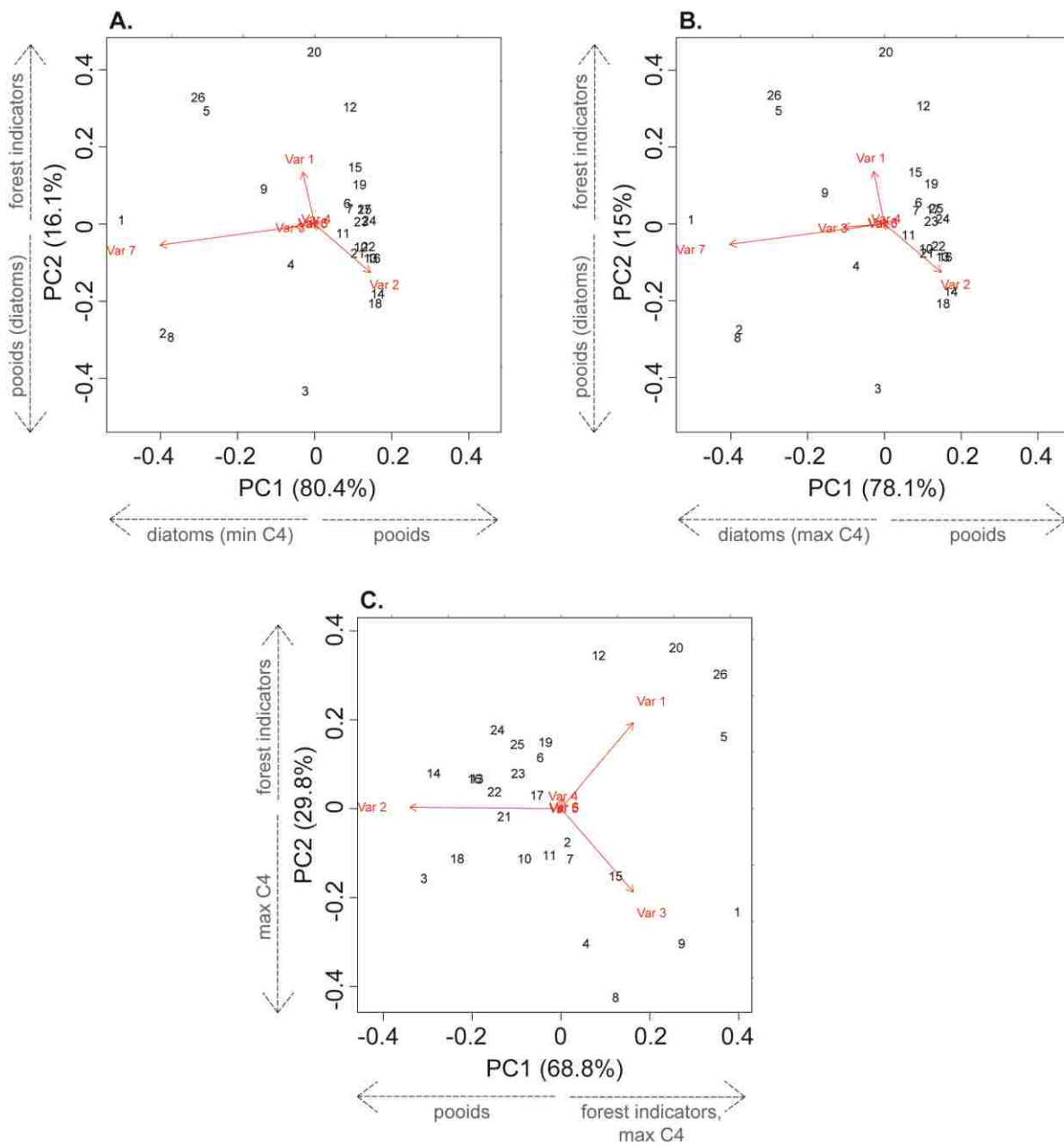
Figure 2.6. Results of principal component analyses for A) Run 1, B) Run 2, and C) Run 3. Var1 = FI-t; Var2 = pooids (in the entire phytolith assemblage); Var3 = maximum C_4 grasses (in the entire phytolith assemblage); Var7 = diatoms.
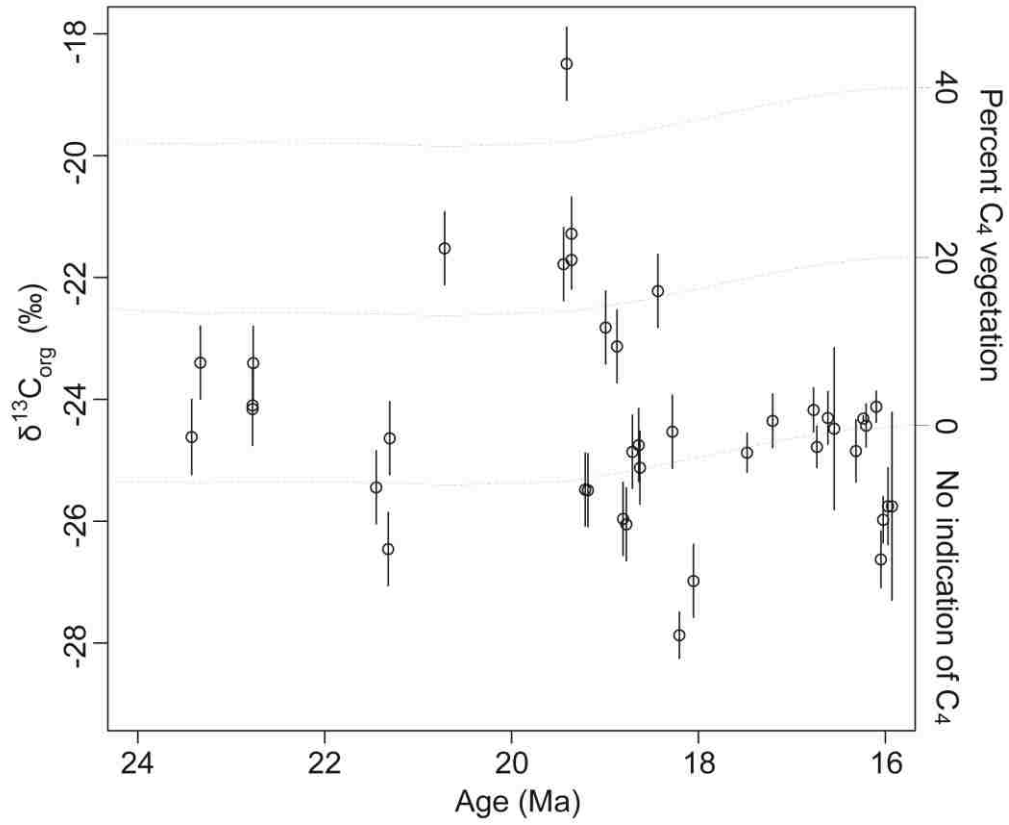
Figure 2.7. Average $\delta^{13}C_{org}$ for individual paleosol samples based on replicate analysis. Dotted lines represent our expectations of %C$_4$ vegetation based on changes in $\delta^{13}C_{atmosphere}$ during the early–middle Miocene.
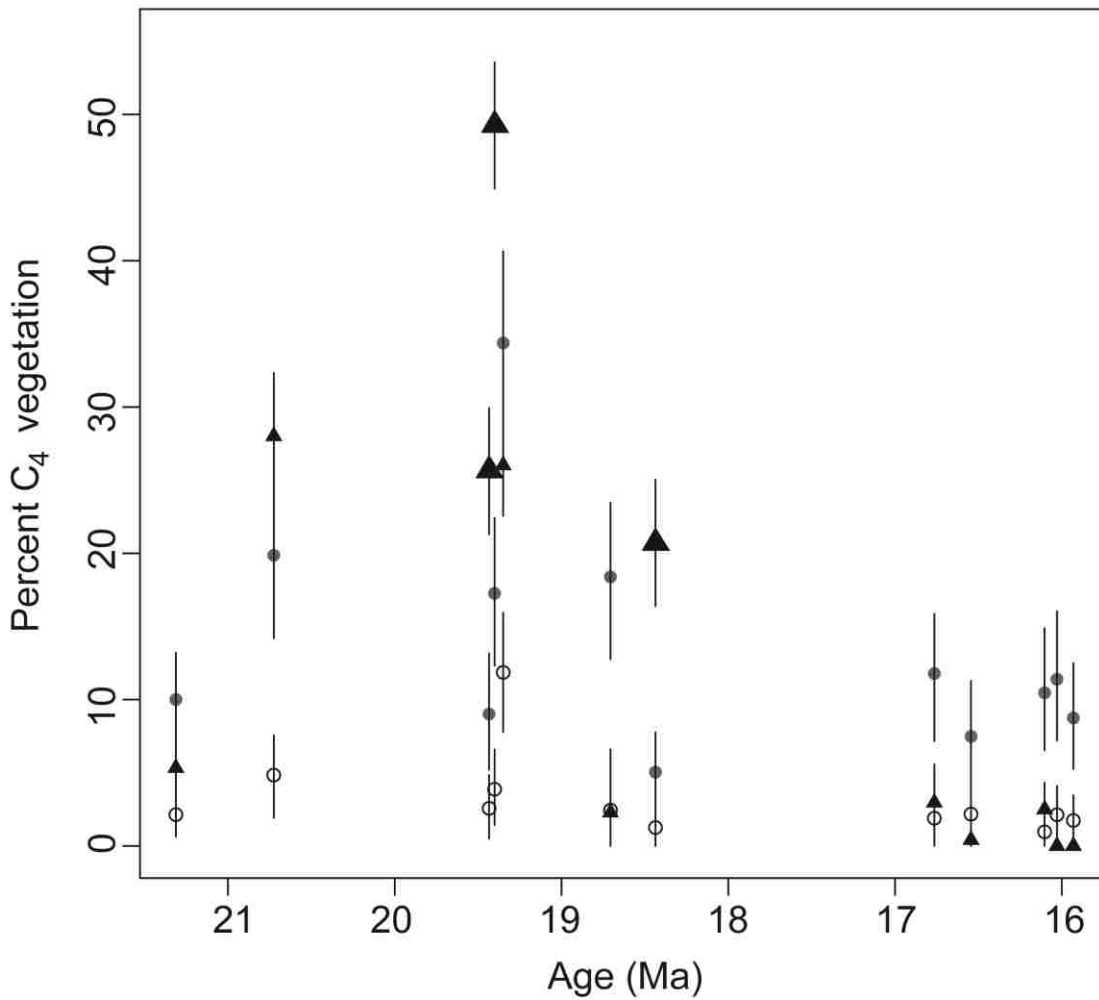
Figure 2.8. Comparison between C_4 reconstructions based on phytolith and isotope analyses. Filled circles indicate phytolith maximum C_4 estimates, empty circles indicate phytolith minimum C_4 estimates, and triangles indicate isotope C_4 estimates. For the majority of samples both methods yield similar results. Bolded triangles indicate samples where C_4 estimates from isotopes exceed those from phytoliths.
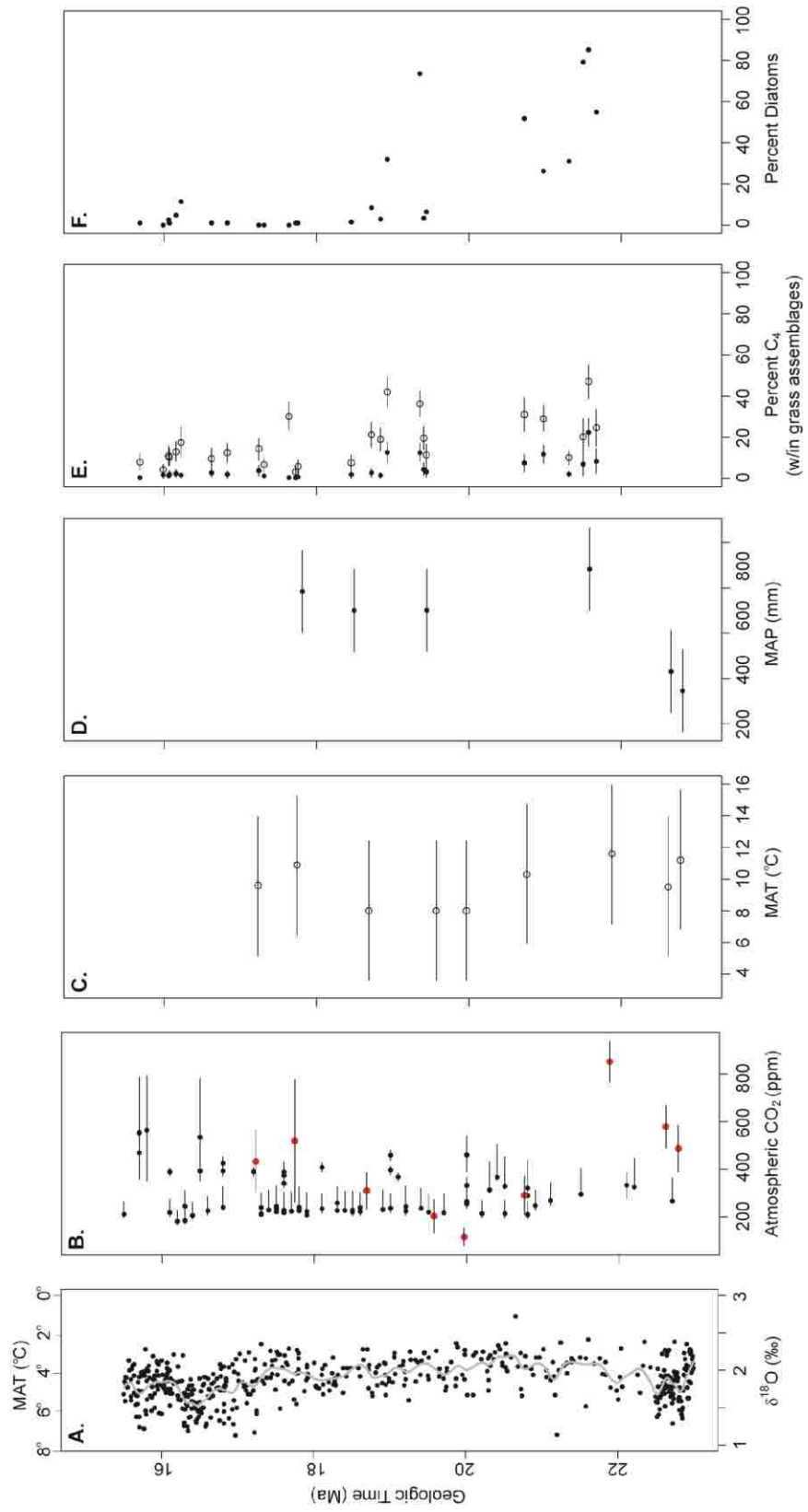
Figure 2.9. Comparison of local and global climate records to trends in local vegetation and diatoms in the RCS. A) Global mean annual temperature (MAT) estimates based on $\delta^{18}O$ of benthic foraminifera (Zachos et al., 2001). B) Estimates of atmospheric CO_2 concentrations with global data in black (Beerling and Royer, 2011) and local data from the RCS in red (based on alleged pedogenic carbonates; Retallack 2007). C) RCS estimates of MAT based on paleosol alkali ratios (Retallack 2007). D) Mean annual precipitation estimates calculated from CIA-K index of Bt horizons (Retallack 2007). E) Phytolith estimate of $\%C_4$ grasses within grass assemblages in the RCS (this study). Closed symbols are minimum estimates of potential C_4 grasses and open symbols are maximum estimates of potential C_4 grasses (i.e., PACMAD GSSCs). F) Relative abundance of diatoms in RCS samples (this study).

CHAPTER 2: TABLES

Table 2.1. Railroad Canyon locality information for sites mentioned in text (arranged stratigraphically).

UWBM locality #	UCMP locality #	Locality synonum	Site name	Abbreviation	Formation	NALMA
C2015	V99490	—	High Dead Squirrel 2	HDS2	Six Mile Creek	Early Barstovian
C2014	V99490	—	High Dead Squirrel 3	HDS3	Six Mile Creek	Hemingfordian
C2013	V99215	MV7325	Dead Squirrel 4	DS4	Six Mile Creek	Hemingfordian
C2012	V99491	MV7325	Dead Squirrel 3	DS3	Six Mile Creek	Hemingfordian
C2011	V99211	—	Snowfence Turtle 3	ST3	Six Mile Creek	Hemingfordian
C2010	V99210	—	Snowfence Turtle 2	ST2	Six Mile Creek	Hemingfordian
C2009	V99209	—	Snowfence Turtle 1	ST1	Six Mile Creek	Late Arikareean
C2008	V99094	MV7338	Snowfence west	SFw	Six Mile Creek	Late Arikareean
C2007	V99094	MV7338	Snowfence east	SFe	Six Mile Creek	Late Arikareean
C2006	V99092	MV7328	West Railroad Cut	WRC	Six Mile Creek	Late Arikareean
C2005	—	MV7337	Whiskey Springs 4	WH4	Renova / Six Mile Creek	Late Arikareean

APPENDIX FOR CHAPTER 2

A1.1. Radiometric dating of the RCS

To improve our comparison to the global record, we provide the first absolute age model for the RCS, using U/Pb dating of zircons extracted from three volcanic ash layers found above and below an erosional unconformity that separates the Renova and Six Mile Creek formations. These new geochronologic results are compared with previously published magnetostratigraphic data (Barnosky et al., 2007; Zheng, 1996) and used build a robust age model for the RCS. Prior to this study, the age of the RCS was poorly constrained. Interpretation of biostratigraphic and magnetostratigraphic data by Barnosky et al. (2007) pointed to a ca. 17.3–13 million year old age for the RCS (Zheng, 1996). This contrasts with a revised age model by Retallack (2009) who proposed that RCS sediments were deposited between 16.4–10.7 Ma based on a revised geologic time scale and by constraining plausible alternative age estimates using faunal biostratigraphic data (Retallack, 2009).

A1.1.1. Geochronology methods.—Within the measured stratigraphic section a series of volcanic ash layers were identified and sampled for zircon U-Pb geochronology (Fig. A1.1). Four ash layers were dated from within the composite section, three collected from Whiskey Springs 4 (RCS1-RCS3) and one from High Dead Squirrel 2 (RCS4).

Zircon crystals concentrated from whole-rock ash samples were picked under a binocular microscope, mounted in epoxy resin, and polished to expose the interior of the grain prior to cathodoluminescence imaging. U-Pb geochronologic analyses were first conducted by laser ablation inductively coupled plasma mass spectrometry (LA-ICP-MS) at the Arizona Laserchron

Center, using a Photon Machines Analyte G2 laser coupled to a Nu Plasma multicollector ICP-MS. Instrumental bias, drift, and inter-element fractionation corrections were performed by the standard-sample bracketing approach, using an in-house Sri Lanka zircon crystal with a known age of 563.5 ± 3.2 Ma (Gehrels et al., 2008) as primary reference material. After LA-ICP-MS analyses, one of our samples from the Whiskey Springs 4 interval (RCS3) was selected for further high-precision dating by chemical abrasion–isotope dilution–thermal ionization mass spectrometry (CA-TIMS), in order to validate the accuracy of the new absolute-age model proposed herein. Select zircons were plucked out of the epoxy mount and subjected to a modified version of the chemical abrasion CA-TIMS method of (Mattinson, 2005) at the MIT isotope geochemistry laboratories.

A1.1.2. LA-ICP-MS U-Pb geochronologic analyses.—Analyses conducted at the Arizona Laserchron laboratory were performed using a laser-beam diameter of 20 µm, firing at a repetition rate of 7 Hz for approximately 14 seconds and using a constant energy fluence of ~7.0 J cm^{-2} on the sample surface. All Pb masses (i.e., 208, 207, 206 and 204) were simultaneously monitored using discrete-dynode ion-multipliers, while ^{232}Th and ^{238}U were measured using Faraday detectors equipped with 3 x 10^{11} Ω resistors. Data processing and uncertainty calculations follow the approach described in Ibañez-Mejia et al. (2014) for time-resolved analyses using ion-multipliers. To assess age accuracy, zircon crystals with a well-established ID-TIMS age of 48.22 ± 0.02 Ma (M.P. Eddy and M. Ibañez-Mejia, unpublished) were frequently analyzed and treated as unknowns during the analytical session; a calculated age of 48.59 ± 0.50 Ma (2σ, n = 58, MSWD = 1.3) using the LA-ICP-MS data indicates that the results are accurate within the quoted uncertainties of ~1–1.5%. Eruption ages discussed in the text are weighted mean ^{206}Pb/^{238}U values, and the quoted uncertainty represents the final propagation of

within-run analytical uncertainties, reproducibility of the primary reference material, and sources of systematic error (i.e., standard calibration and U decay constant uncertainties).

A1.1.3. CA-TIMS U-Pb geochronologic analyses.—Selected crystals previously dated by LA-ICP-MS and plucked out of the epoxy resin were subjected to a modified version of the chemical abrasion method of Mattinson (2005). Zircons were annealed in quartz crucibles in a muffle furnace at 900°C for 60 hours, chemically abraded using a single abrasion step in concentrated HF at 205°C for 12 hours, and processed for isotope dilution thermal ionization mass spectrometry (ID-TIMS) using the EARTHTIME ^{205}Pb-^{233}U-^{235}U mixed tracer (Condon et al., 2015). U-Pb dates and uncertainties were calculated using U-Pb Redux (Bowring et al., 2011), using the algorithms of McLean et al. (2011) and the U decay constants of Jaffey et al. (1971). ^{206}Pb/^{238}U ratios and dates were corrected for initial ^{230}Th disequilibrium using a Th/U$_{[magma]}$ of 2.8 ± 1.0. All common Pb in the analyses was attributed to laboratory blank and subtracted based on the measured laboratory Pb isotopic composition at MIT and associated uncertainty. Quoted errors for individual analyses are presented in the form ±X(Y)[Z] following the scheme of Schoene et al. (2006), where X is solely analytical uncertainty, Y is the combined analytical and tracer uncertainty (i.e., ±<0.03%; McLean et al., 2015), and Z is the combined analytical, tracer and ^{238}U decay constant uncertainty (i.e., ±0.108%; Jaffey et al., 1971). The weighted mean age error includes analytical uncertainties based on counting statistics, mass fractionation correction, spike and blank subtraction, and ^{230}Th disequilibrium correction, and is appropriate when comparing to other ^{206}Pb/^{238}U ages obtained with spikes cross-calibrated with the EARTHTIME gravimetric standards.

A1.1.4. Geochronology results.—Isotopic results and corresponding concordia diagrams from zircon U-Pb analysis using the LA-ICP-MS and CA-TIMS methods are presented in Tables

A1.4. and A1.5., and Figure A1.2. The two ash layers collected within the WH4 interval, near the top of the Renova Formation (RCS1 at 31.2 m in WH4) and the base of the Six Mile Creek Formation (RCS3 at 75 m in WH4), yielded zircon crystallization ages of 22.65 ± 0.37 Ma (2σ, n = 23, MSWD = 2.0) and 21.24 ± 0.27 Ma (2σ, n = 26, MSWD = 1.1), respectively. The third dated horizon, corresponding to a tuff in the upper portion of the Six Mile Creek Formation (RCS4 at 339.9 m in HDS2), yielded a zircon crystallization age of 15.76 ± 0.22 Ma (2σ, n = 21, MSWD = 1.0). A fourth ash layer collected from WH4 (RCS2 at 68.5 m) yielded an age distribution dominated by older inherited zircons and was therefore not included in the age model for the RCS. Further refinement of the age obtained for sample RCS3 by the CA-TIMS method resulted in a $^{206}Pb/^{238}U$ weighted-mean crystallization age of $21.217 \pm 0.027/0.031/0.039$ Ma (2σ, n= 7, MSWD= 0.67), which is in excellent agreement with the initial LA-ICP-MS result and thus provides further support to the accuracy of our new proposed age model. Based on these new dates, we observe that the sedimentation rate between RCS1 and RCS3 was ~31.8 m Ma^{-1} and between RCS3 and RCS4 was ~48.1 m Ma^{-1} (Fig. A1.3). These data suggest that deposition of the Six Mile Creek Formation was associated with a >50% increase in sedimentation rate.

A1.1.5. Revised age estimate for the Railroad Canyon sequence.—The new U-Pb dates from zircons preserved in ashes indicate that the RCS ranges in age from ca. 22.9–15.2 Ma (see Appendix A1.2. for discussion of age model calculations), suggesting that the RCS is ca. 5 Ma older than previously suggested (ca. 17.3–13 Ma from Zheng, 1996; Barnosky et al., 2007; 16.4–10.7 Ma from Retallack, 2009). These new age constraints indicate that the RCS captures pre-MMCO warming as well as build up to peak warming during the global MMCO, rather than documenting peak warming and subsequent cooling (e.g., Retallack, 2009).

However, an alternative possibility is that our substantially older dates for the RCS could be a result of inheritance, producing inaccurate eruption ages. Several observations help us to reject this interpretation: 1) the reported weighted means for the three dated intervals result in ages that progressively decrease up-section, thus not violating stratigraphic first principles, 2) the three horizons from which weighted mean ages are reported contain a proportion between 85 to 95% of zircons with apparent $^{206}Pb/^{238}U$ dates that are statistically undistinguishable, thus validating the hypothesis that they represent a single population within the assigned uncertainties, and 3) although one ash layer collected from the Renova Formation (sample RCS2 at 68.5 m in WH4) yielded a zircon age distribution clearly dominated by inheritance (Table A1.5), indicating an important component of Late Cretaceous detritus being delivered to the Miocene basins of the RCS, the other three dated samples have virtually no zircons with pre-Cenozoic ages, thus suggesting that an inherited zircon component is not prevalent in these horizons. In addition, high-precision CA-TIMS analyses obtained for seven zircons from sample RCS3 also define a statistically single population, and are in excellent agreement with the age obtained by LA-ICP-MS (Table A1.6). Altogether, these lines of evidence support the notion that the reported ages accurately reflect the age of the volcanism that deposited these ash horizons and are not detrital ages influenced by reworking.

A1.1.6. Chrono- and biostratigraphic revisions based on new RCS age model.—At ca. 70 m in the composite section (in WH4) there is an erosional unconformity, regionally termed the "mid-Tertiary unconformity" (MTU), that separates the white beds of the Renova Formation from the predominately buff/pink beds of the Six Mile Creek Formation. The MTU has been widely discussed in paleontological and geological studies in the NRM (e.g., Fields et al., 1985; Hanneman and Wideman, 1991; Barnosky, 2001; Rasmussen, 2003; Barnosky et al., 2007) and

is thought to have occurred ca. 17 Ma in southwestern Montana and northwestern Wyoming (late Hemingfordian; Fields et al., 1985; Barnosky and Labar, 1989; Burbank and Barnosky, 1990). Based on these previous studies as well as biostratigraphy and magnetostratigraphy, Barnosky et al. (2007) suggested that the MTU in the RCS occurred between ca. 17.3 Ma and 16.73 Ma. However, given the new age model for the RCS, the age of the MTU in central-eastern Idaho is now bracketed between ca. 21.5 and 21.4 Ma. This new age estimate suggests that the MTU is time transgressive in the region and lends support to the idea of diachronous regional uplift in western North America leading into the early and middle Miocene (Barnosky et al., 2007; Chamberlain et al., 2012).

The new age model for the RCS also indicates that previously used biostratigraphic dates based on local faunas are not necessarily reliable. The majority of faunal data for the RCS comes from two sites, Snowfence east and Snowfence west, that occur between 125 and 177 m in the composite section. Based on our new age model, these faunas date between ca. 19.8 and 18.8 Ma (latest Arikareean; Albright et al., 2008). In contrast, previous workers proposed that the RCS fauna was late Hemingfordian–late Barstovian (ca. 17.5–13 Ma) in age based on how it and nearby faunas (e.g., Mollie Gulch beds)—which were presumed to be coeval (Barnosky et al., 2007)—compared with regional faunas from the NRM (e.g., Barnosky, 2001). This discrepancy in ages suggests that the biostratigraphy of NRM faunas needs to be reassessed. The current NALMA assignments may indicate that certain species (e.g., *Oreolagus and Pliocyon*) appeared earlier in the NRM compared to the west coast or Great Plains, pointing to diachrony in Cenozoic faunas across North America (Tedford et al., 2004). The needed revisions are beyond the scope of the present manuscript, and are posed as problems for further investigation.

A1.2. Age Model Calculations

Herein we report new radiometric ages for three ash horizons preserved within the Railroad Canyon sequence (RCS). This new data paired with magnetostratigraphy data published by Zheng (1996) and Barnosky et al. (2007) have allowed us create an updated and revised age model for the RCS. Age model calculations are based on the most recently updated geologic time scale of Gradstein et al. (2012).

Three new radiometric dates were used to correlate the RCS magnetostratigraphic record with the global geomagnetic polarity time scale (GPTS; Fig. A1.1). This made it possible to assign ages to specific levels within the RCS that were associated with transitions between normal and reversal magnetic events. Based on this chron ages (Ma) were graphed against meter level height within the RCS and show that sedimentation rates were not constant throughout the RCS (Fig. A1.3). These data were then fit with a polynomial model, which produced the following equation:

$$T = 0.04258 \times M + 0.001616 \times M^2 + 0.00001599 \times M^3 + 0.00000007644 \times M^4$$
$$+ 0.000000000176 \times M^5 + 0.0000000000001559 \times M^6 + 22.48 \qquad (A1)$$

where T is the age in millions of years ago (Ma) and M is the height (in meters) in the composite RCS of the sample of interest. This is the age model used to calculate the age range of the RCS (22.9–15.2 Ma) as well as the age of individual paleosol samples analyzed throughout.

A1.3. Phytolith extraction and assemblage analysis

A1.3.1. Phytolith extraction procedure.—The details of this extraction procedure are covered in detail in Strömberg (2005). To briefly summarize: 1 g of rock was ground with a mortar and pestle, treated with hydrochloric acid to remove carbonates, and large particles were removed using a 250 μm sieve. The sample was treated with Schultze's solution, deflocculated using a 53 μm sieve, and centrifuged with zinc bromide-based heavy liquid to separate phytoliths and other bio-opal from the sediment. Lastly, two slides were made for each sample, one fixed slide using Cargille Meltmount (refractive index = 1.539), and one using immersion oil.

A1.3.2. Phytolith assemblage analysis.—Four-hundred to five-hundred individual phytoliths were counted in each sample to achieve a representative count (>250 diagnostic phytoliths, see below) that yields statistically reliable results (Strömberg, 2009). The remainder of the slide was then scanned for the presence of ecologically important, but rare, morphotypes missed in the original count (these were not included in our quantitative analyses).

Spatiotemporal changes in vegetation structure (e.g., transition from closed to open habitat) were estimated using the relative abundance of FI phytoliths within the sum of FI TOT and GSSC (FI-t ratio; Strömberg et al., 2007b); in addition, the relative abundance of closed-habitat grasses (e.g., bamboos and early-diverging grasses) provides information about habitat openness. Changes in the relative abundances of potential C_4 grasses (minimum and maximum estimates, see below) in the assemblage as a whole were also tracked because comparisons of this metric to the C_4 estimate from stable carbon isotopes are informative in terms of the composition of the PACMAD grass community.

Early-diverging grasses and members of the BEP clade (which contains forest and wetland grasses in the Bambusoideae and Ehrhartoideae) as well as open-habitat grasses in the

Pooideae all exclusively use the C_3 photosynthetic pathway. On the other hand, the PACMAD

clade contains plants that employ both C_3 and C_4 photysunthesis, many of which are open-habitat

adapted today (Aliscioni et al., 2012). Both minimum and maximum estimates of potential C_4

grass cover were estimated following analytical methods published by Strömberg and McInerney

(2011) to account for our current inability to separate GSSC morphotypes produced by C_4 and C_3

PACMAD grasses (McInerney et al., 2011; Erra and Strömberg, 2014). Accordingly, minimum

relative abundances count phytolith forms typically produced in PACMAD subclades that today

include exclusively C_4 species (Chloridoideae) or where C_4 grasses are very abundant

(Panicoideae). Maximum relative abundances count phytolith forms produced by (C_3/C_4) taxa

distributed across the PACMAD clade.

A1.4. Percent C_4 Biomass Calculations from $\delta^{13}C_{org}$

Percent C_4 vegetation was determined using mass balance equations published Wang et

al. (2008), namely:

$$C_3(\%) = [(\delta^{13}C_{SOM} - \delta^{13}C_{C4})/(\delta^{13}C_{C3} - \delta^{13}C_{C4})] \times 100 \qquad (A2)$$

and

$$C_4(\%) = 100 - C_3(\%) \qquad (A3)$$

where $\delta^{13}C_{C3}$ and $\delta^{13}C_{C4}$ are the mean $\delta^{13}C$ values of C_3 and C_4 plants at a given locality at the

time the paleosol being studied was developed. $C_3(\%)$ and $C_4(\%)$ are percentages of C_3 and C_4

plants in the local vegetation. These equations assume that the $\delta^{13}C_{SOM}$ represents the $\delta^{13}C$ value

of bulk local vegetation. Prior to using these equations, we established end member $\delta^{13}C$ values

for C_3 and C_4 plants living in the RCS during the early-middle Miocene. Considering that

precipitation affects the isotopic composition of C_3 plants (Kohn, 2010), we used local MAP

estimates based on paleosol data (350–800 mm yr^{-1}; Retallack, 2007) to estimate the δ^{13}C value

of pure C$_3$ modern biomass as -26.9‰ based on the dataset published by Kohn (2010). We use

the average isotopic composition of modern C$_4$ biomass of -13‰ as our pure C$_4$ end member

(O'Leary, 1988; Tieszen and Boutton, 1989). These two end members were then corrected for

changes in the δ^{13}C of atmospheric CO_2 during the early-middle Miocene, which was enriched in

^{13}C relative to modern (Tipple et al., 2010). We fit a polynomial model to the δ^{13}C$_{atm}$ values

between 22.93–15.14 Ma published by Tipple et al. (2010) to calculate enrichment of

atmospheric CO_2. The equation for our polynomial model is:

$$\delta^{13}C_{atm} = 1418.07521769 \times T + 187.69726105 \times T^2 + 13.10174893 \times T^3 + 0.50860753$$
$$\times T^4 + 0.01041195 \times T^5 + 0.00008783 \times T^6 + 4410 \qquad (A4)$$

where δ^{13}C$_{atm}$ is the carbon isotopic composition of CO_2 in the atmosphere at time T (millions of

years ago, where 15 Ma = -15). For each paleosol sample, we calculated the δ^{13}C$_{atm}$ for the time

in which that paleosol developed (based on its stratigraphic position in the RCS), determined the

amount of δ^{13}C$_{atm}$ enrichment relative to a modern δ^{13}C$_{atm}$ of -8‰, and then adjusted the C$_3$ (-

26.9‰) and C$_4$ (-13‰) biomass end members accordingly. Finally, these newly adjusted C$_3$ and

C$_4$ end members were plugged into the two equations above and percent C$_3$ and C$_4$ biomass were

calculated.

A1.5. Approach for calculating phytolith assemblage change over time

To measure change in vegetation type, we analyze statistical changes in the composition

of phytoliths assemblages over time. Because only a finite sample of phytoliths can be counted

for each assemblage, we estimate the proportion of specific phytolith morphotypes (or

aggregations of those morphotypes – such as all grassland or forest indicator phytoliths), and

then compare that proportion over time. Explicitly, let the number of phytoliths in morphotype i

be denoted as X_i. Then the proportion of phytoliths of a particular morphotype i relative to all

other morphotypes is $Y_i = X_i / \sum_j X_j$. Although this proportion is a point estimate, its confidence

intervalcan be estimated by bootstrap resampling the phytolith counts.

This ratio Y_i can be compared over time to infer changes in phytolith abundance over

time. Because the data are proportions, Y_i is bounded between 0 and 1. To analyze change, we

use a generalized linear model with a logit link function, which converts the morphotype

proportion to a logarithm of the ratio $Y_i/(1 - Y_i)$, rendering the data suitable for regression

analysis. Thus, the equation fitted to the data has the form $\log\left(\frac{Y_i}{1-Y_i}\right) = B_1 T + B_0$, where the B

values are intercepts and the T value is the time index.

While this approach is straightforward if our confidence in Y_i is comparable over time, in

practice different assemblages will have different Y_i and different sample sizes, causing

uncertainty in the observed Y_i, especially if Y_i is far from 0 or 1 and thus has less certainty.

Therefore, when fitting the equation from above, we need to weigh assemblages we are more

confident in more towards the fit, and weigh less confident estimates less towards the fit. To

accomplish this, when we fit the equation above by finding the optimal sum of squares that

minimizes the squared distance of all points to the trend line, we weight the squared distance of

each Y_i from the fit proportionally to our confidence in it.

We choose the simple weight function $1/(Y_i^{upper} - Y_i)$, where Y_i^{upper} is the upper bound

of Y_i. Note, however, that this weight function is 0 when $Y_i = Y_i^{upper} = 0$, a common occurrence

when the morphotype is simply not present in the sample. To circumvent this, a small weight was introduced into the denominator of the weight function $1/\left(\left(Y_i^{upper} - Y_i\right) + w\right)$, which makes it possible to easily vary the balance between weighing all assemblages over time equally and weighing assemblages with higher confidence more.

Ultimately, after applying this methodology, it is possible to interpret the change over time of Y_i in light of varying w. P-values are provided for each analysis which allows for testing the hypothesis that the slope of the weighted regression line is different from zero. However, R^2 values are not provided for these weighted logistic regressions because there is no consensus in the statistical community for how to calculate R^2 for logistic regression, let alone how it should be calculated (or interpreted) for weighted logistic regression (see reviews in Menard, 2000; Mittlbock and Schemper, 1996).
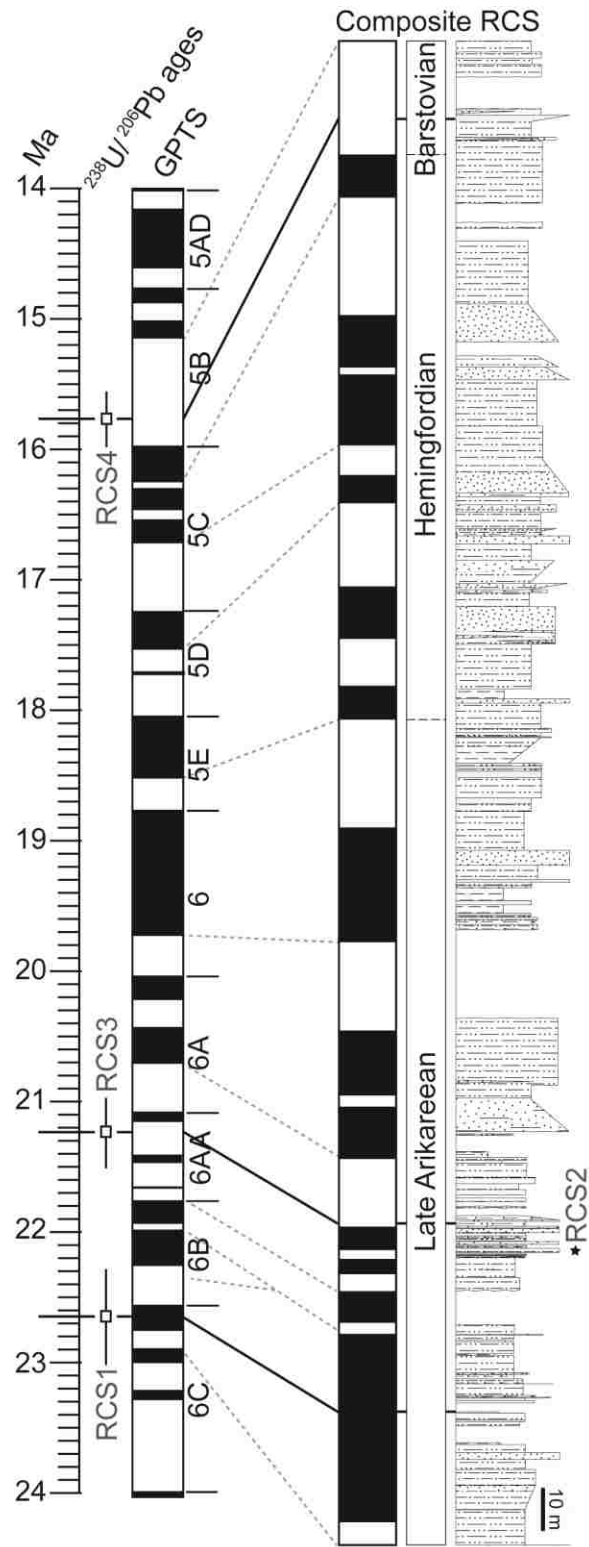
Figure A1.1. Correlation of the Railroad Canyon Sequence (RCS) magnetostratigraphy (Zheng, 1996) with the global geomagnetic polarity time scale (GPTS; Gradstein et al., 2012). Isotopic age determinations are from U-Pb dating of three ash horizons (RCS1, RCS3, RCS4) that can be directly tied from the RCS into the GPTS (solid black lines). Grey dashed lines show possible chron correlation of rock units. North American land Mammal Age (NALMA) durations and age boundaries are from Woodburne (2004) and Albright et al. (2008). Star denotes location of reworked ash, RCS2.
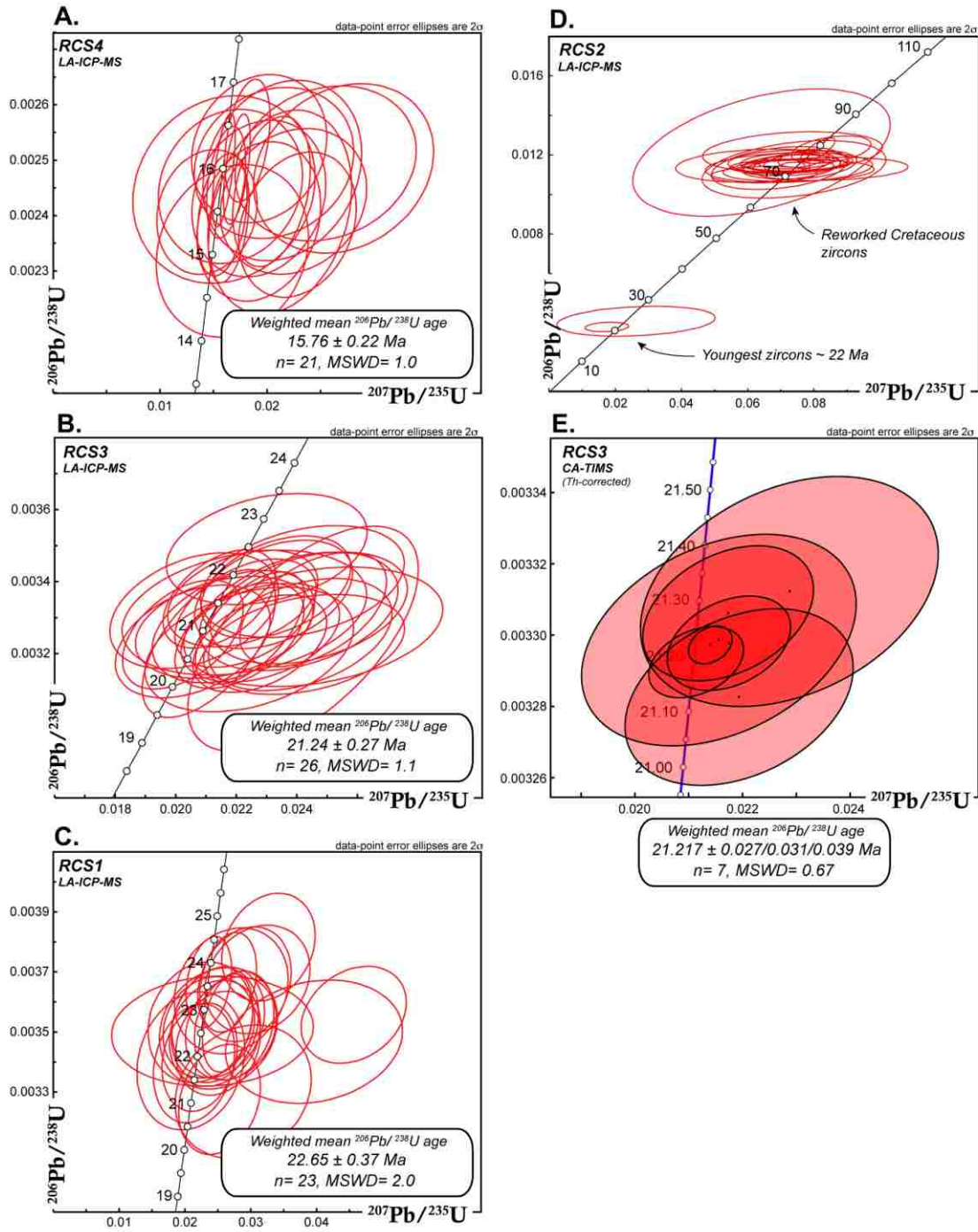
Figure A1.2. U-Pb Concordia diagrams for zircon analyses from four tuffs within the RCS. LA-ICP-MA results for A) RCS4, B) RCS3, and C) RCS1 (Table A1.5). D) LA-ICP-MA results from reworked ash RCS2. E) CA-TIMS results for RCS3 (Table A1.6). All sample error ellipses are plotted at 2σ.
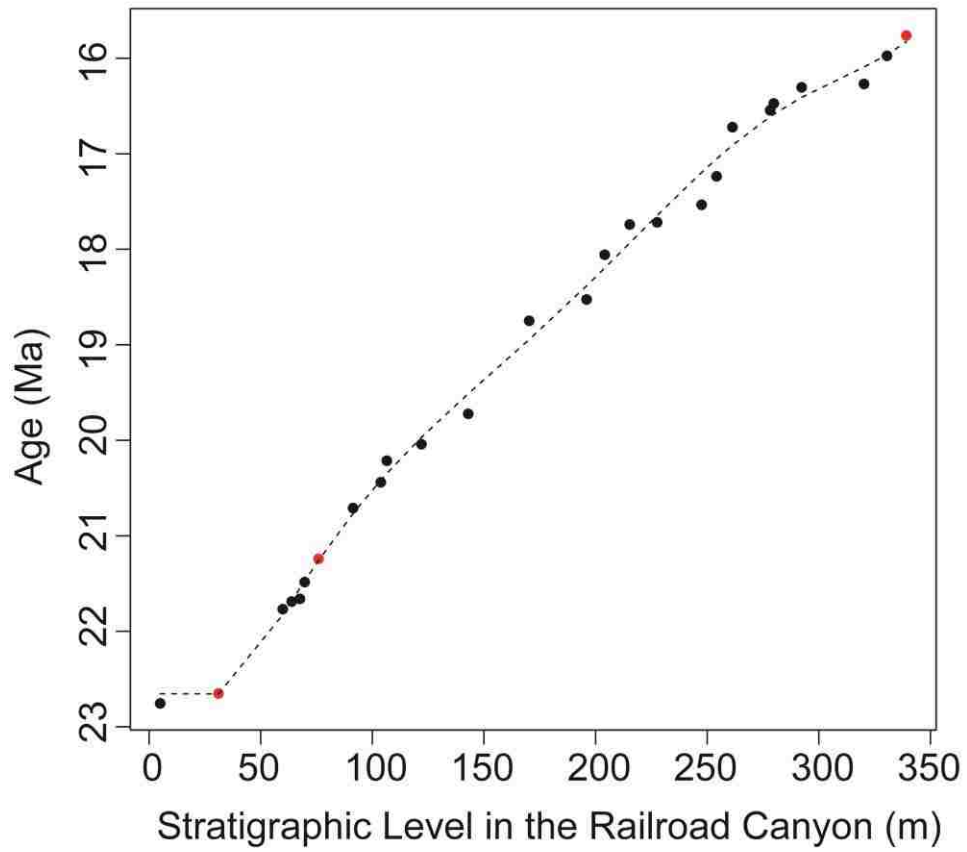
Figure A1.3. Revised age model for the RCS based on new U-Pb dates. Variability in sedimentation rates are apparent. See Appendix for age model equation.
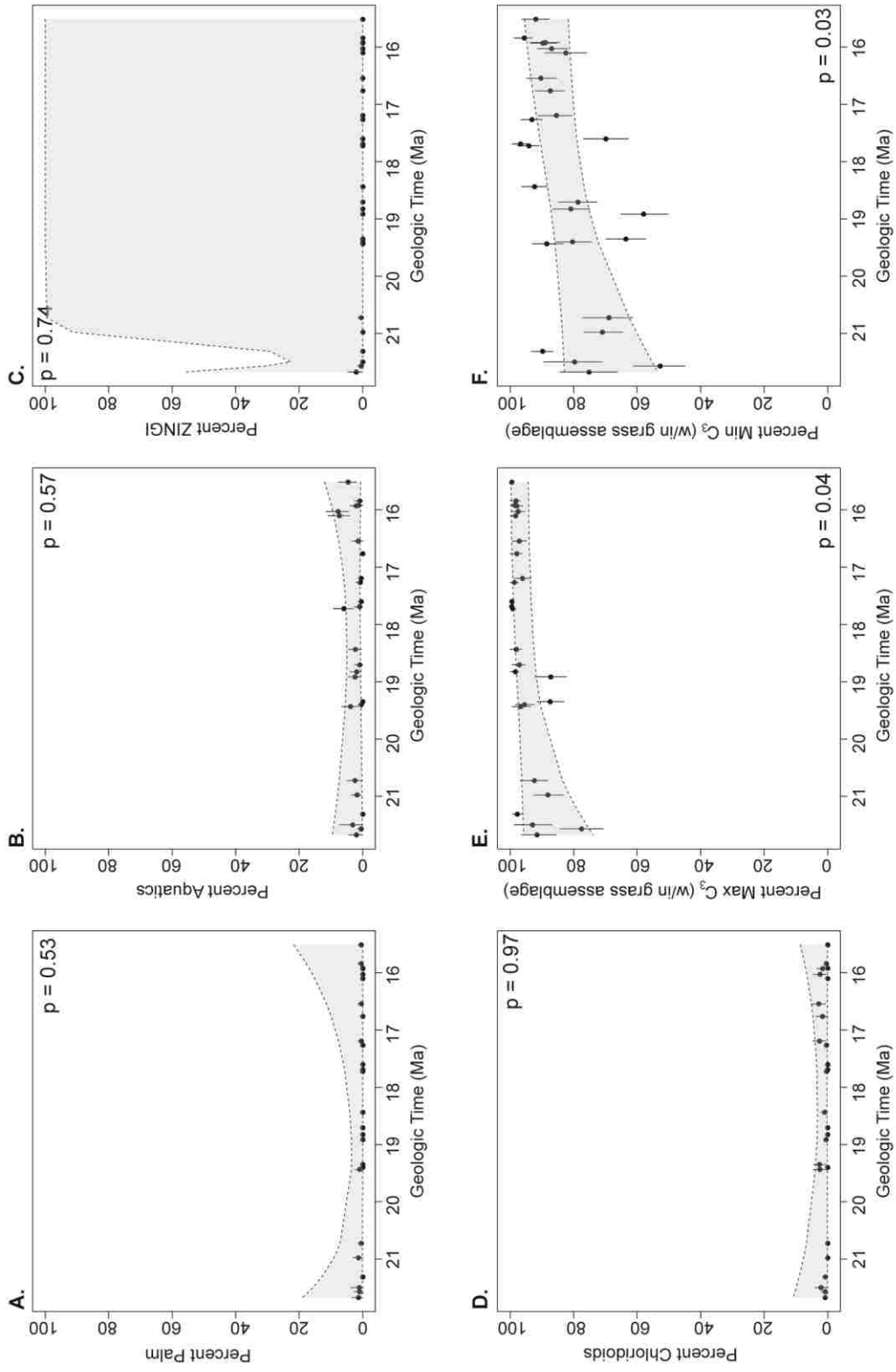
Figure A1.4. Relative abundances of various phytolith vegetation types through time.
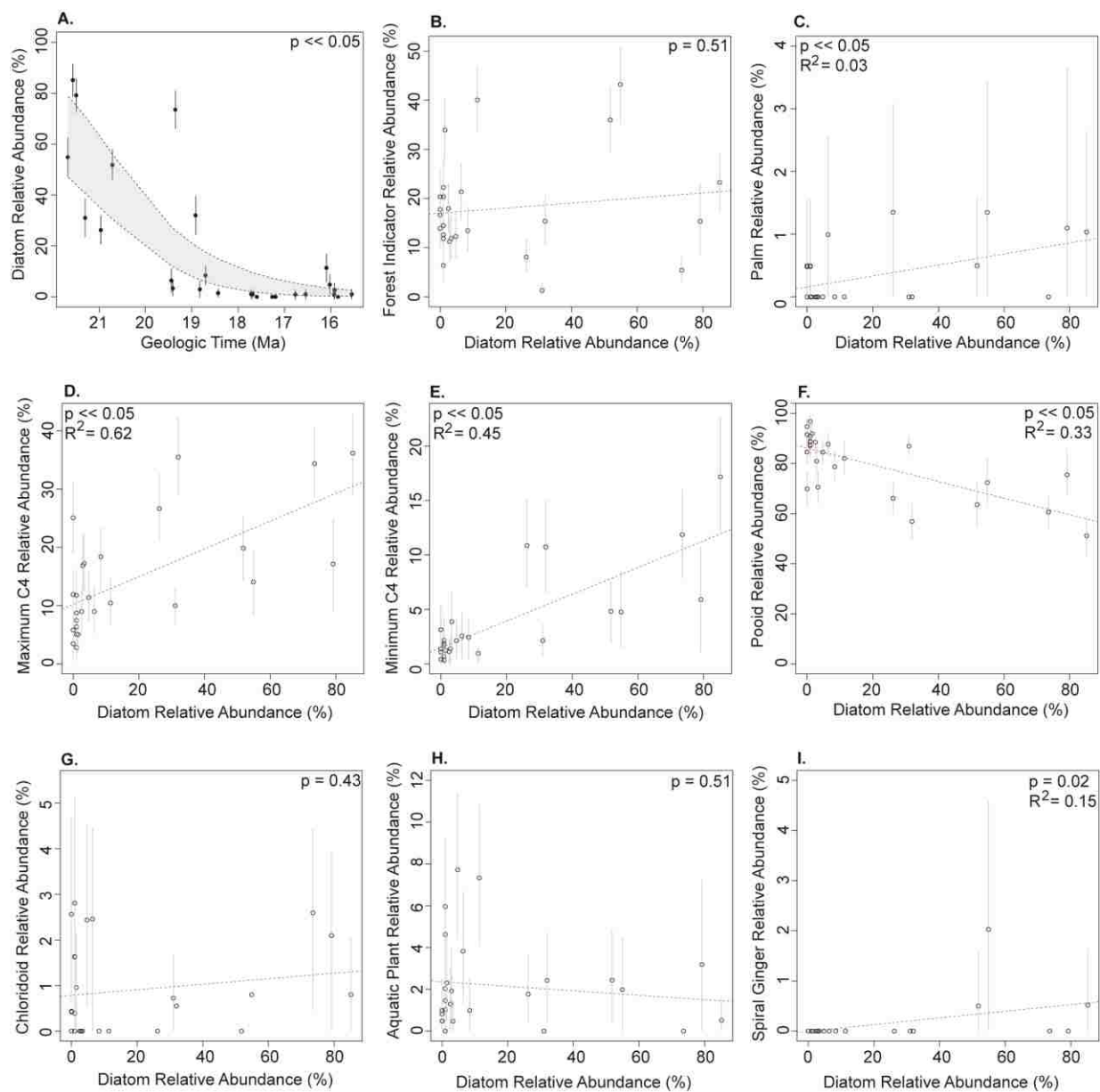
Figure A1.5. A) Relative abundance of diatoms through the RCS. p-value based on 'regression analysis' described in Appendix. B–I) Correlations of different phytolith vegetation types and diatoms in the RCS. Two-tailed p-values are reported.
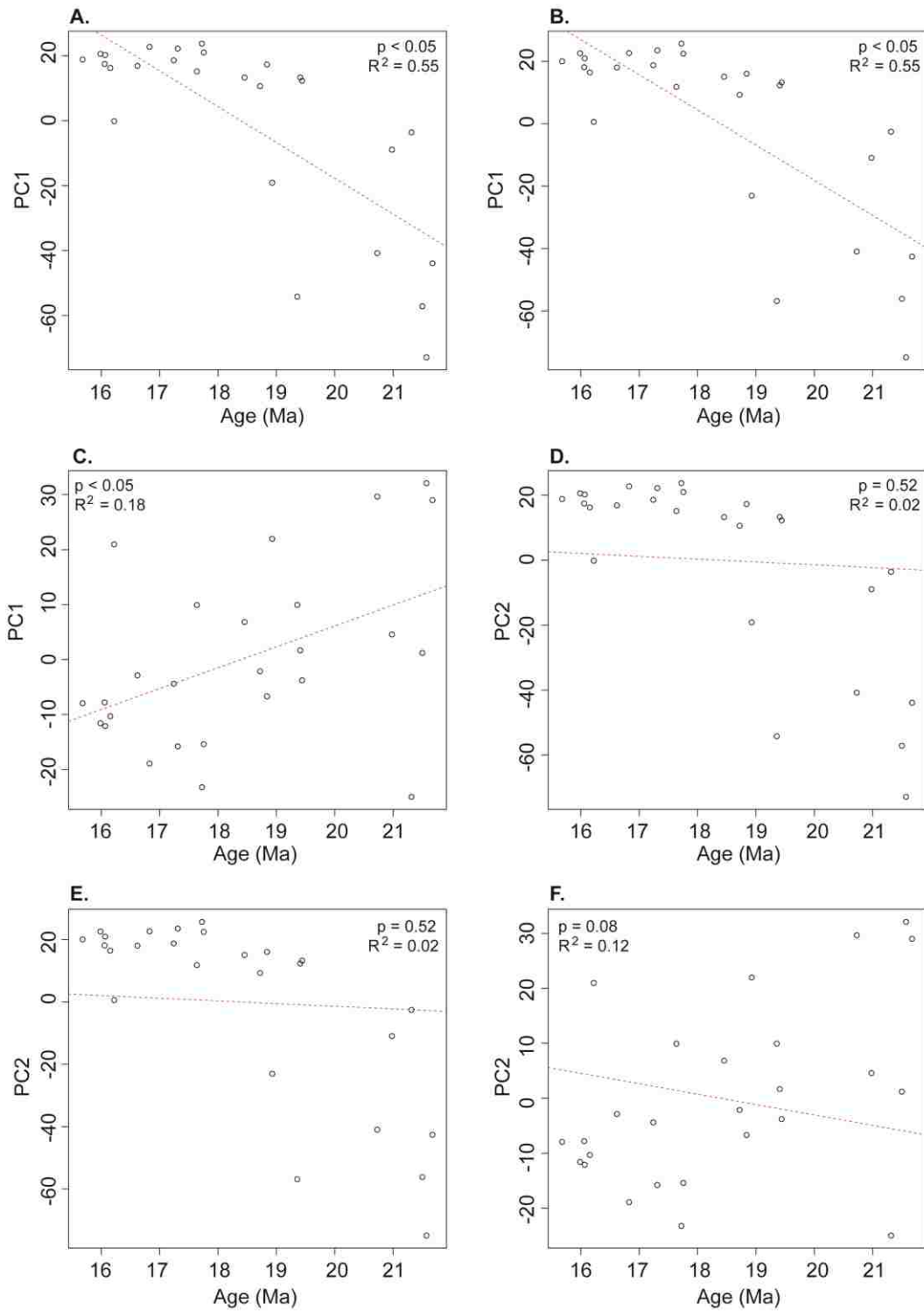
Figure A1.6. Plots of PC1 over time for A) Run 1, B) Run 2, and C) Run 3. Plots of PC2 over time for D) Run 1, E) Run 2, and F) Run 3.
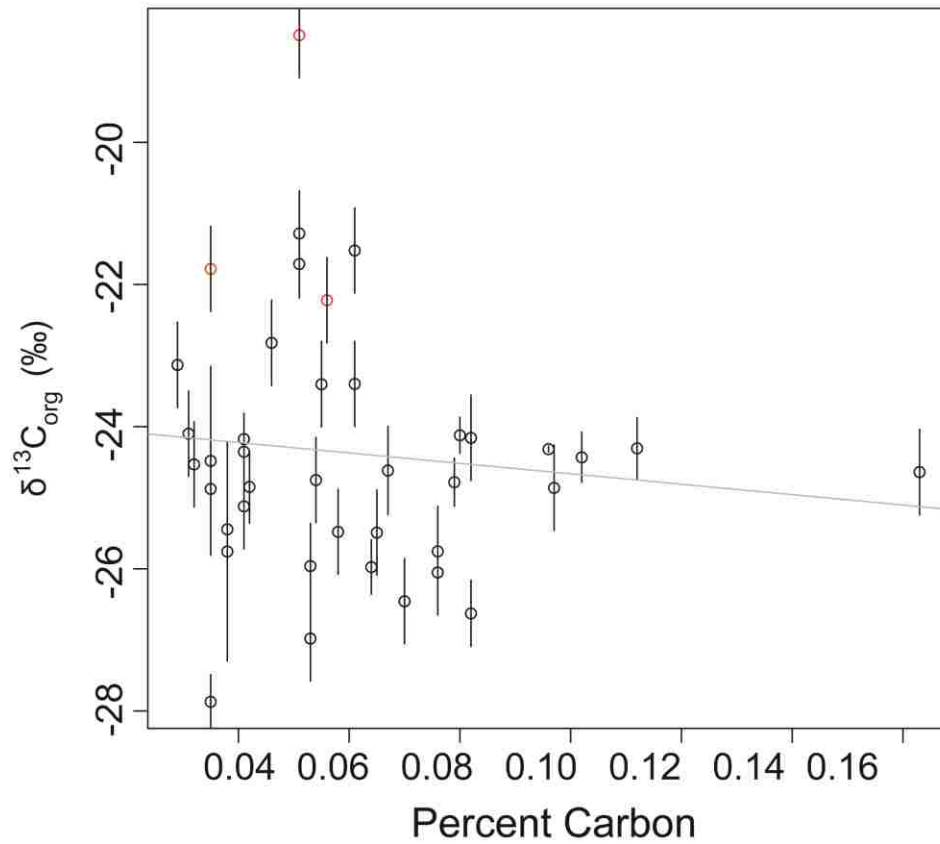
Figure A1.7. Plot of %C_{org} vs. $\delta^{13}C_{org}$ for all RCS samples. The data show that there is no relationship between isotopic composition and percent carbon, indicating that it is unlikely that microbial decomposition or oxidation influenced the isotopic composition of residual carbon in the RCS samples. Red dots highlight samples that would indicate some of the highest %C_4 relative abundances in this study.

Table A1.1. Phytolith assemblage data from the Railroad Canyon. Data reported as percentages of the total number of phytoliths counted in Meltmount™ (permanent mounting medium) slide. Non-GSSC morphotypes: AQ = morphotypes produced by wetland plants (e.g., sedges); ZINGI= morphotypes produced by gingers and relatives; FI = forest indicators; Grass/Mono/Coni = non-diagnostic phytoliths produced by modern grasses, monocots, and conifers. Relative abundance data for diatoms reported as well as presence of chrysophyte cysts and sponge spicules.

Sample #	Abbreviation from Fig. 2.4.	AQ (%)	Palm (%)	ZINGI (%)	Other FI (%)	Grass/Mono/Coni (%)	Other non-GSSC (%)	GSSCs counted in Meltmount (%)	Total phytoliths in Meltmount	Diatom relative abundance (%)	Chrysophyte cysts?	Sponge spicules?	Sample Preservation Quality
PB 30703	a	1.1	0.7	1.1	22.0	10.1	33.6	31.3	268	54.9	few	few	Very good
PB 30614	b	0.3	0.7	0.3	14.4	9.6	23.7	50.9	291	85.1	few	no	Good
PB 30615	c	1.6	0.5	0.0	7.0	12.9	36.6	41.4	186	79.2	few	no	Good
PB 30633	d	0.0	0.0	0.0	0.7	14.0	33.7	51.6	587	31.0	no	no	Good
PB 30648	e	0.8	0.6	0.0	3.1	15.0	38.0	42.4	481	26.2	no	no	Good
PB 30635	f	1.6	0.3	0.3	22.3	7.6	27.1	40.8	314	51.8	no	no	Good
PB 30688	g	2.5	0.6	0.0	12.9	9.4	24.8	49.7	318	6.4	no	no	Good
PB 30649	h	0.3	0.0	0.0	8.6	5.2	22.3	63.6	291	3.3	no	no	Good
PB 30680	i	0.0	0.0	0.0	3.8	10.4	20.5	65.3	346	73.5	no	no	Very good
PB 30651	j	1.9	0.0	0.0	11.8	6.8	14.8	64.6	263	32.0	no	no	Good
PB 30682	k	1.4	0.0	0.0	8.2	5.0	21.3	64.2	282	2.9	no	no	Good
PB 30659	l	0.7	0.0	0.0	9.1	11.1	20.6	58.4	296	8.4	no	no	Good
PB 30683	m	1.6	0.0	0.0	23.5	9.1	20.2	45.6	307	1.5	no	no	Good
PB 30670	n	4.5	0.0	0.0	9.0	5.9	18.7	61.9	289	1.0	no	no	Good
PB 30660	o	0.7	0.0	0.0	8.4	4.4	23.8	62.6	273	1.0	no	no	Good
PB 30654	p	0.3	0.0	0.0	10.8	7.6	27.3	54.0	315	0	no	no	Fair-Good
PB 30655	q	0.4	0.0	0.0	6.7	6.9	44.6	41.4	507	0	no	no	Good
PB 30690	r	0.3	0.3	0.0	11.3	8.8	25.7	53.6	319	0	no	no	Good
PB 30695	s	0.0	0.0	0.0	4.5	4.8	25.4	65.3	291	1.0	no	no	Good
PB 30696	t	1.0	0.3	0.0	15.2	5.2	24.1	54.1	290	1.0	no	no	Good
PB 30698	u	5.4	0.0	0.0	27.4	5.7	20.6	40.9	296	11.4	no	no	Good
PB 30699	v	5.3	0.0	0.0	7.9	6.3	24.5	56.0	318	4.8	no	no	Good
PB 30700	w	1.3	0.0	0.0	9.1	10.7	25.3	53.6	384	1.0	few	no	Good
PB 30685	x	0.7	0.0	0.0	9.0	6.6	42.5	41.2	454	2.5	no	no	Good
PB 30671	y	0.6	0.3	0.0	12.9	7.7	27.0	51.4	311	0	no	no	Good
PB 30672	z	3.5	0.4	0.0	14.4	4.6	19.6	57.5	285	1.0	no	no	Fair-Good

Table A1.2. Grass silica short cell (GSSC) phytolith assemblage data from the Railroad Canyon. Data reported as percentages of the total number of phytoliths counted in oil immersion. Pooid-D = GSSC morphotypes generally diagnostic of pooid grasses; Pooid-ND = GSSC morphotypes commonly abundantly produced by pooid grasses but also by other grasses; PACMAD = GSSC morphotypes produced by grass families that use both the C_3 and C_4 photosynthetic pathways.

Sample #	Abbreviation from Fig. 2.4.	Closed Habitat Grasses (%)	Pooid-D (%)	Pooid-ND (%)	PACMAD (%)	Panicoid (%)	Chloridoid (%)	Other GSSC (%)	Total GSSCs counted in Oil
PB 30703	a	2.2	32.7	24.2	12.9	6.0	0.6	21.4	318
PB 30614	b	1.1	26.9	8.2	17.0	14.8	0.5	31.3	182
PB 30615	c	2.8	32.1	18.9	9.0	3.3	1.4	32.5	212
PB 30633	d	2.3	40.1	29.7	6.4	1.2	0.6	19.8	172
PB 30648	e	3.5	32.2	15.5	12.4	8.5	0.0	27.9	258
PB 30635	f	3.2	27.8	11.1	14.4	4.6	0.0	38.9	216
PB 30688	g	0.6	44.8	21.3	6.2	0.6	1.9	24.7	324
PB 30649	h	6.6	39.7	7.9	10.3	3.0	0.0	32.5	302
PB 30680	i	2.3	25.9	20.6	18.3	7.6	2.0	23.3	301
PB 30651	j	0.8	31.0	11.0	21.6	9.0	0.4	26.1	245
PB 30682	k	0.0	37.6	21.4	12.7	1.2	0.0	27.2	346
PB 30659	l	0.0	31.5	14.5	10.8	1.7	0.0	41.5	241
PB 30683	m	0.4	38.7	32.1	4.4	0.7	0.7	22.9	271
PB 30670	n	4.1	45.0	21.3	3.8	0.3	0.3	25.1	342
PB 30660	o	0.0	43.4	24.4	2.0	0.3	0.0	30.0	357
PB 30654	p	0.0	32.7	13.5	19.5	0.3	0.0	34.0	297
PB 30655	q	1.1	40.0	20.0	3.6	0.6	0.3	34.4	360
PB 30690	r	0.6	30.2	26.7	7.2	0.9	1.7	32.8	348
PB 30695	s	0.0	31.9	36.0	8.2	0.3	1.3	22.4	317
PB 30696	t	2.4	32.4	33.9	5.2	0.0	2.1	23.9	327
PB 30698	u	0.3	39.9	25.1	12.5	1.3	0.0	20.9	311
PB 30699	v	1.9	36.5	28.9	8.2	0.0	1.9	22.6	318
PB 30700	w	0.6	37.6	29.8	6.2	0.3	1.2	24.2	322
PB 30685	x	0.3	34.1	23.1	6.2	0.9	0.0	35.3	337
PB 30671	y	0.6	44.9	20.1	1.8	0.9	0.3	31.4	334
PB 30672	z	0.7	46.3	24.6	5.9	0.4	0.0	22.1	272

Table A1.3. $\delta^{13}C_{org}$ values for sampled paleosols in the Railroad Canyon. Ages are determined by a polynomial interpretation of regional sedimentation rates (see Appendix A1.2).

Sample number	Meter level	Age	$\delta^{13}C_{org}$	St. Dev.	wt. % carbon	n	%C$_4$	%C4 St. Dev.
PB 29587	9.1	22.75	-24.62	0.31	0.07	3	5.4	4.46
PB 30709	14.7	22.80	-23.40	0.3	0.06	1	14.2	4.32
PB 30711	34.25	22.59	-24.16	0.3	0.08	1	8.6	4.32
PB 30712	34.25	22.59	-24.10	0.3	0.03	1	9.0	4.32
PB30612	34.45	22.58	-23.40	0.3	0.06	3	14.0	4.32
PB 30710	74.1	21.33	-26.46	0.3	0.07	1	0	0
PB 30715	70.4	21.46	-25.44	0.3	0.04	1	0	3.78
PB30633	74.6	21.31	-24.64	0.3	0.16	1	5.3	4.32
PB 30713	247	17.25	-24.35	0.22	0.04	3	2.5	3.17
PB 30714	234.75	17.52	-24.87	0.16	0.04	3	0	1.69
PB30635	93.1	20.73	-21.52	0.3	0.06	1	28.0	4.32
PB30688	146.3	19.44	-21.78	0.3	0.04	1	25.6	4.32
PB30649	147.9	19.41	-18.49	0.3	0.05	1	49.3	4.32
PB30680	150.4	19.36	-21.71	0.24	0.05	2	26.0	3.45
PB 29997	150.4	19.36	-21.28	0.3	0.05	1	29.1	4.32
PB 30008	157.5	19.21	-25.48	0.3	0.06	1	0	3.01
PB 30009	158.9	19.18	-25.49	0.3	0.07	1	0	2.90
PB 30010	168	19.00	-22.82	0.3	0.05	1	17.5	4.32
PB 30020	173.75	18.88	-23.13	0.3	0.03	1	15.0	4.32
PB 30015	176.8	18.82	-25.96	0.3	0.05	1	0	0
PB 30023	178.4	18.78	-26.05	0.3	0.08	1	0	0
PB 30659	181.4	18.72	-24.86	0.3	0.10	1	2.3	4.32
PB 30027	184.5	18.65	-24.75	0.3	0.05	1	2.9	4.32
PB 30028	185.1	18.64	-25.12	0.3	0.04	1	0.3	4.32
PB 30683	193.7	18.45	-22.22	0.3	0.06	1	20.7	4.32
PB 30030	200.5	18.30	-24.53	0.3	0.03	1	3.8	4.32
PB 30652	203.75	18.23	-27.87	0.19	0.04	3	0	0
PB 30684	210.25	18.08	-26.98	0.3	0.05	1	0	0
PB 30695	269	16.83	-24.17	0.18	0.04	3	3.0	2.61
PB 30716	271	16.79	-24.78	0.17	0.08	2	0	0.98
PB 30717	278	16.68	-24.30	0.22	0.11	3	1.8	3.11
PB 30696	282.4	16.62	-24.48	0.66	0.04	2	0.4	9.56
PB 30718	300	16.41	-24.85	0.25	0.04	3	0	1.15
PB 30697	307	16.34	-24.32	0.02	0.10	2	1.2	0.31
PB 30719	309.75	16.31	-24.43	0.18	0.10	3	0.4	2.55
PB 30698	319.75	16.22	-24.12	0.13	0.08	2	2.5	1.83
PB 30720	324	16.18	-26.63	0.23	0.08	3	0	0
PB 30699	326	16.15	-25.98	0.19	0.06	2	0	0
PB 30721	330	16.11	-25.75	0.32	0.08	3	0	0
PB 30700	333	16.07	-25.76	0.77	0.04	2	0	0

Table A1.4. Measurement loadings and variance results of Principal Components Analysis of phytolith compound variables.

Run 1

	PC1	PC3	PC3	PC4	PC5	PC6	PC7
Loadings							
Forest indicators	--	0.699	0.649	-0.131	0.259	--	--
Pooids	0.337	-0.653	0.628	--	0.250	--	--
Min potential C4 grasses	-0.118	--	-0.354	--	0.921	--	--
Aquatics	--	--	--	0.986	0.115	--	--
Palms	--	--	--	--	--	-0.869	-0.489
Gingers (ZINGI)	--	--	--	--	--	-0.490	0.870
Diatoms	-0.931	-0.284	0.223	--	--	--	--
Variance							
Percent Variance	0.8037	0.1607	0.0291	0.0036	0.0026	0.0002	0.00006
Cumulative Variance	0.8040	0.9644	0.9935	0.9971	0.9997	0.9999	1.0000

Run 2

	PC1	PC3	PC3	PC4	PC5	PC6	PC7
Loadings							
Forest indicators	--	0.705	-0.403	0.104	-0.567	--	--
Pooids	0.334	-0.649	-0.365	--	-0.570	--	--
Max potential C4 grasses	-0.242	--	0.776	--	-0.573	--	--
Aquatics	--	--	--	-0.993		--	--
Palms	--	--	--	--	0.121	-0.928	0.354
Gingers (ZINGI)	--	--	--	--		-0.346	-0.935
Diatoms	-0.909	-0.275	-0.313	--	--	--	--
Variance							
Percent Variance	0.7808	0.1495	0.0648	0.0034	0.0012	0.0001	0.00006
Cumulative Variance	0.7808	0.9303	0.9951	0.9985	0.9997	0.9998	1.0000

Run 3

	PC1	PC3	PC3	PC4	PC5	PC6
Loadings						
Forest indicators	0.396	0.716		0.559		
Pooids	-0.827			0.548	-0.116	
Max potential C4 grasses	0.397	-0.693		0.591	-0.110	
Aquatics	--		-0.993			
Palms				-0.16	-0.894	-0.419
Gingers (ZINGI)					-0.408	0.907
Variance						
Percent Variance	0.6875	0.2978	0.0101	0.0041	0.0004	0.0001
Cumulative Variance	0.7808	0.9853	0.9954	0.9995	0.9999	1.0000

Table A1.5. U-Pb geochronologic analysis data for zircons from Railroad Canyon section tuffs by LA-ICP-MS.

Analysis	U (ppm)	U/Th	Isotope ratios								Apparent dates (Ma)							
			206Pb/204Pb	206Pb*/207Pb*	±(%)	207Pb*/235U*	±(%)	206Pb*/238U	±(%)	error corr.	206Pb*/238U*	±1s (Ma)	207Pb*/235U	±1s (Ma)	206Pb*/207Pb*	±1s (Ma)	Best date (Ma)	±(Ma)
RCS1_01	34	1.6	353	21.810	14.4	0.0223	14.6	0.0035	2.3	0.16	22.7	0.5	22.4	3.2	-10.2	348.9	22.7	0.5
RCS1_06	57	1.1	3179	10.741	6.9	0.0456	7.2	0.0036	1.9	0.26	22.9	0.4	45.3	3.2	1489.9	130.9	22.9	0.4
RCS1_07	69	1.2	1096	17.674	8.7	0.0275	9.0	0.0035	2.1	0.23	22.7	0.5	27.5	2.4	475.3	193.7	22.7	0.5
RCS1_08	56	1.2	807	19.798	10.8	0.0245	11.0	0.0035	2.2	0.20	22.7	0.5	24.6	2.7	218.5	250.9	22.7	0.5
RCS1_10	59	1.2	1242	19.074	10.3	0.0250	10.5	0.0035	2.0	0.19	22.3	0.5	25.1	2.6	304.2	235.9	22.3	0.5
RCS1_11	184	1.1	3451	19.031	6.4	0.0265	6.6	0.0037	1.8	0.28	23.6	0.4	26.6	1.7	309.3	145.1	23.6	0.4
RCS1_12	57	1.3	852	17.376	9.8	0.0290	10.0	0.0037	2.1	0.27	23.5	0.5	29.1	2.9	512.6	215.1	23.5	0.5
RCS1_13	41	1.7	790	19.303	14.4	0.0251	14.6	0.0035	2.4	0.16	22.6	0.5	25.2	3.6	276.9	331.8	22.6	0.5
RCS1_14	39	1.5	320	21.905	11.6	0.0214	11.8	0.0034	2.4	0.20	21.9	0.5	21.5	2.5	-20.7	280.6	21.9	0.5
RCS1_16	151	1.8	1703	21.402	5.7	0.0236	6.0	0.0037	1.7	0.28	23.6	0.4	23.7	1.4	35.1	137.5	23.6	0.4
RCS1_17	97	1.0	3700	18.390	5.6	0.0265	5.9	0.0035	1.9	0.32	22.7	0.4	26.5	1.5	386.7	125.6	22.7	0.4
RCS1_18	67	1.2	711	19.645	11.3	0.0245	11.5	0.0035	2.1	0.18	22.5	0.5	24.6	2.8	236.4	262.4	22.5	0.5
RCS1_19	43	1.6	951	18.556	12.9	0.0270	13.1	0.0036	2.4	0.18	23.4	0.5	27.1	3.5	366.5	291.1	23.4	0.5
RCS1_20	48	1.2	2807	16.331	10.3	0.0310	10.5	0.0037	2.0	0.19	23.6	0.5	31.0	3.2	647.4	221.7	23.6	0.5
RCS1_21	52	1.3	525	21.197	10.3	0.0222	10.5	0.0034	2.2	0.21	22.0	0.5	22.3	2.3	58.1	246.2	22.0	0.5
RCS1_22	45	0.9	660	17.942	10.3	0.0270	10.5	0.0035	2.0	0.19	22.6	0.5	27.0	2.8	441.8	229.2	22.6	0.5
RCS1_23	53	1.5	645	20.528	11.9	0.0236	12.1	0.0035	2.0	0.16	22.6	0.4	23.7	2.8	134.0	280.4	22.6	0.4
RCS1_24	61	1.9	1310	15.957	8.7	0.0327	8.9	0.0038	2.9	0.22	24.3	0.5	32.6	2.9	697.0	184.8	24.3	0.5
RCS1_25	41	1.7	4390	12.072	13.7	0.0396	13.9	0.0035	2.4	0.17	22.3	0.5	39.4	5.4	1265.4	268.2	22.3	0.5
RCS1_26	42	1.6	403	17.890	9.8	0.0252	10.1	0.0033	2.3	0.23	21.1	0.5	25.3	2.5	448.3	218.6	21.1	0.5
RCS1_28	36	1.0	401	22.471	15.8	0.0209	16.0	0.0034	2.8	0.17	21.9	0.6	21.0	3.3	-82.8	388.6	21.9	0.6
RCS1_29	44	1.7	661	19.991	25.8	0.0242	25.9	0.0035	2.1	0.08	22.5	0.5	24.2	6.2	196.1	609.5	22.5	0.5
RCS1_30	67	1.2	784	19.449	11.3	0.0250	11.5	0.0035	2.1	0.19	22.7	0.5	25.1	2.8	259.5	259.7	22.7	0.5
RCS1_31	48	1.4	670	15.785	14.4	0.0288	14.7	0.0033	2.7	0.19	21.3	0.6	28.9	4.2	720.0	307.1	21.3	0.6
RCS2_01	187	2.6	4675	20.508	12.2	0.0754	12.4	0.0112	2.0	0.16	71.9	1.4	73.8	8.8	136.3	288.4	71.9	1.4
RCS2_02	529	1.7	9687	21.366	5.2	0.0748	5.5	0.0116	1.7	0.30	74.3	1.2	73.3	3.9	39.2	125.2	74.3	1.2
RCS2_03	659	1.2	3371	26.113	15.2	0.0174	15.5	0.0033	2.9	0.19	21.2	0.6	17.5	2.7	-464.7	403.9	21.2	0.6
RCS2_04	1323	2.2	45836	20.832	1.7	0.0811	2.6	0.0123	2.0	0.77	78.5	1.6	79.2	2.0	99.4	39.7	78.5	1.6
RCS2_06	352	1.9	4358	19.879	5.3	0.0852	5.8	0.0123	2.3	0.40	78.7	1.8	83.0	4.6	209.0	123.5	78.7	1.8
RCS2_08	194	1.7	1859	18.841	36.2	0.0263	37.2	0.0036	8.6	0.23	23.1	2.0	26.3	9.7	332.0	846.1	23.1	2.0
RCS2_10	297	2.4	11835	21.505	9.1	0.0747	9.3	0.0117	1.7	0.18	74.7	1.3	73.1	6.6	23.6	219.6	74.7	1.3
RCS2_11	289	1.7	8424	23.408	10.0	0.0649	10.1	0.0110	1.5	0.15	70.6	1.1	63.9	6.3	-183.9	249.9	70.6	1.1
RCS2_12	319	1.9	11334	22.393	9.1	0.0703	9.2	0.0114	1.2	0.14	73.2	0.9	69.0	6.1	-74.3	222.5	73.2	0.9
RCS2_14	140	2.3	18176	11.626	3.2	0.3857	5.5	0.0325	4.4	0.81	206.3	9.0	331.2	15.4	1338.5	61.8	206.3	9.0
RCS2_15	211	1.1	8192	25.075	15.8	0.0631	16.1	0.0115	3.0	0.18	73.5	2.2	62.1	9.7	-358.7	411.0	73.5	2.2
RCS2_16	325	2.2	8331	23.002	6.1	0.0683	6.3	0.0114	1.4	0.23	73.0	1.1	67.1	4.1	-140.4	152.0	73.0	1.1
RCS2_17	928	3.1	15584	21.557	2.5	0.0724	2.7	0.0113	1.1	0.42	72.6	0.8	71.0	1.9	17.9	60.0	72.6	0.8
RCS2_18	123	0.9	4721	26.069	22.3	0.0642	24.8	0.0121	10.8	0.44	77.7	8.4	63.1	15.2	-460.3	594.3	77.7	8.4
RCS2_20	148	1.4	8942	22.811	14.7	0.0735	15.3	0.0122	3.4	0.23	78.0	2.6	72.1	10.5	-119.8	364.5	78.0	2.6
RCS2_21	242	0.9	8772	21.632	14.0	0.0725	14.3	0.0114	2.7	0.19	72.9	2.0	71.0	9.8	9.5	338.1	72.9	2.0
RCS2_22	157	1.9	7260	22.500	11.4	0.0695	12.1	0.0113	3.9	0.32	72.7	2.8	68.2	8.0	-86.0	280.6	72.7	2.8
RCS2_23	274	0.7	3583	18.702	12.1	0.0833	12.3	0.0113	2.1	0.17	72.5	1.5	81.3	9.6	348.8	274.9	72.5	1.5
RCS2_24	334	0.8	11945	21.572	6.2	0.0746	6.3	0.0117	1.3	0.20	74.8	0.9	73.0	4.4	16.2	148.0	74.8	0.9
RCS2_25	372	1.5	16864	21.633	8.1	0.0732	8.3	0.0115	1.9	0.22	73.6	1.4	71.8	5.8	9.4	195.2	73.6	1.4
RCS2_26	255	1.8	4960	22.280	10.1	0.0723	10.3	0.0117	2.0	0.19	74.9	1.5	70.9	7.1	-62.0	247.9	74.9	1.5
RCS2_27	367	2.1	15695	21.188	8.5	0.0749	8.6	0.0115	1.0	0.12	73.8	0.8	73.3	6.1	59.2	204.0	73.8	0.8
RCS2_28	336	1.6	1646	21.022	14.4	0.0740	15.3	0.0113	5.3	0.34	72.3	3.8	72.5	10.7	77.9	343.5	72.3	3.8
RCS2_29	268	3.2	6007	20.551	7.9	0.0772	8.3	0.0115	2.6	0.31	73.8	1.9	75.5	6.0	131.5	185.8	73.8	1.9
RCS2_30	755	2.4	18035	21.234	3.7	0.0769	4.1	0.0118	1.6	0.39	75.9	1.2	75.2	2.9	54.0	89.3	75.9	1.2
RCS3_01	185	1.3	1483	22.203	5.2	0.0206	5.5	0.0033	2.0	0.36	21.4	0.4	20.7	1.1	-53.5	125.6	21.4	0.4
RCS3_02	171	2.2	5024	19.004	5.2	0.0241	5.6	0.0033	2.0	0.36	21.4	0.4	24.1	1.3	312.4	118.0	21.4	0.4
RCS3_03	147	1.4	1538	19.739	5.9	0.0224	6.3	0.0032	2.0	0.35	20.7	0.5	22.5	1.4	225.5	135.8	20.7	0.5
RCS3_04	213	1.2	2897	18.600	4.8	0.0241	5.1	0.0033	2.0	0.38	20.9	0.4	24.2	1.2	361.2	107.2	20.9	0.4
RCS3_05	180	1.1	6421	18.459	5.1	0.0242	6.4	0.0032	3.9	0.61	20.9	0.8	24.3	1.5	378.3	114.2	20.9	0.8
RCS3_06	337	1.2	3363	21.093	3.4	0.0211	4.3	0.0032	2.6	0.61	20.8	0.5	21.2	0.9	69.9	80.4	20.8	0.5
RCS3_07	243	1.6	7875	20.732	1.6	0.0753	2.3	0.0113	1.7	0.73	72.6	1.2	73.7	1.7	110.8	37.6	72.6	1.2
RCS3_08	141	2.0	2872	20.515	7.1	0.0223	7.4	0.0033	2.1	0.29	21.3	0.5	22.4	1.6	135.6	166.9	21.3	0.5
RCS3_09	202	1.3	5051	18.664	3.5	0.0245	4.0	0.0033	1.9	0.48	21.4	0.4	24.6	1.0	353.4	79.8	21.4	0.4
RCS3_10	305	1.0	14697	19.536	5.8	0.0228	4.0	0.0032	1.7	0.43	20.8	0.4	22.9	0.9	249.3	82.2	20.8	0.4
RCS3_11	255	1.3	2230	20.269	3.5	0.0221	3.9	0.0033	1.8	0.47	20.9	0.4	22.2	0.9	163.8	81.3	20.9	0.4
RCS3_12	199	2.4	2178	20.611	4.6	0.0219	5.0	0.0033	1.9	0.39	21.1	0.4	22.0	1.1	124.5	108.3	21.1	0.4
RCS3_13	176	1.7	10031	18.796	5.1	0.0244	5.5	0.0033	1.9	0.35	21.4	0.4	24.5	1.3	337.4	115.8	21.4	0.4
RCS3_14	169	1.8	2161	20.914	5.6	0.0230	5.9	0.0033	1.8	0.31	22.5	0.4	23.1	1.3	90.1	132.9	22.5	0.4
RCS3_16	193	1.5	16376	20.600	1.6	0.1274	2.4	0.0190	1.8	0.74	121.6	2.1	121.7	2.7	125.9	38.2	121.6	2.1
RCS3_17	258	1.9	1365	22.160	3.5	0.0202	4.0	0.0033	1.9	0.47	20.9	0.4	20.3	0.8	-48.8	86.3	20.9	0.4
RCS3_18	323	1.8	1681	21.679	4.7	0.0206	5.1	0.0032	2.0	0.39	20.8	0.4	20.7	1.0	4.3	112.6	20.8	0.4
RCS3_19	217	1.3	3783	20.891	5.3	0.0216	5.5	0.0033	1.8	0.32	21.1	0.4	21.7	1.2	92.7	124.6	21.1	0.4
RCS3_20	632	0.9	3939	19.969	4.2	0.0232	4.6	0.0034	1.8	0.40	21.7	0.4	23.3	1.1	198.6	97.8	21.7	0.4
RCS3_21	219	2.0	3928	19.705	4.4	0.0228	4.7	0.0033	1.7	0.37	21.0	0.4	22.9	1.1	229.5	100.9	21.0	0.4
RCS3_22	224	2.1	1909	20.811	4.3	0.0222	4.6	0.0034	1.6	0.36	21.6	0.4	22.3	1.0	101.8	100.7	21.6	0.4
RCS3_23	355	1.6	2740	21.546	3.1	0.0214	3.5	0.0034	1.7	0.47	21.6	0.4	21.5	0.8	19.1	75.0	21.6	0.4
RCS3_24	337	1.4	14379	20.745	1.2	0.0767	2.1	0.0116	1.8	0.82	74.0	1.3	75.1	1.5	109.3	28.6	74.0	1.3
RCS3_25	394	1.0	6008	20.089	2.6	0.0224	3.3	0.0033	1.9	0.59	21.1	0.4	22.5	0.7	184.6	61.3	21.1	0.4
RCS3_26	233	2.0	1973	18.346	5.3	0.0242	5.6	0.0032	1.8	0.31	20.8	0.4	24.3	1.3	392.1	119.3	20.8	0.4
RCS3_27	119	2.3	1251	18.393	6.8	0.0245	7.1	0.0033	2.1	0.29	21.1	0.4	24.6	1.7	386.4	153.2	21.1	0.4
RCS3_28	205	1.7	2871	20.023	4.0	0.0233	4.3	0.0034	1.7	0.40	21.8	0.4	23.4	1.0	192.4	92.6	21.8	0.4
RCS3_29	215	1.3	3316	20.468	3.9	0.0223	4.3	0.0033	1.9	0.43	21.3	0.4	22.4	0.9	140.9	90.6	21.3	0.4
RCS3_30	165	1.3	2906	19.381	5.4	0.0242	5.7	0.0034	1.9	0.33	21.9	0.4	24.3	1.4	267.5	123.4	21.9	0.4

Table A1.5. *Continued*

Analysis	U (ppm)	U/Th	Isotope ratios								Apparent dates (Ma)							
			206Pb 204Pb	206Pb* 207Pb*	± (%)	207Pb* 235U*	± (%)	206Pb* 238U	± (%)	error corr.	206Pb* 238U*	±1s (Ma)	207Pb* 235U	±1s (Ma)	206Pb* 207Pb*	±1s (Ma)	Best date (Ma)	± (Ma)
RCS4_01	43	1.8	865	13.494	13.4	0.0255	13.6	0.0025	2.3	0.17	16.1	0.4	25.5	3.4	1044.3	271.1	16.1	0.4
RCS4_02	318	1.2	2047	20.967	4.3	0.0162	4.6	0.0025	1.7	0.36	15.8	0.3	16.3	0.7	84.1	101.4	15.8	0.3
RCS4_03	602	0.6	5981	18.745	5.5	0.0199	6.1	0.0027	2.5	0.42	17.4	0.4	20.0	1.2	343.6	124.8	17.4	0.4
RCS4_04	45	1.6	330	20.395	16.4	0.0166	16.6	0.0025	2.3	0.14	15.8	0.4	16.7	2.7	149.4	387.7	15.8	0.4
RCS4_06	68	2.2	2080	14.880	12.3	0.0225	12.5	0.0024	2.2	0.18	15.6	0.3	22.6	2.8	844.1	255.8	15.6	0.3
RCS4_08	66	2.1	750	18.033	13.2	0.0193	13.4	0.0025	2.2	0.16	16.2	0.4	19.4	2.6	430.5	295.7	16.2	0.4
RCS4_10	615	1.3	4511	19.937	2.5	0.0172	3.0	0.0025	1.6	0.55	16.0	0.3	17.3	0.5	202.3	58.0	16.0	0.3
RCS4_11	169	1.7	2519	19.021	6.0	0.0218	6.9	0.0030	3.4	0.50	19.3	0.7	21.9	1.5	310.5	136.6	19.3	0.7
RCS4_12	145	1.1	2068	15.654	12.6	0.0212	12.9	0.0024	3.1	0.24	15.5	0.5	21.3	2.7	737.7	266.6	15.5	0.5
RCS4_14	50	1.4	469	15.956	13.9	0.0214	14.1	0.0025	2.7	0.19	16.0	0.4	21.5	3.0	697.1	297.0	16.0	0.4
RCS4_15	464	1.0	4960	16.975	5.7	0.0231	6.3	0.0028	2.7	0.43	18.3	0.5	23.2	1.4	563.8	123.5	18.3	0.5
RCS4_16	90	1.8	443	23.076	13.2	0.0144	13.3	0.0024	1.9	0.14	15.5	0.3	14.5	1.9	-148.3	328.6	15.5	0.3
RCS4_17	257	1.0	2806	19.249	4.4	0.0182	4.8	0.0025	1.8	0.37	16.3	0.3	18.3	0.9	283.3	101.5	16.3	0.3
RCS4_18	63	1.3	597	17.423	13.1	0.0192	13.3	0.0024	2.4	0.18	15.7	0.4	19.3	2.5	506.8	289.1	15.7	0.4
RCS4_20	172	1.3	3369	19.118	3.8	0.0314	4.4	0.0044	2.2	0.51	28.0	0.6	31.4	1.4	298.8	86.3	28.0	0.6
RCS4_21	43	1.9	362	12.613	12.4	0.0272	12.7	0.0025	2.5	0.20	16.0	0.4	27.2	3.4	1179.2	246.3	16.0	0.4
RCS4_22	38	1.4	295	21.121	21.6	0.0160	21.8	0.0024	2.8	0.13	15.8	0.4	16.1	3.5	66.7	519.1	15.8	0.4
RCS4_23	799	0.9	3401	21.438	2.1	0.0160	2.7	0.0025	1.7	0.62	16.0	0.3	16.1	0.4	31.2	51.4	16.0	0.3
RCS4_24	320	1.5	4411	20.027	4.4	0.0164	4.7	0.0024	1.8	0.39	15.4	0.3	16.5	0.8	191.9	101.5	15.4	0.3
RCS4_25	58	1.2	703	16.656	14.6	0.0206	14.8	0.0025	2.2	0.15	16.1	0.4	20.8	3.0	604.9	317.4	16.1	0.4
RCS4_26	91	2.2	513	14.386	9.6	0.0228	9.8	0.0024	2.2	0.23	15.3	0.3	22.9	2.2	913.9	197.7	15.3	0.3
RCS4_27	103	2.3	1937	16.496	6.9	0.0204	7.3	0.0024	2.3	0.31	15.7	0.4	20.5	1.5	625.8	148.8	15.7	0.4
RCS4_28	198	1.5	1233	20.928	5.7	0.0158	6.0	0.0024	1.9	0.31	15.5	0.3	15.9	0.9	88.6	135.2	15.5	0.3
RCS4_29	87	1.2	984	17.129	12.1	0.0192	12.3	0.0024	2.5	0.20	15.4	0.4	19.3	2.4	544.0	264.4	15.4	0.4
RCS4_30	44	1.6	333	19.227	17.2	0.0167	17.4	0.0023	2.7	0.16	15.0	0.4	16.9	2.9	285.9	394.6	15.0	0.4

Table A1.6. U-Pb geochronologic analysis data for zircons from RCS by CA-TIMS.

	Composition				Isotopic Ratios							Dates (Ma)					
Fraction	Pb_c (pg) [a]	Pb^*/Pb_c [b]	Th/ U [c]	$^{206}Pb/$ ^{204}Pb [d]	$^{208}Pb/$ ^{206}Pb [e]	$^{206}Pb/$ ^{238}U [e, f]	±2σ (%)	$^{207}Pb/$ ^{235}U [e]	±2σ (%)	$^{207}Pb/$ ^{206}Pb [e, f]	±2σ (%)	$^{206}Pb/$ ^{238}U [f, g]	±2σ (abs)	$^{207}Pb/$ ^{235}U [g]	±2σ (abs)	$^{206}Pb/$ ^{207}Pb [f, g]	±2σ (abs)
RCS3																	
z19	0.35	12	0.67	696	0.215	0.003297	0.16	0.02140	1.9	0.047094	1.8	21.221	0.034	21.50	0.40	53	44
z03	0.22	6	0.65	356	0.208	0.003292	0.30	0.02114	4.2	0.046584	4.1	21.189	0.064	21.24	0.88	27	98
z09	0.33	4	0.65	262	0.209	0.003298	0.40	0.0217	5.3	0.047849	5.1	21.224	0.085	21.8	1.1	91	122
z08	0.53	3	0.66	193	0.213	0.003306	0.57	0.0217	7.3	0.047695	7.1	21.28	0.12	21.8	1.6	83	169
z12	0.75	2	0.52	146	0.169	0.003283	0.75	0.0219	9.7	0.048487	9.4	21.13	0.16	22.0	2.1	122	222
z05	1.25	2	0.65	127	0.209	0.003299	0.90	0.0216	12	0.047425	12	21.23	0.19	21.7	2.5	70	275
z04	1.67	2	0.88	116	0.283	0.003312	0.97	0.0229	12	0.050100	12	21.32	0.21	23.0	2.7	199	275

a – Total mass of common Pb.

b – Ratio of radiogenic Pb (including ^{208}Pb) to common Pb.

c – Th contents calculated from radiogenic ^{208}Pb and the ^{207}Pb/^{206}Pb date of the sample and assuming concordance between U-Th and Pb systems.

d – Measured ratio corrected for fractionation and spike contribution only.

e – Measured ratios corrected for fractionation and tracer and blank.

f – Corrected for initial Th/U disequilibrium using radiogenic ^{208}Pb and Th/U[magma] = 2.8.

g – Isotopic dates calculated using the decay constants $\lambda(^{238}U) = 1.55125E-10$ and $\lambda(^{235}U) = 9.8485E-10$ (Jaffey et al. 1971).

APPENDIX: REFERENCES

Albright III, L.B., Woodburne, M.O., Fremd, T.J., Swisher III, C.C., MacFadden, B.J., Scott, G.R., 2008. Revised chronostratigraphy and biostratigraphy of the John Day Formation (Turtle Cove and Kimberly Members), Oregon, with implications for updated calibration of the Arikareean North American Land Mammal Age. J. Geol. 116, 211–237.

Aliscioni, S., Bell, H.L., Besnard, G., Christin, P.A., Columbus, J.T., Duvall, M.R., Edwards, E.J., Giussani, L., Hasenstab-Lehman, K., Hilu, K.W., Hodkinson, T.R., Ingram, A.L., Kellogg, E.A., Mashayekhi, S., Morrone, O., Osborne, C.P., Salamin, N., Schaefer, H., Spriggs, E., Smith, S.A., Zuloaga, F., 2012. New grass phylogeny resolves deep evolutionary relationships and discovers C4 origins. New Phytol. 193, 304–312.

Barnosky, A.D., 2001. Distinguishing the effects of the Red Queen and Court Jester on Miocene mammal evolution in the northern Rocky Mountains. J. Vertebr. Paleontol. 21, 172–185.

Barnosky, A.D., Bibi, F., Hopkins, S.S.B., Nichols, R., 2007. Biostratigraphy and magnetostratigraphy of the Mid-Miocene Railroad Canyon Sequence, Montana and Idaho, and age of the Mid-Tertiary Unconformity west of the Continental Divide. J. Vertebr. Paleontol. 27, 204–224.

Barnosky, A.D., Labar, W.J., 1989. Mid-Miocene (Barstovian) environmental and tectonic setting near Yellowstone Park, Wyoming and Montana. Geol. Soc. Am. Bull. 101, 1448–1456.

Bowring, J.F., McLean, N.M., Bowring, S.A., 2011. Engineering cyber infrastructure for U-Pb geochronology: Tripoli and U-Pb-Redux. Geochemistry, Geophys. Geosystems 12.

Burbank, D.W., Barnosky, A.D., 1990. The Magnetochronology of Barstovian Mammals in Southwestern Montana and Implications for the Initiation of Neogene Crustal Extension in the Northern Rocky Mountains. Geol. Soc. Am. Bull. 102, 1093–1104.

Chamberlain, C.P., Mix, H.T., Mulch, A., Hren, M.T., Kent-Corson, M.L., Davis, S.J., Horton, T.W., Graham, S.A., 2012. The Cenozoic climatic and topographic evolution of the western North American Cordillera. Am. J. Sci. 312, 213–262.

Condon, D.J., Schoene, B., McLean, N.M., Bowring, S. a., Parrish, R.R., 2015. Metrology and traceability of U–Pb isotope dilution geochronology (EARTHTIME Tracer Calibration Part I). Geochim. Cosmochim. Acta 164, 464–480.

Erra, G., Strömberg, C.A.E., 2014. Tracking the deep-time evolution of grasses and grasslands: duilding a key to grass short cell phytolith morphology, in: XI Congreso Latinoamericano de Botânica, Salvador, Bahia, Brazil.

Fields, R.W., Rasmussen, D.L., Tabrum, A.R., Nichols, R., 1985. Cenozoic Rocks of the Intermontane Basins of Western Montana and Eastern Idaho: a summary. Cenozoic Paleogeography of the West-Central United States 9–36.

Gehrels, G.E., Valencia, V.A., Ruiz, J., 2008. Enhanced precision, accuracy, efficiency, and spatial resolution of U-Pb ages by laser ablation–multicollector– inductively coupled plasma–mass spectrometry. Geochemistry, Geophys. Geosystems 9, 1–13.

Gradstein, F.M., Ogg, J.G., Schmitz, M.D., Ogg, G.M. (Eds.), 2012. The Geologic Time Scale 2012. Elsevier, Amsterdam.

Hanneman, D.L., Wideman, C.J., 1991. Sequence stratigraphy of Cenozoic continental rocks, southwestern Montana. Geol. Soc. Am. Bull. 103, 1335–1345.

Ibañez-Mejia, M., Gehrels, G.E., Ruiz, J., Vervoort, J.D., Eddy, M.E., Li, C., 2014. Small-volume baddeleyite (ZrO2) U-Pb geochronology and Lu-Hf isotope geochemistry by LA-ICP-MS. Techniques and applications. Chem. Geol. 384, 149–167.

Jaffey, A.H., Flynn, K.F., Glendenin, L.E., Bentley, W.C., Essling, A.M., 1971. Precision measurement of half-lives and specific activities of 235-U and 238-U. Phys. Rev. C 4, 1889–1906.

Kohn, M.J., 2010. Carbon isotope compositions of terrestrial C3 plants as indicators of (paleo)ecology and (paleo)climate. Proc. Natl. Acad. Sci. U. S. A. 107, 19691–5.

Mattinson, J.M., 2005. Zircon U-Pb chemical abrasion ("CA-TIMS") method: combined annealing and multi-step partial dissolution analysis for improved precision and accuracy of zircon ages. Chem. Geol. 220, 47–66.

McInerney, F.A., Strömberg, C.A.E., White, J.W.C., 2011. The Neogene transition from C3 to C4 grasslands in North America: stable carbon isotope ratios of fossil phytoliths. Paleobiology 37, 23–49.

McLean, N.M., Bowring, J.F., Bowring, S.A., 2011. An algorithm for U-Pb isotope dilution data reduction and uncertainty propagation. Geochemistry, Geophys. Geosystems 12.

McLean, N.M., Condon, D.J., Schoene, B., Bowring, S.A., 2015. Evaluating Uncertainties in the Calibration of Isotopic Reference Materials and Multi-Element Isotopic Tracers (EARTHTIME Tracer Calibration Part II). Geochim. Cosmochim. Acta 164, 481–501.

Menard, S., 2000. Coefficients of determination for multiple logistic regression analysis. Am. Stat. 54, 17–24.

Mittlbock, M., Schemper, M., 1996. Explained variation in logistic regression. Stat. Med. 15, 1987–1997.

O'Leary, M.H., 1988. Carbon isotopes in photosynthesis. Bioscience 38, 328–336.

Rasmussen, D.L., 2003. Tertiary history of western Montana and east-central Idaho: a synopsis, in: G., R.R., Flores, R.M. (Eds.), Cenozoic Systems of the Rocky Mountain Region. Rocky Mountain Section Society for Sedimentary Geology, Denver, pp. 459–478.

Retallack, G.J., 2009. Refining a pedogenic-carbonate CO2 paleobarometer to quantify a middle Miocene greenhouse spike. Palaeogeogr. Palaeoclimatol. Palaeoecol. 281, 57–65.

Retallack, G.J., 2007. Cenozoic Paleoclimate on Land in North America. J. Geol. 115, 271–294.

Schoene, B., Crowley, J.L., Condon, D.J., Schmitz, M.D., Bowring, S.A., 2006. Reassessing the uranium decay constants for geochronology using ID-TIMS U-Pb data. Geochim. Cosmochim. Acta 70, 426–445.

Strömberg, C.A.E., 2009. Methodological concerns for analysis of phytolith assemblages: Does count size matter? Quat. Int. 193, 124–140.

Strömberg, C.A.E., 2005. Decoupled taxonomic radiation and ecological expansion of open-habitat grasses in the Cenozoic of North America. Proc. Natl. Acad. Sci. U. S. A. 102, 11980–4.

Strömberg, C.A.E., McInerney, F.A., 2011. The Neogene transition from C3 to C4 grasslands in North America : assemblage analysis of fossil phytoliths. Paleobiology 37, 50–71.

Strömberg, C.A.E., Werdelin, L., Friis, E.M., Saraç, G., 2007. The spread of grass-dominated habitats in Turkey and surrounding areas during the Cenozoic: Phytolith evidence.

Palaeogeogr. Palaeoclimatol. Palaeoecol. 250, 18–49.

Tedford, R.H., Albright III, L.B., Barnosky, A.D., Ferrusquia-Villafranca, I., Hunt Jr., R.M., Storer, J.E., Swisher III, C.C., Voorhies, M.R., Webb, S.D., Whistler, D.P., 2004. Mammalian Biochronology of the Arikareean Through Hemphillian Interval (Late Oligocene Through Early Pliocene Epochs), in: Woodburne, M.O. (Ed.), Late Cretaceous and Cenozoic Mammals of North America. Columbia University Press, pp. 169–231.

Tieszen, L.L., Boutton, T.W., 1989. Stable carbon isotopes in terrestrial ecosystem research, in: Stable Isotopes in Ecological Research. pp. 167–195.

Tipple, B.J., Meyers, S.R., Pagani, M., 2010. Carbon isotope ratio of Cenozoic CO2: A comparative evaluation of available geochemical proxies. Paleoceanography 25, 1–11.

Wang, G., Feng, X., Han, J., Zhou, L., Tan, W., Su, F., 2008. Paleovegetation reconstruction using d13C of Soil Organic Matter. Biogeosciences 5, 1325–1337.

Zheng, J., 1996. Magnetostratigraphy of a Miocene sedimentary sequencen Railroad Canyon, Idaho. University of Pittsburgh.

CHAPTER 3. Stable isotope compositions from herbivore teeth indicate climatic stability leading into the middle Miocene in Idaho

Elisha B. Harris, Matthew J. Kohn, Caroline A.E. Strömberg

ABSTRACT

To reconstruct local paleoclimate leading into the mid-Miocene Climatic Optimum in the Northern Rocky Mountains, we measured oxygen and carbon isotope compositions of herbivore tooth enamel from the Railroad Canyon section (RCS) of central-eastern Idaho. We investigated how mean annual precipitation (MAP), mean annual temperature (MAT), coldest month mean temperature (CMMT), and temperature seasonality varied during the early–middle Miocene and how the local RCS record compares to global records of climate change during this interval. Isotope compositions of fossil equids and rhinocerotids (*Merychippus* and *Diceratherium*, respectively) were compared across five time bins at 21.98 Ma, 20.23 Ma, 19.1 Ma, 17.92 Ma, and 16.32 Ma. Bulk $\delta^{18}O_{H2O}$ compositions of both taxa indicate meteoric water compositions were unchanged during the early–middle Miocene (consistently ~14.9‰) but were ~2.6‰ higher than meteoric water compositions in that region today. This difference could in part indicate a warmer climate in the RCS during the Miocene and could also be due to topographic uplift in western North America since the Miocene. The presence of palm phytoliths in low abundance through the RCS also suggests warmer MAT and CMMT of ≥11ºC and ≥5ºC, respectively. Serial sampling of enamel suggests seasonal fluctuations in water compositions and temperature. Bulk

δ^{13}C compositions indicate that MAP was 188 ± 104 mm yr^{-1} through the RCS, similar to today's MAP (236 mm yr $^{-1}$), with no significant change through time. The reconstructed semi-arid, seasonal, warm climate for the RCS is in contrast to previously held ideas that the northern Rocky Mountains were regionally warm and wet during the middle Miocene. Our study therefore highlights the importance of studying intervals of global climate change at local–regional scales when trying to assess potential abiotic drivers of biotic change at the ecosystem level.

1. INTRODUCTION

Paleontologists and modern ecologists have increasingly realized the utility of using the fossil record to gain knowledge about ecosystem change in the face of anthropogenically driven global climate change (e.g., Froyd and Willis, 2008). However, most studies of important climatic transitions during the Cenozoic and further back lack the temporal continuity and appropriate geographic scale necessary to assess biotic community and climate change within local ecosystems (e.g., Barnosky, 2001; Bennington et al., 2009). Rather, these studies tend to draw broad, regional- to continental-scale conclusions about climate and biotic change that dampen local-scale signals relevant for understanding ecosystem-level perturbations (see discussion in Barnosky, 2001). Most investigations into ecological changes during the mid-Miocene Climatic Optimum (MMCO) fall into this category (e.g., Barnosky 2001; Barnosky et al., 2003), preventing analysis of linkages between climate and biotic change during this most recent global warming event. Herein, we take a first step to address this issue by reconstructing early–middle Miocene climate from a near-continuous sedimentary record deposited during build up to global warming during the MMCO.

According to Cenozoic global temperature estimates (Zachos et al., 2001, 2008), Earth began to warm during the early Miocene ca. 18 million years ago (Ma) and experienced peak warming during the MMCO ca. 17–14.75 Ma. The MMCO was associated with elevated global atmospheric CO_2 levels in terrestrial settings (500–600 ppm, possibly as high as 850 ppm; Beerling and Royer, 2011) as well as increased global temperatures that were ~3–6°C warmer than today (Flower and Kennett, 1994; You et al., 2009). The MMCO broadly coincided with global-scale ecological transformations as temperate grasslands expanded in geographic range across many continents and mammalian browsers were replaced by grazers in paleocommunities (e.g., Badgley et al., 2008; Barnosky et al., 2003; Blois and Hadly, 2009; Jacobs et al., 1999; Strömberg, 2011; Tedford et al., 2004), yet causal links remain unclear. To test if middle Miocene biotic changes were driven fully or in part by the MMCO continuous, long-term and high temporal-resolution records of local climate associated with plant and animal fossils are necessary. However, to date very few such continuous records that preserve climate information leading into the MMCO have been described from around the world.

One exception is the Railroad Canyon section (RCS) of central-eastern Idaho, USA, which preserves a nearly uninterrupted record of fossil plants, animals, and paleoclimate that spans five million years leading into peak mid-Miocene warming (ca. 22.9 – 15.2 Ma; Fig. 3.1; Barnosky et al., 2007; Harris et al., 2016a, 2016b; Retallack, 2009, 2007; Strömberg, 2005). Using this study system, we aim to test the local-scale effects of the MMCO on biota over macroevolutionary timescales in North America. To do this, we first establish a record of local climate for the RCS prior to and during the MMCO.

Multiple lines of evidence including sedimentary deposits (e.g., occasional gypsum and halite deposits in the Renova Formation; Fields et al., 1985), faunal data (Barnosky and

Carrasco, 2002; Barnosky et al., 2007, 2003), and new biosilica assemblages from the RCS (showing a decrease in diatoms and increase in dry-adapted pooid, open-habitat grasses; Harris et al., 2016b) have been used to suggest that water availability decreased through time in the Northern Rocky Mountains (NRM) as the local climate became increasingly arid during the early–middle Miocene. Conversely, paleosol data suggest the NRM had a warmer and wetter, sub-humid climate during the middle Miocene (Retallack, 2007). To tease apart these contradictory interpretations, we establish a paleoclimate record of precipitation, temperature, and seasonality for the RCS based on new carbon and oxygen stable isotope data from herbivore tooth enamel as well as palm phytolith data. We then compare our new record to published records of climate and biotic change to test the following hypotheses: (1) Local climate became increasingly arid in the RCS; (2) Local climate became warmer through the early–middle Miocene in the RCS coincident with the global MMCO; (3) Warming temperatures were associated with changes in local temperature seasonality; and (4) Faunal changes in the Northern Rocky Mountains occurred in parallel with climate change recorded in the RCS.

2. BACKGROUND

2.1 Geologic setting

The Miocene was a tectonically and biologically active epoch in the geologic history of western North America. Crustal extension led to development of the Basin and Range province by ca. 17.5 Ma, which created dramatic topographic relief in the region through the late Miocene (Atwater and Stock, 1998; Chamberlain et al., 2012; McMillan et al., 2002). Columbia River Basalt flow deposits in eastern Washington, northeastern Oregon, and western Idaho indicate increased regional volcanism ca. 17.5 Ma (Swanson et al., 1979; Liu and Stegman, 2012). The

Yellowstone Hotspot initiated intense volcanic activity in northern Nevada ca. 16 Ma, and, in the course of migrating towards its present location in northwestern Wyoming, it created the Snake River Plain in its path (Pierce and Morgan, 1992).

The RCS of central-eastern Idaho was deposited during the early–middle Miocene (Harris et al., 2016b) and preserves a ~380 m thick sedimentary sequence belonging to the Renova and Six Mile Creek Formations. A transition between these two formations occurs at ~70 m in the composite section and is thought to correspond to the mid-Tertiary unconformity (MTU). Recently, the RCS, whose age had previously been debated, was firmly dated to 22.9–15.2 Ma using U/Pb zircon dating. This new age has challenged local chronostratigraphy and has pushed back the age of the MTU in central-eastern Idaho (now ca. 21.4–21.5 Ma; Harris et al., 2016b).

2.2 Floral and faunal record

The NRM hosts a rich fossil record of both plants (e.g., Graham, 1999; Strömberg, 2011) and mammals (e.g., Barnosky and Carrasco, 2002; Barnosky et al., 2007, 2003; Janis et al., 1998) documenting biotic change during the Cenozoic. Regional floral evidence mainly from phytoliths documents that vegetation dominated by C_3 pooid grasses, but with a low abundance of potential C_4 PACMADs had spread across the NRM by the early Miocene (Chen et al., 2015; Cotton et al., 2012; Harris et al., 2016b; Hyland et al., *in review*; Strömberg, 2005). This can be compared to analyses using compilations of NRM faunal records showing an increase in herbivores with adaptations linked to grazing in faunal communities and a transition from oreodont-, camel- and rhino-dominated communities in the early Miocene to equid-dominated communities in the middle Miocene (Barnosky and Carrasco, 2002; Barnosky, 2001). This

region also experienced to major immigration events at ca. 18.5 Ma and ca. 17.2 Ma (e.g., Woodburne and Swisher, 1995; Woodburne 2004), as well as a radiation of ungulates (Janis et al., 2004) and diversification of endemic clades in the northern Rocky Mountains (Barnosky, 2001) during the early–middle Miocene. Many recent studies have used regional faunal databases to explicitly test for temporal correlation of faunal change, tectonism, and climate change during the early–middle Miocene across the NRM region (e.g., Barnosky and Carrasco, 2002; Barnosky, 2001; Kent-Corson et al., 2013; Kohn and Fremd, 2008). Barnosky (2001) suggested that a peak in mammalian species richness during the late early–middle Miocene was driven by the MMCO (i.e., an increase in mammals adapted to warmer, more arid environments suggest an increase in regional temperatures), while others pointed to increased endemism within the NRM, perhaps as a result of increased topographic heterogeneity over short distances, as a driver of increased faunal diversity ca. 15–16 Ma (Barnosky and Carrasco, 2002; Kohn and Fremd, 2008).

The strata in the RCS was deposited during this interval of increased tectonic activity and faunal change in the early–middle Miocene (Harris et al., 2016b). The RCS paleosol record was described by Retallack (2009) as containing mostly Aridisols but later revision by Harris et al., (2016b) indicates that most soils are actually quite immature (Entisols or Inceptisols) and thus limited in their applicability for climatic reconstructions. Nonetheless, Retallack (2007, 2009) interpreted the record as showing an expansion of short sod grasslands and woodlands in an otherwise sagebrush-dominated habitat in response to the warm-wet climates of the early–middle Miocene. In contrast, local phytolith records and stable carbon isotopic data from the RCS indicate the landscape was an open-habitat, C_3 grassland with a mosaic of woodland patches and a low abundance of C_4 grasses in an increasingly water-limited habitat (Harris et al., 2016b;

Strömberg, 2005). Fossil mammals have been collected from throughout the RCS by Nichols (1979, 1976), Barnosky and colleagues (2007), as well as by Elisha Harris and colleagues from the University of Washington, resulting in large collections at the University of Montana Paleontology Center (UMPC), University of California Museum of Paleontology (UCMP), and University of Washington's Burke Museum of Natural History and Culture (UWBM). See table 2 in Barnosky et al. (2007) for a list of the taxa reported from each locality in the composite RCS. Most fossils come from between 146 m and 255 m, with Snowfence east and west being the most productive field site (Fig. 3.4). Some of the biostratigraphically significant taxa from the RCS include *Merychippus*, *Hypohippus*, *Aepycamelus*, *Diceratherium*, and *Merychyus* (see Barnosky et al., 2007, table 2). We have chosen to focus on equids and rhinos for our isotope analyses because their teeth were found in abundance throughout the RCS.

2.3 Carbon isotopic composition of mammalian tooth enamel

The carbon isotopic composition of mammalian herbivore tooth enamel reflects the isotopic composition of ingested vegetation, with a known offset due to metabolic enrichment (Cerling and Harris, 1999; Koch, 1998; Lee-Thorp and van der Merwe, 1987; Passey et al., 2005). The carbon isotopic composition of plants is influenced by CO_2 fractionation during photosynthesis. Because different plants employ different photosynthetic pathways, this results in distinctly different carbon isotopic compositions in these plants (Ehleringer et al., 1991; O'Leary, 1988; Vogel, 1978). Modern C_3 plants (typically trees, shrubs, and cool-growing-season grasses) have an average $\delta^{13}C$ value of -28.5‰ and range between -20‰ to -37‰ (Kohn, 2010), whereas C_4 plants (warm-growing-season grasses and sedges) have an average $\delta^{13}C$ value of -13‰ and range between -9‰ to -19‰ (Cerling et al., 1997). Metabolic and

biomineralization processes fractionate ingested carbon resulting in $\delta^{13}C$ enrichment between plant material and herbivore enamel that is $14.6 \pm 0.3‰$ for ruminants and $13.3 \pm 0.3‰$ for non-ruminants (Cerling and Harris, 1999; Passey et al., 2005). Ultimately this leads to a correlation between $\delta^{13}C$ diets and enamel such that animals that eat C_3 plants will have enamel depleted in ^{13}C and animals that eat C_4 plants will have enamel enriched in ^{13}C (e.g., Cerling and Harris, 1999). Many studies have used this correlation to infer the diets and habitats of ancient mammals based on the carbon isotopic composition of their teeth (e.g., Boardman and Secord, 2013; Feranec and Macfadden, 2006; Feranec et al., 2009; MacFadden, 2000; Secord et al., 2008). For further discussion of RCS herbivore diets see Harris et al. (2016a).

$\delta^{13}C$ compositions can also be used to estimate mean annual precipitation (MAP) in the fossil record. Many studies have observed a negative relationship between $\delta^{13}C$ values of C_3 plants and MAP (excluding plants living in dense, closed forest understories; Diefendorf et al., 2010; Kohn, 2010; Stewart et al., 1995), resulting from changes in C_3-plant water use efficiency in increasingly arid environments (Heaton, 1999). Because the $\delta^{13}C$ of ingested plants can be calculated from the $\delta^{13}C_{enamel}$ (after correcting for metabolic enrichment), the $\delta^{13}C_{enamel}$ from herbivores in pure C_3 ecosystems can be used to infer MAP (Kohn and McKay, 2012; Kohn, 2010). In times when C_4 plants were not present or abundant, such as the early–middle Miocene of Idaho (Harris et al., 2016b), $\delta^{13}C_{enamel}$ can be applied in this way.

2.4 Oxygen isotopic composition of mammalian tooth enamel

Tooth enamel is made up of the diagenetically resistant mineral hydroxylapatite (Kohn and Cerling, 2002) that contains carbonate substitutions for the phosphate and hydroxyl groups. Because of the stability of this hard tissue, the stable isotopic composition of enamel is

particularly useful in paleoecological and paleoclimatic studies (see reviews in Koch, 1998; Kohn and Cerling, 2002).

The oxygen isotopic composition of tooth enamel ($\delta^{18}O_{enamel}$) in large-bodied, mammalian herbivores is affected by many factors including the $\delta^{18}O$ of ingested water, fractionation of oxygen isotopes between body water and enamel during mineralization, and the physiology of a particular taxon (e.g., Kohn, 1996; Kohn et al., 1998, 1996; Longinelli, 1984; Luz and Kolodny, 1985). The $\delta^{18}O$ of ingested water is largely dependent on the source, whether primarily taken in through drinking or eating plant material (Luz and Kolodny, 1985). Modern observations and modeling results indicate that enamel $\delta^{18}O$ in obligate drinkers (e.g., horse, rhino, and bovines) is primarily dependent on the $\delta^{18}O$ composition of ingested rainwater (Kohn, 1996). In contrast, enamel $\delta^{18}O$ of drought-resistant species (e.g., goat and gazelle) that derive the majority of water from ingested plant tissues have enamel relatively enriched in ^{18}O (Ayliffe and Chivas, 1990; Balasse et al., 2003; Kohn, 1996; Levin et al., 2006; Luz et al., 1990). The reason for this is that plant leaf water tends to be enriched in ^{18}O due to fractionation by transpiration, and enrichment increases with increasing aridity and insolation (e.g., Yakir, 1992; Yakir et al., 1990). Therefore, animals that rely on plants as their main source of water are expected to have much higher $\delta^{18}O_{enamel}$ values relative to obligate drinkers from the same area with similar physiologies.

The isotopic composition of surface water reservoirs is primarily controlled by the composition of rainwater (although it can also be influenced by evaporation, mean annual temperature, and continental effects; e.g., Koch, 1998; Kohn and Cerling, 2002). At mid- to high-latitudes, the $\delta^{18}O$ of rainwater is primarily influenced by temperature (Dansgaard, 1964; Rozanski and Araguás-Araguás, 1992), where warmer temperatures result in more positive

$\delta^{18}O_{precipitation}$ values and cooler temperatures result in more negative $\delta^{18}O_{precipitation}$ values (due to Rayleigh fractionation and local air temperatures; Dansgaard, 1964). These changes in $\delta^{18}O_{precipitation}$ are reflected in the $\delta^{18}O_{enamel}$ values of large-bodied, obligate drinkers and thus, the $\delta^{18}O_{enamel}$ values of these animals can be used to estimate local surface and meteoric water compositions (Kohn and Fremd, 2007; Kohn, 1996), which can then be used to infer general changes in temperature through time. Furthermore, $\delta^{18}O_{precipitation}$ generally decreases with increasing elevation (e.g., Poage and Chamberlain, 2001; Rozanski et al., 1993) due to rainout of ^{18}O in ascending and cooling air masses (Dansgaard, 1964). This process ultimately results in lower $\delta^{18}O_{precipitation}$ values in areas of high elevation or in orographic rain shadows compared to the $\delta^{18}O_{precipitation}$ composition of the initial air mass (see discussion in Kohn and Dettman, 2007).

Tooth enamel forms over the course of a few months to 1–2 years (e.g., Fricke and O'Neil, 1996; Fricke et al., 1998). Because of this, any changes in $\delta^{18}O$ composition or inputs/outputs in mammals during tooth formation will result in isotopic changes in the composition of enamel, resulting in isotopic zoning in teeth. Studies of isotopic zoning in teeth have shown that variation in $\delta^{18}O$ compositions within a tooth closely track seasonal changes that result from changes in the oxygen isotope composition of rainwater and plant compositions (with high values in the summer and low values in the winter; e.g., Fricke and O'Neil, 1996; Kohn, 1996; Kohn et al., 1998). Seasonality signals are preserved as sinusoidal patterns in δ18Oenamel curves reconstructed from serial sampling down the length of a tooth. However, there are many factors that can dampen climatically-induced isotopic zoning signals within teeth (e.g., Kohn and Cerling, 2002). For example, large bodies of water are isotopically averaged relative to seasonal $\delta^{18}O$ compositions of precipitation. Additionally, the $\delta^{18}O$ composition of animal body water does not immediately change as environmental $\delta^{18}O$ fluctuates. Thus, these

factors dampen environmental $\delta^{18}O$ extremes and induce a time lag between environmental change and compositional change reflected in enamel. Ultimately, enamel of drought-resistant species will experience greater dampening and time lag in seasonal $\delta^{18}O$ signals than water-dependent animals (Kohn and Cerling, 2002). Lastly, dampening can occur over the course of enamel precipitation and maturation (Passey and Cerling, 2002). However, sampling teeth with relatively thin enamel can minimize this dampening effect (Kohn and Cerling, 2002). Despite these issues, many studies have successfully used fossil teeth to make inferences about changes in climate seasonality (e.g., Fricke and O'Neil, 1996; Fricke et al., 1998; Kohn et al., 2015; Nelson, 2005; van Dam and Reichart, 2009).

3. MATERIALS AND METHODS

3.1 Fossil samples

Isotope compositions were obtained from fossils collected mostly as float during the summers of 2013 and 2014 as well as specimens from the UMPC collections. Specimens were collected from ten sites within the composite RCS and four nearby sites from Mollie Gulch, which, based on lithological similarities including presence of the MTU, correlates with the lower 80 m of the RCS (Harris et al., 2016a, fig. 1). A total of 71 teeth (59 equids, 11 rhinos) were isotopically analyzed and all are housed at either the UWBM or the UMPC. When possible, fossils were identified to genus using fossil reference material from either the UWBM or UMPC, and identifications were cross-checked with published biostratigraphic ranges (e.g., Janis et al., 1998; Tedford et al., 2004). Additionally, because of the limited number and distribution of individual teeth collected from fossil-bearing sites in the RCS, we have grouped our data into five time bins to increase sample sizes for each time interval. Time bins represent the following

average ages: 21.98 Ma (representing ca. 1 million years), 20.23 Ma (representing ca. 1.7 million years), 19.1 Ma (representing ca. 0.7 million years), 17.92 Ma (representing ca. 1.6 million years), and 16.32 Ma (representing ca. 1.5 million years), following the age model of Harris et al. (2016b; Fig. 3.1).

Bulk tooth enamel samples were analyzed from 42 *Merychippus*, three *Parahippus*, three *Miohippus*, 11 unidentified equids, and 12 *Diceratherium* (Table 3.1). Serial sampling of enamel was conducted on 15 Equidae and eight Rhinocerotidae specimens (Table 3.2). Additionally, all of these individuals were assumed to be obligate-drinkers based on the inferred large body sizes of these organisms and the drinking habits of their modern relatives (i.e., modern perissodactyls are hindgut fermenters and require large amounts of ingested water for digestion; McNab, 2002).

3.2 Stable isotope geochemistry

All teeth were sampled according the method established by Koch et al. (1997) for bulk and serial sampling of tooth enamel; preparatory work and analyses were performed in the Stable Isotope Laboratory, Department of Geosciences, Boise State University. Approximately 5–10 mg of enamel powder was collected from each tooth using a 0.5 mm inverted cone carbide drill bit attached to a Dremel™. For bulk enamel analysis, samples were taken from a single groove carved down the length of each tooth parallel to the growth axis; serial samples were drilled perpendicular to the growth axis. Enamel powder was treated with 30% hydrogen peroxide overnight to remove organics. Samples were then decanted, washed with deionized water, and soaked in 1M calcium acetate buffered acetic acid overnight to remove any diagenetic carbonate. The following day, samples were again decanted, washed repeatedly with deionized water, and dried overnight at 50°C in an oven.

After pre-treatment samples were dissolved overnight in 100% phosphoric acid at 90°C and the carbonate component of enamel was analyzed in a 2010 ThermoFisher Delta V Plus continuous flow mass spectrometer coupled with a GasBench II. Two samples of NIST120c (phosphorite rock) were prepared with each batch of unknown enamel samples following the guidelines above. Six to eight NBS-18 and NBS-19 calcite samples were analyzed alongside the unknown enamel samples to verify mass spectrometer performance and reference gas calibrations. All samples were repeatedly sub-sampled 15 times and standard deviations of the replicates were calculated for each sample. All stable isotope analyses presented in this study are from the carbonate component of tooth enamel and are reported in units permil relative to the Vienna Standard Mean Ocean Water (V-SMOW) for $\delta^{18}O$, and the Vienna PeeDee Belemnite (V-PDB) for $\delta^{13}C$. Mean values for NIST standards were $\delta^{18}O = 28.3 \pm 0.5‰$ (2σ) and $\delta^{13}C = -6.5 \pm 0.2‰$ (2σ), which is within reported ranges (Kohn et al., 2005, 2015). Errors include intra-run and day-to-day variations in sample preparation and analysis.

3.3 Modeling MAP

Mean annual precipitation was calculated following the method outlined in Kohn (2010) and Kohn et al. (2015), which is based on the $\delta^{13}C$ of modern C_3 plants:

$$MAP = 10 \, \char`\^[\delta^{13}C - 2.01 + 0.000198 \times elevation - 0.0129 \times |lat| / 5.88] - 300 \qquad (1)$$

where

$$\delta^{13}C = (\delta^{13}C_{atm} - \delta^{13}C_{leaf})/(1 + \frac{\delta^{13}C_{leaf}}{1000}) \qquad (2)$$

and $\delta^{13}C_{atm}$ and $\delta^{13}C_{leaf}$ are the carbon isotope compositions of atmospheric CO_2 (-5.63‰ on average for 22.9–15.2 Ma; Tipple et al., 2010) and leaves (estimated from diet), respectively.

$\delta^{13}C_{enamel}$ values were converted to $\delta^{13}C_{leaf}$ values by correcting for known fractionation between diet and enamel (Cerling and Harris, 1999; Passey et al., 2005). For application in the RCS, we calculated MAP from average $\delta^{13}C_{enamel}$ values from all herbivores in each time bin. All herbivores are assumed to have pure C_3 diets based on habitat modeling of RSC herbivores (Harris et al., 2016a) and habitat reconstruction indicating a C_3, grass-dominated open-habitat in the RCS (Harris et al., 2016b). Altitude of the RCS locality was estimated as ~2000 m during the early–middle Miocene. This conservative estimate was established by considering the site's modern elevation (2342 m), the fact that nearby isotopic records suggest little to no evidence for uplift after 15 Ma in southwestern Montana, and that regional paleoelevation was likely over 2000 m by the late Miocene (Chamberlain et al., 2012). This estimate also accounts for the fact that regional uplift was ongoing during and after deposition of the RCS (Chamberlain et al., 2012; McMillan et al., 2002). Uncertainties in elevation do not propagate to significant uncertainties in MAP (Kohn, 2010).

Calculations of MAP from tooth enamel-based carbon isotope compositions presume that an average composition adequately represents plant compositions across a landscape. When only one or two taxa are analyzed, dietary or niche selectivity can bias isotope compositions to higher or lower values, in turn biasing MAP calculations. Analysis of medium- to large-bodied, non-selective herbivores, such as equids and rhinos, should provide a better estimate of mean compositions than more selective feeders such as camelids. Comparisons of mid-Miocene compositions among diverse herbivores shows that equids and rhino $\delta^{13}C$ values are typically nearly identical to or at most ca. 0.5‰ higher than the median or midpoint of the range exhibited by all herbivores (e.g., Biasatti et al., 2010; Domingo et al., 2012). Consequently we calculate

leaf $\delta^{13}C$ and MAP both for the mean $\delta^{13}C$ values of rhinos plus equids (0‰ offset), and assuming a maximum 0.5‰ lower value for leaf $\delta^{13}C$.

3.4 Modeling meteoric water compositions

To estimate surface water compositions from $\delta^{18}O$ of equid and rhinocerotid teeth, mean $\delta^{18}O_{CO3}$ values for each time bin are first converted to $\delta^{18}O_{PO4}$ values (Iacumin et al., 1996):

$$\delta^{18}O_{PO4\ (VSMOW)} = \delta^{18}O_{CO3\ (VSMOW)} \times 0.98 - 8.5 \tag{3}$$

Kohn (1996) showed that diet and physiological adaptations have significant impacts on the $\delta^{18}O$ compositions of biological phosphate ($\delta^{18}O_{PO4}$). Therefore, we estimated local surface water compositions ($\delta^{18}O_{H2O}$) using the generalized herbivore equation published by Kohn (1996) for animals living in temperate climates:

$$\delta^{18}O_{H2O\ (VSMOW)} = \frac{\delta^{18}O_{PO4\ (VSMOW)} - 26.8 + 8.9h}{0.76} \tag{4}$$

where h is relative humidity from 0 to 1, here assumed to be 0.5. Calculated $\delta^{18}O_{H2O}$ values are assumed to approximate meteoric water compositions.

Kohn and Fremd (2007) showed a strong correlation between modern horse phosphate $\delta^{18}O$ compositions and local water composition. They argued that rhinos and equids share plesiomorphic digestive strategies and generally overlap in consumption. Consequently, the dependence of tooth enamel isotope composition on local water is probably similar. Thus, we use the Kohn and Fremd (2007) equation to model local water compositions ($\delta^{18}O_{LW}$) for both taxa:

$$\delta^{18}O_{LW\ (VSMOW)} = \frac{\delta^{18}O_{PO4\ (VSMOW)} - 23.5}{0.83} \tag{5}$$

4. RESULTS

4.1 Stable isotope results from bulk enamel sampling

Enamel carbon isotope compositions for all taxa ranged from -11.3‰ to -8.1‰ with an average of -9.2‰ (Table 3.1). Mean $\delta^{13}C$ values are -9.1 ± 0.9‰ for equids and -9.5 ± 0.9‰ for rhinos. MAP estimates based on the $\delta^{13}C$ of all taxa are 205 ± 164 mm yr^{-1} (mean ± 2 S.E.) at 17.92 Ma, 187 ± 107 mm yr^{-1} at 19.1 Ma, 269 ± 191 mm yr^{-1} at 20.23 Ma, and 151 ± 153 mm yr^{-1} at 21.98 Ma. There are no statistically significant differences in MAP across time bins (ANOVA, p > 0.05; Fig. 3.3).

Bulk enamel oxygen isotope compositions for all taxa ranged from 15.9‰ to 25.5‰ (Table 3.1). Mean $\delta^{18}O_{CO3}$ values for equids are 19.5 ± 1.6‰ and for rhinos are 19.0 ± 2.9‰. Conversions of $\delta^{18}O_{CO3}$ to $\delta^{18}O_{H2O}$ following Kohn (1996) and of $\delta^{18}O_{CO3}$ to $\delta^{18}O_{LW}$ following Kohn and Fremd (2007) yield similar average $\delta^{18}O$ values ($\delta^{18}O_{H2O}$ and $\delta^{18}O_{LW}$) for each time bin (Fig. 3.2). Because these two calculations give similar results and because the Kohn (1996) equation also takes humidity into account, we will only discuss results from Equation 2 moving forward. $\delta^{18}O_{H2O}$ values averaged through all of the RCS are -15.4‰ for equids and -16.1‰ for rhinos (based on Equation 2). $\delta^{18}O_{H2O}$ values reconstructed from equids and rhinos show no statistically significant change through time (ANOVA, p > 0.05).

4.2 Stable isotope results from serial enamel sampling

$\delta^{18}O_{CO3}$ values for the equid teeth range from 16.3‰ to 23.2‰ and show on average 2.7‰ intra-tooth isotope variation (Table 3.2). $\delta^{18}O_{CO3}$ values for the rhino teeth range from 15.9‰ to 27.6‰ and show on average 2.3‰ intra-tooth isotope variation. The magnitude of

$\delta^{18}O$ seasonal variation for most sampled teeth was less than ~ 3.5‰ with the exception of specimens UMVP 4453E (*Merychippus*, 4.1‰; Fig. 3.4E), UMVP 5723 (*Merychippus*, 3.6‰; Fig. 3.4H), UMVP 5724 (*Merychippus*, 3.9‰; Fig. 3.4G), UMVP 4452A (*Merychippus*, 4.8‰; Fig. 3.3C), and UWBM 100082 (*Diceratherium*, 3.7‰, Fig. 3.3B). In addition, equid teeth tended to show sinusoidal seasonal variation more often than rhino teeth. In particular, equid specimens UMVP 5723 (Fig. 3.4H), UMVP 5724 (Fig. 3.4G) and UMVP 4452A (Fig. 3.4C) show clear seasonal patterns, whereas seasonality in UMVP 9426 (Fig. 3.4D) and UWBM 100066 (Fig. 3.4F) appears more subdued. The remaining equids do not appear to preserve markedly seasonal patterns or have 'dampened' seasonal signals (e.g., Fig. 3.4I). Of the rhino teeth sampled, specimens UMVP 4482E (Fig. 3.4A) and UWBM 100082 (Fig. 3.4B) appear to preserve a seasonal signal, even though the amplitude is small compared to some of the equids. The remaining rhino specimens are more difficult to interpret and appear to preserve highly dampened seasonal signals. Additionally, there are no significant changes over time in the mean magnitude of $\delta^{18}O$ seasonal variation recorded by equids or rhinos (ANOVA; $p > 0.05$).

5. DISCUSSION

5.1 Mean annual precipitation estimates for the RCS

Modern MAP for Leadore, Idaho (located 13 miles south of the RCS) is 236 mm yr^{-1} (U.S. climate data, 2016), within the range of errors estimated for MAP through the early–middle in the RCS (Fig. 3.3). This suggests that the RCS was likely a semi-arid environment during the early–middle Miocene, which is in line with phytolith vegetation reconstructions suggesting dry, C_3-dominated, open-habitats (Harris et al., 2016b). Additionally, our isotope based MAP proxy-record further suggests that the observed decrease in diatoms and C_3 water-loving PACMAD

grasses through the RCS are not a result of a change in mean annual precipitation or rainfall seasonality. Instead, we propose these changes signal a decrease in permanent lakes and standing water on the landscape linked to a change in depositional regime in the basin, namely a transition from low-energy, floodplain deposition to alluvial fan deposition in increasingly upland environments (Harris et al. 2016b).

In contrast to our new precipitation estimates, independent MAP estimates based on the chemical index of alteration without potash (CIA-K index) of paleosol Bt horizons in the RCS suggest much higher MAP for the RCS (ranging from ~345 ± 182 mm yr^{-1} to 883 ± 182 mm yr^{-1} with a marked increase between ca. 22.5 and 21.5 Ma, based on revised age model from Harris et al., 2016b; Retallack, 2007). Although seemingly at odds with our isotope data, we believe the significantly wetter paleosol MAP estimates previously reported are inaccurate, a result of improper application of the CIA-K index to RCS paleosols. We argue that the paleosol CIA-K estimates are suspect for two main reasons: First, the CIA-K index methodology does not apply to soils formed on significant topographic relief (e.g., hillslope or montane soils; Sheldon et al., 2002). As discussed above, that the RCS depositional environment represents an increasingly upland environment (e.g., alluvial fan deposit) above 70 m in the composite section (Harris et al., 2016b), indicating that the majority of RCS paleosols were formed in hillslope settings, hence are inappropriate for paleosol MAP reconstruction. Second, the CIA-K index is based on the modern relationship between degree of soil weathering and MAP for well-developed Alfisols, Mollisols, and Ultisols, not for poorly developed soils such as Entisols and Inceptisols, which are the abundant paleosol type preserved throughout the RCS. For these reasons, we propose that our isotope MAP estimates are a more accurate reflection of RCS climate during the early–middle Miocene than previous paleosol-based values (Retallack, 2007).

115

5.2 Meteoric water compositions and temperature estimates in the RCS

The nearly indistinguishable average $\delta^{18}O$ compositions of RCS equids and rhinos indicate that these taxa had similar water dependencies (i.e., water-dependent digestive physiologies) during the early–middle Miocene and, thus, did not fractionate ^{18}O significantly differently. This supports our earlier view that for our data it is appropriate to model local water compositions for both taxa using the modern correlation equation between horse phosphate $\delta^{18}O$ and local water compositions (Kohn and Fremd, 2007).

Modern meteoric water compositions are -17.5‰ VSMOW near the RCS in Heise, Idaho (Coplen and Kendall, 2000). Comparatively, meteoric water in the RCS is estimated to have been -14.9‰ during the early–middle Miocene and to not have changed significantly during this time. The difference between modern and Miocene water compositions could in part be due to topographic evolution of western North American landscapes since the Miocene. Basin and range extension was occurring during the early-middle Miocene (Atwater and Stock, 1998; Chamberlain et al., 2012; McMillan et al., 2002) and the development of complex basin systems could have resulted in different rain-out patterns that led to depleted $\delta^{18}O_{H2O}$ values. Additionally, a decrease in local temperatures since the Miocene as well as changes in source water could have contributed to decreased modern local $\delta^{18}O_{H2O}$ values. A lack of independent local paleotemperature estimates precludes explicit testing of this hypothesis; however, many terrestrial and marine records across the globe suggest climatic cooling following the MMCO (Holbourn et al., 2007, 2015), it is possible this may also have been the case in the NRM.

Regional differences in $\delta^{18}O_{H2O}$ in the Pacific Northwest also provide insight into potential topographic barriers during the early–middle Miocene. For example, estimated $\delta^{18}O_{H2O}$ for RCS is ~5–7‰ lower than $\delta^{18}O_{H2O}$ estimated from central Oregon over the same time period

(-9 to -10‰; Kohn and Fremd, 2007; Kohn et al., 2002). The continental effect, in which isotope values of precipitation tend to decrease away from coastlines (Dansgaard, 1964), could explain 1–2‰ of this difference. The remaining disparity likely indicates higher elevations either at the RCS or between the RCS and central Oregon (or both) during the early–middle Miocene.

In addition to using isotopes to glean information about climate during the early–middle Miocene, the presence of climate-sensitive plants from the same strata can be used as well. Harris et al. (2016b) reported low relative abundances of palm phytoliths preserved throughout the RCS ($< 2\%$). Because modern palms are typically tropical and frost-intolerant taxa (especially seedlings), they can serve as indicators of minimum winter temperatures (e.g., Archibald et al., 2014; Greenwood and Wing, 1995). The natural distribution of modern palms are typically limited to regions with coldest month mean temperatures (CMMT) >5ºC (Greenwood and Wing, 1995; Larcher and Winter, 1981), although some palms can withstand brief intervals of freezing temperatures. This tolerance is further reduced under high atmospheric CO_2 concentrations (>800 ppm increases CMMT estimates by +1.5ºC to +3ºC; Royer et al., 2002), such as has been proposed for the MMCO (e.g., Beerling and Royer, 2011; Retallack, 2009). A compiled dataset of mean annual temperature (MAT) and CMMT climate profiles for a range of modern cold tolerant palm clades indicates that the lowest MAT threshold for palms is ~11ºC and the CMMT is typically >5ºC (Archibald et al., 2014). Assuming similar climatic tolerances of palms in the early–middle Miocene, the inferred presence of palms suggests that MAT and CMMT for the RCS were likely above 11ºC and 5ºC, respectively. Consistently warm MAT in the RCS is also supported by salinization index-based MAT estimates from RCS paleosols of ~10.3°C for the early–middle Miocene (Retallack, 2007). All of these reconstructed values are much warmer than modern MAT and CMMT for Leadore, Idaho today (3.8°C and -

8.4°C, respectively; U.S. climate data, 2016), indicating that local climate in this region has cooled considerably since the early–middle Miocene.

5.3 Seasonality

Our oxygen isotopic data from serially sampled equid and rhino teeth indicate that there was seasonality in either temperature or source of precipitation in RCS, but that this did not change substantially from the early to middle Miocene.

The differences in magnitude and shape of seasonal $\delta^{18}O$ variation between equids and rhinos could be due to taxon-specific differences in tooth mineralization or even migration. Large-bodied herbivores that migrate (e.g., modern horses) typically consume different water sources as well as different plants (i.e., species or different parts of plants) throughout the year, which results in higher intra-tooth variability in $\delta^{18}O$ and $\delta^{13}C$ compared with non-migratory herbivores (e.g., Feranec et al., 2009; Julien et al., 2012). Non-migratory, resident herbivores are known to display high $\delta^{18}O$ variation (associated with seasonal changes in temperature or water source) with little to no variability in $\delta^{13}C$ (Julien et al., 2012). RCS herbivores display intra-tooth isotopic variability (high $\delta^{18}O$ variation associated with no $\delta^{13}C$ variation; Harris et al., 2016a) most similar to what we expect from non-migratory herbivores. Therefore, we believe it unlikely that migration was a main driving force for $\delta^{18}O$ variation between equids and rhinos. High variation in strontium isotopes ($^{87}Sr/^{86}Sr$) curves is also associated with migratory behavior since $^{87}Sr/^{86}Sr$ varies with the isotopic composition of soil mineral compositions. Although we did not test for the strontium composition of RCS herbivore teeth, doing so in the future could provide additional support to our hypothesis that RCS herbivores were non-migratory, thereby, allowing us to use their teeth as indicators of local climate.

Another reason why seasonal $\delta^{18}O$ variation among sampled specimens is not ubiquitous could be that herbivores were drinking water from different sources, each with different compositional averages. For example, we would expect to see little to no seasonal variation in the enamel of herbivores that drank water from (or ate plants growing nearby) lakes or other large bodies of water, which have less isotopic variability than seasonal precipitation (see discussion in Kohn and Cerling, 2002). Additionally, due to the scarcity of fossil teeth recovered from the RCS, we could not selectively choose to analyze the same tooth position (e.g., M3) among individuals sampled. Because different teeth erupt and form over the course of a few months to years, each tooth records a slightly different (although at times overlapping) sinusoidal seasonal isotopic signature (e.g., Fricke and O'Neil, 1996; Kohn et al., 1998). Therefore, it is possible that the differences in $\delta^{18}O$ variation that we observe between samples could relate to having sampled different molar positions, which preserve different portions of the seasonal $\delta^{18}O$ cycles over which the enamel formed (Kohn et al., 1998). Despite this, we can still use the largest amplitudes of isotopic change to infer that some RCS herbivores were drinking water from sources that experienced changes in $\delta^{18}O$ over the course of tooth formation (likely driven by seasonal changes in temperature).

5.4 Did climatic events in the RCS coincide with Miocene faunal change in the NRM?

Our climate data indicate relative stasis in MAP, MAT, and temperature seasonality in the RCS during the early–middle Miocene. Comparing these climate data with the relatively stable plant community composition and habitat structure throughout the RCS indicates that many aspects of the environment remained constant in the RCS during this time, even as the depositional regime appears to have shifted (Harris et al., 2016b). Although we are comparing

our local environmental reconstruction for the RCS basin to more regional faunal data, this discrepancy in patterns nonetheless suggests that the major faunal changes recorded for the early–middle Miocene of the NRM were not likely driven by changes in local climate and vegetation. Instead we propose that these faunal changes could have been driven by increased immigration or even increased endemism due to tectonic factors in this mountainous region (Barnosky and Carrasco, 2002; Woodburne 2004; Woodburne and Swisher, 1995). These faunal data are addressed further in Harris et al. (2016a).

5.5 Regional climatic differences in response to the MMCO

How does our record of relative climate stasis compare to other reconstructions from around the world of regional climate leading into the MMCO? Mosbrugger et al. (2005) used 45 megafloras to infer climate during the last 45 million years in Central Europe and found an overall trend towards increased MAT and CMMT leading into middle Miocene (although with some short-term variations regionally that were attributed to different paleogeographic settings). Herpetological proxy data from nearby sites also indicate MAT values 9º to 12ºC warmer than modern (Böhme, 2003). In Central Europe MAP was relatively high during the early–middle Miocene (>1000 mm yr^{-1}), and although estimates in some regions appear to indicate increases leading into the MMCO, there are generally weaker trends regionally (Böhme et al., 2011; Mosbrugger et al., 2005). Overall, these climatic data from Europe generally agree with estimates of increased global temperatures leading into the MMCO based on oxygen isotopes from benthic foraminifera (Zachos et al., 2001, 2008).

Similarly, Hinojosa and Villagrán (2005) used multiple fossil floras to characterize climate parameters in southern South America (Chile) during the early–middle Miocene. These

authors found that MAT rose markedly by >6ºC from ~23–15 Ma and CMMT increased to 15.9ºC by ca. 15 Ma. Local MAP appears to have risen from ~750 to 1000 mm yr^{-1} during the early–middle Miocene as well. These findings are generally supported by faunal and wood morphological analyses from the early Miocene of southern Argentina, indicating warm (>14ºC), wet conditions (~1500 mm yr^{-1}) with small mean annual ranges of temperature ($\geq$ 4ºC; Brea et al., 2012; Kay et al., 2012).

In contrast to the above-mentioned studies are early–middle Miocene-aged pollen assemblages from sediment cores taken off the coast of New Jersey (in the shallow coastal shelf) that indicate consistently warm (~14ºC) climate during the MMCO (Kotthoff et al., 2013). Miocene MAT estimates are ~2ºC warmer than modern estimates from the hinterlands of New Jersey. Additionally, paleovegetation reconstructions reveal stable floral communities during the MMCO (with only minor increases in deciduous-evergreen mixed forest taxa and a decrease in swamp forest taxa during this time; Kotthoff et al., 2013). The striking aspect of this study is that there is no evidence of climate or vegetation change leading into the MMCO. In these regards the results from Kotthoff et al. (2013) parallel our results from the RCS.

From these data it seems clear that the MMCO did not have a uniform impact on climate across the globe. These differences highlight how crucial it is to study many different regions to gain a full understanding of the local impacts of climate change in deep time. Specifically, data from the RCS provide insight into the response of a high-elevation site located in the continental interior to global warming during the MMCO. Given that inland, high-elevation sites are generally under-represented in the fossil record, the RCS is an important field area that has the potential to provide a unique piece to the puzzle that is the climate, ecology, and evolution of ecosystems during the early–middle Miocene.

6. CONCLUSION

Stable isotopes from herbivore teeth suggest the RCS was characterized by a semi-arid, seasonal climate during the early–middle Miocene with warmer mean annual temperatures than central-eastern Idaho today. These local climate conditions remained stable and more or less unchanged during the lead-up to peak warming during the middle Miocene. Our findings contrast with previously held ideas that the northern Rocky Mountains, and western North America in general, shifted to warm and wet conditions during the middle Miocene (e.g., Chaney and Axelrod, 1959; Retallack, 2007), and suggest that this region of the Northern Rocky Mountains was climatically buffered from the long-term effects of global climate forcing leading into the MMCO. A similar pattern of no climate change during the early–middle Miocene is inferred from pollen extracted from shallow coastal shelf deposits off of New Jersey (Kotthoff et al., 2013), whereas other sites, for example in Europe and South America, show the expected shift to warm-wet conditions during the MMCO (Böhme, 2003; Hinojosa and Villagrán, 2005; Mosbrugger et al., 2005). Geographically variable manifestations of global climate change are no surprise in light of current knowledge of how the ongoing global warming differentially affects local ecosystems across the Earth (e.g., Walther et al., 2002). Nonetheless, the discrepancy between local/regional and global climatic trends in RCS and other areas emphasizes the importance of investigating geologic intervals of extreme global climate change at local scales instead of relying on studies at the regional or global scale. This is especially vital when testing hypotheses about biotic responses to potential abiotic drivers during major climate change. Out of necessity, paleontologists often rely on comparing patterns of vegetation or faunal change at the basin level to global climate curves (e.g., Dunn et al., 2015; Janis et al., 2000; Kohn et al., 2015; Strömberg et al., 2013), however, it can lead to erroneous conclusions about ecological or

122

evolutionary processes involved in biotic turnover. The RCS, which represents a depositional

environment ('uplands') not typically represented in paleontological surveys, therefore adds a

key piece to our understanding of ecological and evolutionary change during long-term climatic

alteration.

ACKNOWLEDGEMENTS

REFERENCES

Archibald, S.B., Morse, G.E., Greenwood, D.R., Mathewes, R.W., 2014. Fossil palm beetles refine upland winter temperatures in the Early Eocene Climatic Optimum. Proc. Natl. Acad. Sci. U. S. A. 111, 8095–8100.

Atwater, T., Stock, J., 1998. Pacific-North America Plate Tectonics of the Neogene Southwestern United States–An Update. Int. Geol. Rev. 40, 375–402.

Ayliffe, L.K., Chivas, A.R., 1990. Oxygen isotope composition of the bone phosphate of Australian kangaroos: Potential as a palaeoenvironmental recorder. Geochim. Cosmochim. Acta 54, 2603–2609.

Badgley, C., Barry, J.C., Morgan, M.E., Nelson, S. V, Behrensmeyer, A.K., Cerling, T.E., Pilbeam, D., 2008. Ecological changes in Miocene mammalian record show impact of prolonged climatic forcing. Proc. Natl. Acad. Sci. U. S. A. 105, 12145–9.

Balasse, M., Smith, A.B., Ambrose, S.H., Leigh, S.R., 2003. Determining sheet birth seasonality by analysis of tooth enamel oxygen isotope ratios: the Late Stone Age site of Kasteelberg (South Africa). J. Archaeol. Sci. 30, 205–215.

Barnosky, A.D., 2001. Distinguishing the effects of the Red Queen and Court Jester on Miocene mammal evolution in the northern Rocky Mountains. J. Vertebr. Paleontol. 21, 172–185.

Barnosky, A.D., Bibi, F., Hopkins, S.S.B., Nichols, R., 2007. Biostratigraphy and magnetostratigraphy of the Mid-Miocene Railroad Canyon Sequence, Montana and Idaho, and age of the Mid-Tertiary Unconformity west of the Continental Divide. J. Vertebr.

Paleontol. 27, 204–224.

Barnosky, A.D., Carrasco, M.A., 2002. Effects of Oligo-Miocene global climate changes on
mammalian species richness in the northwestern quarter of the USA. Evol. Ecol. Res. 4,
811–841.

Barnosky, A.D., Hadly, E. a., Bell, C.J., 2003. Mammalian Response To Global Warming on
Varied Temporal Scales. J. Mammal. 84, 354–368.

Beerling, D.J., Royer, D.L., 2011. Convergent Cenozoic CO2 history. Nat. Geosci. 4, 418–420.

Bennington, J.B., Dimichele, W.A., Badgley, C., Bambach, R.K., Barrett, P.M., Behrensmeyer,
A.K., Bobe, R., Burnham, R.J., Daeschler, E.B., Dam, J. V., Eronen, J.T., Erwin, D.H.,
Finnegan, S., Holland, S.M., Hunt, G., Jablonski, D., Jackson, S.T., F., J.B., Kidwell, S.M.,
Koch, P.L., Kowalewski, M.J., Labandeira, C.C., Looy, C. V., Lyons, S.K., Novack-
Gottshall, P.M., Potts, R., Roopnarine, P.D., Stromberg, C.A.E., Sues, H.-D., Wagner, P.J.,
P., W., Wing, S.L., 2009. Critical Issues of Scale in Paleoecology. Palaios 24, 1–4.

Biasatti, D., Wang, Y., Deng, T., 2010. Strengthening of the East Asian summer monsoon
revealed by a shift in seasonal patterns in diet and climate after 2-3Ma in northwest China.
Palaeogeogr. Palaeoclimatol. Palaeoecol. 297, 12–25.

Blois, J.L., Hadly, E.A., 2009. Mammalian Response to Cenozoic Climatic Change. Annu. Rev.
Earth Planet. Sci. 37, 181–208.

Boardman, G.S., Secord, R., 2013. Stable isotope paleoecology of White River ungulates during
the Eocene-Oligocene climate transition in northwestern Nebraska. Palaeogeogr.
Palaeoclimatol. Palaeoecol. 375, 38–49.

Böhme, M., 2003. The Miocene Climatic Optimum: evidence from ectothermic vertebrates of

    Central Europe. Palaeogeogr. Palaeoclimatol. Palaeoecol. 195, 389–401.

Böhme, M., Winklhofer, M., Ilg, A., 2011. Miocene precipitation in Europe: Temporal trends

    and spatial gradients. Palaeogeogr. Palaeoclimatol. Palaeoecol. 304, 212–218.

Brea, M., Zucol, A.F., Iglesias, A., 2012. Fossil plant studies from late Early Miocene of Santa

    Cruz Formation: paleoecology and paleoclimatology at the passive margin of Patagonia,

    Argentina, in: Vizcaíno, S.F., Kay, R.F., Bargo, M.S. (Eds.), Early Miocene Paleobiology in

    Patagonia: High-Latitude Paleocommunities of the Santa Cruz Formation. Cambridge

    University Press, London, pp. 104–128.

Cerling, T.E., Harris, J.M., 1999. Carbon isotope fractionation between diet and bioapatite in

    ungulate mammals and implications for ecological and paleoecological studies. Oecologia

    120, 347–363.

Cerling, T.E., Harris, J.M., Macfadden, B.J., Leakey, M.G., Quade, J., Eisenmann, V.,

    Ehleringer, J.R., 1997. Global vegetation change through the Miocene/Pliocene boundary.

    Nature 389, 153–158.

Chamberlain, C.P., Mix, H.T., Mulch, A., Hren, M.T., Kent-Corson, M.L., Davis, S.J., Horton,

    T.W., Graham, S.A., 2012. The Cenozoic climatic and topographic evolution of the western

    North American Cordillera. Am. J. Sci. 312, 213–262.

Chaney, R.W., Axelrod, D.I., 1959. Miocene floras of the Columbia Plateau, 617th ed. Carnegie

    Institute Washington Publication.

Chen, S.T., Smith, S.Y., Sheldon, N.D., Strömberg, C.A.E., 2015. Regional-scale variability in

    the spread of grasslands in the late Miocene. Palaeogeogr. Palaeoclimatol. Palaeoecol. 437,

42–52.

Coplen, T.B., Kendall, C., 2000. Stable isotope and oxygen isotope ratios for selected sites of the U.S. Geological Survey's NASQAN and Benchmark surface-water networks.

Cotton, J.M., Sheldon, N.D., Strömberg, C.A.E., 2012. High-resolution isotopic record of C4 photosynthesis in a Miocene grassland. Palaeogeogr. Palaeoclimatol. Palaeoecol. 337-338, 88–98.

Dansgaard, W., 1964. Stable isotopes in precipitation. Tellus 16, 436–468.

Diefendorf, A.F., Mueller, K.E., Wing, S.L., Koch, P.L., Freeman, K.H., 2010. Global patterns in leaf 13C discrimination and implications for studies of past and future climate. Proc. Natl. Acad. Sci. 107, 5738–5743.

Domingo, M.S., Domingo, L., Badgley, C., Sanisidro, O., Morales, J., 2012. Resource partitioning among top predators in a Miocene food web. Proc. Biol. Sci. 280, 20122138.

Dunn, R.E., Strömberg, C.A.E., Madden, R.H., Kohn, M.J., Carlini, A.A., 2015. Linked canopy, climate, and faunal change in the Cenozoic of Patagonia. Science (80-.). 347, 2–5.

Ehleringer, J.R., Sage, R.F., Flanagan, L.B., Pearcy, R.W., 1991. Climate Change and the Evolution of C4 Photosynthesis. Trends Evol. Ecol. 6, 95–99.

Feranec, R.S., Hadly, E.A., Paytan, A., 2009. Stable isotopes reveal seasonal competition for resources between late Pleistocene bison (Bison) and horse (Equus) from Rancho La Brea, southern California. Palaeogeogr. Palaeoclimatol. Palaeoecol. 271, 153–160.

Feranec, R.S., Macfadden, B.J., 2006. Isotopic discrimination of resource partitioning among ungulates in C3-dominated communities from the Miocene of Florida and California.

Paleobiology 32, 191–205.

Fields, R.W., Rasmussen, D.L., Tabrum, A.R., Nichols, R., 1985. Cenozoic Rocks of the
Intermontane Basins of Western Montana and Eastern Idaho: a summary. Cenozoic
Paleogeography of the West-Central United States 9–36.

Flower, B.P., Kennett, J.P., 1994. The Middle Miocene climatic transition: East Antarctic ice
sheet development, deep ocean circulation and global carbon cycling. Palaeogeogr.
Palaeoclimatol. Palaeoecol. 108, 537–555.

Fricke, H.C., Clyde, W.C., O'Neil, J.R., Gingerich, P.D., 1998. Evidence for rapid climate
change in North America during the latest Paleocene thermal maximum: oxygen isotope
compositions of biogenic phosphate from the Bighorn Basin (Wyoming). Earth Planet. Sci.
Lett. 160, 193–208.

Fricke, H.C., O'Neil, J.R., 1996. Inter- and intra-tooth variation in the oxygen isotope
composition of mammalian tooth enamel phosphate: implications for palaeoclimatological
and palaeobiological research. Palaeogeogr. Palaeoclimatol. Palaeoecol. 126, 91–99.

Froyd, C. a., Willis, K.J., 2008. Emerging issues in biodiversity and conservation management:
The need for a palaeoecological perspective. Quat. Sci. Rev. 27, 1723–1732.

Graham, A., 1999. Late Cretaceous and Cenozoic history of North American vegetation. Oxford
University Press, New York.

Greenwood, D.R., Wing, S.L., 1995. Eocene continental climates and latitudinal temperature
gradients. Geology 23, 1044–1048.

Harris, E.B., Strömberg, C.A.E., Kohn, M.J., 2016a. Stable isotopes reveal differential dietary

evolution in large ungulates during the early–middle Miocene in the Northern Rocky Mountains. *Chapter 4*.

Harris, E.B., Strömberg, C.A.E., Sheldon, N.D., Smith, S.Y., Ibanez-Mejia, M., Vilhena, D.A., 2016b. Vegetation response during the lead-up to the middle Miocene warming event in the Northern Rocky Mountains. *Chapter 2*.

Heaton, T.H.E., 1999. Spatial, Species, and Temporal Variations in the 13C/12C Ratios of C3 Plants: Implications for Palaeodiet Studies. J. Archaeol. Sci. 26, 637–649.

Hinojosa, L.F., Villagrán, C., 2005. Did South American Mixed Paleofloras evolve under thermal equability or in the absence of an effective Andean barrier during the Cenozoic? Palaeogeogr. Palaeoclimatol. Palaeoecol. 217, 1–23.

Holbourn, A., Kuhnt, W., Kochhann, K.G.D., Andersen, N., Sebastian Meier, K.J., 2015. Global perturbation of the carbon cycle at the onset of the Miocene Climatic Optimum. Geology 43, 123–126.

Holbourn, A., Kuhnt, W., Schulz, M., Flores, J.A., Andersen, N., 2007. Orbitally-paced climate evolution during the middle Miocene "Monterey" carbon-isotope excursion. Earth Planet. Sci. Lett. 261, 534–550.

Hyland, E.G., Sheldon, N.D., Smith, S.Y., Strömberg, C.A.E., *in review*. Late Miocene rise and fall of C4 grasses in the western United States. Geology.

Iacumin, P., Bocherens, H., Mariotti, A., Longinelli, A., 1996. Oxygen isotope analyses of co-existing carbonate and phosphate in biogenic apatite: a way to monitor diagenetic alteration of bone phosphate? Earth Planet. Sci. Lett. 142, 1–6.

Jacobs, B.F., Kingston, J.D., Jacobs, L.L., 1999. The origin of grass-dominated ecosystems. Ann. Missouri Bot. Gard. 86, 590–643.

Janis, C.M., Damuth, J., Theodor, J.M., 2004. The species richness of Miocene browsers, and implications for habitat type and primary productivity in the North American grassland biome. America (NY). 207, 371 – 398.

Janis, C.M., Damuth, J., Theodor, J.M., 2000. Miocene ungulates and terrestrial primary productivity: where have all the browsers gone? Proc. Natl. Acad. Sci. U. S. A. 97, 7899–7904.

Janis, C.M., Scott, K.M., Jacobs, L.L., 1998. Evolution of Tertiary Mammals of North America, 1st ed. Cambridge University Press, Cambridge.

Julien, M.A., Bocherens, H., Burke, A., Drucker, D.G., Patou-Mathis, M., Krotova, O., Péan, S., 2012. Were European steppe bison migratory? 18O, 13C and Sr intra-tooth isotopic variations applied to a palaeoethological reconstruction. Quat. Int. 271, 106–119.

Kay, R.F., Vizcaíno, S.F., Bargo, M.S., 2012. A review of the paleoenvironment and paleoecology of the Miocene Santa Cruz Formation, in: Vizcaíno, S.F., Kay, R.F., Bargo, M.S. (Eds.), Early Miocene Paleobiology in Patagonia: High-Latitude Paleocommunities of the Santa Cruz Formation. Cambridge University Press, London, pp. 331–364.

Kent-Corson, M.L., Barnosky, A.D., Mulch, A., Carrasco, M. a., Chamberlain, C.P., 2013. Possible regional tectonic controls on mammalian evolution in western North America. Palaeogeogr. Palaeoclimatol. Palaeoecol. 387, 17–26.

Koch, P., Tuross, N., Fogel, M., 1997. The effects of sample treatment and diagenesis on the isotopic integrity of carbonate in biogenic hydroxylapatite. J. Archaeol. Sci. 24, 417–429.

Koch, P.L., 1998. Isotopic Reconstruction of Past Continental Environments. Annu. Rev. Earth Planet. Sci. 26, 573–613.

Kohn, M.J., 2010. Carbon isotope compositions of terrestrial C3 plants as indicators of (paleo)ecology and (paleo)climate. Proc. Natl. Acad. Sci. U. S. A. 107, 19691–5.

Kohn, M.J., 1996. Predicting animal δ18O: accounting for diet and physiological adaptation. Geochim. Cosmochinica Acta 60, 4811–4829.

Kohn, M.J., Cerling, T.E., 2002. Stable Isotope Compositions of Biological Apatite. Rev. Mineral. Geochemistry 48, 455–488.

Kohn, M.J., Dettman, D.L., 2007. Paleoaltimetry from stable isotope compositions of fossils. Rev. Mineral. Geochemistry 66, 119–154.

Kohn, M.J., Fremd, T.J., 2008. Miocene tectonics and climate forcing of biodiversity, western United States. Geology 36, 783–786.

Kohn, M.J., Fremd, T.J., 2007. Tectonic controls on isotope composition and species diversification, John Day Basin, central Oregon. PaleoBios 27, 48–61.

Kohn, M.J., McKay, M.P., 2012. Paleoecology of late Pleistocene–Holocene faunas of eastern and central Wyoming, USA, with implications for LGM climate models. Palaeogeogr. Palaeoclimatol. Palaeoecol. 326-328, 42–53.

Kohn, M.J., McKay, M.P., Knight, J.L., 2005. Dining in the Pleistocene - Who's on the menu? Geology 33, 649–652.

Kohn, M.J., Miselis, J.L., Fremd, T.J., 2002. Oxygen isotope evidence for preogressive uplift of the Cascade Range, Oregon. Earth Planet. Sci. Lett. 204, 151–165.

132

Kohn, M.J., Schoeninger, M.J., Valley, J.W., 1998. Variability in oxygen isotope compositions of herbivore teeth: reflections of seasonality or developmental physiology? Chem. Geol. 152, 97–112.

Kohn, M.J., Schoeninger, M.J., Valley, J.W., 1996. Herbivore tooth oxygen isotope compositions: effects of diet and physiology. Geochim. Cosmochinica Acta 60, 3889–3896.

Kohn, M.J., Strömberg, C.A.E., Madden, R.H., Dunn, R.E., Evans, S., Palacios, A., Carlini, A.A., 2015. Quasi-static Eocene–Oligocene climate in Patagonia promotes slow faunal evolution and mid-Cenozoic global cooling. Palaeogeogr. Palaeoclimatol. Palaeoecol. 435, 24–37.

Kotthoff, U., Greenwood, D.R., McCarthy, F.M.G., Müller-Navarra, K., Prader, S., Hesselbo, S.P., 2014. Late Eocene to middle Miocene (33 to 13 million years ago) vegetation and climate development on the North American Atlantic Coastal Plain (IODP Expedition 313, Site M0027). Clim. Past 10, 1523–1539.

Larcher, W., Winter, A., 1981. Frost susceptibility of palms: experimental data and their interpretation. Principes 25, 143–152.

Lee-Thorp, J., van der Merwe, N.J., 1987. Carbon isotope analysis of fossil bone apatite. S. Afr. J. Sci. 83, 712–715.

Levin, N.E., Cerling, T.E., Passey, B.H., Harris, J.M., Ehleringer, J.R., 2006. A stable isotope aridity index for terrestrial environments. Proc. Natl. Acad. Sci. 103, 11201.

Liang, M., Bruch, a, Collinson, M., Mosbrugger, V., Li, C., Sun, Q., Hilton, J., 2003. Testing the climatic estimates from different palaeobotanical methods: an example from the Middle Miocene Shanwang flora of China. Palaeogeogr. Palaeoclimatol. Palaeoecol. 198, 279–301.

Liu, L., Stegman, D.R., 2012. Origin of Columbia River flood basalt controlled by propagating

    rupture of the Farallon slab. Nature 482, 386–389.

Longinelli, A., 1984. Oxygen isotopes in mammal bone phospate: a new tool for

    paleohydrological and paleoclimatological research? Geochim. Cosmochinica Acta 48,

    385–390.

Luz, B., Cormie, A.B., Schwarcz, H.P., 1990. Oxygen isotope variations in phosphate of deer

    bones. Geochim. Cosmochim. Acta 54, 1723–1728.

Luz, B., Kolodny, Y., 1985. Oxygen isotope variations in phosphate of biogenic apatites, IV.

    Mammal teeth and bones. Earth Planet. Sci. Lett. 75, 29–36.

MacFadden, B.J., 2000. Cenozoic mammalian herbivores from the Americas: reconstructing

    ancient diets and terrestrial communities. Annu. Rev. Ecol. Syst. 31, 33–59.

McMillan, M.E., Angevine, C.L., Heller, P.L., 2002. Postdepositional tilt of the Miocene-

    Pliocene Ogallala Group on the western Great Plains: Evidence of late Cenozoic uplift of

    the Rocky Mountains. Geology 30, 63–66.

McNab, B.K., 2002. The physiological ecology of vertebrates. A view from energetics. Cornell

    University Press, Ithica, NY.

Mosbrugger, V., Utescher, T., Dilcher, D.L., 2005. Cenozoic continental climatic evolution of

    Central Europe. Proc. Natl. Acad. Sci. U. S. A. 102, 14964–14969.

Nelson, S. V., 2005. Paleoseasonality inferred from equid teeth and intra-tooth isotopic

    variability. Palaeogeogr. Palaeoclimatol. Palaeoecol. 222, 122–144.

Nichols, R., 1979. Additional early Miocene mammals from the Lemhi Valley of Idaho. Tebiwa

17, 1–12.

Nichols, R., 1976. Early Miocene mammals from the Lemhi Valley of Idaho. Tebiwa 18, 9–37.

O'Leary, M.H., 1988. Carbon isotopes in photosynthesis. Bioscience 38, 328–336.

Passey, B.H., Cerling, T.E., 2002. Tooth enamel mineralization in ungulates: implications for recovering a primary isotopic time-series. Geochim. Cosmochinica Acta 66, 3225–3234.

Passey, B.H., Robinson, T.F., Ayliffe, L.K., Cerling, T.E., Sphonheimer, M., Dearing, M.D., Roeder, B.L., Ehleringer, J.R., 2005. Carbon isotope fractionation between diet, breath CO_2, and bioapatite in different mammals. J. Archaeol. Sci. 32, 1459–1470.

Pierce, K.L., Morgan, L.A., 1992. The track of the Yellowstone hot spot: volcanism, faulting and uplift. Geol. Soc. Am. Mem. 1–53.

Poage, M.A., Chamberlain, C.P., 2001. Empirical relationships between elevation and the stable isotope composition of precipitation and surface waters: considerations for studies of paleoelevation change. Am. J. Sci. 301, 1–15.

Retallack, G.J., 2009. Refining a pedogenic-carbonate CO_2 paleobarometer to quantify a middle Miocene greenhouse spike. Palaeogeogr. Palaeoclimatol. Palaeoecol. 281, 57–65.

Retallack, G.J., 2007. Cenozoic Paleoclimate on Land in North America. J. Geol. 115, 271–294.

Royer, D.L., Osborne, C.P., Beerling, D.J., 2002. High CO_2 increases the freezing sensitivity of plants: Implications for paleoclimatic reconstructions from fossil floras. Geology 30, 963–966.

Rozanski, K., Araguás-Araguás, L., 1992. Relation between long-term trends of oxygen-18 isotope composition of precipitation and climate. Science (80-.). 258, 981–985.

Rozanski, K., Araguas-Araguas, L., Gonfiantini, R., 1993. Isotopic patterns in modern global precipitation, in: Climate Change in Continental Isotopic Records. pp. 1–36.

Secord, R., Wing, S.L., Chew, A., 2008. Stable isotopes in early Eocene mammals as indicators of forest canopy structure and resource partitioning. Paleobiology 34, 282–300.

Sheldon, N.D., Retallack, G.J., Tanaka, S., 2002. Geochemical Climofunctions from North American Soils and Application to Paleosols across the Eocene-Oligocene Boundary in Oregon. J. Geol. 110, 687–696.

Stewart, G.R., Turnbull, M.H., Schmidt, S., Erskine, P.D., 1995. 13C natural abundance in plant communities along a rainfall gradient: A biological integrator of water availability. Aust. J. Plant Physiol. 22, 51–55.

Strömberg, C. a. E., 2011. Evolution of Grasses and Grassland Ecosystems. Annu. Rev. Earth Planet. Sci. 39, 517–544.

Strömberg, C.A.E., 2005. Decoupled taxonomic radiation and ecological expansion of open-habitat grasses in the Cenozoic of North America. Proc. Natl. Acad. Sci. U. S. A. 102, 11980–4.

Strömberg, C.A.E., Dunn, R.E., Madden, R.H., Kohn, M.J., Carlini, A.A., 2013. Decoupling the spread of grasslands from the evolution of grazer-type herbivores in South America. Nat. Commun. 4, 1478.

Strömberg, C.A.E., Friis, E.M., Liang, M.-M., Werdelin, L., Zhang, Y.-I., 2007. Palaeoecology of an Early-Middle Miocene late in China: preliminary interpretations based on phytoliths from the Shanwang Basin. Vertebr. Palasiat. 45, 145–160.

Swanson, D.A., Wright, T.L., Hooper, P.R., Bentley, R.D., 1979. Revisions in stratigraphic
nomenclature of the Columbia River Basalt Group. U.S. Geol. Surv. Bull. 1457-G.

Tedford, R.H., Albright III, L.B., Barnosky, A.D., Ferrusquia-Villafranca, I., Hunt Jr., R.M.,
Storer, J.E., Swisher III, C.C., Voorhies, M.R., Webb, S.D., Whistler, D.P., 2004.
Mammalian Biochronology of the Arikareean Through Hemphillian Interval (Late
Oligocene Through Early Pliocene Epochs), in: Woodburne, M.O. (Ed.), Late Cretaceous
and Cenozoic Mammals of North America. Columbia University Press, pp. 169–231.

Tipple, B.J., Meyers, S.R., Pagani, M., 2010. Carbon isotope ratio of Cenozoic CO2: A
comparative evaluation of available geochemical proxies. Paleoceanography 25, 1–11.

U.S. climate data [WWW Document], 2016. . Your Weather Serv. URL
http://www.usclimatedata.com/ (accessed 10.20.15).

van Dam, J.A., Reichart, G.J., 2009. Oxygen and carbon isotope signatures in late Neogene horse
teeth from Spain and application as temperature and seasonality proxies. Palaeogeogr.
Palaeoclimatol. Palaeoecol. 274, 64–81.

Vogel, J.C., 1978. Isotopic assessment of the dietary habits of ungulates. S. Afr. J. Sci. 74, 298–
301.

Walther, G.-R., Post, E., Convey, P., Menzel, A., Parmesan, C., Beebee, T.J.C., Fromentin, J.-
M., Hoegh-Guldberg, O., Bairlein, F., 2002. Ecological responses to recent climate change.
Nature 416, 389–395.

Woodburne, M.O., Swisher, C.C., 1995. Land mammal high-resolution geochronology,
intercontinental overland dispersals, sea level, climate, and vicariance, in: Berggren, W.A.,
Kent, D.V., Aubry, M.-P., Hardenbol, J. (Eds.), Geochronology, Time Scales and Global

Stratigraphic Correlation. Society of Sedimentary Geology Special Publication 54, pp. 336–364.

Woodburne, M.O. (Ed.), 2004. Late Cretaceous and Cenozoic Mammals of North America: Biostratigraphy and Geochronology. Columbia University Press.

Yakir, D., 1992. Variations in the natural abundance of oxygen-18 and deuterium in plant carbohydrates. Plant Cell Environ. 15, 1005–1020.

Yakir, D., DeNiro, M.J., Gat, J.R., 1990. Natural deuterium and oxygen-18 enrichment in leaf water of cotton plants grown under wet and dry conditions: evidence for water compartmentation and its dynamics. Plant Cell Environ. 13, 49–56.

You, Y., Huber, M., Müller, R.D., Poulsen, C.J., Ribbe, J., 2009. Simulation of the Middle Miocene Climate Optimum. Geophys. Res. Lett. 36.

Zachos, J., Pagani, M., Sloan, L., Thomas, E., Billups, K., 2001. Trends, rhythms, and aberrations in global climate 65 Ma to present. Science 292, 686–93.

Zachos, J.C., Dickens, G.R., Zeebe, R.E., 2008. An early Cenozoic perspective on greenhouse warming and carbon-cycle dynamics. Nature 451, 279–83.
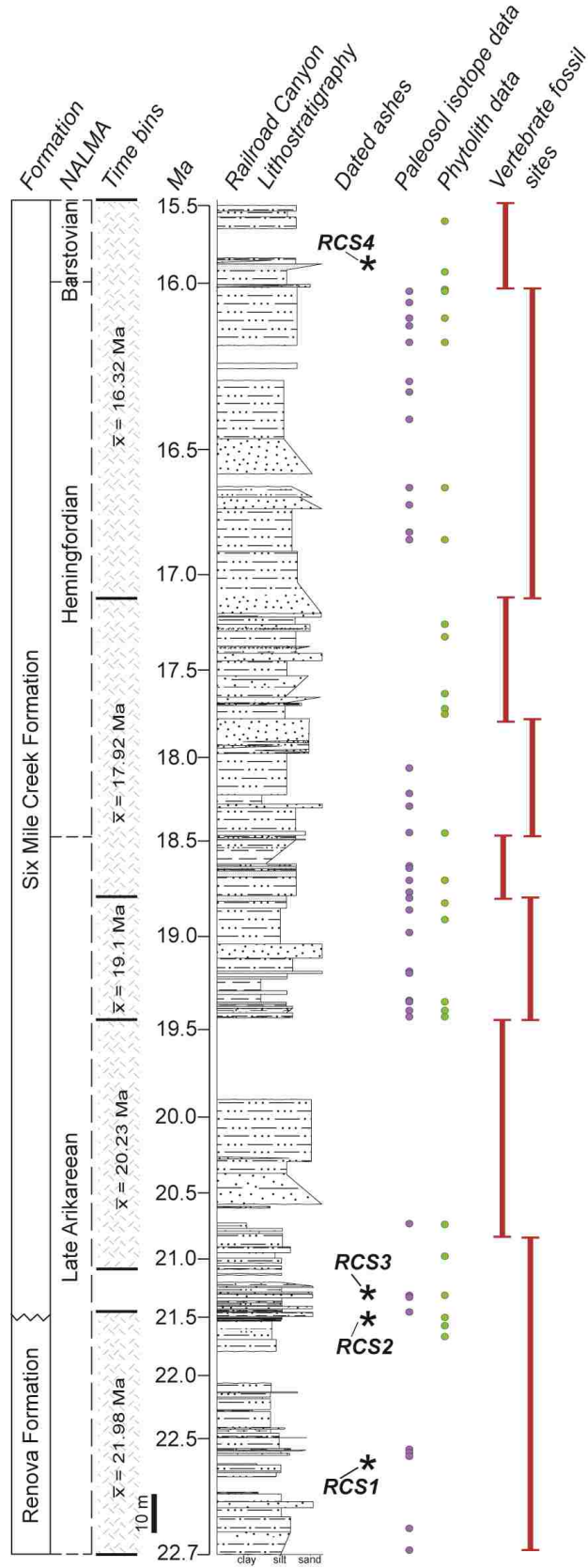
Figure 3.1. Stratigraphic section for the Railroad Canyon section showing formation boundaries, North American Land Mammal Ages (NALMAs), time bins used in this study, location of dated ashes, location of paleosols sampled for $\delta^{13}C_{org}$ and phytoliths (Chapter 2), and location of vertebrate fossil sites.
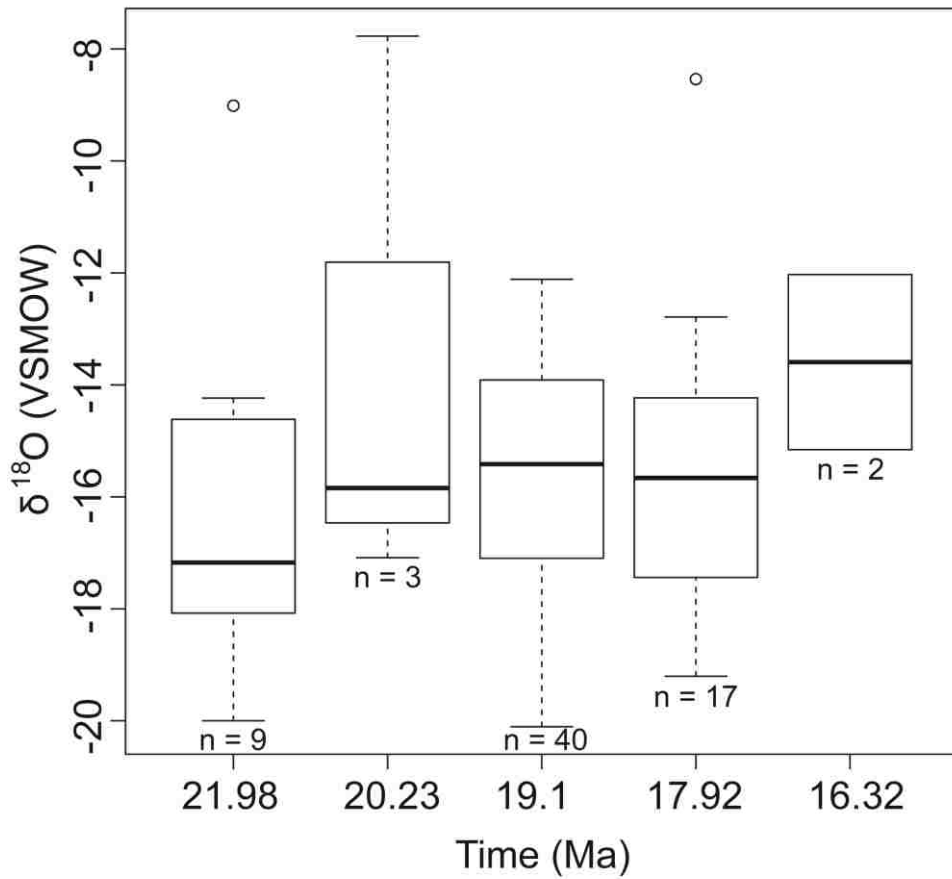
Figure 3.2. δ^{18}O of local water for all taxa during each time bin in the Railroad Canyon section. For each boxplot the dark line indicates the median, the box represents the interquartile range, the dashed lines indicate the range of measured values, and circles indicate outliers (greater than 1.5 times the interquartile range from the median), n = the number of samples.
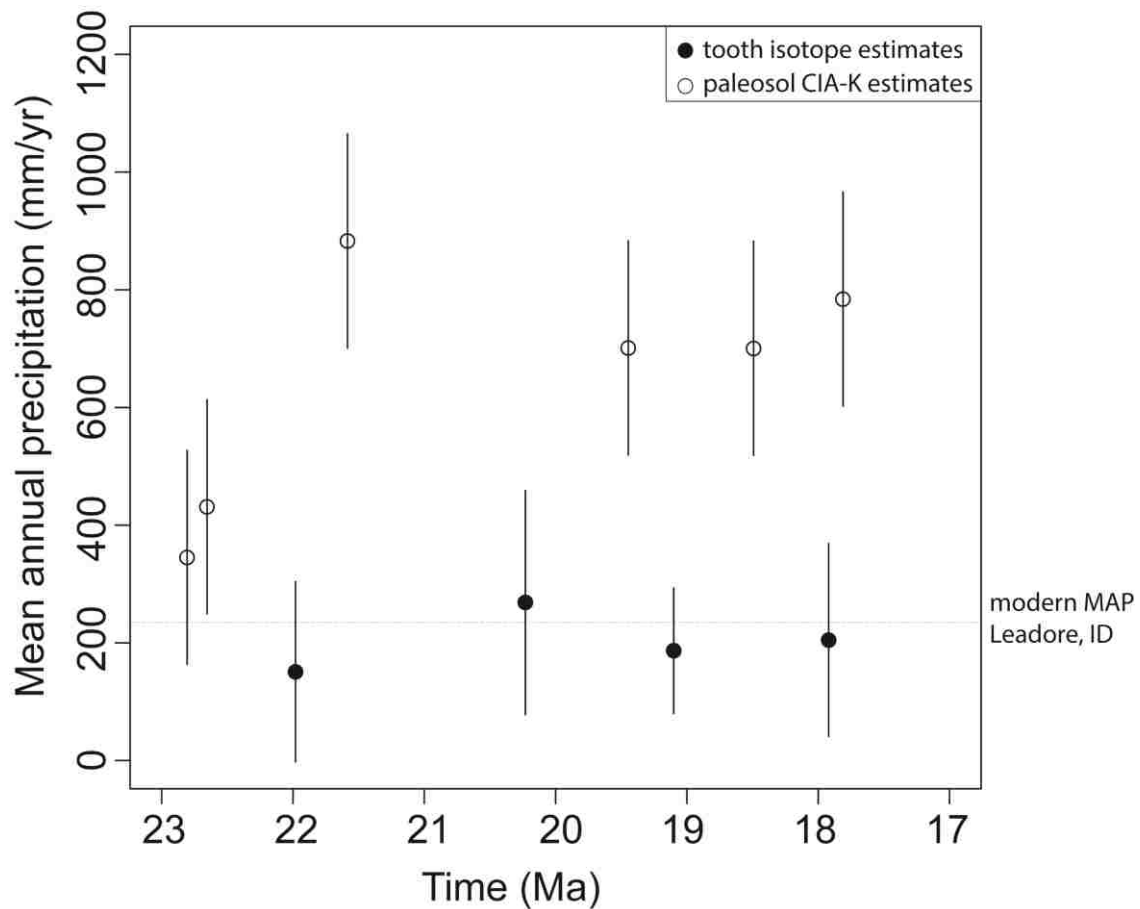
Figure 3.3. Estimates of mean annual precipitation (MAP in mm/yr) through time in the Railroad Canyon section (RCS). Filled circles are MAP estimates calculated from enamel $\delta^{13}C$ values for four RCS time bins (this study; Time bins as in Fig. 1) and hollow circles are estimates from paleosols (Retallack 2007). Dashed line represents modern MAP for Leadore, ID located ~12 miles south of the RCS.
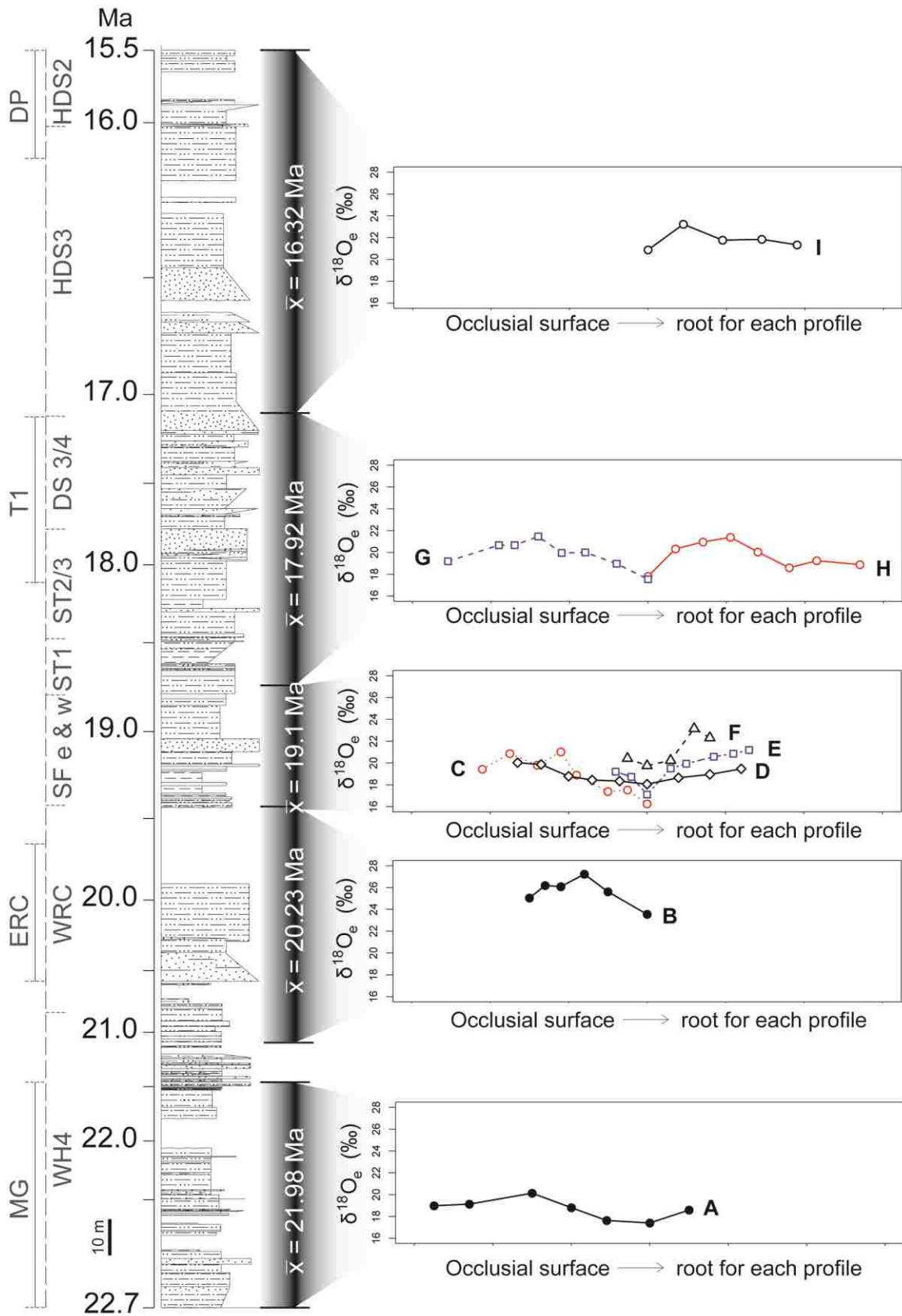
Figure 3.4. Bulk $\delta^{18}O$ enamel results from nine serial sampled equid and rhino teeth (some of which show quasi-sinusoidal seasonal variation) placed into the stratigraphic framework of the RCS. Hollow symbols are data from equid teeth and filled symbols are data from rhino teeth. Different line, color, and symbol types signify different individual teeth. A) UMVP 4482E; B) UWBM 100082; C) UMVP 4452A; D) UMVP 9426; E) UMVP 4453E; F) UWBM 100066; G) UMVP 5724; H) UMVP 5723; I) UMVP 4400. Vertebrate fossil locality names are abbreviated as follows: WH4, Whiskey Springs 4; MG, Mollie Gulch; WRC, West Railroad Cut; ERC, East Railroad Cut; SF e&w, Snowfence east and west; ST1, Snowfence Turtle 1; ST2/3, Snowfence Turtle 2 and 3; DS 3/4, Dead Squirrel 3 and 4; T1, Turtle 1; HDS3, High Dead Squirrel 3; HDS2, High Dead Squirrel 2; DP, Deadman Pass.

Table 3.1. Bulk $\delta^{18}O$ and $\delta^{13}C$ compositions of herbivore teeth from the Railroad Canyon

section, Idaho.

Sample number	Taxa	Time bin	δ13C (VPDB)	δ13C st. dev.	δ18O (VSMOW)	δ18O st. dev.
UWBM 100084	*Diceratherium*	17.92	-10.88	0.11	24.86	0.05
UWBM 100029	*Diceratherium*	19.1	-10.00	0.12	17.52	0.07
UWBM 100038	*Diceratherium*	19.1	-9.34	0.14	17.96	0.05
UWBM 100040	*Diceratherium*	19.1	-8.83	0.16	18.88	0.08
UWBM 100082	*Diceratherium*	20.23	-10.05	0.13	25.45	0.08
UMVP 5721	*Diceratherium*	17.92	-10.86	0.10	16.59	0.08
UMVP 4434	*Diceratherium*	19.1	-9.74	0.13	18.73	0.06
UMVP 4482A	*Diceratherium*	21.98	-10.24	0.13	16.18	0.08
UMVP 4482B	*Diceratherium*	21.98	-8.76	0.12	18.16	0.09
UMVP 4482C	*Diceratherium*	21.98	-9.20	0.12	17.46	0.08
UMVP 4482D	*Diceratherium*	21.98	-8.21	0.11	18.13	0.06
UMVP 4482E	*Diceratherium*	21.98	-8.35	0.11	18.37	0.11
UWBM 100012	Equid	19.1	-8.16	0.12	20.11	0.05
UWBM 100014	Equid	19.1	-9.15	0.07	16.62	0.03
UWBM 100026	Equid	19.1	-9.57	0.13	16.14	0.10
UWBM 100034	Equid	19.1	-11.25	0.12	20.56	0.07
UWBM 100035	Equid	19.1	-10.07	0.11	20.95	0.07
UWBM 100039	Equid	19.1	-10.25	0.12	18.38	0.07
UWBM 100042	Equid	19.1	-9.13	0.12	17.51	0.10
UWBM 100047	Equid	19.1	-10.33	0.06	20.21	0.03
UWBM 100052	Equid	19.1	-8.54	0.13	20.68	0.06
UMVP 99996	Equid	19.1	-8.30	0.10	17.42	0.07
UMVP 4483	Equid	21.98	-8.16	0.10	15.97	0.08
UWBM 100097	*Merychippus*	16.32	-8.89	0.10	19.73	0.07
UWBM 100107	*Merychippus*	17.92	-7.48	0.08	17.41	0.04
UWBM 102404	*Merychippus*	17.92	-11.00	0.10	19.36	0.06
UWBM 99988	*Merychippus*	17.92	-8.12	0.13	17.76	0.07
UWBM 100081	*Merychippus*	19.1	-7.43	0.11	18.05	0.05
UWBM 100002	*Merychippus*	19.1	-8.59	0.13	19.26	0.08

Table 3.1. *Continued*

Sample number	Taxa	Time bin	δ13C (VPDB)	δ13C st. dev.	δ18O (VSMOW)	δ18O st. dev.
UWBM 100005	*Merychippus*	19.1	-9.04	0.14	17.92	0.08
UWBM 100022	*Merychippus*	19.1	-9.06	0.07	15.89	0.05
UWBM 100049	*Merychippus*	19.1	-10.57	0.10	18.88	0.06
UWBM 100054	*Merychippus*	19.1	-9.36	0.11	21.22	0.06
UWBM 100055	*Merychippus*	19.1	-8.49	0.09	17.78	0.04
UWBM 100062	*Merychippus*	19.1	-9.54	0.10	19.38	0.07
UWBM 100063	*Merychippus*	19.1	-9.02	0.13	19.08	0.08
UWBM 100066	*Merychippus*	19.1	-8.06	0.11	20.08	0.07
UWBM 100070	*Merychippus*	19.1	-8.58	0.08	21.14	0.03
UMVP 4400	*Merychippus*	16.32	-7.73	0.12	22.15	0.06
UMVP 4159	*Merychippus*	17.92	-8.25	0.08	20.44	0.07
UMVP 4160	*Merychippus*	17.92	-8.77	0.10	20.45	0.04
UMVP 4219	*Merychippus*	17.92	-8.11	0.13	21.56	0.09
UMVP 5723	*Merychippus*	17.92	-7.94	0.11	20.06	0.08
UMVP 5724	*Merychippus*	17.92	-8.77	0.11	21.00	0.08
UMVP 4154A	*Merychippus*	17.92	-8.31	0.12	17.46	0.11
UMVP 4154B	*Merychippus*	17.92	-10.16	0.11	17.96	0.07
UMVP 4154C	*Merychippus*	17.92	-8.17	0.05	19.24	0.07
UMVP 4154D	*Merychippus*	17.92	-9.77	0.11	19.95	0.07
UMVP 4154E	*Merychippus*	17.92	-10.99	0.13	18.07	0.07
UMVP 4154F	*Merychippus*	17.92	-8.12	0.08	19.33	0.07
UMVP 5891	*Merychippus*	19.1	-8.43	0.09	19.95	0.05
UMVP 6420	*Merychippus*	19.1	-8.49	0.12	19.25	0.08
UMVP 6423	*Merychippus*	19.1	-7.89	0.13	19.74	0.06
UMVP 6424	*Merychippus*	19.1	-9.58	0.07	21.08	0.06
UMVP 7238	*Merychippus*	19.1	-8.65	0.12	20.80	0.05
UMVP 9218	*Merychippus*	19.1	-8.14	0.09	19.37	0.05
UMVP 9424	*Merychippus*	19.1	-9.99	0.09	19.67	0.05
UMVP 9426	*Merychippus*	19.1	-8.44	0.10	18.79	0.07
UMVP 4452a	*Merychippus*	19.1	-9.25	0.12	20.58	0.09

Table 3.1. *Continued*

Sample number	Taxa	Time bin	δ13C (VPDB)	δ13C st. dev.	δ18O (VSMOW)	δ18O st. dev.
UMVP 4453e	*Merychippus*	19.1	-8.33	0.11	20.04	0.09
UMVP 4453f	*Merychippus*	19.1	-7.84	0.12	21.48	0.07
UMVP 7160	*Merychippus*	20.23	-9.65	0.07	18.23	0.03
UMVP 9394	*Merychippus*	20.23	-9.06	0.10	19.19	0.06
UMVP 4547	*Merychippus*	21.98	-11.29	0.12	24.49	0.05
UMVP 4548	*Merychippus*	21.98	-8.38	0.09	20.44	0.07
UWBM 99995	*Miohippus*	19.1	-9.98	0.14	20.70	0.09
UWBM 100045	*Miohippus*	19.1	-7.22	0.12	20.97	0.10
UWBM 100050	*Miohippus*	19.1	-9.49	0.10	22.09	0.07
UWBM 99977	*Parahippus*	17.92	-9.18	0.07	18.96	0.04
UWBM 100064	*Parahippus*	19.1	-9.65	0.11	20.89	0.05
UMVP 4472	*Parahippus*	21.98	-8.56	0.11	20.15	0.07

Table 3.2. δ^{18}O compositions for serially sampled equid and rhino teeth from the Railroad Canyon.

Sample number	Taxa	Distance from occlusial surface (mm)	Time bin (Ma)	δ18O (VSMOW)	δ18O st. dev.
UWBM 100055-b	*Merychippus*	2.25	19.1	20.02	0.05
UWBM 100055-d		4.5		19.90	0.04
UWBM 100055-h		10.5		18.70	0.05
UWBM 100055-k		13.5		18.45	0.09
UWBM 100055-o		20.5		20.47	0.04
UWBM 100062-a	*Merychippus*	1	19.1	21.61	0.05
UWBM 100062-c		4.25		20.84	0.08
UWBM 100062-h		10.5		19.79	0.08
UWBM 100062-k		14.5		19.77	0.08
UWBM 100062-n		19		18.39	0.08
UWBM 100062-q		23.5		18.31	0.06
UWBM 100066-a	*Merychippus*	1.5	19.1	20.42	0.08
UWBM 100066-b		4		19.75	0.06
UWBM 100066-d		7		20.24	0.08
UWBM 100066-f		10		23.15	0.07
UWBM 100066-g		12		22.31	0.07
UWBM 100081-a	*Merychippus*	2	19.1	18.88	0.06
UWBM 100081-b		4		19.38	0.08
UWBM 100081-c		6		19.17	0.06
UWBM 100081-d		8		20.71	0.08
UWBM 100081-e		10		21.05	0.07

Table 3.2. *Continued*

Sample number	Taxa	Distance from occlusial surface (mm)	Time bin (Ma)	δ18O (VSMOW)	δ18O st. dev.
UMVP 4453Eb	*Merychippus*	1.5	19.1	19.20	0.07
UMVP 4453Eb		3.5		18.73	0.05
UMVP 4453Ec		5.5		17.10	0.06
UMVP 4453Ee		8.5		19.50	0.05
UMVP 4453Ef		10.5		19.93	0.06
UMVP 4453Eh		14		20.57	0.08
UMVP 4453Ei		16.5		20.85	0.07
UMVP 4453Ej		18.5		21.19	0.11
UMVP 5723a	*Merychippus*	2.5	17.92	17.81	0.10
UMVP 5723c		6		20.33	0.08
UMVP 5723e		9.5		20.95	0.07
UMVP 5723g		13		21.39	0.07
UMVP 5723i		16.5		20.04	0.05
UMVP 5723k		20.5		18.60	0.08
UMVP 5723m		24		19.24	0.08
UMVP 5723p		29.5		18.88	0.06
UMVP 5724a	*Merychippus*	2	17.92	19.18	0.08
UMVP 5724b		8.5		20.67	0.09
UMVP 5724c		10.5		20.67	0.05
UMVP 5724e		13.5		21.46	0.07
UMVP 5724g		16.5		19.96	0.09
UMVP 5724i		19.5		20.00	0.05
UMVP 5724k		23.5		18.97	0.05
UMVP 5724m		27.5		17.54	0.08

Table 3.2. *Continued*

Sample number	Taxa	Distance from occlusial surface (mm)	Time bin (Ma)	δ18O (VSMOW)	δ18O st. dev.
UMVP 9305a	*Merychippus*	1.5	19.1	20.73	0.10
UMVP 9305c		5		19.93	0.08
UMVP 9305e		8		20.32	0.09
UMVP 9305g		11		20.25	0.09
UMVP 9305i		14.5		20.07	0.07
UMVP 9305k		17.5		20.17	0.09
UMVP 9305l		19.5		20.58	0.03
UMVP 9426a	*Merychippus*	2	19.1	20.02	0.07
UMVP 9426c		5		19.87	0.08
UMVP 9426e		8.5		18.78	0.08
UMVP 9426g		11.5		18.44	0.07
UMVP 9426i		15		18.34	0.06
UMVP 9426k		18.5		18.06	0.07
UMVP 9426m		22.5		18.65	0.08
UMVP 9426o		26.5		18.95	0.06
UMVP 9426q		30.5		19.46	0.06
UMVP 4400 a	*Merychippus*	2	16.32	20.88	0.05
UMVP 4400 b		6.5		23.23	0.12
UMVP 4400 c		11.5		21.77	0.10
UMVP 4400 d		16.5		21.85	0.13
UMVP 4400 e		21		21.34	0.08

Table 3.2. *Continued*

Sample number	Taxa	Distance from occlusial surface (mm)	Time bin (Ma)	δ18O (VSMOW)	δ18O st. dev.
UMVP 4154Ea	*Merychippus*	2	17.92	19.98	0.11
UMVP 4154Ec		5.5		19.74	0.09
UMVP 4154Ee		8.5		19.44	0.06
UMVP 4154Eg		11.5		19.65	0.07
UMVP 4154Ei		14.5		19.26	0.08
UMVP 4154Ek		17.5		19.42	0.04
UMVP 4154Em		20.5		18.51	0.05
UMVP 4154Eo		24.5		19.03	0.10
UMVP 4159a	*Merychippus*	2.5	17.92	21.16	0.09
UMVP 4159c		5.5		21.50	0.06
UMVP 4159e		8.5		21.61	0.10
UMVP 4159g		11.5		21.23	0.06
UMVP 4159i		15.5		21.22	0.07
UMVP 4159k		19		20.33	0.08
UMVP 4159m		22.5		19.70	0.09
UMVP 4159o		26		19.97	0.07
UMVP 4154Fa	*Merychippus*	3.5	17.92	22.08	0.10
UMVP 4154Fc		6.5		20.45	0.09
UMVP 4154Fe		10.5		20.01	0.06
UMVP 4154Fg		14.5		19.03	0.07
UMVP 4154Fi		17.5		19.15	0.07
UMVP 4154Fk		21.5		19.26	0.05
UMVP 4154Fm		25.5		19.58	0.06
UMVP 4154Fn		27.5		19.67	0.07

151

Table 3.2. *Continued*

Sample number	Taxa	Distance from occlusial surface (mm)	Time bin (Ma)	δ18O (VSMOW)	δ18O st. dev.
UMVP 4452Aa	*Merychippus*	1.5	19.1	19.43	0.05
UMVP 4452Ac		5		20.86	0.08
UMVP 4452Ae		8.5		19.80	0.08
UMVP 4452Af		11.5		21.02	0.11
UMVP 4452Ag		13.5		18.89	0.07
UMVP 4452Ai		17.5		17.38	0.05
UMVP 4452Aj		20		17.53	0.09
UMVP 4452Ak		22.5		16.26	0.07
UMVP 6424a	*Merychippus*	2	19.1	19.84	0.06
UMVP 6424c		5.5		19.33	0.05
UMVP 6424e		9		19.95	0.06
UMVP 6424g		12.5		19.82	0.06
UMVP 6424i		16		19.63	0.07
UMVP 6424k		19		20.60	0.08
UMVP 6424m		23		20.65	0.10
UMVP 6424o		26.5		18.72	0.08
UWBM 100038-a	*Diceratherium*	3	19.1	17.60	0.09
UWBM 100038-c		7		18.68	0.07
UWBM 100038-e		10		18.12	0.05
UWBM 100038-g		13		17.61	0.07
UWBM 100038-i		16		17.64	0.03
UWBM 100038-k		19		17.08	0.06
UWBM 100038-m		21		17.66	0.04
UWBM 100038-o		25		18.50	0.07
UWBM 100038-q		30		17.43	0.07
UWBM 100038-r		32		16.97	0.07

Table 3.2. *Continued*

Sample number	Taxa	Distance from occlusial surface (mm)	Time bin (Ma)	δ18O (VSMOW)	δ18O st. dev.
UWBM 100084-a	*Diceratherium*	0	17.92	24.83	0.08
UWBM 100084-b		2		25.54	0.08
UWBM 100084-c		5		24.98	0.08
UWBM 100084-e		8		24.42	0.05
UWBM 100084-f		11		23.79	0.08
UWBM 100084-g		13.5		23.07	0.06
UWBM 100082-a	*Diceratherium*	1	20.23	25.04	0.06
UWBM 100082-b		3		26.19	0.07
UWBM 100082-c		5		26.09	0.09
UWBM 100082-e		8		27.23	0.05
UWBM 100082-g		11		25.61	0.06
UWBM 100082-i		16		23.55	0.04
UMVP 4482D-A	*Diceratherium*	4	21.98	19.96	0.03
UMVP 4482D-B		8		20.52	0.09
UMVP 4482D-C		12.5		19.15	0.05
UMVP 4482D-D		17		19.56	0.09
UMVP 4482D-E		21.5		19.50	0.04
UMVP 4482D-F		27		20.76	0.08
UMVP 4482D-G		31.5		19.42	0.10
UMVP 4482E-A	*Diceratherium*	1.5	21.98	18.98	0.05
UMVP 4482E-B		6		19.13	0.07
UMVP 4482E-D		14		20.13	0.10
UMVP 4482E-E		19		18.80	0.11
UMVP 4482E-F		23.5		17.63	0.08
UMVP 4482E-G		29		17.40	0.05
UMVP 4482E-H		34		18.59	0.07

Table 3.2. *Continued*

Sample number	Taxa	Distance from occlusial surface (mm)	Time bin (Ma)	δ18O (VSMOW)	δ18O st. dev.
UMVP 5721-A	*Diceratherium*	3	17.92	17.29	0.07
UMVP 5721-B		7		17.30	0.06
UMVP 5721-C		10.5		17.78	0.12
UMVP 5721-D		15.5		15.89	0.06
UMVP 5721-E		18		17.31	0.11
UMVP 4482C-A	*Diceratherium*	1	21.98	18.15	0.07
UMVP 4482C-B		5		19.31	0.14
UMVP 4482C-D		14		20.23	0.09
UMVP 4482C-E		18.5		19.28	0.08
UMVP 4482C-F		23		17.03	0.11
UMVP 4482C-G		27.5		18.53	0.10
UWBM 100040-a	*Diceratherium*	2	19.1	19.28	0.10
UWBM 100040-b		4		19.42	0.08
UWBM 100040-c		6		18.60	0.08
UWBM 100040-d		8		18.00	0.07
UWBM 100040-e		9		17.97	0.06

Table 3.3. MAP estimates calculated from δ^{13}C enamel compositions for four times bins in the Railroad Canyon.

	16.32 Ma	17.92 Ma	19.1 Ma	20.23 Ma	21.98 Ma	Avg. across all sites
MAP (mm/yr)	--	205	187	269	151	188
max estimate	--	369	294	460	304	292
min estimate	--	41	80	78	-2	84

Table 3.4. Number of individuals of each taxon that were analyzed per time bin.

	16.32 Ma	17.92 Ma	19.1 Ma	20.23 Ma	21.98 Ma
Taxa Bulk Sampled					
Diceratherium	--	2	4	1	5
Merychippus	2	14	22	2	2
Parahippus	--	1	1	--	1
Miohippus	--	--	3	--	--
unidentified equids	--	--	10	--	1
Taxa Serially Sampled					
Diceratherium	--	2	2	1	3
Merychippus	1	5	9	--	--

CHAPTER 4. Stable isotopes reveal differential dietary evolution in large ungulates during the early–middle Miocene in the Northern Rocky Mountains, USA

Elisha B. Harris, Caroline A.E. Strömberg, Matthew J. Kohn

ABSTRACT

Stable carbon isotope compositions of herbivore tooth enamel from the Railroad Canyon section (RCS) of Idaho are analyzed to investigate the long-term effects of climate and biotic change on mammalian dietary patterns leading into the mid-Miocene Climatic Optimum (MMCO). We investigate diet and patterns of resource partitioning among equids and rhinocerotids of the RCS in an attempt to better understand faunal change during the early–middle Miocene in western North America. In particular we focus on *Merychippus*, *Parahippus*, *Miohippus*, and *Diceratherium* across five time bins with average ages of 21.98 Ma, 20.23 Ma, 19.1 Ma, 17.92 Ma, and 16.32 Ma. Bulk $\delta^{13}C$ compositions range from –11.3‰ to –7.2‰ and indicate that RCS herbivores exclusively consumed C_3 vegetation likely in open habitats during the early–middle Miocene. Members of the equid genus *Merychippus* consistently fed in open habitats throughout the early–middle Miocene, whereas members of the rhinoceratid genus *Diceratherium* shifted to feeding in more closed canopy microhabitats through time, potentially as a result of competition with other herbivores. Additionally, *Merychippus* specimens have a larger dietary breadth (on average ~2.3‰) than *Diceratherium* (on average ~1.1‰) in all time

bins sampled suggesting this taxon was consuming a broader range of vegetation likely in a wider range of habitats. Negative correlations between $\delta^{13}C$ and $\delta^{18}O$ curves of serially sampled teeth suggest isotopic shifts that are likely explained by seasonal variations in plant growth and water availability. Our dietary data coupled with data from other RCS studies of vegetation and climate show patterns of ecosystem change that appear to be decoupled from global climate, illustrating the importance of testing for links between climate, vegetation, and faunas at the appropriate spatial scales during periods of global climate change such as the MMCO.

1. INTRODUCTION

The late early–middle Miocene is characterized by an interval of global climatic warming known as the mid-Miocene Climatic Optimum (MMCO; ca. 17–14.75 Ma) that is followed by long-term global climatic cooling (Zachos et al., 2001, 2008). In North America, pollen, phytolith, and paleosol data from the Great Plains and western North America suggest the structure and composition of vegetation changed leading up to the MMCO, as open-habitat, mainly C3 grasslands and woodlands spread and replaced forested habitats (Gabel et al., 1998; Harris et al., 2016b; Leopold and Denton, 1987; Retallack, 2007; Strömberg, 2005). Evidence from the Northern Rocky Mountains and the Great Plains also points to changes in ungulate species richness and composition during this time, including a dramatic increase in browser generic richness (Barnosky and Carrasco, 2002; Barnosky, 2001; Janis et al., 2000). In addition, whereas the MMCO coincided broadly with these major ecological transformations and biotic turnover events, it is unclear if global climate change was the ultimate driver in all cases (e.g., (Barnosky and Carrasco, 2002; Kohn and Fremd, 2008).

Our inability to directly evaluate links between climate, vegetation, and faunal change during the MMCO stems in part from the rarity of continuous, long-term records around the world that document ecosystem-level floral and faunal change for this global warming event. Recently, the early–middle Miocene Railroad Canyon section (RCS; Fig. 4.1) of Idaho has emerged as a rare opportunity to test such linkage during the lead-up to the MMCO (Harris et al., 2016a, 2016b).

The RCS (located in central-eastern Idaho; Fig. 4.1) was deposited ca. 23–15 Ma (Harris et al., 2016b) and preserves a seven million-year long fossil record of plants, animals, and climatic proxy data from a single basin in the Northern Rocky Mountains (NRM; Barnosky et al., 2007; Harris et al., 2016a; Retallack, 2009, 2007; Strömberg, 2005). During deposition of the RCS, global temperatures peaked at ~18°C and global atmospheric CO_2 levels increased as well (Beerling and Royer, 2011; Zachos et al., 2001, 2008). In contrast, locally within the RCS the climate appears to have been seasonally cool and semi-arid during the early–middle Miocene, with no dramatic changes in climate during this interval (Harris et al., 2016a). Local phytolith records from the RCS indicate open-habitat, mainly C_3 grasslands with a mosaic of woodland patches, and a gradual decrease in potential C_4 grasses within grass communities during the early–middle Miocene (Harris et al., 2016b). Regional data from the NRM, including the RCS, indicates an increase in grazers in faunal communities during the early–middle Miocene and a transition from oreodont-, camel-, chalicothere-, and rhino-dominated communities in the early Miocene to equid-dominated communities in the middle Miocene (Barnosky and Carrasco, 2002; Barnosky, 2001).

This discrepancy between subtle environmental changes and the more marked faunal shifts in northern Idaho begs the question: How did herbivores use available vegetation in RCS

through the lead-up to the MMCO and can changes in diet or habitat be used to explain faunal turnover? To address this over-arching question, we studied stable carbon and oxygen isotope values from the enamel of early–middle Miocene-aged herbivore teeth from the RCS. In particular, we address the following questions: (1) How were resources partitioned (e.g. C_3 vs. C_4 vegetation) among mammalian herbivore taxa that inhabited the RCS and did this partitioning change through time? (2) Did RCS herbivores display seasonal shifts in diet associated with observed, local seasonal shifts in climate (Harris et al., 2016a)? And (3) how do temporal patterns of diet or diet partitioning compare with faunal turnover during the early–middle Miocene in the NRM?

2. BACKGROUND

2.1 Northern Rocky Mountain fauna and changes through time

Many studies have attempted to test for relationships among faunal change, tectonism, and climate change during the early–middle Miocene in the Northern Rocky Mountains (NRM) by analyzing regional mammalian fossil datasets (e.g., Barnosky and Carrasco, 2002; Barnosky, 2001; Kent-Corson et al., 2013; Kohn and Fremd, 2008). Some of these studies suggested that a peak in mammalian species richness during the late early–middle Miocene was driven by the MMCO (Barnosky, 2001). However, others have concluded that tectonism in the NRM is more likely to have been the driver of increased diversity because less tectonically active provinces nearby (i.e., the northern Plains or Northwest) did not experience concurrent increases in richness and because the NRM faunas were unaffected by the Late Oligocene warming event (ca. 27–24 Ma; Barnosky and Carrasco, 2002). Instead, these authors suggest increased endemism in

the NRM may have led to increased faunal diversity ca. 15–16 Ma, potentially as a result of increased topographic heterogeneity over short distances (Barnosky and Carrasco, 2002).

Within the NRM, mammalian fossils have been recovered from 50 localities in and near the RCS (see Barnosky et al., 2007, table 1). These fossils suggest that the NRM faunas transitioned from being dominated by oreodonts, camels, chalicotheres, and rhinos prior to ca. 19.5 Ma to being increasingly dominated by equids in the latest Arikareean–Barstovian (after 19.5 Ma; Barnosky et al., 2007; timescale updated from Harris et al., 2016b). The composite stratigraphic section for the RCS was described across 11 field sites, ten of which were productive for fossil herbivore teeth (some field sites, such as Snowfence east and west, were much more productive than others, e.g., Whiskey Springs 4). Some of the biostratigraphically significant taxa from the RCS are shown in Figure 2 including two taxa, *Merychippus* and *Diceratherium*, which are present throughout the majority of the RCS. We have chosen to focus on these two taxa for our isotope analyses because they are abundant throughout the section and, therefore, should provide the best opportunity to test for changes in herbivore diets through the early–middle Miocene.

2.2 Isotopic composition of mammalian tooth enamel and inferring habitat structure

2.2.1 Bulk tooth enamel.—Tooth enamel is made up of the diagenetically resistant mineral hydroxylapatite that contains carbonate substitutions for the phosphate and hydroxyl groups (Kohn and Cerling, 2002). Because of the stability of this hard tissue, enamel is far less susceptible to diagenetic isotopic alteration than other biological tissues. Therefore, the stable isotopic composition of enamel is particularly useful in paleoecological and paleoclimatic studies (see reviews in Koch, 1998; Kohn and Cerling, 2002; Clementz, 2012).

161

The carbon isotopic composition of mammalian herbivore tooth enamel reflects the isotopic composition of ingested vegetation, with a known offset due to metabolic enrichment (Cerling and Harris, 1999; Koch, 1998; Lee-Thorp and van der Merwe, 1987; Passey et al., 2005). Because the carbon of ingested plant material is incorporated into the mineralized tissues of an herbivore, the carbonate component of dental enamel reflects the $\delta^{13}C$ composition of the plants that were eaten. Relative to the bulk $\delta^{13}C$ composition of ingested plant material, dental enamel is enriched in ^{13}C due to metabolic and biomineralization fractionation (DeNiro and Epstein, 1978). Metabolic enrichment between plant material and herbivore enamel is ~ +14.6 ± 0.3‰ for ruminants and +14‰ for non-ruminants (Cerling and Harris, 1999; Passey et al., 2005).

Mammalian herbivores with a C_3 diet can be distinguished from mammals with a C_4 or mixed C_3/C_4 diet because the distinct $\delta^{13}C$ signatures of these plants are compositionally preserved in dental enamel. The carbon isotopic compositions of plants are influenced by CO_2 fractionation during photosynthesis. Because plants can employ different photosynthetic pathways, this results in distinctly different carbon isotopic compositions for plants using each pathway (Ehleringer et al., 1991; O'Leary, 1988; Vogel, 1978). Modern C_3 plants (typically trees, shrubs, and cool-growing-season grasses) have an average $\delta^{13}C$ value of -28.5‰ and range between -20‰ to -37‰ (Kohn, 2010), whereas C_4 plants (warm-growing-season grasses and sedges) have an average $\delta^{13}C$ value of -13‰ and range between -9‰ to -19‰ (Cerling et al., 1997). Because C_3 and C_4 plants have nearly non-overlapping carbon isotopic ranges, pure C_3 and C_4 consumers are expected to have non-overlapping $\delta^{13}C_{enamel}$ ranges, whereas mixed C_3/C_4 feeders will have intermediate $\delta^{13}C_{enamel}$ values (Cerling et al., 1998, 1997; Koch, 1998; Macfadden and Cerling, 1996; Quade and Cerling, 1995).

Local floral records from the early–middle Miocene RCS suggest that mammals living in this study area inhabited open-habitat grasslands dominated by C_3 vegetation (Harris et al., 2016b; Strömberg, 2005). Within C_3 ecosystems, isotopic variability among C_3 plants can be driven by differences in temperature, nutrient availability, water stress, and light intensity (Heaton, 1999; Koch, 1998; O'Leary et al., 1992). For example, the $\delta^{13}C$ values of leaves are known to decrease with increasing precipitation/humidity and increase with increasing irradiance and certain plant functional types (e.g., evergreen species; Diefendorf et al., 2010; Ehleringer et al., 1986; Kohn, 2010; Stewart et al., 1995). This ultimately results in lower $\delta^{13}C$ values for plants growing in wet, forested habitats relative to the isotopic compositions of plants living in C_3-dominated, dry, open habitats. These isotopically unique compositions of plants are then transferred to and preserved in mammalian dental enamel, resulting in lower $\delta^{13}C_{enamel}$ values for herbivores feeding in closed, forested habitats and higher values for those feeding in more open, dry habitats (e.g., Cerling and Harris, 1999; Koch, 1998; O'Leary et al., 1992). However, because the $\delta^{13}C$ of individual plants within a species can vary depending on environmental conditions (e.g., C_3 grasses growing in forested regions are expected to have more depleted $\delta^{13}C$ values than C_3 grasses in open habitats), it is not possible to distinguish between individuals consuming C_3 grass and C_3 browse.

In addition to reconstructing the diets of specific taxa, $\delta^{13}C_{enamel}$ values from multiple mammals can be analyzed to determine how herbivorous taxa partitioned resources within ancient communities. Many of these applications have been particularly useful for determining niche partitioning (i.e., resource partitioning) among ungulates in C_3-dominated habitats (e.g., Bibi, 2007; Clementz, 2012; Feranec and Macfadden, 2006; Secord et al., 2008). Recent work has also demonstrated the effectiveness of using stable carbon isotopes in teeth to assess diets

and niche partitioning among carnivores from ancient communities (e.g., Domingo et al., 2012; Kohn et al., 2005).

    2.2.2 Serial sampling of tooth enamel.—Because tooth enamel forms over the course of a few months to 1–2 years (e.g., Fricke and O'Neil, 1996; Fricke et al., 1998; Kohn et al., 1998), serially sub-sampling teeth can reveal information about seasonal variations in diet that resulted from seasonal changes in the availability of food sources on the landscape (e.g., Clementz, 2012). Many modern ecological studies have shown that herbivores can change their diets seasonally with variation in vegetation abundance, such as the abundance of C_3 and C_4 grasses on the landscape (e.g., Muldavin et al., 2008; Seamster et al., 2014; Warne et al., 2010). This modern work provides a framework by which we can interpret seasonal isotopic changes in fossil teeth.

3. MATERIALS AND METHODS

3.1 Sites, samples and isotope analysis

    The Railroad Canyon section (RCS) is located in Bannock Pass, Idaho and consists of a series of field sites that outcrop along Idaho State Highway 29 (Fig. 4.1; Harris et al., 2016b). Isotope data presented here come from fossils collected mostly as float during the summers of 2013 and 2014 as well as specimens from the University of Montana's Paleontological Center (UMPC) collections. Overall, these fossils were collected from ten sites within the composite RCS (22.9–15.2 Ma) and four sites from the contemporaneous Mollie Gulch sections of the Lemhi Valley sequence, located 15-25 km north of Leadore, Idaho (Barnosky et al., 2007; Harris et al., 2016b; fig. 1). All analyzed specimens are housed at either the University of Washington's Burke Museum of Natural History and Culture (UWBM) or the UMPC.

The details of our sampling protocol are outlined in detail in Harris et al. (2016a; their section 3.2), and involved using a dental drill to remove enamel powder either in a single groove along the length of the tooth, or in a series of parallel grooves perpendicular to the growth axis of the tooth. Enamel powders were pretreated and analyzed according to the method outlined by Koch et al. (1997). Isotope compositions were determined by using a 2010 ThermoFisher Delta V Plus continuous flow mass spectrometer coupled with a GasBench II housed in the Stable Isotope Laboratory, Department of Geosciences, Boise State University.

We analyzed bulk carbon isotope samples from 59 equid (*Merychippus*, *Parahippus*, *Miohippus*, and Equidae undifferentiated), 12 rhinocerotid (*Diceratherium*), one unidentified perissodactyl, and two unidentified artiodactyl specimens (see also Harris et al., 2016a). Fifteen *Merychippus* and eight *Diceratherium* teeth were serially sampled and analyzed for the stable carbon (this study) and oxygen isotope compositions (Harris et al., 2016a). Fossils were identified to genus using fossil reference material from either the UWBM or UMPC, and identifications were crosschecked with published biostratigraphic ranges (e.g., Janis et al., 1998; Tedford et al., 2004). Due to uncertain species-level taxonomic identifications, interpretation of these data are made with the understanding that the observed generic diets could represent a range of diets from individuals representative of multiple species (see similar approaches in Maguire, 2015; Zanazzi and Kohn, 2008). Additionally, because of the limited number and distribution of individual teeth collected from fossil-bearing sites in the RCS, we have grouped our data into four time bins to increase sample sizes for each time interval. Time bins have the following mean ages: 21.98 Ma (representing ca. 1 million years), 20.23 Ma (representing ca. 1.7 million years), 19.1 Ma (representing ca. 0.7 million years), 17.92 Ma (representing ca. 1.6

million years), and 16.32 Ma (representing ca. 1.5 million years), following the age model of Harris et al. (2016b; Fig. 4.1).

3.2 Modeling carbon isotope values for middle Miocene mammals

Following the general methods of Passey et al. (2002) and Kohn et al. (2005) we developed a model to predict the habitats in which RCS taxa were likely feeding during the early-middle Miocene (Fig. 4.3). Because far more $\delta^{13}C$ values have been published for modern plants than for modern mammals, this model is based on $\delta^{13}C$ values of extant plants, which provides approximated cutoffs for particular habitat types (e.g., the absolute maximum C_3 vegetation limit, the upper isotopic boundary for closed-canopy forests; Kohn, 2010). These modern plant $\delta^{13}C$ values were normalized to parameters of the early-middle Miocene of Idaho by correcting for factors such as: (1) the effect of latitude on the $\delta^{13}C$ values of vegetation; (2) the effect of elevation on the $\delta^{13}C$ values of vegetation; (3) diet-enamel isotope enrichment; and (4) changes in the $\delta^{13}C$ composition of atmospheric CO_2 between the Miocene and present.

We corrected for the isotopic effects of latitude on plant $\delta^{13}C$ using the correction factor of 0.0124‰ per degree latitude published by Kohn (2010). We used the modern latitude of the RCS today (44.8º N) for this correction, which we believe is a fair assumption since paleogeographic reconstructions indicate that North America was approximately at the same latitude during the Miocene as it is today (e.g., Atwater and Stock, 1998). We also accounted for the effect of elevation on the $\delta^{13}C$ values of plants using the correction factor of 0.19‰ per km of elevation published by Kohn (2010). To account for this, we normalized our modern $\delta^{13}C$ plant data to 2 km, which is our estimate of RCS elevation during the early–middle Miocene. This conservative elevation estimate was established by considering the site's modern elevation

(~2.3 km), the fact that nearby isotopic records suggest little to no evidence for uplift after 15 Ma

in southwestern Montana, and that regional paleoelevation was likely over 2 km by the late

Miocene (Chamberlain et al., 2012). This estimate accounts for the fact that regional uplift was

ongoing during and after deposition of the RCS (Chamberlain et al., 2012; McMillan et al.,

2002).

To correct for diet-enamel enrichment of RCS ungulate teeth, we assume an average

enrichment of 14.1 ± 0.5‰, which is the enrichment factor for extant, large-bodied ungulates

(Cerling and Harris, 1999; Passey et al., 2005). Based on a dataset of atmospheric $\delta^{13}C$ values

inferred from the isotopic composition of benthic foraminifera (Tipple et al., 2010), we estimate

that the early–middle Miocene atmosphere was ~0.87‰ more positive (-5.63‰) than during the

pre-industrial Holocene (~-6.5‰), or ~2.4‰ more enriched in ^{13}C than in 2000 AD. This

estimate of atmospheric $\delta^{13}C$ is an average estimate calculated from values between 22.9–15.2

Ma in the global dataset published by Tipple et al. (2010).

4. RESULTS

4.1 Stable carbon isotope results from bulk enamel sampling

Enamel carbon isotope compositions for all RCS specimens ranged from –11.3‰ to

–7.2‰ with an average of –9.1‰ (Table 4.1). Mean $\delta^{13}C_{enamel}$ values by taxa are as follows: –8.8

± 0.95‰ for *Merychippus*, –8.9 ± 1.48‰ for *Miohippus*, –9.1 ± 0.55‰ for *Parahippus*, –9.4 $\pm$

1.03‰ for unidentified equids, and –9.5 ± 0.91‰ for *Diceratherium*. All specimens preserve

$\delta^{13}C$ values that fall within the range expected for a pure C$_3$ diet (Fig. 4.3).

Additionally, we compared $\delta^{13}C_{enamel}$ values of multiple taxa within each time bin

(assuming each taxon is represented by >1 individual specimen) with the exception of the

youngest time bin (16.32 Ma) where we only have data for *Merychippus*. No statistically significant differences in $\delta^{13}C_{enamel}$ values were found for any pairwise comparisons of coeval taxa (Welch's t-test, p>0.05), except for *Diceratherium* and *Merychippus* at 17.92 Ma (Welch's t-test, p << 0.05).

Merychippus and *Diceratherium* are the only taxa sufficiently sampled (> 1 specimen per time bin) across multiple time bins to allow for comparison of $\delta^{13}C_{enamel}$ over time. Data for *Merychippus* shows no statistically significant difference in $\delta^{13}C_{enamel}$ values through all five time bins (ANOVA, p = 0.05; Fig. 4.4A). Data for *Diceratherium* (two time bins only) shows a statistically significant decrease in $\delta^{13}C_{enamel}$ values from 21.98 Ma to 17.92 Ma (ANOVA, p << 0.05; Fig. 4.4B).

4.2 Stable isotope results from serial enamel sampling

$\delta^{13}C_{enamel}$ values for all *Merychippus* specimens across all time bins range from –11.4‰ to –7.0‰ with an average $\delta^{13}C$ value of –9.2‰ (Table 4.2). $\delta^{13}C_{enamel}$ values for all *Diceratherium* specimens across all time bins range from –12.4‰ to –8.6‰ with an average $\delta^{13}C$ value of –9.9‰. The magnitude of $\delta^{13}C$ seasonal variation for the majority (~70%) of serially specimens was less than 1‰ with the exception of specimens UMVP 4400 (*Merychippus*, 1.32‰), UMVP 6424 (*Merychippus*, 1.32‰), UMVP 9426 (*Merychippus*, 1.07‰), UWBM 100062 (*Merychippus*, 1.11‰), UMVP 5721 (*Diceratherium*, 1.44‰), UWBM 100040 (*Diceratherium*, 2.12‰), and UMVP 4482C (*Diceratherium*, 1.88‰). Seven (30%) of the serially sampled teeth display negative correlations between $\delta^{13}C$ and $\delta^{18}O$ values (Fig. 4.5), namely UWBM 100040 (p << 0.05, R^2 = 0.96; *Diceratherium*), UMVP 4482E (p << 0.05, R^2 = 0.64; *Diceratherium*; Fig. 4.6A), UWBM 100062 (p << 0.05, R^2 = 0.87; *Merychippus*; Fig.

4.6D), UMVP 4154F ($p \ll 0.05$, $R^2 = 0.72$; *Merychippus*; Fig. 4.6G), UMVP 5724 ($p \ll 0.05$, $R^2 = 0.43$; *Merychippus*; Fig. 4.6F), UMVP 4452A ($p \ll 0.05$, $R^2 = 0.57$; *Merychippus*; Fig. 4.6C), and UMVP 4453E ($p \ll 0.05$, $R^2 = 0.62$; *Merychippus*; Fig. 4.6B).

4.3 Habitat modeling

Our model results predict the following approximate vegetation boundaries based on the $\delta^{13}C$ enamel compositions of RCS ungulates: –14.1‰ for closed canopy forests; –8.1‰ for the lower bound for dry C_3 ecosystems; –6.8‰ for average C_3 vegetation limit (above this are mixed C_3/C_4 open habitats); and –5.6‰ for absolute maximum C_3 vegetation limit (above this MAP is <10 mm per year and limited to C_4 plants, lichen, or plants using Crassulacean acid metabolism; Fig. 4.3).

5. DISCUSSION

5.1 Dietary stasis and niche partitioning

$\delta^{13}C$ values for all RCS taxa fall below –7.03‰ suggesting the diets of these herbivores consisted solely of C_3 vegetation, likely from open habitat environments, during the early–middle Miocene. This is consistent with local vegetation records that indicate primarily open habitats dominated by C_3 grasses in the RCS during this time (Harris et al., 2016b). Additionally, our data are consistent with $\delta^{13}C_{enamel}$ records from North America and around the world that do not suggest definitive C_4 plant consumption until the late Miocene–Pliocene (Cerling et al., 1997). Tracking $\delta^{13}C_{enamel}$ compositions for *Merychippus* through the RCS indicates that members of this taxon did not change their diets through the early–middle Miocene (Fig. 4.4A). Instead these

individuals consistently fed on C_3 vegetation open-habitat environments (Fig. 4.3). The variability in $\delta^{13}C_{enamel}$ compositions for *Merychippus* specimens throughout the RCS likely suggests these animals were able to take advantage of a range of food sources in a variety of environments at this site. This observation falls in line with analyses by Mihlbachler et al. (2011), who suggested that *Merychippus* had crown heights and mesowear patterns consistent with those of modern mixed feeders and grazers, and Feranec (2007), who suggested hypsodonty enabled a broader feeding strategy beyond purely grazing.

In contrast to the relatively static dietary strategy of *Merychippus*, members of the genus *Diceratherium* preserve $\delta^{13}C_{enamel}$ compositions that potentially indicate a shift in diets between 19.1 Ma and 17.92 Ma (Fig. 4.4B). From 21.98 to at least 19.1 Ma, RCS rhinoceratids fed on C_3 vegetation in both wet and dry open-canopy environments, similarly to *Merychippus*. However, by 17.92 Ma RCS *Diceratherium* specimens (n = 2) indicate this taxon began feeding in the wettest parts of the local mesic, open-canopy forests with $\delta^{13}C$ values very close to the isotopic boundary for closed canopy forest biomes (Fig. 4.3). Unfortunately, due to sampling only a few *Diceratherium* at 17.92 Ma and a lack of data for *Diceratherium* at 16.3 Ma, we are unable to discern if this shift in diet was universal within this taxon after 17.92 Ma or if these data represent a long-term shift in dietary preference. Most literature published on *Diceratherium* is purely taxonomic in nature (e.g., Prothero and Rasmussen, 2008; Prothero, 2005, 1998), although some oxygen isotope data for this taxon have been reported from the John Day Basin, Oregon (Kohn and Fremd, 2007). Additionally, there is no quantitative paleoecological data published on *Diceratherium*. That being said, Prothero (2005) concluded, based on skull shape, occiput, and premaxillary dentition that *Diceratherium* were likely browsers that fed on bushes and trees growing near water sources. Our data do not reject this hypothesis and may even

support it given that RCS *Diceratherium* at 21.98 Ma and 19.1 Ma (Fig. 4.3) have more depleted

$\delta^{18}O$ values than many of the herbivores they co-occur with, potentially suggesting eating

vegetation in a higher humidity environment (e.g., in more closed microhabitats near water

sources).

Our data also provide insights into how various herbivores partitioned dietary niche (i.e.,

resource) space among herbivores through time in the RCS. Thus, at 21.98 Ma *Merychippus* and

Diceratherium have overlapping carbon and oxygen isotope values (Fig. 4.3; Fig. 4.7C; Fig.

4.7F), and at 19.1 Ma, all of the taxa overlap when only $\delta^{13}C$ is considered (Fig. 4.7B). This

pattern suggests that these herbivores were feeding on isotopically similar C_3 food sources and

this behavior persisted through the early–middle Miocene. However, when only $\delta^{18}O$ is

considered at 19.1 Ma, *Diceratherium* teeth are significantly more depleted in ^{18}O than

Miohippus (Fig. 4.7E). This difference suggests that although these taxa were eating in and

occupying the same area of the landscape, they may have drank water from different sources.

Alternatively, the data may suggest taxon-specific differences in tooth enamel mineralization

processes.

Lastly, at 17.92 Ma our data suggest habitat and resource partitioning ($\delta^{13}C$ differences)

between *Diceratherium* and *Merychippus* (Fig. 4.7A). At this time, *Merychippus* continued to

feed on C_3 plants in open-habitat environments, whereas *Diceratherium* began feeding in slightly

wetter parts of open habitat. This transition from a broad to narrow feeding strategy for RCS

Diceratherium is evident when tracking the $\delta^{13}C$ of this taxon through time (Fig. 4.4B). If a real

biological phenomenon, it is unlikely that changes in *Diceratherium* diets were driven by

changes in the distribution and availability of mesic forest biomes on the landscape because

phytolith data do not indicate such a transition through the RCS (Harris et al., 2016b). However,

increased local competition with other herbivores such as *Menoceras* (the only other North American rhino of that time; Prothero 1998; Prothero 2005), or contemporaneous horses, which were increasing in species diversity in the Northern Rocky Mountains during the early–middle Miocene (e.g., Barnosky et al., 2003), could have forced *Diceratherium* to alter its feeding habits. Given that we currently have only two rhino specimens sampled at 17.92 Ma, additional data will be necessary to further test this hypothesis and determine if this isotopic shift is a real biological phenomenon.

5.2 Dietary niche breadth

Comparing the variance in $\delta^{13}C$ for *Merychippus* and *Diceratherium* through the RCS reveals that whenever these two taxa co-occur in a single time bin, *Diceratherium* always has a smaller variance (Fig. 4.7A-C). These data could indicate that *Diceratherium* occupied a narrower dietary niche, for example consuming more browse or understory plants in the mesic open canopy forest. Conversely, contemporaneous *Merychippus* individuals may have consumed more C_3 grasses from a variety of habitats in both wet and dry, woodland and open-habitat environments. However, with our current dataset we cannot determine if the breadth in *Merychippus* and *Diceratherium* diets was a true feature of the lifestyle of these animals or a result of insufficient sample sizes and/or taxonomic resolution. Alternatively, the broad dietary range for *Merychippus* in the RCS may reflect changes in diet due to seasonality, time averaging, or differences in tooth enamel mineralization.

5.3 Seasonality of diets

The majority of serially sampled specimens from the RCS show relatively low variability in δ^{13}C (<1‰ difference between the highest and lowest δ^{13}C values) with seven specimens (four *Merychippus* and two *Diceratherium*) showing between 1–2.1‰ variation. If this isotopic variation was due to seasonal changes in diet, we would expect to see obvious sinusoidal patterns in δ^{13}C that correspond with summer maxima and winter minima δ^{18}O values. In some cases (Fig. 4.6A and 4.6F) the corresponding δ^{18}O curves record summer maxima and winter minima, however, the associated δ^{13}C curves do not show obvious sinusoidal patterns. This suggests that the small variations in δ^{13}C associated with seasonal variations in δ^{18}O are not likely a result of seasonal variations in diet but rather more likely result from seasonal variations in plant water use efficiency.

Comparing δ^{13}C and δ^{18}O curves for serially sampled teeth reveals negative correlations for seven specimens (five *Merychippus* and two *Diceratherium*; Fig. 4.5). Previous studies of stable isotopes in large mammals have shown similar inverse correlations (e.g., Barnosky et al., 2007; Biasatti et al., 2010; Bocherens et al., 2001; Feranec et al., 2009; Kohn and McKay, 2012). Kohn and McKay (2012) suggest that these inverse correlations could result from a combination of factors related to seasonality of available food sources and seasonality of plant growth. For example, Farquhar et al. (1989) and Kohn (2010) show that δ^{13}C values of plant tissues decrease with increasing moisture availability. Accordingly, if summer growing seasons (intervals of high δ^{18}O) in the RCS were relatively wet during the early–middle Miocene like they are today (i.e., Leadore, ID receives ~54% of its annual rainfall between May–August) then we might expect to see correspondingly lower plant δ^{13}C values during this time of the year. The fact that we see this

pattern in some of our samples points to a seasonally arid climate with summer precipitation had become established in the NRM by the early Miocene.

Another potential explanation for negative correlations between δ^{13}C and δ^{18}O values is that these animals consumed different parts of the same plants during different seasons. Different parts of the same plant can have different δ^{13}C compositions; for example, leaf litter, bark, and twigs, are known to be enriched in ^{13}C (Dawson et al., 2002). During portions of the year when temperatures are cool and precipitation limited, new plant growth is relatively uncommon. As a result, herbivores may need to rely on alternative food sources during those seasons, which could result in minimum δ^{18}O values of enamel during the winter associated with enriched δ^{13}C values (Kohn and McKay, 2012).

Why do only some specimens exhibit these seasonal variations in isotope compositions? One explanation is that seasonal variations in water and resource availability were not constant or consistent throughout deposition of the RCS. This would result in different individuals experiencing slightly different levels of seasonality of water and food, thus resulting in different δ^{18}O and δ^{13}C relationships in serial sampled teeth. This source of variation becomes amplified by temporal binning because we grouped individuals that did not co-occur. Despite the fact that not all serially sampled teeth preserve δ^{13}C and δ^{18}O seasonal patterns, those individuals that do are likely explained by seasonal variations in plant growth and water availability.

5.4 Paleoecology of the Railroad Canyon section

The RCS was deposited during a tectonically active period in the geologic history of North America. A broad regional plateau that had been created from the mid-Mesozoic through Eocene (DeCelles, 2004) began to collapse with initiation of Basin and Range extension in the

mid-Miocene (e.g., Atwater and Stock, 1998). An erosional unconformity, regionally termed the Mid-Tertiary Unconformity, perhaps indicates regional uplift ca. 21.4–21.5 Ma (see discussion in Harris et al., 2016b). Diatom relative abundance data coupled with carbon-isotope based mean annual precipitation estimates suggest the RCS transitioned from a floodplain depositional environment to an increasingly upland, alluvial fan depositional environment (Harris et al., 2016a). Oxygen isotope records from the RCS suggest a seasonally warm and wet, semi-arid climate during the early–middle Miocene, similar to the climate of this region today (Harris et al., 2016a). Additionally, these climatic patterns persisted relatively unchanged throughout deposition of the RCS.

Vegetation during the early–middle Miocene in the RCS was characterized by an open-habitat mosaic with large regions dominated by C_3-pooid grasslands and other areas with a mix of open woodlands (Harris et al., 2016b). Wetter microhabitats were also present at this time and may have provided a refuge for seemingly water-loving PACMAD grasses, potentially located near sources of water. Given that local climate was seasonally wet, it is likely that the productivity of plants living in these grassland and woodland patches varied throughout the course of the year, providing variation in the timing of food availability for some local herbivores (see discussion in Section 5.3).

The fauna of the RCS contains numerous small mammals (e.g., lagomorphs and rodents), a diversity of ungulates (including a variety of horses, oreodonts, antilocaprids, and camels), and a several carnivores (Barnosky et al., 2007). The isotope data here indicate that the horse *Merychippus* and rhino *Diceratherium* lived in open habitat, C_3 grassland environments and had pure C_3 diets during the early–middle Miocene. These data are consistent with vegetation reconstructions from this site and suggest that these herbivores had rather generalist C_3 diets,

175

consuming the plants that were abundant on the landscape. Previous studies of tooth crown

heights and mesowear patterns in *Merychippus* have suggested that these horses were likely

mixed feeders and grazers (Mihlbachler et al., 2011). Given that C_3, pooid grasses were the most

dominant vegetation in the RCS (Harris et al., 2016b) and that the majority of *Merychippus*

specimens sampled have carbon isotope values that fall within our reconstruction of a dry, open-

canopy habitat, it is probable that the majority of individuals we sampled in this study were

consuming mainly C_3, pooid grasses. If Prothero (2005) is correct in his assertion that

Diceratherium species were browsers, then it is likely that these rhinos fed on C_3 plants in the

woodland patches that characterized parts of the RCS landscape (Harris et al., 2016b).

In general, Barnosky (2001) suggested that ungulate faunas changed compositionally

during the early–middle Miocene with equids, camelids, and antilocaprids replacing oreodontids

as the dominant, large-bodied herbivores of the NRM (Fig. 4.2). These faunal changes also

meant a transition from taxa with low-crowned teeth to taxa with higher-crowned dentition,

interpreted as a shift from browsers to grazers and/or mixed feeders (Barnosky 2001) that likely

inhabited increasingly open habitats (Harris et al., 2016b; Strömberg, 2006). Broadly speaking,

these faunal changes signal a modernization of faunas in the region and indicate increased

abundance and diversity of grazers living in open-habitats. Phytolith data from the RCS suggest

there were no concurrent changes in vegetation that can explain the changes in faunal

communities observed in the NRM (Harris et al., 2016b). Furthermore, there is no broad

correlation between timing of faunal change and onset of mid-Miocene warming or even peak

global warming during the MMCO. Therefore, climate and vegetation could not have been the

trigger for these faunal changes. So then, could changes in diet or niche partitioning have led to

these faunal changes in the NRM? Our limited dataset from the RCS do not show dramatic

changes in diet or niche partitioning during the early–middle Miocene that are associated with these broad scale faunal changes in the NRM. Additionally, we do not have isotope data for oreodonts that would allow us to explicitly test for concurrent dietary changes in oreodonts, horses, and rhinos during the critical transition from oreodont- to horse-dominated faunal communities. Therefore, we cannot robustly test the hypothesis that diet was a main driver of faunal turnover in the NRM. However, we can say that for a subset of the herbivores within faunal communities during the early–middle Miocene (equids and rhinos) there were no changes in diet that coincided with their increase in relative abundances during this time. Yet there is a broad correlation in time with a change in *Diceratherium* diets in the RCS (this study) and a regional immigration event that occurred ca. 18.5 Ma (Woodburne and Swisher, 1995). It is possible this immigration event could have resulted in competition for resources and thus, resulted in shifts in *Diceratherium* diets. However, additional data for *Diceratherium* as well as data for some of these immigrant taxa (e.g., *Menoceras*) are necessary to test this explicitly.

5.5 Merychippus regional dietary comparison during the early–middle Miocene

The John Day Fossil Beds National Monument (JDNM) in eastern Oregon is similar to the RCS in that it preserved a relatively continuous sequence of rocks and fossils deposited around the mid-Miocene climatic optimum (Dillhoff et al., 2009). A recent study by Maguire (2015) details the dietary preferences and niche partitioning among equids that inhabited central and eastern Oregon (including fossils from the JDNM) from the late Oligocene to the interval following MMCO peak warming ca. 16 Ma (with sparse data between ca. 23 Ma to ca. 16 Ma). Our results are consistent with the $\delta^{13}C$ enamel results from Oregon equids (Maguire 2015) in that both studies indicate pure C_3 diets for equids during the middle Miocene. Although the

equids from Oregon and those from the RCS have similarly variable isotopic ranges, the

$\delta^{18}O_{enamel}$ values of the Oregon equids are higher on average. This pattern is likely a result of

differences in elevation between these sites and because the RCS received more rainout relative

to the Oregon sites (due to distance from moisture sources). Our $\delta^{13}C_{enamel}$ results are also in

keeping with contemporaneous isotope results from California and Nebraska that show that

Merychippus consumed solely C$_3$ vegetation during the middle Miocene (ca. 17.5 to 15 Ma;

Wang et al., 1994).

6. CONCLUSION

Our study of the $\delta^{13}C$ of tooth enamel showed that ungulate herbivores in central-eastern

Idaho exploited C$_3$ vegetation as a food source and lived in open habitats during the early–

middle Miocene. Members of the equid genus *Merychippus* consistently fed in open habitats

throughout the early–middle Miocene, whereas members of the rhino genus *Diceratherium* may

have shifted to feeding in more moist, open-microhabitats through time, potentially as a result of

competition with other herbivores. Additionally, *Merychippus* had a larger dietary breadth than

Diceratherium in all time bins sampled suggesting that, relative to *Diceratherium*, this taxon was

consuming a broader range of vegetation likely in a wider range of habitats. Furthermore,

analysis of serially sampled enamel indicates seasonal shifts in enamel oxygen isotope

compositions but minimal shifts in carbon isotope compositions in multiple specimens of

Merychippus and *Diceratherium*. This pattern suggests that these herbivores were not changing

their food sources seasonally. Our findings of niche conservatism and dietary stasis among

horses are consistent with contemporaneous isotope studies from North America. Our dietary

data coupled with data from other RCS studies of vegetation and climate illustrate the

importance of studying periods of global climate change at small spatial scales because not all regions on Earth experience climate change to the same magnitude and degree. Studying smaller geographic regions and integrating multiple lines of evidence are critical for piecing together the dynamics of abiotic and biotic change leading into and beyond the MMCO.

ACKNOWLEDGEMENTS

REFERENCES

Atwater, T., Stock, J., 1998. Pacific-North America Plate Tectonics of the Neogene
Southwestern United States–An Update. Int. Geol. Rev. 40, 375–402.

Barnosky, A.D., 2001. Distinguishing the effects of the Red Queen and Court Jester on Miocene
mammal evolution in the northern Rocky Mountains. J. Vertebr. Paleontol. 21, 172–185.

Barnosky, A.D., Bibi, F., Hopkins, S.S.B., Nichols, R., 2007. Biostratigraphy and
magnetostratigraphy of the Mid-Miocene Railroad Canyon Sequence, Montana and Idaho,
and age of the Mid-Tertiary Unconformity west of the Continental Divide. J. Vertebr.
Paleontol. 27, 204–224.

Barnosky, A.D., Carrasco, M.A., 2002. Effects of Oligo-Miocene global climate changes on
mammalian species richness in the northwestern quarter of the USA. Evol. Ecol. Res. 4,
811–841.

Barnosky, A.D., Hadly, E. a., Bell, C.J., 2003. Mammalian Response To Global Warming on
Varied Temporal Scales. J. Mammal. 84, 354–368.

Beerling, D.J., Royer, D.L., 2011. Convergent Cenozoic CO2 history. Nat. Geosci. 4, 418–420.

Biasatti, D., Wang, Y., Deng, T., 2010. Strengthening of the East Asian summer monsoon
revealed by a shift in seasonal patterns in diet and climate after 2-3Ma in northwest China.
Palaeogeogr. Palaeoclimatol. Palaeoecol. 297, 12–25.

Bibi, F., 2007. Dietary niche partitioning among fossil bovids in late Miocene C3 habitats:
Consilience of functional morphology and stable isotope analysis. Palaeogeogr.

Palaeoclimatol. Palaeoecol. 253, 529–538.

Bocherens, H., Mashkour, M., Billiou, D., Pellé, E., Mariotti, A., 2001. A new approach for
studying prehistoric herd management in arid areas: intra-tooth isotopic analyses of
archaeological caprine from Iran. Earth Planet. Sci. 332, 67–74.

Cerling, T.E., Ehleringer, J.R., Harris, J.M., 1998. Carbon dioxide starvation, the development of
C4 ecosystems, and mammalian evolution. Philos. Trans. Biol. Sci. 353, 159–171.

Cerling, T.E., Harris, J.M., 1999. Carbon isotope fractionation between diet and bioapatite in
ungulate mammals and implications for ecological and paleoecological studies. Oecologia
120, 347–363.

Cerling, T.E., Harris, J.M., Macfadden, B.J., Leakey, M.G., Quade, J., Eisenmann, V.,
Ehleringer, J.R., 1997. Global vegetation change through the Miocene/Pliocene boundary.
Nature 389, 153–158.

Chamberlain, C.P., Mix, H.T., Mulch, A., Hren, M.T., Kent-Corson, M.L., Davis, S.J., Horton,
T.W., Graham, S.A., 2012. The Cenozoic climatic and topographic evolution of the western
North American Cordillera. Am. J. Sci. 312, 213–262.

Clementz, M.T., 2012. New insight from old bones: stable isotope analysis of fossil mammals. J.
Mammal. 93, 368–380.

Dawson, T., Mambelli, S., Plamboeck, A., Templer, P., Tu, K., 2002. Stable isotopes in plant
ecology. Annu. Rev. Ecol. Syst. 33, 507–559.

DeCelles, P.G., 2004. Late Jurassic to Eocene evolution of the Cordilleran thrust belt and
foreland basin system, western U.S.A. Am. J. Sci. 304, 105–168.

DeNiro, M.J., Epstein, S., 1978. Influence of diet on the distribution of carbon isotopes in animals. Geochim. Cosmochim. Acta 42, 495–506.

Diefendorf, A.F., Mueller, K.E., Wing, S.L., Koch, P.L., Freeman, K.H., 2010. Global patterns in leaf 13C discrimination and implications for studies of past and future climate. Proc. Natl. Acad. Sci. 107, 5738–5743.

Dillhoff, R.M., Dillhoff, T.A., Dunn, R.E., Myers, J.A., Strömberg, C.A.E., 2009. Cenozoic paleobotany of the John Day Basin , central Oregon. Geol. Soc. Am. 015, 135–164.

Domingo, M.S., Domingo, L., Badgley, C., Sanisidro, O., Morales, J., 2012. Resource partitioning among top predators in a Miocene food web. Proc. Biol. Sci. 280, 20122138.

Ehleringer, J.R., Field, C.B., Lin, Z.F., Kuo, C.Y., 1986. Leaf carbon isotope ratio and mineral composition in subtropical plants along an irradiance cline. Oecologia 70, 520–526.

Ehleringer, J.R., Sage, R.F., Flanagan, L.B., Pearcy, R.W., 1991. Climate Change and the Evolution of C4 Photosynthesis. Trends Evol. Ecol. 6, 95–99.

Farquhar, G.D., Ehleringer, J.R., Hubick, K.T., 1989. Carbon isotope discrimination and photosynthesis. Annu. Rev. Plant Physiol. Plant Mol. Biol. 40, 503–537.

Feranec, R.S., 2007. Ecological generalization during adaptive radiation: Evidence from Neogene mammals. Evol. Ecol. Res. 9, 555–577.

Feranec, R.S., Hadly, E.A., Paytan, A., 2009. Stable isotopes reveal seasonal competition for resources between late Pleistocene bison (Bison) and horse (Equus) from Rancho La Brea, southern California. Palaeogeogr. Palaeoclimatol. Palaeoecol. 271, 153–160.

Feranec, R.S., Macfadden, B.J., 2006. Isotopic discrimination of resource partitioning among

ungulates in C3-dominated communities from the Miocene of Florida and California. Paleobiology 32, 191–205.

Fricke, H.C., Clyde, W.C., O'Neil, J.R., Gingerich, P.D., 1998. Evidence for rapid climate change in North America during the latest Paleocene thermal maximum: oxygen isotope compositions of biogenic phosphate from the Bighorn Basin (Wyoming). Earth Planet. Sci. Lett. 160, 193–208.

Fricke, H.C., O'Neil, J.R., 1996. Inter- and intra-tooth variation in the oxygen isotope composition of mammalian tooth enamel phosphate: implications for palaeoclimatological and palaeobiological research. Palaeogeogr. Palaeoclimatol. Palaeoecol. 126, 91–99.

Gabel, M.L., Backlund, D.C., Haffner, J., 1998. The Miocene Macroflora of the Northern Ogallala Group, Northern Nebraska and Southern South Dakota. J. Paleontol. 72, 388–397.

Harris, E.B., Strömberg, C.A.E., Kohn, M.J., 2016a. Stable Isotope Compositions from Herbivore Teeth Suggest Climatic Stability leading into the Middle Miocene in Idaho. *Chapter 3*.

Harris, E.B., Strömberg, C.A.E., Sheldon, N.D., Smith, S.Y., Ibanez-Mejia, M., Vilhena, D.A., 2016b. Vegetation response during the lead-up to the middle Miocene warming event in the Northern Rocky Mountains. *Chapter 2*.

Heaton, T.H.E., 1999. Spatial, Species, and Temporal Variations in the 13C/12C Ratios of C3 Plants: Implications for Palaeodiet Studies. J. Archaeol. Sci. 26, 637–649.

Janis, C.M., Damuth, J., Theodor, J.M., 2000. Miocene ungulates and terrestrial primary productivity: where have all the browsers gone? Proc. Natl. Acad. Sci. U.S.A. 97, 7899–7904.

Janis, C.M., Scott, K.M., Jacobs, L.L., 1998. Evolution of Tertiary Mammals of North America, 1st ed. Cambridge University Press, Cambridge.

Kent-Corson, M.L., Barnosky, A.D., Mulch, A., Carrasco, M. a., Chamberlain, C.P., 2013. Possible regional tectonic controls on mammalian evolution in western North America. Palaeogeogr. Palaeoclimatol. Palaeoecol. 387, 17–26.

Koch, P., Tuross, N., Fogel, M., 1997. The effects of sample treatment and diagenesis on the isotopic integrity of carbonate in biogenic hydroxylapatite. J. Archaeol. Sci. 24, 417–429.

Koch, P.L., 1998. Isotopic Reconstruction of Past Continental Environments. Annu. Rev. Earth Planet. Sci. 26, 573–613.

Kohn, M.J., 2010. Carbon isotope compositions of terrestrial C3 plants as indicators of (paleo)ecology and (paleo)climate. Proc. Natl. Acad. Sci. U. S. A. 107, 19691–5.

Kohn, M.J., Cerling, T.E., 2002. Stable Isotope Compositions of Biological Apatite. Rev. Mineral. Geochemistry 48, 455–488.

Kohn, M.J., Fremd, T.J., 2008. Miocene tectonics and climate forcing of biodiversity, western United States. Geology 36, 783–786.

Kohn, M.J., Fremd, T.J., 2007. Tectonic controls on isotope composition and species diversification, John Day Basin, central Oregon. PaleoBios 27, 48–61.

Kohn, M.J., McKay, M.P., 2012. Paleoecology of late Pleistocene–Holocene faunas of eastern and central Wyoming, USA, with implications for LGM climate models. Palaeogeogr. Palaeoclimatol. Palaeoecol. 326-328, 42–53.

Kohn, M.J., McKay, M.P., Knight, J.L., 2005. Dining in the Pleistocene - Who's on the menu?

Geology 33, 649–652.

Kohn, M.J., Schoeninger, M.J., Valley, J.W., 1998. Variability in oxygen isotope compositions of herbivore teeth: reflections of seasonality or developmental physiology? Chem. Geol. 152, 97–112.

Lee-Thorp, J., van der Merwe, N.J., 1987. Carbon isotope analysis of fossil bone apatite. S. Afr. J. Sci. 83, 712–715.

Leopold, E.B., Denton, M.F., 1987. Comparative Age of Grassland and Steppe East and West of the Northern Rocky Mountain. Ann. Missouri Bot. Gard. 74, 841.

Macfadden, B.J., Cerling, T.E., 1996. Mammalian herbivore communities, ancient feeding ecology, and carbon isotopes: A 10 million-year sequence from the Neogene of Florida. J. Vertebr. Paleontol. 16, 103–115.

Maguire, K.C., 2015. Dietary niche stability of equids across the mid-Miocene Climatic Optimum in Oregon, USA. Palaeogeogr. Palaeoclimatol. Palaeoecol. 426, 297–307.

McMillan, M.E., Angevine, C.L., Heller, P.L., 2002. Postdepositional tilt of the Miocene-Pliocene Ogallala Group on the western Great Plains: Evidence of late Cenozoic uplift of the Rocky Mountains. Geology 30, 63–66.

Mihlbachler, M.C., Rivals, F., Solounias, N., Semprebon, G.M., 2011. Dietary change and evolution of horses in North America. Science (80-.). 331, 1178–81.

Muldavin, E.H., Moore, D.I., Collins, S.L., Wetherill, K.R., Lightfoot, D.C., 2008. Aboveground net primary production dynamics in a northern Chihuahuan Desert ecosystem. Oecologia 155, 123–132.

O'Leary, M.H., 1988. Carbon isotopes in photosynthesis. Bioscience 38, 328–336.

O'Leary, M.H., Madhavan, S., Paneth, P., 1992. Physical and chemical basis of carbon isotope fractionation in plants. Plant, Cell, Environ. 15, 1099–1104.

Passey, B.H., Cerling, T.E., Perkins, M.E., Voorhies, M.R., Harris, J.M., Tucker, S.T., 2002. Environmental Change in the Great Plains: An Isotopic Record from Fossil Horses. J. Geol. 110, 123–140.

Passey, B.H., Robinson, T.F., Ayliffe, L.K., Cerling, T.E., Sphonheimer, M., Dearing, M.D., Roeder, B.L., Ehleringer, J.R., 2005. Carbon isotope fractionation between diet, breath CO_2, and bioapatite in different mammals. J. Archaeol. Sci. 32, 1459–1470.

Prothero, D.R., 2005. The Evolution of North American Rhinoceroses. Cambridge University Press, Cambridge.

Prothero, D.R., 1998. Rhinocerotidae, in: Janis, C.M., Scott, K.M., Jacobs, L.L. (Eds.), Evolution of Tertiary Mammals of North America. Cambridge University Press, Cambridge, pp. 595–605.

Prothero, D.R., Rasmussen, D.L., 2008. New giant rhinoceros from the Arikareean (Oligocene–Miocene) of Montana, South Dakota and Wyoming, in: Lucas, S.G., Morgan, G.S., Spielmann, J.A., Prothero, D.R. (Eds.), Neogene Mammals: Bulletin 44. New Mexico Museum of Natural History and Science Bulletins, Albuquerque, pp. 323–330.

Quade, J., Cerling, T.E., 1995. Expansion of C4 grasses in the Late Miocene of Northern Pakistan: evidence from stable isotopes in paleosols. Palaeogeogr. Palaeoclimatol. Palaeoecol. 115, 91–116.

Retallack, G.J., 2009. Refining a pedogenic-carbonate CO2 paleobarometer to quantify a middle Miocene greenhouse spike. Palaeogeogr. Palaeoclimatol. Palaeoecol. 281, 57–65.

Retallack, G.J., 2007. Cenozoic Paleoclimate on Land in North America. J. Geol. 115, 271–294.

Seamster, V.A., Waits, L.P., Macko, S.A., Shugart, H.H., 2014. Coyote (Canis latrans) mammalian prey diet shifts in response to seasonal vegetation change. Isotopes Environ. Health Stud. 50, 343–60.

Secord, R., Wing, S.L., Chew, A., 2008. Stable isotopes in early Eocene mammals as indicators of forest canopy structure and resource partitioning. Paleobiology 34, 282–300.

Stewart, G.R., Turnbull, M.H., Schmidt, S., Erskine, P.D., 1995. 13C natural abundance in plant communities along a rainfall gradient: A biological integrator of water availability. Aust. J. Plant Physiol. 22, 51–55.

Strömberg, C.A.E., 2006. Evolution of hypsodonty in equids : testing a hypothesis of adaptation. Paleobiology 32, 236–258.

Tedford, R.H., Albright III, L.B., Barnosky, A.D., Ferrusquia-Villafranca, I., Hunt Jr., R.M., Storer, J.E., Swisher III, C.C., Voorhies, M.R., Webb, S.D., Whistler, D.P., 2004. Mammalian Biochronology of the Arikareean Through Hemphillian Interval (Late Oligocene Through Early Pliocene Epochs), in: Woodburne, M.O. (Ed.), Late Cretaceous and Cenozoic Mammals of North America. Columbia University Press, pp. 169–231.

Tipple, B.J., Meyers, S.R., Pagani, M., 2010. Carbon isotope ratio of Cenozoic CO2: A comparative evaluation of available geochemical proxies. Paleoceanography 25, 1–11.

Vogel, J.C., 1978. Isotopic assessment of the dietary habits of ungulates. S. Afr. J. Sci. 74, 298–301.

Wang, Y., Cerling, T.E., MacFadden, B.J., 1994. Fossil horses and carbon isotopes : new evidence for Cenozoic dietary , habitat , and ecosystem changes in North America. Palaeogeogr. Palaeoclimatol. Palaeoecol. 107, 269–279.

Warne, R.W., Pershall, A.D., Wolf, B.O., 2010. Linking precipitation and C3-C4 plant production to resource dynamics in higher-trophic-level consumers. Ecology 91, 1628–1638.

Woodburne, M.O., Swisher, C.C., 1995. Land mammal high-resolution geochronology, intercontinental overland dispersals, sea level, climate, and vicariance, in: Berggren, W.A., Kent, D.V., Aubry, M.-P., Hardenbol, J. (Eds.), Geochronology, Time Scales and Global Stratigraphic Correlation. Society of Sedimentary Geology Special Publication 54, pp. 336–364.

Zachos, J., Pagani, M., Sloan, L., Thomas, E., Billups, K., 2001. Trends, rhythms, and aberrations in global climate 65 Ma to present. Science 292, 686–93.

Zachos, J.C., Dickens, G.R., Zeebe, R.E., 2008. An early Cenozoic perspective on greenhouse warming and carbon-cycle dynamics. Nature 451, 279–83.

Zanazzi, A., Kohn, M.J., 2008. Ecology and physiology of White River mammals based on stable isotope ratios of teeth. Palaeogeogr. Palaeoclimatol. Palaeoecol. 257, 22–37.
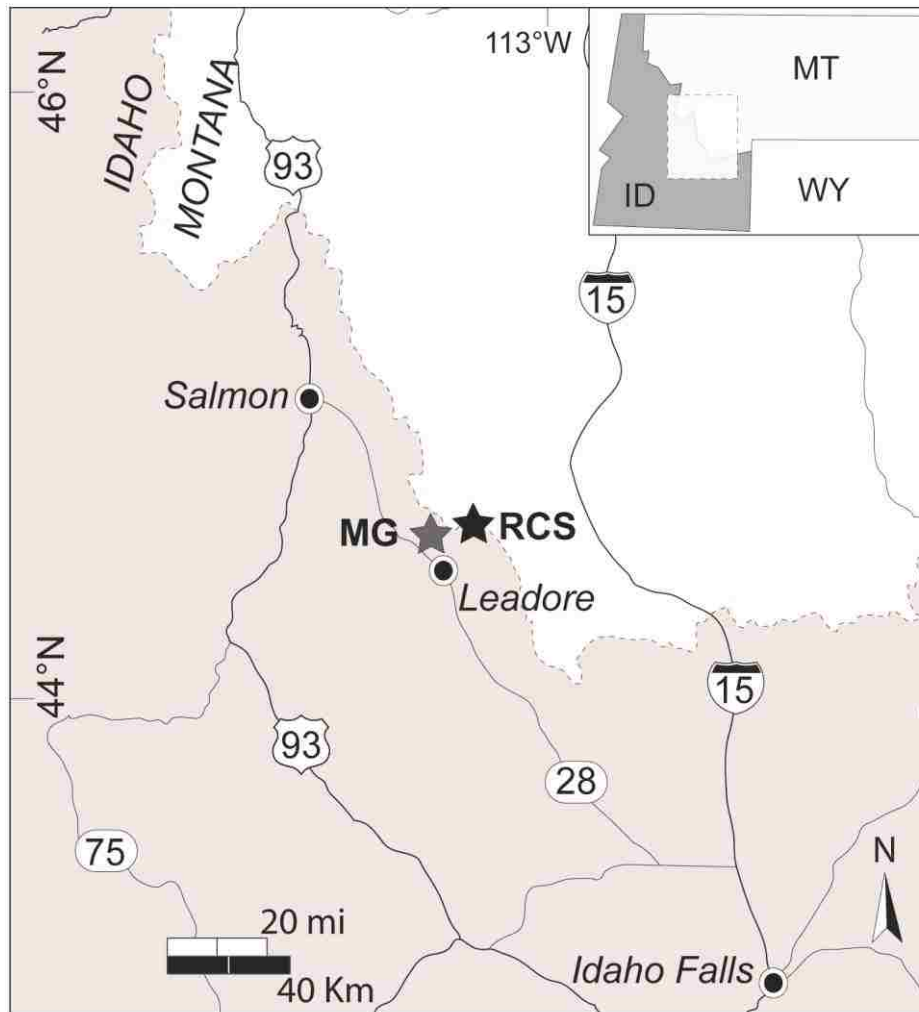
Figure 4.1. Locality map showing the location of the Railroad Canyon section (RCS; black star) and the Mollie Gulch sites (MG; grey star) in east-central Idaho.
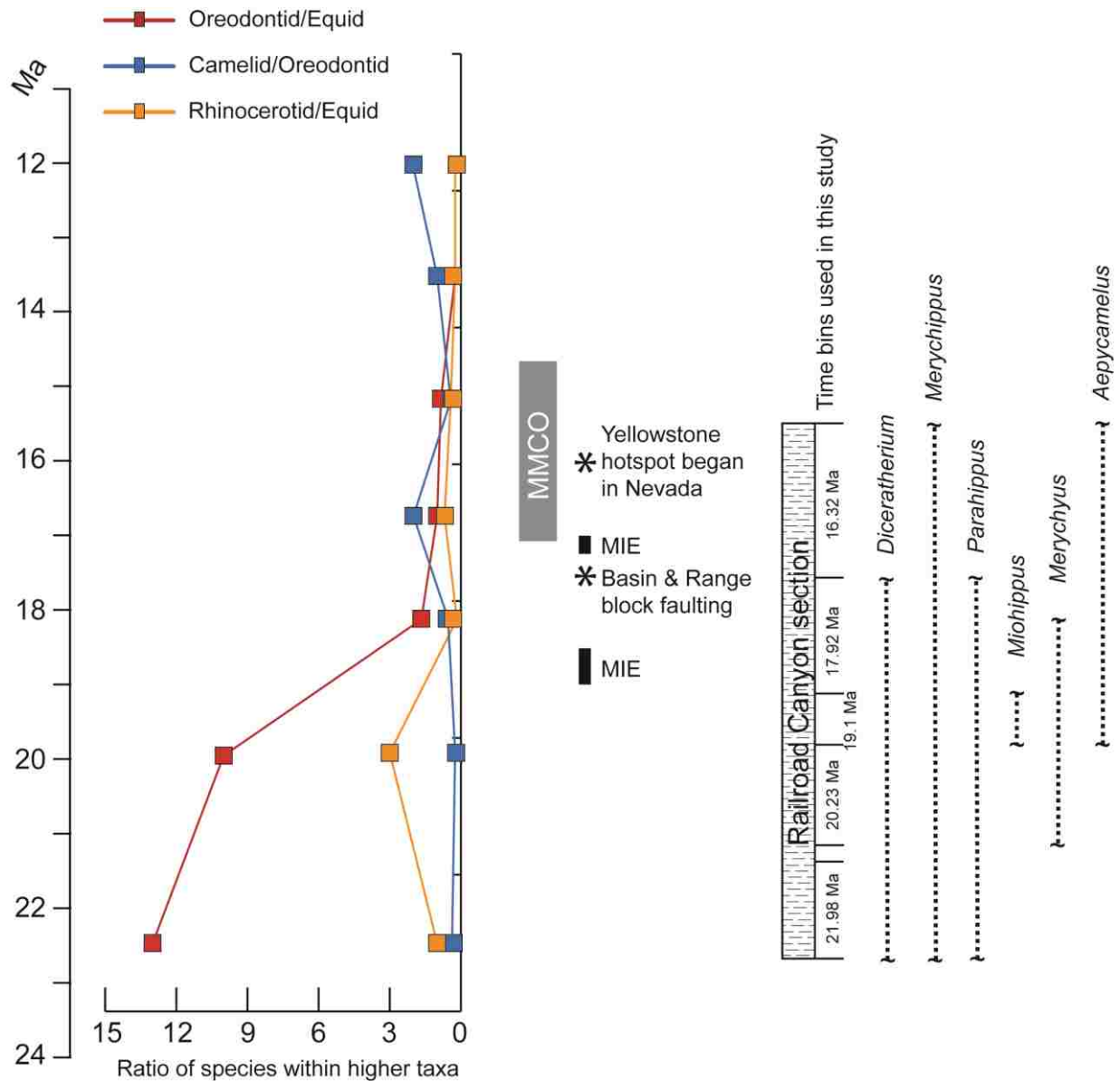
Figure 4.2. Faunal, climatic, and tectonic events from the early–middle Miocene in the Northern Rocky Mountains and stratigraphic ranges of biostratigraphically significant taxa within the Railroad Canyon section (RCS). Faunal data (i.e., ratios of species within higher taxa) from Barnosky et al. (2001). RCS mammal ranges modified from Barnosky et al. (2007). MMCO = mid-Miocene Climatic Optimum. MIE = mammalian immigration event (Woodburn and Swisher, 1995).
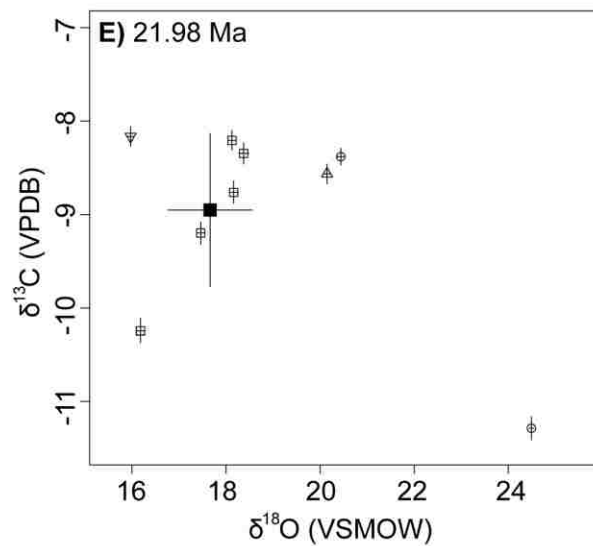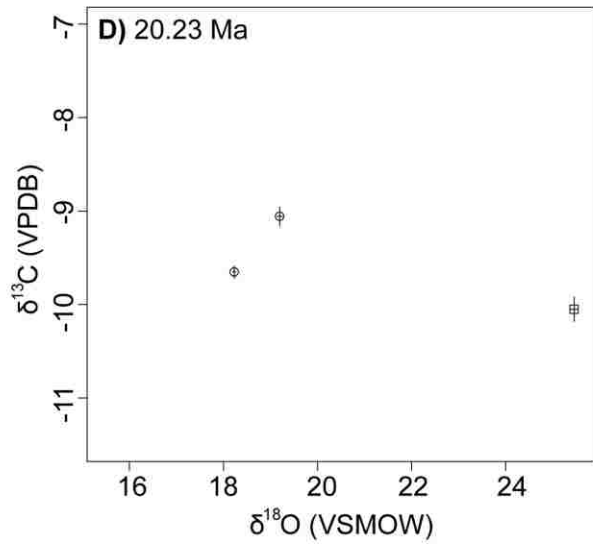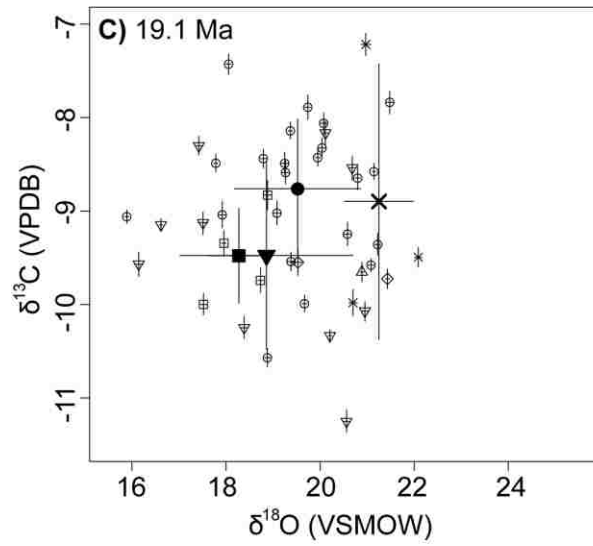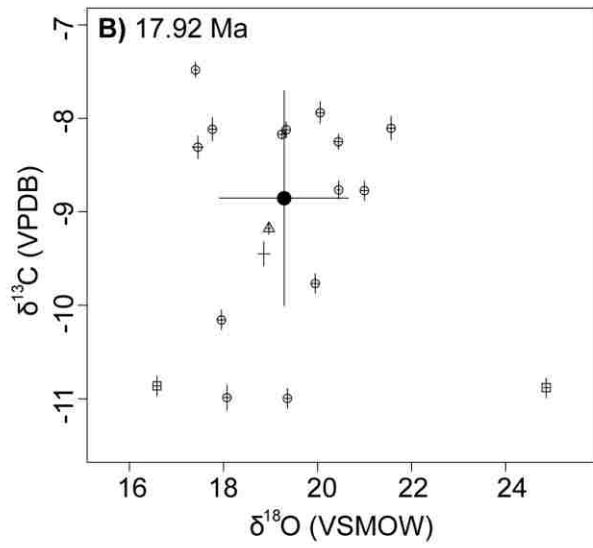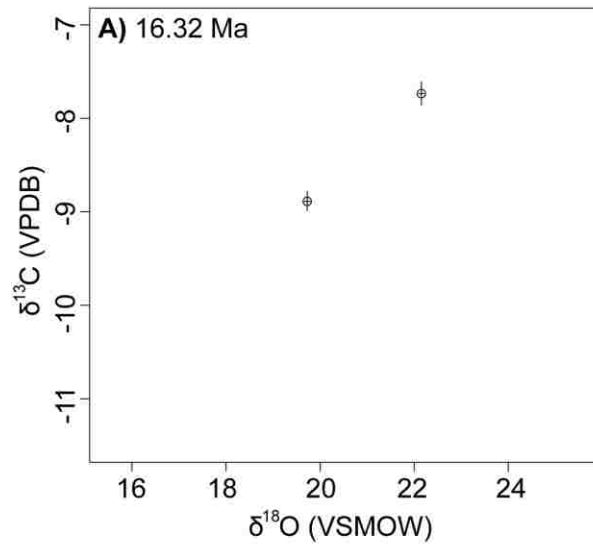
191

Figure 4.3. $\delta^{13}C_{enamel}$ and $\delta^{18}O_{enamel}$ values for RCS taxa in each time bin. Boundaries between vegetation types are predictions based on $\delta^{13}C$ values from modern floras normalized to 44.8° N latitude in North America and adjusted for diet-enamel enrichment and early–middle Miocene changes in $\delta^{13}C_{atmosphere}$ (see methods). Means are designated by bold symbols and error bars represent standard deviation around each mean.
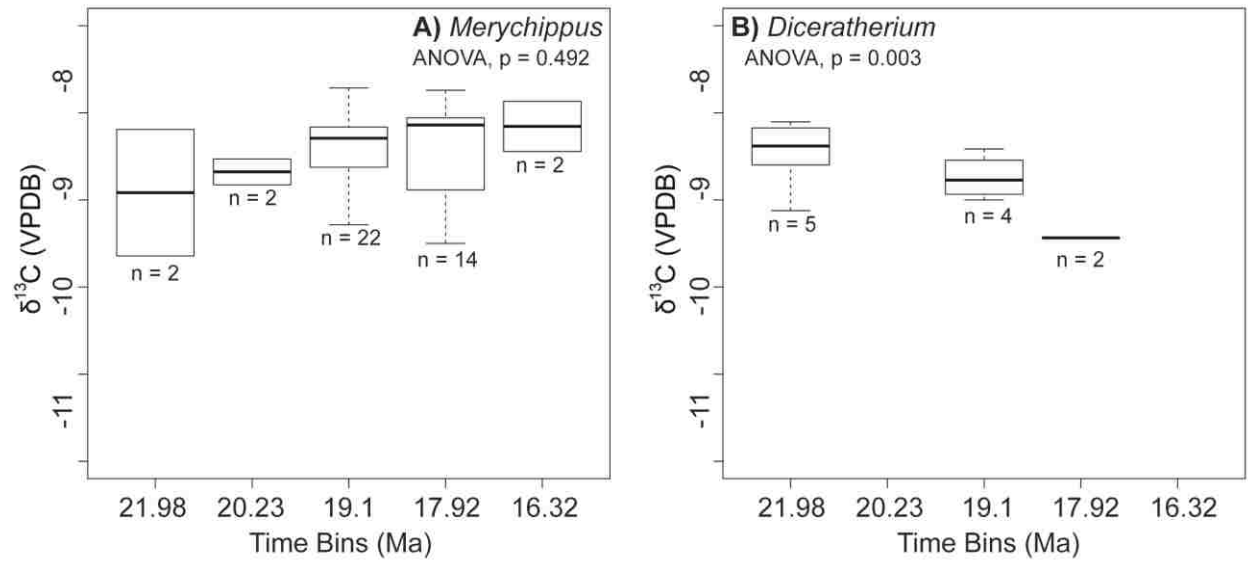
Figure 4.4. Bulk δ^{13}C values for A) *Merychippus* and B) *Diceratherium* in each time bin. For each boxplot, the dark line indicates the median, the box represents the interquartile range, and the dashed lines indicate the range of isotope values. n = the number of samples.
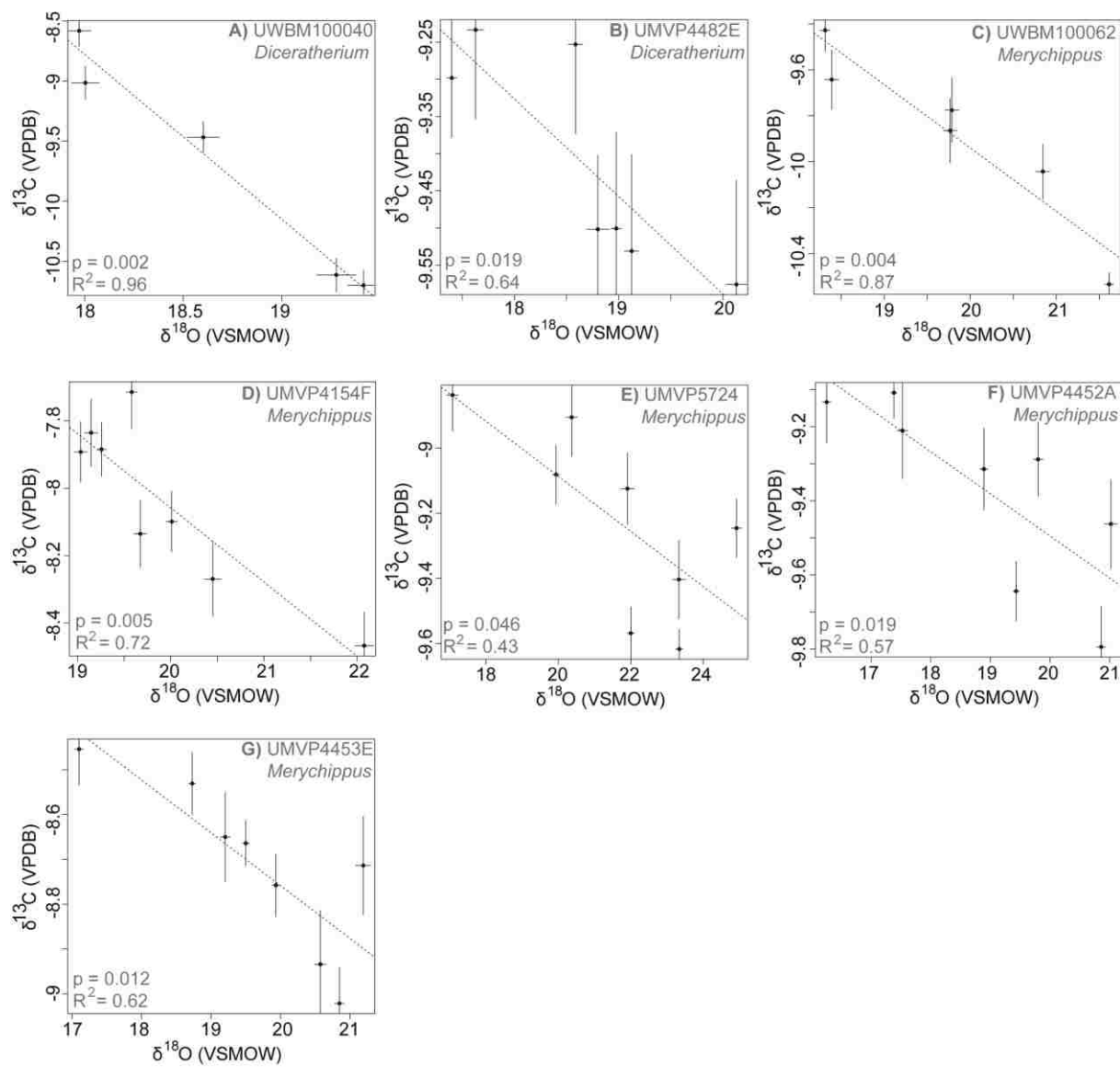
Figure 4.5. Negative correlations between δ¹³C vs. δ¹⁸O for seven serially sampled specimens.
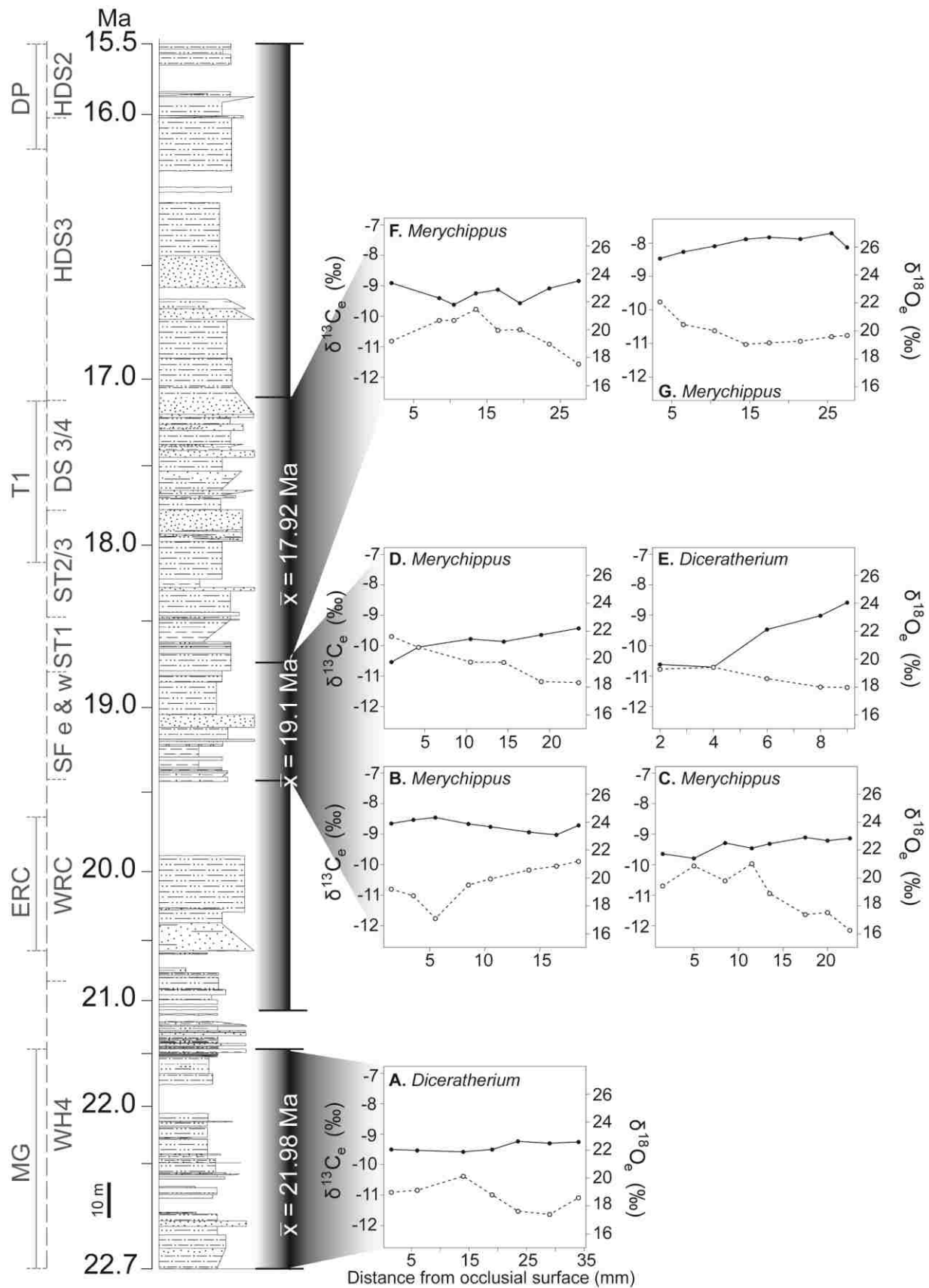
Figure 4.6. $\delta^{13}C$ vs. $\delta^{18}O$ enamel results from seven serially sampled equid and rhino teeth that exhibit seasonal variation. Filled circles are $\delta^{13}C$ results and open circles are $\delta^{18}O$ results. A) UMVP 4482e (*Diceratherium*); B) UMVP 4453e (*Merychippus*); C) UMVP 4452a (*Merychippus*); D) UWBM 100062 (*Merychippus*); E) UWBM 100040 (*Diceratherium*); F) UMVP 5724 (*Merychippus*); G) UMVP 4154f (*Merychippus*). Vertebrate fossil locality names are abbreviated as follows: WH4, Whiskey Springs 4; MG, Mollie Gulch; WRC, West Railroad Cut; ERC, East Railroad Cut; SF e&w, Snowfence east and west; ST1, Snowfence Turtle 1; ST2/3, Snowfence Turtle 2 and 3; DS ¾, Dead Squirrel 3 and 4; T1, Turtle 1; HDS3, High Dead Squirrel 3; HDS2, High Dead Squirrel 2; DP, Deadman Pass.
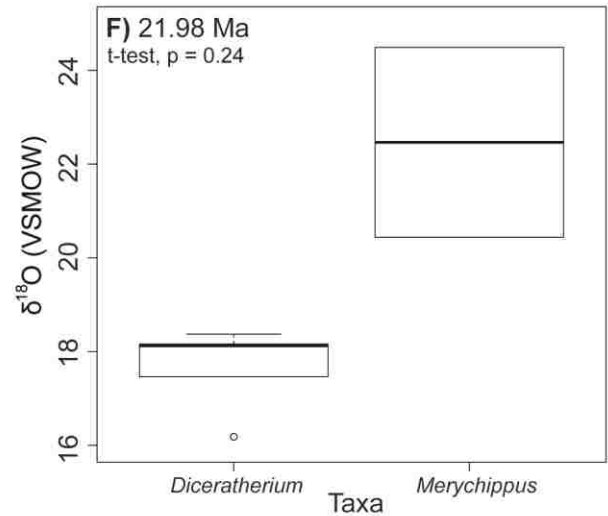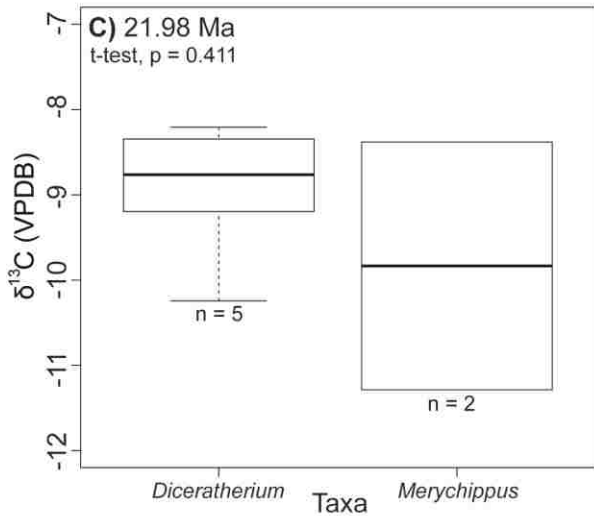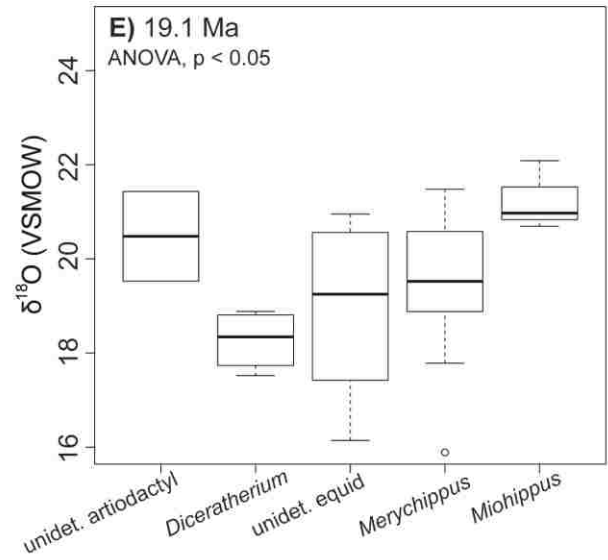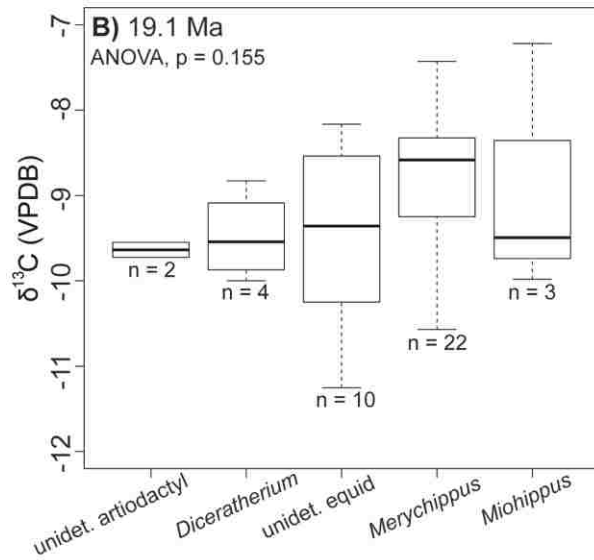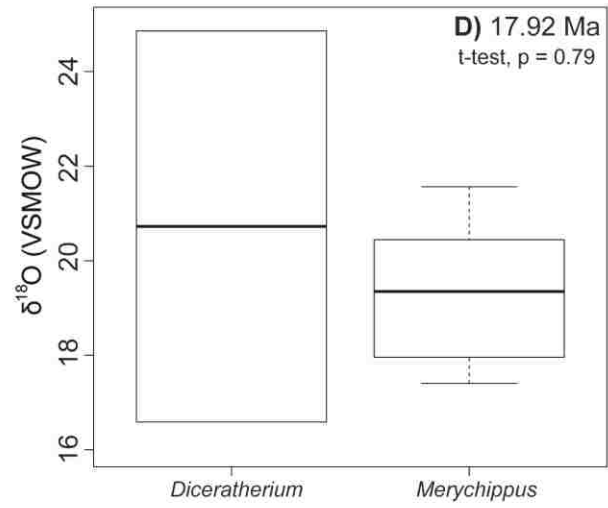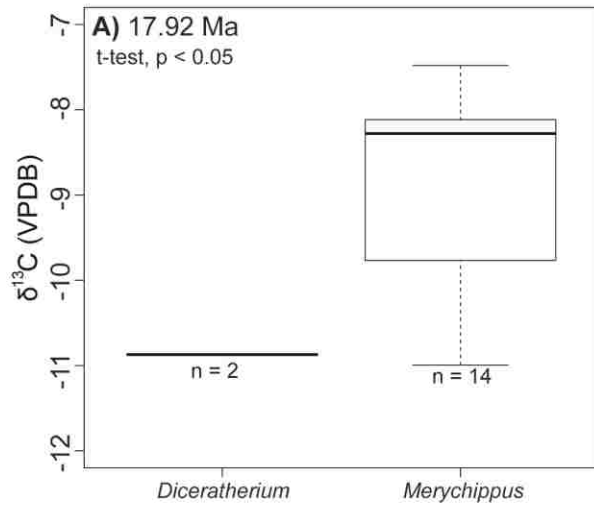
Figure 4.7. Bulk $\delta^{13}C$ and $\delta^{18}O$ values for various taxa at A) 17.92 Ma, B) 19.1 Ma, and C) 21.98 Ma. For each boxplot, the dark line indicates the median, the box represents the interquartile range, and the dashed lines indicate the range of isotope values. n = the number of samples.

CHAPTER 4: TABLES

Table 4.1. Bulk δ^{13}C and δ^{18}O compositions of herbivore teeth from the Railroad Canyon

section, Idaho.

| Sample number	Taxa	Time bin	δ^{13}C (VPDB)	δ^{13}C st. dev.	δ^{18}O (VSMOW)	δ^{18}O st. dev.
UWBM 100057	Artiodactyl	19.1	-9.73	0.11	21.43	0.05
UWBM 100051	Artiodactyl	19.1	-9.55	0.14	19.53	0.08
UWBM 100084	*Diceratherium*	17.92	-10.88	0.11	24.86	0.05
UMVP 5721	*Diceratherium*	17.92	-10.86	0.10	16.59	0.08
UWBM 100038	*Diceratherium*	19.1	-9.34	0.14	17.96	0.05
UWBM 100029	*Diceratherium*	19.1	-10.00	0.12	17.52	0.07
UWBM 100040	*Diceratherium*	19.1	-8.83	0.16	18.88	0.08
UMVP 4434	*Diceratherium*	19.1	-9.74	0.13	18.73	0.06
UWBM 100082	*Diceratherium*	20.23	-10.05	0.13	25.45	0.08
UMVP 4482D	*Diceratherium*	21.98	-8.21	0.11	18.13	0.06
UMVP 4482C	*Diceratherium*	21.98	-9.20	0.12	17.46	0.08
UMVP 4482A	*Diceratherium*	21.98	-10.24	0.13	16.18	0.08
UMVP 4482B	*Diceratherium*	21.98	-8.76	0.12	18.16	0.09
UMVP 4482E	*Diceratherium*	21.98	-8.35	0.11	18.37	0.11
UWBM 100047	Horse	19.1	-10.33	0.06	20.21	0.03
UWBM 100014	Horse	19.1	-9.15	0.07	16.62	0.03
UWBM 100012	Horse	19.1	-8.16	0.12	20.11	0.05
UWBM 100052	Horse	19.1	-8.54	0.13	20.68	0.06
UWBM 99996	Horse	19.1	-8.30	0.10	17.42	0.07
UWBM 100039	Horse	19.1	-10.25	0.12	18.38	0.07
UWBM 100035	Horse	19.1	-10.07	0.11	20.95	0.07
UWBM 100034	Horse	19.1	-11.25	0.12	20.56	0.07
UWBM 100026	Horse	19.1	-9.57	0.13	16.14	0.10
UWBM 100042	Horse	19.1	-9.13	0.12	17.51	0.10
UMVP 4483	Horse	21.98	-8.16	0.10	15.97	0.08
UWBM 100097	*Merychippus*	16.32	-8.89	0.10	19.73	0.07
UMVP 4400	*Merychippus*	16.32	-7.73	0.12	22.15	0.06
UWBM 100107	*Merychippus*	17.92	-7.48	0.08	17.41	0.04
UWBM 102404	*Merychippus*	17.92	-11.00	0.10	19.36	0.06
UWBM 99988	*Merychippus*	17.92	-8.12	0.13	17.76	0.07
UMVP 4160	*Merychippus*	17.92	-8.77	0.10	20.45	0.04
UMVP 4154E	*Merychippus*	17.92	-10.99	0.13	18.07	0.07

200

Table 4.1. *Continued*

Sample number	Taxa	Time bin	δ13C (VPDB)	δ13C st. dev.	δ18O (VSMOW)	δ18O st. dev.
UMVP 4154C	*Merychippus*	17.92	-8.17	0.05	19.24	0.07
UMVP 4154F	*Merychippus*	17.92	-8.12	0.08	19.33	0.07
UMVP 4159	*Merychippus*	17.92	-8.25	0.08	20.44	0.07
UMVP 4154D	*Merychippus*	17.92	-9.77	0.11	19.95	0.07
UMVP 4154B	*Merychippus*	17.92	-10.16	0.11	17.96	0.07
UMVP 5723	*Merychippus*	17.92	-7.94	0.11	20.06	0.08
UMVP 5724	*Merychippus*	17.92	-8.77	0.11	21.00	0.08
UMVP 4219	*Merychippus*	17.92	-8.11	0.13	21.56	0.09
UMVP 4154A	*Merychippus*	17.92	-8.31	0.12	17.46	0.11
UWBM 100070	*Merychippus*	19.1	-8.58	0.08	21.14	0.03
UWBM 100055	*Merychippus*	19.1	-8.49	0.09	17.78	0.04
UWBM 100022	*Merychippus*	19.1	-9.06	0.07	15.89	0.05
UWBM 100081	*Merychippus*	19.1	-7.43	0.11	18.05	0.05
UWBM 100049	*Merychippus*	19.1	-10.57	0.10	18.88	0.06
UWBM 100054	*Merychippus*	19.1	-9.36	0.11	21.22	0.06
UWBM 100066	*Merychippus*	19.1	-8.06	0.11	20.08	0.07
UWBM 100062	*Merychippus*	19.1	-9.54	0.10	19.38	0.07
UWBM 100063	*Merychippus*	19.1	-9.02	0.13	19.08	0.08
UWBM 100005	*Merychippus*	19.1	-9.04	0.14	17.92	0.08
UWBM 100002	*Merychippus*	19.1	-8.59	0.13	19.26	0.08
UMVP 9218	*Merychippus*	19.1	-8.14	0.09	19.37	0.05
UMVP 9424	*Merychippus*	19.1	-9.99	0.09	19.67	0.05
UMVP 7238	*Merychippus*	19.1	-8.65	0.12	20.80	0.05
UMVP 5891	*Merychippus*	19.1	-8.43	0.09	19.95	0.05
UMVP 6423	*Merychippus*	19.1	-7.89	0.13	19.74	0.06
UMVP 6424	*Merychippus*	19.1	-9.58	0.07	21.08	0.06
UMVP 9426	*Merychippus*	19.1	-8.44	0.10	18.79	0.07

Table 4.1. *Continued*

Sample number	Taxa	Time bin	δ13C (VPDB)	δ13C st. dev.	δ18O (VSMOW)	δ18O st. dev.
UMVP 4453f	*Merychippus*	19.1	-7.84	0.12	21.48	0.07
UMVP 6420	*Merychippus*	19.1	-8.49	0.12	19.25	0.08
UMVP 4452a	*Merychippus*	19.1	-9.25	0.12	20.58	0.09
UMVP 4453e	*Merychippus*	19.1	-8.33	0.11	20.04	0.09
UMVP 7160	*Merychippus*	20.23	-9.65	0.07	18.23	0.03
UMVP 9394	*Merychippus*	20.23	-9.06	0.10	19.19	0.06
UMVP 4547	*Merychippus*	21.98	-11.29	0.12	24.49	0.05
UMVP 4548	*Merychippus*	21.98	-8.38	0.09	20.44	0.07
UWBM 100050	*Miohippus*	19.1	-9.49	0.10	22.09	0.07
UWBM 99995	*Miohippus*	19.1	-9.98	0.14	20.70	0.09
UWBM 100045	*Miohippus*	19.1	-7.22	0.12	20.97	0.10
UWBM 99977	*Parahippus*	17.92	-9.18	0.07	18.96	0.04
UWBM 100064	*Parahippus*	19.1	-9.65	0.11	20.89	0.05
UMVP 4472	*Parahippus*	21.98	-8.56	0.11	20.15	0.07
UWBM 99954	Perissodactyl	17.92	-9.45	0.13	18.86	0.06

Table 4.2. $\delta^{13}C$ compositions for serially sampled equid and rhino teeth from the Railroad Canyon.

Sample number	Taxa	Distance from occlusial surface (mm)	Time bin (Ma)	$\delta^{13}C$ (VPDB)	$\delta^{13}C$ st. dev.
UWBM 100055-b	*Merychippus*	2.25	19.1	-9.57	0.08
UWBM 100055-d		4.5		-9.40	0.08
UWBM 100055-h		10.5		-9.12	0.11
UWBM 100055-k		13.5		-9.07	0.12
UWBM 100055-o		20.5		-9.19	0.07
UWBM 100062-a	*Merychippus*	1	19.1	-10.53	0.05
UWBM 100062-c		4.25		-10.04	0.12
UWBM 100062-h		10.5		-9.78	0.14
UWBM 100062-k		14.5		-9.86	0.14
UWBM 100062-n		19		-9.64	0.13
UWBM 100062-q		23.5		-9.43	0.09
UWBM 100066-a	*Merychippus*	1.5	19.1	-8.28	0.12
UWBM 100066-b		4		-8.51	0.12
UWBM 100066-d		7		-8.69	0.13
UWBM 100066-f		10		-8.31	0.13
UWBM 100066-g		12		-9.01	0.13
UWBM 100081-a	*Merychippus*	2	19.1	-8.13	0.11
UWBM 100081-b		4		-7.94	0.12
UWBM 100081-c		6		-8.34	0.13
UWBM 100081-d		8		-8.70	0.14
UWBM 100081-e		10		-8.54	0.12

Table 4.2. *Continued*

Sample number	Taxa	Distance from occlusial surface (mm)	Time bin (Ma)	δ13C (VPDB)	δ13C st. dev.
UMVP 4453Ea	*Merychippus*	1.5	19.1	-8.65	0.10
UMVP 4453Eb		3.5		-8.53	0.07
UMVP 4453Ec		5.5		-8.45	0.08
UMVP 4453Ee		8.5		-8.66	0.05
UMVP 4453Ef		10.5		-8.76	0.07
UMVP 4453Eh		14		-8.93	0.12
UMVP 4453Ei		16.5		-9.02	0.08
UMVP 4453Ej		18.5		-8.71	0.11
UMVP 5723a	*Merychippus*	2.5	17.92	-8.56	0.11
UMVP 5723c		6		-8.56	0.10
UMVP 5723e		9.5		-8.54	0.11
UMVP 5723g		13		-8.38	0.09
UMVP 5723i		16.5		-8.23	0.08
UMVP 5723k		20.5		-8.23	0.11
UMVP 5723m		24		-7.88	0.14
UMVP 5723p		29.5		-8.30	0.09
UMVP 5724a	*Merychippus*	2	17.92	-8.91	0.12
UMVP 5724b		8.5		-9.40	0.12
UMVP 5724c		10.5		-9.62	0.06
UMVP 5724e		13.5		-9.25	0.09
UMVP 5724g		16.5		-9.12	0.11
UMVP 5724i		19.5		-9.57	0.08
UMVP 5724k		23.5		-9.08	0.09
UMVP 5724m		27.5		-8.84	0.11

Table 4.2. *Continued*

Sample number	Taxa	Distance from occlusial surface (mm)	Time bin (Ma)	δ13C (VPDB)	δ13C st. dev.
UMVP 9305a	*Merychippus*	1.5	19.1	-10.66	0.12
UMVP 9305c		5		-10.03	0.12
UMVP 9305e		8		-10.17	0.12
UMVP 9305g		11		-10.52	0.09
UMVP 9305i		14.5		-10.57	0.12
UMVP 9305k		17.5		-10.85	0.12
UMVP 9305l		19.5		-10.29	0.09
UMVP 9426a	*Merychippus*	2	19.1	-9.02	0.10
UMVP 9426c		5		-9.52	0.10
UMVP 9426e		8.5		-9.19	0.10
UMVP 9426g		11.5		-9.07	0.09
UMVP 9426i		15		-9.28	0.11
UMVP 9426k		18.5		-9.33	0.12
UMVP 9426m		22.5		-9.62	0.12
UMVP 9426o		26.5		-9.53	0.11
UMVP 9426q		30.5		-10.09	0.11
UMVP 4400 a	*Merychippus*	2	16.32	-7.02	0.20
UMVP 4400 b		6.5		-7.50	0.15
UMVP 4400 c		11.5		-8.35	0.12
UMVP 4400 d		16.5		-8.07	0.29
UMVP 4400 e		21		-7.91	0.20

Table 4.2. *Continued*

Sample number	Taxa	Distance from occlusial surface (mm)	Time bin (Ma)	δ13C (VPDB)	δ13C st. dev.
UMVP 4154Ea	*Merychippus*	2	17.92	-10.79	0.11
UMVP 4154Ec		5.5		-10.11	0.11
UMVP 4154Ee		8.5		-10.87	0.10
UMVP 4154Eg		11.5		-10.58	0.11
UMVP 4154Ei		14.5		-10.64	0.08
UMVP 4154Ek		17.5		-10.38	0.07
UMVP 4154Em		20.5		-10.21	0.06
UMVP 4154Eo		24.5		-10.05	0.11
UMVP 4159a	*Merychippus*	2.5	17.92	-8.62	0.12
UMVP 4159c		5.5		-8.82	0.11
UMVP 4159e		8.5		-8.74	0.11
UMVP 4159g		11.5		-8.60	0.11
UMVP 4159i		15.5		-8.44	0.11
UMVP 4159k		19		-8.58	0.11
UMVP 4159m		22.5		-8.74	0.11
UMVP 4159o		26		-8.58	0.11
UMVP 4154Fa	*Merychippus*	3.5	17.92	-8.47	0.10
UMVP 4154Fc		6.5		-8.27	0.11
UMVP 4154Fe		10.5		-8.10	0.09
UMVP 4154Fg		14.5		-7.89	0.09
UMVP 4154Fi		17.5		-7.84	0.10
UMVP 4154Fk		21.5		-7.88	0.08
UMVP 4154Fm		25.5		-7.71	0.11
UMVP 4154Fn		27.5		-8.14	0.10

Table 4.2. *Continued*

Sample number	Taxa	Distance from occlusial surface (mm)	Time bin (Ma)	δ13C (VPDB)	δ13C st. dev.
UMVP 4452Aa	*Merychippus*	1.5	19.1	-9.64	0.08
UMVP 4452Ac		5		-9.79	0.11
UMVP 4452Ae		8.5		-9.29	0.10
UMVP 4452Af		11.5		-9.46	0.12
UMVP 4452Ag		13.5		-9.31	0.11
UMVP 4452Ai		17.5		-9.11	0.07
UMVP 4452Aj		20		-9.21	0.13
UMVP 4452Ak		22.5		-9.13	0.11
UMVP 6424a	*Merychippus*	2	19.1	-11.16	0.10
UMVP 6424c		5.5		-11.04	0.06
UMVP 6424e		9		-11.19	0.08
UMVP 6424g		12.5		-10.87	0.10
UMVP 6424i		16		-11.43	0.12
UMVP 6424k		19		-10.70	0.12
UMVP 6424m		23		-11.33	0.12
UMVP 6424o		26.5		-10.12	0.12
UWBM 100038-a	*Diceratherium*	3	19.1	-9.98	0.13
UWBM 100038-c		7		-9.33	0.11
UWBM 100038-e		10		-9.23	0.12
UWBM 100038-g		13		-9.52	0.12
UWBM 100038-i		16		-9.36	0.12
UWBM 100038-k		19		-9.21	0.14
UWBM 100038-m		21		-9.78	0.11
UWBM 100038-o		25		-9.24	0.14
UWBM 100038-q		30		-9.36	0.14
UWBM 100038-r		32		-9.35	0.12

Table 4.2. *Continued*

Sample number	Taxa	Distance from occlusial surface (mm)	Time bin (Ma)	δ13C (VPDB)	δ13C st. dev.
UWBM 100084-a	*Diceratherium*	0	17.92	-10.34	0.13
UWBM 100084-b		2		-10.92	0.12
UWBM 100084-c		5		-10.92	0.14
UWBM 100084-e		8		-10.78	0.13
UWBM 100084-f		11		-10.76	0.12
UWBM 100084-g		13.5		-10.20	0.10
UWBM 100082-a	*Diceratherium*	1	20.23	-10.51	0.14
UWBM 100082-b		3		-10.52	0.12
UWBM 100082-c		5		-10.39	0.13
UWBM 100082-e		8		-10.16	0.12
UWBM 100082-g		11		-9.88	0.09
UWBM 100082-i		16		-9.62	0.11
UMVP 4482D-A	*Diceratherium*	4	21.98	-9.41	0.05
UMVP 4482D-B		8		-9.02	0.15
UMVP 4482D-C		12.5		-9.31	0.08
UMVP 4482D-D		17		-9.21	0.13
UMVP 4482D-E		21.5		-9.44	0.10
UMVP 4482D-F		27		-9.08	0.12
UMVP 4482D-G		31.5		-9.45	0.19
UMVP 4482E-A	*Diceratherium*	1.5	21.98	-9.50	0.13
UMVP 4482E-B		6		-9.53	0.13
UMVP 4482E-D		14		-9.58	0.14
UMVP 4482E-E		19		-9.50	0.10
UMVP 4482E-F		23.5		-9.23	0.12
UMVP 4482E-G		29		-9.30	0.08
UMVP 4482E-H		34		-9.25	0.12

Table 4.2. *Continued*

Sample number	Taxa	Distance from occlusial surface (mm)	Time bin (Ma)	δ13C (VPDB)	δ13C st. dev.
UMVP 5721-A	*Diceratherium*	3	17.92	-11.16	0.08
UMVP 5721-B		7		-12.05	0.16
UMVP 5721-C		10.5		-11.52	0.14
UMVP 5721-D		15.5		-12.42	0.11
UMVP 5721-E		18		-10.97	0.12
UMVP 4482C-A	*Diceratherium*	1	21.98	-8.82	0.17
UMVP 4482C-B		5		-8.84	0.18
UMVP 4482C-D		14		-9.23	0.11
UMVP 4482C-E		18.5		-9.28	0.13
UMVP 4482C-F		23		-10.70	0.13
UMVP 4482C-G		27.5		-9.03	0.13
UWBM 100040-a	*Diceratherium*	2	19.1	-10.61	0.14
UWBM 100040-b		4		-10.70	0.13
UWBM 100040-c		6		-9.47	0.13
UWBM 100040-d		8		-9.01	0.14
UWBM 100040-e		9		-8.58	0.13

CHAPTER 5. Conclusion

This work is the culmination of an integrative and collaborative endeavor that used phytoliths, enamel-based stable isotopes (oxygen and carbon), and stable carbon isotopes from fossil soils to create a comprehensive picture of ecosystem change in a single basin during the early–middle Miocene. This study is the first to create a high-resolution, temporally constrained fossil dataset that documents relative stasis in terrestrial climate, plant and animal communities leading into the mid-Miocene Climatic Optimum in North America. As one of Earth's most recent, prolonged major global warming events, the MMCO has the potential to provide us with information critical to projecting impacts of climate change on future ecosystems. Thus, this work is particularly relevant because the Northern Rocky Mountains region is expected to be greatly impacted by global warming in 21st century (National Assessment Synthesis Team, 2001) but the consequences of this for local biota remain largely unknown. Because different areas on Earth respond differently to global climate change events, region-by-region studies of biota are particularly important for piecing together the larger global pattern of biotic change.

Whether biotic communities are restructured mostly by abiotic change or intrinsic biotic forces is a paramount issue in evolutionary ecology. This issue is especially pertinent in light of modern and future climate change, which may have different effects across lineages, biomes, and geographic space. Throughout Earth's history, climatic events have had a continual role in sculpting and reshaping biotic communities. Biological events of the geologic past can be viewed as natural experiments that have played out in countless different worlds unlike the one we live in today. Although we can never recreate these natural experiments, we can identify patterns across these climatic events, and use these patterns to constrain and delimit the causal

mechanisms of biotic community transitions. Knowledge of the past can only enhance our ability to understand, manage, and mitigate future biotic change.

REFERENCE

National Assessment Synthesis Team, 2001. Climate Change Impacts on the United States: The Potential Consequances of Climate Variability and Change. Cambridge University Press, Cambridge.

VITA

Elisha B. Harris was born and raised in upstate New York and has been conducting paleontological research since 2007. She began her research career at Hobart and William Smith Colleges, NY, under the supervision of Dr. Nan C. Arens. The culmination of her undergraduate thesis resulted in the publication of two peer-reviewed papers on the climate and vegetation of a mid-Cretaceous flora from the Cedar Mountain Formation, UT. Elisha began her graduate studies in 2010 under the supervision of Dr. Caroline A.E. Strömberg at the University of Washington. While at the UW, Elisha excelled at teaching undergraduates through various teaching assistant positions she held in the Biology department. In addition, she spent many hours volunteering at the Burke Museum of Natural History and Culture and mentoring undergraduates in the field and in the lab. In addition to her dissertation research, Elisha co-authored a peer-reviewed paper on bivalve networks during the end-Cretaceous mass extinction as well as a book chapter on the application of phytoliths in paleoecology. In addition to her academic interests, Elisha is an avid baker and naturalist. When not in the lab she can be found whipping up amazingly sweet confections, working in her garden, or hiking and camping in the beautiful Pacific Northwest.